Exploring the multiple techniques available for developing an understanding of soil erosion in the UK

Submitted by Pia Emma Benaud to the University of Exeter

as a thesis for the degree of

Doctor of Philosophy in Physical Geography

In September 2017

I certify that all material in this thesis which is not my own work has been identified and that no material has previously been submitted and approved for the award of a degree by this or any other University.

Signature: ……..

ABSTRACT

Accelerated soil erosion and the subsequent decline in soil depth has negative environmental, and consequently financial, impacts that have implications across all land cover classifications and scales of land management. Ironically, although attempts to quantify soil erosion nationally have illustrated that soil erosion can occur in the UK, understanding whether or not the UK has a soil erosion problem still remains a question to be answered. Accurately quantifying rates of soil erosion requires capturing both the volumetric nature of the visible, fluvial pathways and the subtle nature of the less-visible, diffuse pathways, across varying spatial and temporal scales. Accordingly, as we move towards a national-scale understanding of soil erosion in the UK, this thesis aims to explore some of the multiple techniques available for developing an understanding of soil erosion in the UK.

The thesis first explored the information content of existing UK-based soil erosion studies, ascertaining the extent to which these existing data and methodological approaches can be used to develop an empirically derived understanding of soil erosion in the UK. The second research chapter then assessed which of two proximal sensing technologies, Terrestrial Laser Scanning and Structure-from-Motion Multi-view Stereo (SfM-MVS), is best suited to a cost-effective, replicable and robust assessment of soil erosion within a laboratory environment. The final research chapter built on these findings, using both Rare Earth Oxide tracers and SfM-MVS to elucidate retrospective information about sediment sources under changing soil erosion conditions, also within a laboratory environment

Given the biased nature of the soil erosion story presented within the existing soil erosion research in the UK, it is impossible to ascertain if the frequency and magnitude of soil erosion events in the UK are problematic. However, this study has also identified that without 'true' observations of soil loss i.e. collection of sediment leaving known plot areas, proxies, such as the novel techniques presented in the experimental work herein and the methods used in the existing landscape scale assessments of soil erosion as included in the database chapter, are not capable of providing a complete assessment of soil erosion rates. However, this work has indicated that despite this limitation, each technique can present valuable information on the complex and spatially variable nature of soil erosion and associated processes, across different observational environments and scales.

ACKNOWLEDGEMENTS

Thanks first goes to my lead supervisor, Richard Brazier, for giving me the opportunity to carry out this research and for providing me with patience, guidance and encouragement throughout the process. Thank you to my other supervisors, Tim Quine and Karen Anderson, for always being enthusiastic about my research findings and providing support and feedback when needed.

My research was funded by Defra and situated within a broader research project. From within the project I would like to give a special thanks to Miriam Glendell for her support and advice; Jane Rickson for organising access to soil erosion records at Cranfield; John Quinton for sharing his enthusiasm and REO supply with me; and finally to Mike James for imparting some of his SfM-MVS wisdom on me.

Throughout my PhD I have also been incredibly fortunate to have an amazing support network of colleagues and friends within the Geography Department, here at Exeter. There are a few too many people to thank everyone individually, but I am incredibly grateful for the moral support, wisdom, ideas, laughter and pints I have shared. A special thanks to Alan Puttock and Emilie Grand-Clement for their constant availability as sounding boards, providing academic and personal support. Alan, Dave, Donna, Emilie, Gemma, Jo, Josie, Naomi and Paul – thank you for your assistance with running my experiments. Andy and Hugh, thank for the stimulating discussions, sounding out ideas in the blue room. I also need to thank the Exeter Geography support staff, with a special mention to Joana Zaragoza-Castells and Angela Elliott for going above and beyond with their support in the lab and to Neville England for saving the day with his epic supply of bolts and screws.

To my family and friends, both near and far, thank you for keeping me sane and grounded, for your patience, supply of cherry ripes and for believing in me.

Finally, Annie, thank you. You had no idea what you were getting yourself into, so thank you for your constant support, all the dinners, and for donning a lab-coat to help sieve my 2 tonne mound of soil.

Devon and the Streatham campus have been a wonderful backdrop to the process, and the unusually cold and soggy spring has presented ideal working conditions for getting it all finished. Now, to explore it all from somewhere other than the Blue Room…

TABLE OF CONTENTS

Abstract ..... **ii**

Acknowledgements ..... **iv**

List of tables ..... **ix**

List of figures ..... **x**

Glossary ..... **xiv**

1. Introduction **15**

1.1 Research context 15
1.2 Objective 1 18
1.3 Objective 2 19
1.4 Objective 3 20
1.5 Thesis structure 20

2. Literature review **22**

2.1 Soil Erosion Processes 22
2.1.1 Water erosion 23
2.1.2 Tillage erosion 27
2.1.3 Wind erosion 30
2.1.4 Soil loss via crop harvest 31
2.2 Quantification of soil erosion processes 31
2.2.1 Plot-based techniques 32
2.2.2 Field Surveys 34
2.2.3 Tracers 36
2.2.3.1 Naturally occurring and fallout tracers 38
2.2.3.2 Locally applied tracers 40
2.2.1 Fine-scale proximal sensing technologies 42
2.2.1.1 LiDAR and Terrestrial Laser scanning 43
2.2.1.2 Structure-from-Motion Photogrammetry 44
2.3 Summary 45

3. What can we learn from National-scale geodata describing soil erosion in the UK? 47

3.1 Overview 47
3.2 Introduction 47
3.3 Building a national-scale geodatabase of soil erosion observations 49
3.4 The occurrence of soil erosion in the UK 52
3.5 Understanding the impact of environmental conditions on rates of soil erosion 56
3.5.1 Soil texture 56
3.5.2 The role of slope 58
3.5.3 Precipitation 58
3.6 The relationship between erosion observations and monitoring approaches 59
3.6.1 Scale and soil erosion rates 60
3.6.2 Monitoring techniques 61

3.6.3 Site selection 63
3.7 Towards a national-scale understanding of soil erosion in the UK 64
4. Experimental Methods 68
4.1 Overview 68
4.2 Spatial scales and experimental setup 68
4.3 Preliminary characterisation work 69
4.3.1 Rainfall uniformity 69
4.3.2 Soil particle size distribution 70
4.4 Soil surface conditions 70
4.4.1 Experimental soil 70
4.4.2 Soil preparation – Rare Earth Oxide tracers 71
4.4.3 Soil bed preparation 73
4.4.4 Experimental runs 73
4.5 Sediment flux 75
4.6 Terrestrial Laser Scanning 75
4.7 Structure-from-Motion Photogrammetry 76
4.7.1 Camera properties 77
4.7.2 Ground control points 77
4.7.3 Lens calibration imagery 78
4.7.4 Experimental imagery 79
4.7.5 Data processing 80
5. Testing a suite of innovative soil erosion monitoring techniques 83
5.1 Overview 83
5.2 Introduction 83
5.3 Research methods 86
5.3.1 Experimental conditions 86
5.3.2 Runoff and sediment collection 86
5.3.3 TLS point clouds 86
5.3.4 SfM MVS point clouds 87
5.4 Precision and replicability of the SfM MVS methods 87
5.5 Predicting volumes of soil loss 91
5.6 Results 95
5.6.1 Sediment yields 95
5.6.2 Plot experiments 95
5.6.3 Flume experiments 102
5.7 Discussion 104
5.7.1 Model spatial resolution 105
5.7.2 Calculated mass of soil loss 106
5.8 Conclusions 108
6. Using REO and SfM based techniques to identify source apportinment of soil erosion at laboratory scales 110
6.1 Overview 110
6.2 Introduction 110
6.3 Methods 111

6.3.1 Experimental conditions 111
6.3.2 Runoff and sediment collection 112
6.3.3 REO analysis 112
6.3.4 Structure-from-Motion Multi-View-Stereo data 113
6.4 Results 114
6.4.1 Plot scale experiments 114
6.4.2 Flume scale experiment 117
6.4.3 REO versus SfM MVS Calculations 121
6.5 Discussion 122
6.5.1 Plot scale erosion experiments 122
6.5.2 Flume scale erosion experiment 124
6.6 Conclusions 126
7. Discussion and Conclusions 128
7.1 Existing soil erosion observations 128
7.2 Quantification of soil erosion using proximal technologies 129
7.3 Source apportionment under different soil erosion processes 131
7.4 Study limitations and future research 133
7.5 Conclusions 134
8. Supplementary Material 136
9. References 146

LIST OF TABLES

Table 2.1: Applied tracers used in soil erosion studies. 41

Table 2.2: Comparison between proximal sensing technology, data resolutions and application to soil erosion using examples. 43

Table 2.3: Summary of the advantages and disadvantages of the techniques presented in relation the erosion pathways. 46

Table 3.1: Summary statistics for the records held within the database. *The values reported for the upland environment represent the presence of erosion at a single point in time, rather than annual rates. 53

Table 4.1: Outline of the basic properties of the plots and flumes used, where dimensions represents the volume filled with soil. The bottom of the flume was filled with 8 cm of sand. 68

Table 4.2: PSD of soil used in plot and flume experiments, based on three replicates. 71

Table 4.3: Summary of mass of REO tracers used for plot scale experiments 73

Table 4.4: Summary of REO tracers and soil used for flume scale experiments 73

Table 4.5: Outline of the basic experimental conditions for each plot experiment. Rainfall is correct to +/- 5 mm hr^{-1} and run-on varied by +/- 50 mL min^{-1}. 74

Table 4.6: Outline of the basic experimental conditions for each flume experiment, where rainfall intensity is +/- 25 mm hr^{-1} 75

Table 5.1: RMSE values of the control and check points for each plot SfM MVS point cloud. 88

Table 5.2: RMSE values of the control and check scalebars for each flume SfM MVS point cloud. 88

Table 5.3: Properties and results for the models used for the precision analysis. 90

Table 5.4: Summary of sediment collected (g) during each plot and flume experimental run and the calculated volume (cm^3) based on ρb 1.3 g cm^{-3}. 95

Table 5.5: Summary table showing the point density of the raw TLS point clouds and the volume of change predicted (cm^3) following each experimental run at 5, 10 and 20 mm resolution. The calculated volume of observed sediment loss is included for reference. 96

Table 5.6: Summary table showing the point density of the raw SfM MVS point clouds and predicted volume of soil loss for each event, at 0.5, 2, 5, 10 and 20 mm grid resolutions. The calculated volume of observed sediment loss is included for reference. 99

Table 5.7: Summary table showing the point density of the SfM MVS point clouds and the volume of change detected following each experimental run based on 5 mm DoD. Error is the relationship between sediment and DoD calculations. 102

Table 8.1: Summary table illustrating the structure of records held within the geodatabase, when limited to records with a presence of erosion. 136

Table 8.2: Processing and error properties following plot scale camera calibration. 137

Table 8.3: SfM MVS processing properties and quality of plot scale experimental models, based on Photoscan metrics. 138

LIST OF FIGURES

Figure 2.1: Complexities of soil erosion processes. (From Brazier, 2013: Figure 15.1, p. 254) 26

Figure 2.2: (A) Ephemeral gully, (B) Evidence of preferential flow and increased erosion along tramlines, with a visible deposition feature at the foot of the slope. (Both authors own photos) 27

Figure 2.3: Schematic diagram of variable tillage translocation rate as a result of up- and down-slope tillage operation (from Govers *et al.*, 1999: Figure 1) 28

Figure 2.4: Factors of tillage erosion (From Van Oost *et al.*, 2006: Figure 6, p.451) 29

Figure 2.5: Bubble plot indicating the distribution of erosion studies with tracers (from Guzman *et al.*, 2013: Figure 1) 38

Figure 3.1: Screenshot from the online geodatabase illustrating the spatial distribution of records and an example of the information contained within the interactive dialogue box. 51

Figure 3.2: Distribution of soil texture classes based on relative percentage of sand, silt and clay particles (© Landis, Cranfield University). 52

Figure 3.3: Graphical representations of the distribution of erosion records: A) histogram of the frequency of erosion rates (t ha^{-1} yr^{-1}) for arable records with erosion (n = 260), B) histogram of the frequency of total erosion observed (t ha^{-1}), for the 1999 upland observations with erosion visible (n = 206) from McHugh et al. (2002), C) boxplots comparing all arable and grassland observations, and D) boxplots comparing arable and grassland records with erosion. 54

Figure 3.4: Map illustrating the spatial distribution and erosion magnitude of records (t ha^{-1} yr^{-1} for arable and grassland classes, and total t ha^{-1} for upland classes). The darker shading indicates the distribution of arable or improved grassland areas in the UK, based on LCM2000map. 55

Figure 3.5: The spatial distribution of soil textures in England and Wales, with the locations of soil erosion records held within the geodatabase shown in black. The soil texture information was sourced from the National Soil Map of England and Wales, NATMAP topsoil texture, 1:250,000 © Cranfield University. N values in parentheses indicate the number of sites with erosion (first value) and the total number of studies per soil texture class presented in Figure 3.2. 56

Figure 3.6: Boxplot illustrating the distribution of erosion rates (t ha^{-1} yr^{-1}), on a log scale, within each soil texture class, for arable records with a presence of erosion. 57

Figure 3.7: Boxplot illustrating the relationship between erosion risk (Evans, 1990b) and erosion rates (t ha^{-1} yr^{-1}) on a log scale for A) all values, and B) records with a presence of soil erosion 58

Figure 3.8: Scatter plot illustrating the relationship between erosion rates (t ha^{-1} yr^{-1}) on a log scale and A) slope gradient with 95% confidence intervals shaded, and B) precipitation (mm) 59

Figure 3.9: Boxplots illustrating the relationship between study extent and soil erosion rates (t ha^{-1} yr^{-1}) on a log scale for A) all arable records, and B) arable records with a presence of erosion. 61

Figure 3.10: Boxplot illustrating the relationship between erosion rates (t ha^{-1} yr^{-1}) and the monitoring technique employed for the study, for A) all arable and grassland records, and B) arable and grassland records with a presence of erosion. 62

Figure 3.11: Boxplot illustrating the relationship between erosion rate (t ha^{-1} yr^{-1}) and the criteria used for selecting the study location, for sites with a presence of erosion, for A) all arable and grassland records, and B) arable and grassland records with a presence of erosion. 64

Figure 4.1: Experimental setup for the A) plot-scale rilling experimental runs and B) flume rainsplash and compaction experimental run. 69

Figure 4.2: Schematic diagram illustrating the set-up of the rainfall nozzles in relation to the experimental areas. Dashed circles indicate the nozzles engaged for both the plot and flume scale experiments, open circles the nozzles engaged for only the flume scale experiments, and the crossed are nozzles that were not engaged. 70

Figure 4.3: Schematic diagram illustrating the REO tagging design for the plots (A) and flume (B) 71

Figure 4.4: A) Schematic diagram of the control frame used for calibration and the plot scale experiments, B) example 12-bit markers printed from PhotoScan (Agisoft LLC). 78

Figure 4.5: a) example geometry of image network surrounding the control frame, and b) the control frame and board used for calibration. 79

Figure 4.6: Schematic diagram illustrating the set-up of the imaging station used to collect experimental images for the plot scale experiments. 80

Figure 4.7: Schematic diagram showing the set-up used to collect experimental imagery for the flume scale experiments. 80

Figure 4.8: Workflow for the production of georeferenced dense point clouds using PhotoScan. Dashed lines indicated the calibration phase, while solid lines the processing for dense point clouds. 81

Figure 5.1: 'z' axis precision for A) P5E2 and B) P5E3, based on the mean precision of the tie points within in a 5 mm grid cell. 91

Figure 5.2: 'z' axis precision for F2E2 A) georeferenced and B) shape only, based on the mean precision of the tie points within in a 10 mm grid cell. 91

Figure 5.3: Illustration of the application of a cell-by-cell LoD to the prediction of elevation change for P5E3, where, A) and B) are the original DoDs processed from SfM MVS and TLS point clouds, respectively, C) and D) are the 95% confidence intervals LoD for the SfM MVS and TLS DoDs, respectively, and E) and F) are the LoD filtered DoDs for the SfM MVS and TLS clouds, respectively. 94

Figure 5.4: Graphical illustration of the distribution of results for the TLS predictions, showing A) the TLS relative measurement error (%) for all grid resolutions, and B) the relationship between the TLS predictions from a 5 mm DoD and sediment observations (cm3), where the dotted line represents a 1:1 relationship. 96

Figure 5.5: 5 mm resolution DoD showing changes in surface elevation following the rilling event (E3), for Plot 2 (A), Plot 3 (B), Plot 4 (C), and Plot 5(D). White represents areas with zero change detected. 97

Figure 5.6: A true colour photo of P5 following E3 (A) and DoDs for the same at the following grid resolutions B) 5 mm and C) 10 mm and D) 20 mm. White represents areas with zero change detected. 98

Figure 5.7: Graphical illustration of the distribution of results for the SfM MVS predictions, showing A) the SfM MVS relative measurement error (%) for all grid resolutions, and B) the relationship between the SfM MVS predictions from a 0.5 mm DoD and sediment observations (cm^3), where the dotted line represents a 1:1 relationship. 100

Figure 5.8: 0.5 mm resolution DoD showing changes in surface elevation following E1, E2 and E3, for Plot 2 (A), Plot 3 (B), Plot 4 (C), and Plot 5(D). E) and F) show the same DoD and the original nadir image for the areas identified in D. Where, white represents areas with zero elevation change, blue indicates areas of elevation decreases and red areas of increased surface elevation. 101

Figure 5.9: A) True colour SfM MVS point cloud of Plot 5, after the rilling event (E3), and DoD for surface elevation change between E2 and E3, after application of LoD, at B) 0.5 mm, C) 5 mm, and D) 20 mm grid resolution. Where, white represents areas with zero elevation change, blue indicates areas of elevation decreases and red areas of increased surface elevation. 102

Figure 5.10: A) True colour SfM MVS point cloud of F2, after E2, and B)DoD for total surface elevation change at 5 mm resolution. Where, white represents areas with zero elevation change, blue indicates areas of elevation decreases and red areas of increased surface elevation. 103

Figure 5.11: A) True colour SfM MVS point cloud of F1, after E2, and B)DoD for total surface elevation change at 5 mm resolution. Where, white represents areas with zero elevation change, blue indicates areas of elevation decreases and red areas of increased surface elevation. 104

Figure 6.1: Schematic diagram illustrating the REO tagging design for the plots (A), where the tracer changes 0 – 5 mm, 5 – 15 mm and >15 mm into the soil profile, and the flume (B), where the upper segments were tagged to a depth of 10 mm and change every 1 m from the top of the flume. 112

Figure 6.2: PSD for bulked sediment samples following experimental runs two and three, presented as mass faction (%) for each φ interval. 114

Figure 6.3: Calculated contribution from each tagged layer in the soil profile based on REO concentrations in the bulked sediment samples for A) the sheetwash events (E2), and B) the rilling event (E3). Note the different y-axis scales. 115

Figure 6.4: Calculated contribution from each tagged layer in the soil profile based on SfM-derived elevation and volumetric change for A) event 2, and B) event 3, where 'Dep.' represents the positive change resulting from sediment deposition. Note the different y-axis scales. 116

Figure 6.5: SfM-derived 0.5 mm DoD for P3 (A) and P5 (B) following E3, showing the area and magnitude of negative elevation changes in layers consistent with the REO tagging of the 0.3 x 0.5 m plots. 117

Figure 6.6: Summary of discharge (A), sediment concentration (B), Enrichment of particle size fractions (C), REO-based concentrations calculated from the sediment samples (D), and REO-based sediment apportionment (E), for Flume 3 through time during Event 2. 119

Figure 6.7: Calculated contribution from each section in the flume based on REO concentrations in the bulked sediment samples (A) and SfM elevations changes within each section (B) where 'Depos.' indicates the mass calculated from positive elevation changes at the lower end of the flume. Note the different y axis scales..... 120

Figure 6.8: SfM based raw point cloud showing the surface of Flume 3 following the erosion experiment (A), and the SfM-derived DoD, illustrating the spatial distribution of elevation changes (B). 121

Figure 6.9: The relationship between mass calculated by REO and SfM, presented as the relative error of the SfM predictions when compared to the REO results. Tot. indicates the total measurement error, including the estimated mass of deposited sediment. 122

Figure 7.1: Modified complexities of soil erosion processes diagram illustrating the contribution of REOs (green) and SfM-MVS (blue) to the understanding of soil erosion processes. Dashed lines indicates areas of further research (From Brazier, 2013: Figure 15.1, p. 254). 132

Figure 8.1 : Precision estimates for P5E2 based on methods presented by James et al., (2017b) 139

Figure 8.2: Precision estimates for P5E3 based on methods presented by James et al., (2017b) 140

Figure 8.3: Variation in tie point precision as a function of the number of Monte Carlo iterations. 141

Figure 8.4: Precision estimates for F2E2 based on methods presented by James et al., (2017b) 142

Figure 8.5: Formula for determination of cell-by-cell LoD using Surfer. 143

Figure 8.6: Discharge (A) and sediment flux concentrations (B) for the plot scale sheetwash experiment (E2) 144

Figure 8.7: Discharge (A) and sediment flux concentrations (B) for the plot scale rilling experiment (E3) 144

Figure 8.8: The bulked PSD for the sediment collected during the flume rainfall/runoff event (E2), presented as mass faction (%) for each φ interval, presented for all Flumes, while F3 was studied in Chapter 6. 145

GLOSSARY

AOI – Area of interest

DTM – Digital terrain model

DoD – DTM of difference

GSD – Ground sampling distance

GCP – Ground control point

LoD – Level of detection

PSD – Particle size distribution

REO – Rare Earth Oxide

RMSE – Root mean square error

SfM-MVS – Structure-from-Motion Multi-View Stereo (colloquially – SfM Photogrammetry)

TLS – Terrestrial Laser Scanner

σ_z - Standard deviation of the elevation (within a grid cell)

1. INTRODUCTION

1.1 Research context

Evans' 1971 paper, in drawing together evidence of soil erosion and highlighting the need for soil conservation, marked the start of a new era of soil erosion monitoring in the United Kingdom (Boardman, 2002; Brazier, 2004; Evans, 1971). More specifically, there was a shift towards quantitative assessments of soil erosion (Boardman, 2013). As a result, the 1980s and 1990s saw a peak in soil erosion monitoring in the UK and studies such as those carried out for the (then) Ministry of Agriculture, Fisheries and Food (MAFF) by the Soil Survey of England and Wales (SSEW), (Evans, 1988a, 2005) or Soil Survey and Land Research Centre (SSLRC) (Harrod, 1998) have been some of the most extensive attempts at quantifying soil erosion, on a national scale, to date. However, whilst observations of soil erosion in the UK have been carried out along-side agricultural development and intensification (e.g. Fisher, 1868; Morgan, 1985b; Quinton & Catt, 2004), the question remains: does the United Kingdom have a soil erosion problem?

Accelerated soil erosion and the subsequent decline in soil depth has negative environmental, and consequently financial, impacts that have implications across all land cover classifications and scales of land management (Montgomery, 2007; Pimentel *et al.*, 1995). The loss of top soil and the nutrients bound to soil particles can result in a substantial decline in soil fertility (Bakker *et al.*, 2005; Davidson & Harrison, 1995; Kirkbride & Reeves, 1993; Kosmas *et al.*, 2000; Lal, 1998; Palmer & Smith, 2013; Pimentel, 2006; Quine & Zhang, 2002), leading to potential losses in productivity, unless fertilizers are re-applied, in-turn increasing management costs and raising the risk of further environmental degradation (Bilotta & Brazier, 2008; Lal, 1998; Pimentel, 2006). Furthermore, large erosion and runoff events are particularly prevalent when crop cover is low, such as times of new growth, leading to further losses in annual crop yields (Duck & McManus, 1987; Evans, 1990a). In addition to on-site costs, off-site impacts such as decreases in surface water quality (Bilotta & Brazier, 2008; Brazier *et al.*, 2007; Tilman *et al.*, 2002), the sedimentation of waterways (Chapman *et al.*, 2005; Rickson, 2014; Vandaele & Poesen, 1995; Walling *et al.*, 2002) and large muddy flooding events (Boardman, 1995; Holman *et al.*, 2000), can have significant clean-up and mitigation costs (Pimentel *et al.*, 1995).

Unfortunately, sustainably managing soil resources is quite often perceived as a balance between costs, and frequently the upfront cost of strategies to reduce soil erosion in the long-term outweighs the short-term losses associated with erosion (Posthumus *et al.*, 2013). Consequently, strong policy is needed to drive change and reduce land degradation. Fortunately, the increased understanding of accelerated erosion, derived from the work of researchers since late in the last century, has led to some policy-based, soil management controls (Evans, 2010). At the EU level, the Soil Thematic Strategy aims to ensure the sustainable use of soil and proposes a Framework Directive (COM(2006) 232) to set the common principles of soil management. Such policy, however, only sought to encourage EU Member States to manage soils through their own strategies and remains a proposal to date (CEC, 2006). Subsequently, the 2009 Defra Soil Strategy set to prioritise soil management, launching the vision: "*By 2030, all England's soils will be managed sustainably and degradation threats tackled successfully*" (Defra, 2009). However, like the Soil Thematic Strategy, the Defra Soil Strategy sought to achieve better soil management through promoting best practice, rather than strict legislative guidelines. Furthermore, at present, current guidelines are top-down in nature and are not based on contemporary soil erosion research. Therefore, there is a real need for a strong body of soil erosion research aligned with the development of new legislation pertaining to the sustainable management of our soil resource, which is of particular importance in light of the contemporary changes to the UK's political environment.

Quantifying rates of soil erosion requires capturing both the volumetric nature of the visible, fluvial pathways (e.g. rills and gullies) and the subtle nature of the less-visible, diffuse pathways (e.g. sheetwash, tillage and wind), across varying spatial and temporal scales. However, often in response to policy needs, soil erosion studies in the UK have been largely *ad hoc* in nature, typically covering relatively small areas, over short time frames, at locations with a known history of erosion (e.g. Evans, 1988; Walling & Quine, 1991). Historically, evidence of soil erosion was often collected after erosion events using labour-intensive volumetric surveys of erosion features, whereby the depths of rills and/or gullies were measured at intervals along transects on the ground or estimated from aerial imagery (e.g. Chambers & Garwood, 2000; Davidson & Harrison, 1995), and was thus biased towards fluvial processes and localities known to erode. Since the late 1980s tracer technologies, such as ^{137}Cs fall-out surveys, have been utilised to quantify diffuse erosion pathways, through capturing long-term soil redistribution patterns in the case of using fall-out tracers,

or short-term patterns when tracers are locally applied (Govers *et al.*, 1996; Guzmán *et al.*, 2013; Quine *et al.*, 1997; Quine & Walling, 1991). Determining rates of soil redistribution, and thus loss, through the use of tracer methodologies requires a strong understanding of initial tracer concentrations through the soil profile, accordingly it can be difficult to establish a sound reference inventory using naturally occurring or fall-out tracers (Mabit *et al.*, 2013; Parsons & Foster, 2011, 2013). While the use of these methodologies has provided some evidence of soil erosion in the UK, due to their resource-intensive nature these methods are not practical for long-term, national-scale studies.

Recently, the use of point cloud technologies, namely Terrestrial Laser Scanning (TLS) and Structure-from-Motion photogrammetry (SfM), have experienced a rapid uptake in the geosciences for the fine-scale modelling of complex terrain (Smith *et al.*, 2015; Telling *et al.*, 2017). As a result, they have gained attention as an alternative approach for volumetric surveys of rills and gully soil erosion features (D'Oleire-Oltmanns *et al.*, 2012; Eltner *et al.*, 2014; Glendell *et al.*, 2017; Ouédraogo *et al.*, 2014; Vericat *et al.*, 2014). SfM in particular offers a cost-effective and accessible opportunity for high-resolution assessments of soil loss, across changing scales, though the technique is still being refined (James *et al.*, 2017a, 2017b). While SfM has been successfully applied to large erosion features, with the correct experimental design and control, relationships between sampling distance and errors suggest there is scope for SfM to monitor sub-millimetre changes to surface elevation using close-range imagery (Smith & Vericat, 2015), thus presenting an opportunity for the quantification of both fluvial and diffuse erosion pathways. TLS is often employed as the benchmark technique when assessing the efficiency of SfM in both field (Glendell *et al.*, 2017; James & Robson, 2012; Micheletti *et al.*, 2014) and laboratory environments (Morgan *et al.*, 2017; Nouwakpo *et al.*, 2014), however the validity of dong such, particularly for the quantification of small-scale erosion features remains unknown.

With expanding computing capabilities there has been a move away from field-based data collection to a heavy reliance on modelling soil erosion (Brazier, 2004). Derived from process-based understanding and/or using empirical data from controlled erosion plots or other smaller scale studies, models provide a platform from which rates of soil erosion can be inferred for larger spatial or temporal extents (e.g. Brazier et al., 2001; Kirkby et al., 2008; Morgan et al., 1998; Panagos et al., 2015; Wainwright et al., 2008a, 2008b, 2008c). However, as soil erosion is not a spatially uniform process, correlations between soil erosion rates and

scales are non-linear, leading to complex uncertainties within predictions (Beven & Brazier, 2010; Brazier *et al.*, 2000). As a result, there is often little correlation between results obtained from field studies and rates predicted through erosion models (Brazier *et al.*, 2010; Evans & Boardman, 2016a; Evans & Brazier, 2005). Consequently, there is an argument for both the empirical validation of models and the development of soil erosion monitoring techniques that provide a deeper spatial and temporal understanding of soil erosion processes (de Vente et al., 2013; Peeters et al., 2008; Wainwright et al., 2008).

Finally, there are several arguments for the development of a new national-scale understanding of soil erosion in support of national-scale modelling and subsequent decision-making. Accordingly, as we move towards a national-scale understanding of soil erosion in the UK, this thesis aims to explore some of the multiple techniques available for developing an understanding of soil erosion in the UK. This has been achieved through addressing the objectives and sub-objectives listed below:

1.2 Objective 1

Identify the extent to which existing data and approaches can be used to develop an empirically-derived understanding of soil erosion in the UK.

The UK has a rich history of soil erosion research, comprising of a mixture of large-scale monitoring schemes (Evans, 1988a; Harrod, 1998; McHugh *et al.*, 2002), assessments of single events (Boardman *et al.*, 1996; Evans & Morgan, 1974) and *ad hoc* studies targeting a greater understanding of erosion processes (Deasy *et al.*, 2011; Quinton & Catt, 2004). However, despite numerous reviews of the existing research (Boardman, 2013; Boardman *et al.*, 1990; Brazier, 2004; Evans, 2005), there is not an accessible resource that pools together all of this work, in an open access framework, to the benefit of the whole soil erosion community. Furthermore, there is no conclusive understanding of the severity of soil erosion in the UK (Brazier *et al.*, 2011), the significance of different environmental controls, and the impact the monitoring approaches employed by researchers has had on the perception of soil erosion rates in the UK (Evans *et al.*, 2015). Consequently, to best focus future soil erosion research, it is suggested that a synthesis and critique of existing data and approaches is conducted. This was achieved through addressing the following sub-objectives:

1.1 Collate all available, UK-based and empirically-derived soil erosion datasets into a spatially explicit and open-source resource.

1.2 Develop an understanding of potential magnitudes of soil erosion in the UK.

1.3 Explore the significance of environmental controls on erosion rates, in a UK setting.

1.4 Evaluate the impact that monitoring approaches have had on the rates of soil erosion that have been observed.

1.3 Objective 2

Test a suite of innovative soil erosion monitoring techniques and identify those best suited for a cost-effective, replicable and robust assessment of soil erosion within laboratory environments

The quantification of soil erosion rates in laboratory and field environments has traditionally been resource intensive and heavily reliant on expert knowledge and/or specialist equipment (Berger *et al.*, 2010; Harrod, 1998; Heng *et al.*, 2010; Jester & Klik, 2005; McHugh *et al.*, 2002; Walling, 2008; Watson & Evans, 1991). Furthermore, due to the breadth of approaches employed across the research community, there is little consistency and thus compatibility between soil erosion observations obtained under different research projects (Brazier *et al.*, 2011, 2016). Consequently, there is a need to develop monitoring techniques that can be utilised by all soil erosion researchers, along-side a clear understanding of the limitation of the technique(s). To this end, three-dimensional structural information collected via Terrestrial Laser Scanning (TLS) and Structure-from-Motion photogrammetry (SfM) provide an interesting platform from which to evolve a standardised approach for monitoring soil erosion rates. TLS, which uses timed returns from a pulsed laser, is often considered the benchmark for collecting spatial/topographic data (James & Robson, 2012; Smith & Vericat, 2015). In contrast, although the full scope for SfM application is yet to be explored, the rapidly developing tool is argued to provide a cost effective alternative to TLS (Glendell *et al.*, 2017). Therefore, the following sub-objectives were addressed to determine the suitability of each technique for a replicable and robust assessment of soil erosion:

2.1 Identify the resolution of information attainable through each technique, under changing experimental conditions.

2.2 Numerically compare the use of point cloud technologies for the volumetric quantification of soil loss.

2.3 Explore the roles changing soil erosion magnitudes and spatial complexities have on the accuracy of erosion quantification.

1.4 Objective 3

Evaluate the ability of REO tracers and SfM point clouds to elucidate retrospective information about soil sources during erosion experiments at two laboratory scales.

Identifying patterns of soil loss and source apportionment during soil erosion events is crucial to building an understanding of soil erosion processes, which can in turn feed into soil erosion models (Wainwright et al., 2008a). Soil erosion via water can be divided into diffuse and concentrated processes, which have different impacts on the landscape and relative contributions to the total soil lost from the landscape. With less erosive energy, diffuse erosion is primarily associated with the relatively uniform transport of fines (Armstrong *et al.*, 2011). In contrast, rill erosion shows less evidence of size selectivity and leaves visible evidence of concentrated flow pathways (Alberts *et al.*, 1980). Consequently, accurately describing soil loss via each process requires employing monitoring techniques capable of spatially quantifying the magnitude of both processes. To this end, applying a combination of REO tracers and SfM to different soil erosion conditions within a controlled laboratory environment presents a novel platform for building an understanding of patterns of soil loss and source apportionment. Accordingly, fulfilling the following sub-objectives assessed the suitability and information content of both techniques:

3.1 Apply REO tracers and SfM-based volumetric techniques to understand soil source apportionment at two discrete scales.

3.2 Discussion of the information content and/or value of the different techniques under changing soil erosion conditions within laboratory environments.

1.5 Thesis structure

The research objectives have been addressed in a series of chapters, which are presented in the style of the journals they will be submitted to, consequently there is some repetition in the content of each chapter's introduction section. First, however, a literature review examines the current state of knowledge on soil erosion processes and details the breadth of monitoring techniques that have been used to quantify soil erosion. In line with the first objective, Chapter 3 then collates and analyses all available, UK-based and empirically-derived soil erosion observations, building an understanding of the potential magnitudes of soil erosion in the UK and highlighting the strengths and weaknesses in the approaches adopted to-date. To minimise repetition, a research methods chapter then outlines the steps undertaken to create and capture soil erosion features, within a laboratory

environment. Chapter 5 then addresses the second objective, through assessing the capabilities of SfM and TLS for the quantification of soil erosion via water processes, in a laboratory setting. The final results chapter addresses objective three through using both REO tracers and SfM point clouds to elucidate retrospective information about sediment sources under changing soil erosion conditions, within a laboratory environment. Finally, Chapter 7 provides a discussion of how the findings of the individual chapters are situated within the broader discourse before articulating the limitations of the research presented herein and suggesting potential areas for future research.

2. LITERATURE REVIEW

2.1 Soil Erosion Processes

Boardman (2013) highlights that, when considering causes or pathways of accelerated soil erosion, it is important to distinguish between ultimate and immediate causes. In this context, ultimate causes can be described as the socio-economic drivers of land use and management, whereas immediate causes include the "erodibility of soils, farm management and weather events" (Boardman, 2013: p. 423). The following sections will therefore define the pathways of soil erosion based on the 'immediate causes' from a process-based perspective, rather than focusing on the arguably socio-political 'ultimate causes'. Furthermore, soil erosion pathways can act in isolation, though they often act simultaneously or sequentially. However, for the purpose of this literature review, the processes will be considered individually as: water, wind, soil loss via crop harvest, and tillage erosion.

Soil erosion, occurring through a range of physical processes and pathways, can be defined as:

> *"the wearing away of the land surface by physical forces such as rainfall, flowing water, wind, ice, temperature change, gravity or other natural or anthropogenic agents that abrade, detach and remove soil or geological material from one point on the earth's surface to be deposited elsewhere"* (Soil Science Society of America, 2001, in Verheijen *et al*., 2009: p. 24)

Building on this, the physical process of soil erosion can be divided into three phases, namely: detachment, transportation and deposition. Detachment involves the removal of soil particles or aggregates by physical forces including: rainsplash, flowing water, wind, and mechanical cultivation; allowing the easy removal of soil by transport agents (Morgan, 1995). Following detachment, the same forces can then act as transport agents, removing soil via diffuse or concentrated soil erosion processes (Govers *et al.*, 1999). Deposition then may occur when the driving erosive forces lose energy or reach a maximum carrying capacity. Consequently, it is possible to have detachment- or transport-limited erosion, and thus the resulting volume of soil eroded from an event is a function of the erodibility of the soil, the erosivity of transport agents and the influence of topography on the transport agents (Kirkby, 2010; Morgan, 1995).

Antecedent soil and landscape conditions, and therefore the energy of the erosion agents, influence the rate of soil erosion. Within diffuse erosion processes, soil transport rate is primarily controlled by slope gradient and the processes typically decrease relief, smoothing the landscape (Govers *et al.*, 1999). In contrast, the soil transport rate of concentrated pathways is a function of slope gradient and length, and acts to increase topographical relief and creates incisions in the landscape (Govers *et al.*, 1999). Consequently, changes in land use and management from natural conditions can result in the soil system becoming unbalanced and the rate of soil erosion exceeding the rate of soil formation, thus accelerating soil erosion rates. Herein, discussion will focus on accelerated soil erosion.

2.1.1 Water erosion

As introduced, erosion involves the detachment and transportation of soil particles by erosive agents – this section will focus on the soil erosion processes linked directly to the hydrological cycle. The understanding of the processes and interactions involved within water erosion pathways is continuously being expanded through a combination of laboratory work (allowing researchers to conduct highly focused analysis of research hypotheses, through controlled conditions), field based research (which allows for the theories developed under laboratory conditions to be tested under natural conditions) and computer modelling (trialling the application of assumptions over greater spatial and temporal extents) (Bennett, 1974; Kinnell, 2005; Parsons *et al.*, 2004, 2006; Wainwright *et al.*, 2008b). Consequently, the body of work pertaining to water erosion pathways is ever-expanding and, as such, the following section will provide a summary of the current understanding of the processes, rather than an in-depth detailing of the evolution of the scientific understanding.

Within the hydrological cycle, rainsplash and flowing water act to both detach and transport soil particles and aggregates, through processes that are divided into rainsplash, rill and interrill erosion. Rainfall, landing on the soil either directly as through-fall or following interception by vegetation as leaf-drainage – both described as rainsplash – has erosive potential. The erosive potential relates to the energy of the falling raindrop, and consequently, with increased velocity and mass comes greater erosivity (Bryan, 2000; Morgan, 1995). Interception by vegetation therefore reduces the erosivity of rainfall, and greater vegetation cover results in lower rates of soil erosion (Fullen, 1998; Gyssels *et al.*, 2005). Vegetation can, however, also act to filter runoff, preferentially removing coarse

particles and leading to runoff with a higher percentage of fine sediment (Brazier *et al.*, 2007).

When rainsplash does strike the soil surface with sufficient energy, soil aggregates are broken-down into smaller, more mobile, fragments, and particles and/or micro-aggregates are detached and transported (Farres, 1987; Kinnell, 2005; Salles & Poesen, 2000; Torri *et al.*, 1987). Transportation occurs when soil particles become entrained within the rain droplet and are transported with the resulting upward force or refraction of the water. The downward force of the raindrop also acts to reorganise the particles at the surface of the soil, consolidating or sealing the surface. The sealed surface can harden, forming a crust, which then further reduces the infiltration capacity of the soil leading to increased runoff. Decreased clay and organic matter have been associated with an increase in surface crusting; consequently loams and sandy loams are more susceptible to crust formation (Le Bissonnais *et al.*, 2005).

Following the initial disturbance, the rainfall either infiltrates into the soil, filling pore spaces, until the storage or infiltration capacity of the soil is reached, or is stored in depressions on the soil surface as a result of impermeable layers formed through surface sealing or crusting (Morgan, 1995). Runoff occurs when the soil infiltration rate or capacity is exceeded (Shaw, 1994), or if soil moisture content is such that there is a pressure equilibrium between soil and surface water (Foth, 1990). Similarly, as surface depressions reach capacity (ponding), runoff is also generated. Runoff can either flow across the surface of the soil in relatively uniform thickness (called sheetwash or Hortonian overland flow), or can converge to form concentrated flow paths – increasing the energy of the moving water (Morgan, 1995).

Through carrying soil particles trapped via rainsplash action, or those entrained through the erosive action of moving water, sheetwash and channelled water erode the soil surface. Given that the erosivity of any erosion agent is related to energy, the faster-moving, concentrated water can result in greater levels of surface transport when compared to un-concentrated sheetwash (Kinnell, 2005). Consequently, both rainsplash and sheetwash remove soil of a relatively uniform thickness, though the spatial variability of soil physical properties and changes in topography act as secondary controls on the amount of material removed (Bryan, 2000). In contrast, concentrated water flows cut into the soil surface

through entrainment, forming rills that can develop into gullies, should there be sufficient energy (Kirkby & Bracken, 2009).

As coarse and fine grain sizes are transported as a function of rainsplash and un-concentrated overland flow, surface roughness decreases (Idowu *et al.*, 2002; Rai *et al.*, 2010) which in turn increases the speed of surface flows, and further encourages concentrated flow paths. The formation of concentrated flow paths intensifies particle entrainment, scouring the soil surface and rills are formed (Morgan, 1995; Parsons & Wainwright, 2006). A secondary process of up-slope incision commences with the formation of a head-cut (Slattery & Bryan, 1992). The up-slope incision of a rill, from the head-cut, is controlled by soil cohesiveness, headwall properties and flow, whereas the down-slope extension is a function of the erosive potential (energy) of the concentrated flow and the erosivity of the soil (Morgan, 1995; Robinson *et al.*, 2000). Consequently, rill erosion (if there is sufficient energy within overland flow to create concentrated flows) has been found to be responsible for a larger percentage of soil loss through water erosion processes, when compared to interrill erosion (Govers & Poesen, 1988).

As detailed, sediment, in the form of soil aggregates or particles, is entrained into un-concentrated or concentrated flowing water through a combination of rainsplash and flow detachment (Kinnell, 2005). While relationships between dispersed and un-dispersed particle size distribution (PSD) in sediment sources and depositions sediments can be used to identify the breakdown of aggregates and the preferential transportation of different sized sediments, whereby a relatively small difference between dispersed (i.e. by an ultrasonic bath) and un-dispersed PSD in sediment would indicate aggregate breakdown (Michaelides *et al.*, 2010), changes in the consistency of exported sediment can also be a function of slope length. For example, resulting from either shorter coarse particle travel distances (Parsons *et al.*, 2004), the preferential deposition of coarse particles as transport capacity decreases (Kirkby, 2010), or changing relationships between sediment yields and slope length (Parsons *et al.*, 2006). Consequently, when looking to describe erosion processes, it important to identify the source of sediment.

Figure 2.1 further highlights the multifaceted nature of water erosion processes, where complex interactions exists between these often dynamic variables (Brazier, 2013). Accordingly, it has proven challenging to accurately describe the modes of sediment

transport and, in turn, sediment transport distances. This is best reflected in the difficulties in modelling soil erosion rates and the discrepancies between studies carried out over different spatial extents (Evans & Brazier, 2005; Govers *et al.*, 2007; Wainwright *et al.*, 2008b). As a result, there has been an often lively discourse on the mechanisms of water erosion processes, within the soil erosion community (Evans & Boardman, 2016a; Hairsine & Sander, 2009; Kinnell, 2008; Panagos *et al.*, 2016; Wainwright *et al.*, 2009).

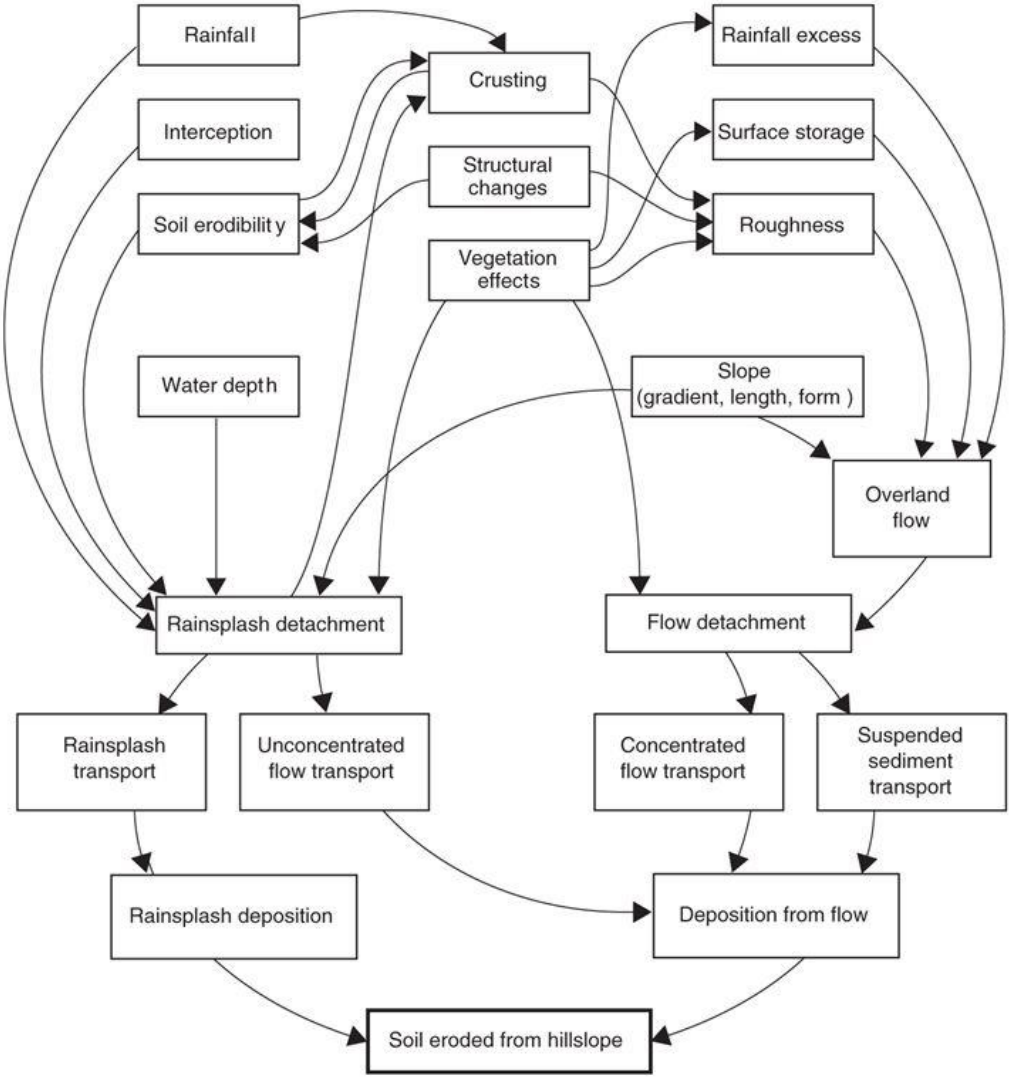

Figure 2.1: Complexities of soil erosion processes. (From Brazier, 2013: Figure 15.1, p. 254)

Due to the relatively uniform removal of soil through sheetwash and rainsplash, evidence for this type of water erosion is rarely visible in the landscape. Rills and gullies, however, leave highly visible incisions through the landscape, increasing topographic variability (see Figure 2.2). Patterns of rilling or gullying may relate directly to topographic features, particularly changes in slope and convexities that stimulate the forming of channels (Davidson & Harrison, 1995; Morgan, 1995). Additionally, artificial features, such as wheeling or tramlines and compaction, have a strong influence on the preferential flow of

water, thus also resulting in increased erosion rates, as visible in Figure 2.2 (Chambers *et al.*, 1992; Deasy *et al.*, 2009a; Deasy & Quinton, 2010; Etana *et al.*, 2013; Fullen, 1985a; Stevens & Quinton, 2008). Therefore, fully quantifying water erosion pathways would require a methodology or suite of techniques that capture both the volumetric nature of the more visible, fluvial pathways and the subtle nature of the less visible, diffuse erosion.

Figure 2.2: (A) Ephemeral gully, (B) Evidence of preferential flow and increased erosion along tramlines, with a visible deposition feature at the foot of the slope. (Both authors own photos)

2.1.2 Tillage erosion

The soil movement associated with a pass of tillage equipment is referred to as *translocation*, defined as the "mass of soil moved by the tillage in a specific direction per metre width" (Van Oost *et al.*, 2006: 446). Though it is common practice to till whole fields, operational and environmental conditions can result in the variable magnitude of soil movement within a field (see Figure 2.3). Different tillage implements, speed, depth, soil type and slope, have all been associated with differing volumes of soil being translocated (Quine & Zhang, 2004; Van Muysen *et al.*, 2002; Van Oost *et al.*, 2000). Furthermore, Lobb *et al.* (1999) found operations to vary considerably even under the control of a single machine (or operator) in response to conditions, noting on-going changes in speed and plough depth within a single pass.

Given the largely non-visible nature of tillage processes, tracer-based research has strongly supported the development of the understanding of subsequent soil re-distribution patterns. Work such as the ^{137}Cs derived modelling carried out by Walling and Quine (1991), which studied the long-term spatial re-distribution of soils within fields, identified un-accounted for soil loss after combining results from field studies with models of water and diffuse erosion pathways. Additionally, patterns of soil redistribution didn't match those typically associated with soil erosion, namely, losses were found in convexities in the landscape and deposition appeared in concavities. Govers *et al.* (1999) argue that development of the technique also marked the change in the way tillage processes were studied. Other methods, such as the incorporation of aluminium cubes (e.g. Govers et al., 1994) or additional levels of ^{137}Cs into the plough layer (Lobb *et al.*, 1995), have allowed for short-term studies on soil translocation via tillage.

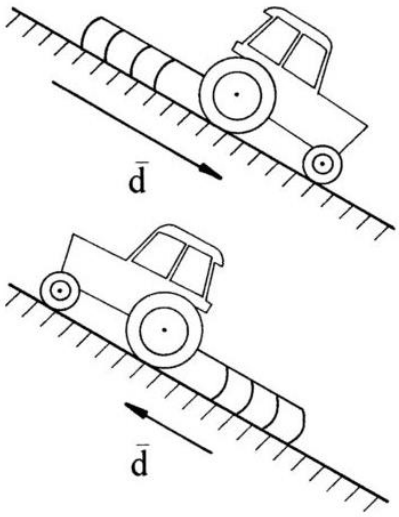

Figure 2.3: Schematic diagram of variable tillage translocation rate as a result of up- and down-slope tillage operation (from Govers *et al.*, 1999: Figure 1)

Unlike water erosion pathways, tillage has been found to cause soil loss on slope crests or shoulders (convexities) and increased soil accumulation in hollows or footslopes (concavities) (Govers *et al.*, 1994; Lindstrom *et al.*, 1992; Lobb *et al.*, 1995; Van Oost *et al.*, 2006; Walling & Quine, 1991). Studies on translocation rates have identified that this is related to an increase in soil translocation during downslope passes over convexities, when compared to upslope passes, and *vice versa* on concavities, as illustrated in Figure 2.3 (Van Muysen *et al.*, 2002). Furthermore, Govers *et al.* (1999) note that it is in fact "the change in slope gradient between the boundaries of the segment rather than its absolute value" (p.167) that has the greatest effect on translocation rates. Consequently, it is now acknowledged that tillage and the subsequent unequal redistribution of soil is a largely gravity-driven process.

To-date tillage erosion studies have largely focussed on understanding the role of the tillage process and slope on the rate of soil translocation. However, there are a limited number of studies looking at other controls, such as the work of Van Muysen *et al.* (1999) who looked at soil conditions prior to tillage. The study identified that loose, pre-tilled soil, through reduced cohesion allowed for greater tillage depths, resulted in the greater downslope translocation of soil within known risk areas. Furthermore, agricultural practice typically incorporates a range of crops and tillage operations – therefore it is important to not only consider the erosivity of each tillage device, but also the impact of a combination or sequence of operations, each with erosive potential – making accurate quantification or prediction of soil loss quite difficult (Van Muysen & Govers, 2002).

Van Oost *et al.* (2006) through the review of a wide body of tillage erosion literature developed Figure 2.4, capturing the above-described complexities. The equation within, i.e. $E_t = f(T_E , L_E)$ acknowledges that the rate of tillage erosion (E_t) resulting from any individual tillage operation is a function of both the erosivity of a tillage process (T_E) and the erodibility of the landscape being worked (L_E).

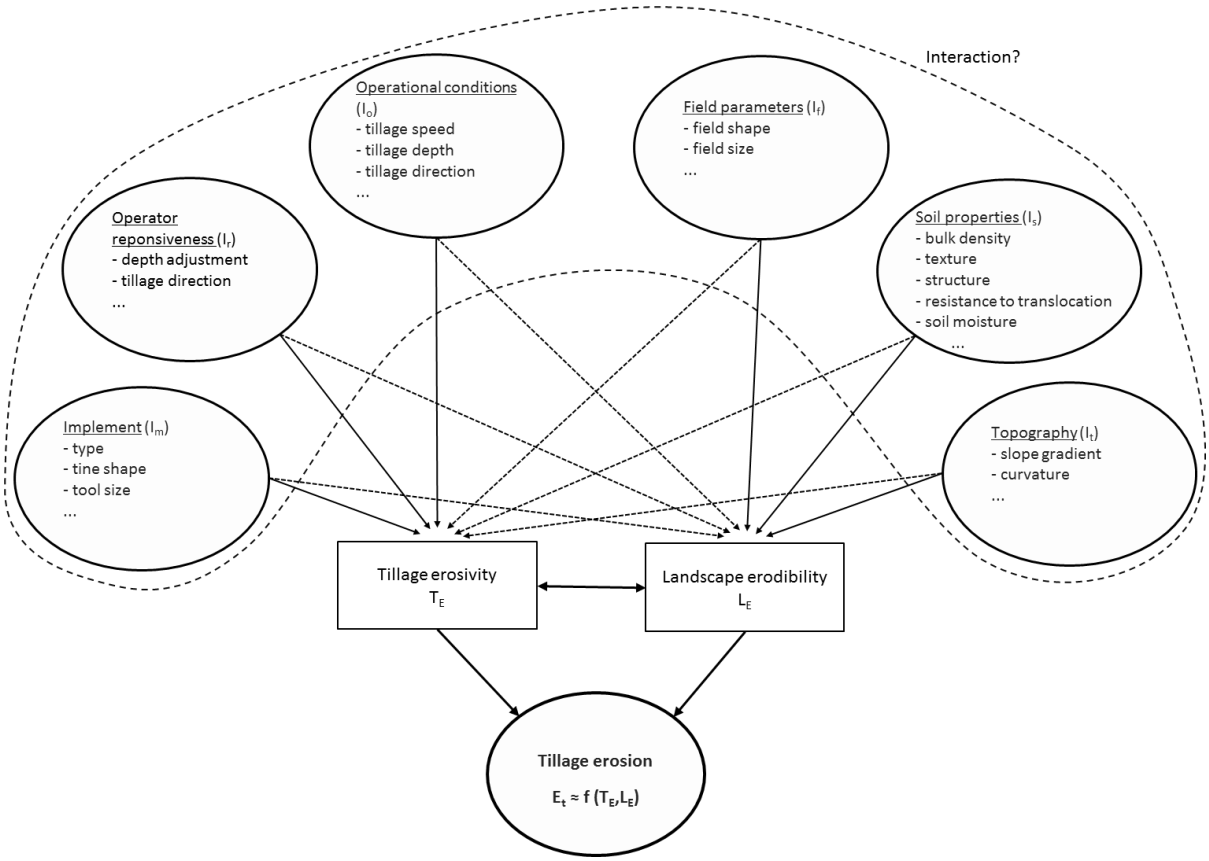

Figure 2.4: Factors of tillage erosion (From Van Oost *et al.*, 2006: Figure 6, p.451)

To summarise, in addition to changing soil properties with the aim of boosting productivity, tillage can increase rates of soil erosion through altering the erodibility of soils and gravity-driven variable rates of soil translocation. Tillage erosion consists of two components, and can be defined as such, i.e. the loss and subsequent accumulation of soils, as the result of variable translocation rates (Lobb *et al.*, 1995). Furthermore, tillage operations have an impact on soil erosion via water-driven pathways, through decreasing resistance to detachment by rain-splash and flowing water (Desmet & Govers, 1997; Gómez *et al.*, 2005; Gómez & Nearing, 2005; Takken *et al.*, 2001a, 2001b). Due to the time it takes for signs of tillage erosion to become visible within the landscape, tracer methods (often teamed with modelling) have proven useful for gaining an understanding of the spatial distribution of the processes involved, and will be discussed further within Section 2.2.3. Finally, as highlighted by Van Oost *et al.*(2006), despite the success of such techniques, a number of gaps remain within the understanding on the relationship between tillage and soil loss.

2.1.3 Wind erosion

Wind erosion occurs in three processes of particle movement: creep, saltation and suspension. Whereby, surface creep is the rolling of coarse grains along the ground surface, saltation is the process of grains moving in a series of jumps and suspension, perhaps the most dramatically visible of the processes, involves the movement of fine particles, usually less than 0.2 mm in diameter, high in the air and over long distances, forming dust storms (Morgan, 1995). As with water erosion pathways, the occurrence of wind erosion is dependent on the erodibility of the soil surface and the wind having sufficient energy to entrain material. Soil type, moisture content and vegetation cover are particularly important controls on rates of wind erosion (Owens *et al.*, 2006). Due to the low cohesion between particles, sandy soils are the most susceptible to wind erosion (Boardman & Evans, 2006; Fullen, 1985b). Furthermore, decreasing soil moisture content acts to further increase the erodibility of soils by wind (Wiggs *et al.*, 2004). Increasing vegetation cover can, through increasing roughness, however, decrease the risk of wind erosion by reducing the wind sheer stress (Owens *et al.*, 2006) or acting as a windbreak and encouraging deposition (Chappell & Warren, 2003).

Though wind erosion has been largely un-studied in the UK, following the work of Morgan (1985b) and Evans, (1990b), Boardman and Evans (2006) map wind (and water) erosion risks in the UK, using the typical soil physical characteristics within each of the main soil associations and work carried out by the SSEW between 1982 and 1986. Based on the

assumptions and mapping, it was determined that 9.1% of the soil associations are at risk of wind erosion (Boardman & Evans, 2006). However, events of wind erosion are highly episodic and, whilst anecdotal evidence of wind erosion exists in the UK (Chappell & Manchester, 2002), quantification is difficult due to the high temporal and spatial variability (Owens *et al.*, 2006).

2.1.4 Soil loss via crop harvest

Soil is also lost with the harvesting of crops and as a result of machinery leaving the field, in a process known as soil loss via crop harvest (SLCH). Typically associated with root crops, Ruysschaert *et al.,*(2004) suggest the soil moisture content and texture have the most significant effect on rates of soil loss, though note that little research has been done on these processes. Owens *et al.*,(2006) identified that whilst SLCH can be a significant route of soil loss from arable land within certain fields, accounting for up to 1 t ha^{-1} yr^{-1}, at a national-scale SLCH accounts for approximately 0.1 t ha^{-1} yr^{-1}, across all arable land in the UK.

2.2 Quantification of soil erosion processes

The previous sections have identified that through studying the interaction between soil, transport agents and land management, research has significantly contributed to our understanding of the various pathways of accelerated soil erosion, particularly in terms of water and tillage erosion. Previously Evans (1995) and Brazier (2004) have provided summaries of the methods that had been used to understand and quantify water erosion, on arable land in the UK. However, while many of the techniques reviewed in these papers are still in use, there has been significant development in research methodologies over the last decade, including further development of tracing techniques and more recently a move towards laser scanning or novel photogrammetry techniques for volumetric surveys. Consequently, this section aims to provide an update on soil erosion monitoring techniques, first introducing existing methods, but then providing an analysis of the more novel approaches to studying soil erosion which may also be able to provide quantification of both the visible and non-visible erosion pathways.

The review will focus on the following monitoring techniques: plot-based techniques, volumetric surveys, tracers and fine-scale remote sensing; as they provide a platform from which fine scale erosion processes can be quantified. Coarse scale proxies, for example; catchment sediment budgets (e.g. Bilotta *et al.*, 2010; Walling *et al.*, 2002), reservoir bathymetry studies (Duck & McManus, 1994; Rowan *et al.*, 1995) or satellite remote sensing

techniques (Vrieling, 2006) have been excluded, as they provide little understanding of the processes involved, and are typically carried out at a scale that precludes understanding of on-site soil erosion. Through summarising the techniques that have been used to quantify and develop the current understanding of soil erosion, this section will also identify some of the key gaps or shortcomings that need to be addressed in order to select a suite of methods best suited to building a national-scale understanding of soil erosion, in the UK.

2.2.1 Plot-based techniques

Small, bounded study plots, designed for the purpose of hypothesis testing, have a number of benefits for carrying out soil erosion studies. They allow for experimental control on the conditions contributing to erosion and an accurate quantification of soil loss, from a known area. Plot studies are particularly useful for the quantification of water erosion pathways, as sedimentation and runoff can be collected at the bottom of a plot with a known contributing area. However, plots can also be used to quantify any of the soil pathways described within the previous section. Additionally, unlike catchment-scale studies, replication is possible due to size and the ability to control experimental conditions (Nearing *et al.*, 1999a).

Lab-based plot studies allow for a high level of experimental control, providing an opportunity to develop a thorough understanding of how the variables identified in Figure 2.1 influence erosion rates. For example, Abrahams *et al.* (1998) through carrying out over 1500 repeat experiments in a 5.2 x 0.4 m flume, and changing variables such as rainfall intensity, slope, roughness size and discharge, were able to identify that flow depth and energy accounted for 89.8 per cent of variance in sediment transport capacity, when quantifying the effect of surface roughness. The control and ability to replicate experimental conditions available at the lab-scale, also provides a useful platform for assessing other monitoring techniques. For example, Ventura *et al*. (2001) used plots in the development of a magnetic tracer, applying different styles and concentrations to erosion pans (0.32 x 0.45 m), to assess applicability in studying interrill erosion, and to a small flume (1.0 x 0.1 m) to determine the best application in the assessment of rill erosion. However, whilst studies carried out on these plots are ideal for developing a fine-scale understanding of soil degradation and erosion processes, and assessing methodologies, they cannot be assumed to represent field-sized responses due to artificial boundary effects, often single-intensity rainfall rates and artificial soil depths/composition (Evans, 2002).

There have been a number of both short- and long-term, field-based erosion plot studies carried out in the UK, studying a wide range of soil and land management practices. Robinson and Boardman (1988), for example, monitored and compared the erosion rates of plots under a range of traditional and conservation cultivation techniques, over one growing season. Fullen (1992) reported on studies carried out at Hilton Experimental Site, Shropshire, where erosion rates from only bare plots were related to variations in hydrological events and slope gradients, over five years. The Woburn Erosion Reference Experiment, in Bedfordshire, also hosted a number of plot-based erosion studies, from which Quinton and Catt (2004) collate data collected over ten years at the site, with a particular focus on erosion rates during periods of low vegetation cover, whilst also looking at the role of cultivation technique. Sediment exhaustion can limit the meaningful use long term use of plots, particularly when plots are bound (Boix-Fayos *et al.*, 2006).

In an attempt to increase the representation of the results, or standardise to units that are universally employed, most studies report observations in units of t ha^{-1} yr^{-1}, which carries an implicit assumption about the whole plot yielding eroded soil (Parsons *et al.*, 2006). For example, Quinton and Catt (2004) report results from plots of 0.0875 ha in units of t ha^{-1}, including both a mean total over the 10-year period and also an annual average. The total amount of eroded sediment collected at the site was 6.899 t from the 0.6712 ha studied (Quinton, *pers. comm.* 2014) which, when up-scaled to 1 ha linearly, would be 10.278 t ha^{1}. However, Quinton and Catt (2004) report mean rates ranging from 4.18 t ha^{-1} (+/- 4.57) to 17.49 t ha^{-1} (+/- 17.20) over the same ten-year period – noting the large standard deviations – this use of standard areal units of ha, thus potentially over-reports the results. Brazier (2004) also reports the findings for the site as a mean erosion rate of 2.0 t ha^{-1} yr^{-1} and maximum of 2.93 t ha^{-1} yr^{-1} between 1990 and 1995 (a period that captures big rainfall events). Accordingly, these three representations of the same data highlight the difficulties in upscaling observations beyond the scale from which they were collected and the importance of recognising the assumptions that have been used in the process, when drawing comparisons between studies.

As a well-established method for monitoring soil erosion, plot studies have contributed substantially to the understanding of soil erosion processes, there are, however, a number of shortfalls with the method. As summarised by (Parsons *et al.*, 2006), one of the prevailing issues relate to up-scaling the results. Through isolating plots, so as to create a strong (and

replicable) scientific understanding of processes acting within, the resulting data are arguably limited to describing just that. Namely, plots describe a set of responses to specific conditions, and the influence of erosive agents acting over a greater area, such as the formation of rills or gullies, are excluded (Boix-Fayos *et al.*, 2006; Leys *et al.*, 2010). Furthermore, the full extent of the spatial patterns of sediment entrainment are rarely studied (Michaelides *et al.*, 2010), and studies have identified varying relationships between plot length and sediment loads (Chaplot & Le Bissonnais, 2000; Parsons *et al.*, 2006; Sadeghi *et al.*, 2013). Some studies look at soil erosion rates at the hill-slope scale (Deasy *et al.*, 2009a; Stevens *et al.*, 2009), in open scenarios, to overcome this issue at the cost of an uncertain hydrological perimeter and less control over experimental parameters.

2.2.2 Field Surveys

Whilst plot studies can provide fine-resolution data from a heavily controlled environment, increasing study areas to the field-scale can increase the representativeness of the dataset and relevance for land managers. At the field scale, where it can be impractical to capture all runoff and sediment, work by authors such as Bilotta *et al.* (2008) and Deasy *et al.* (2011) instead record total discharge and collect water samples on timed intervals during rainfall events. At larger scales, such as catchment, regional or national-scale, this approach is not pragmatic, consequently qualitative or volumetric surveys of erosion features are often carried out. Qualitative studies, such as the work carried out in Scotland by Kirkbride and Reeves (1993) and Davidson and Harrison (1995) allow for the rapid identification of the extent of erosion within arable land, through the classification of erosion features from site walk-overs, and allow researchers to postulate possible causes, sources of sediment and pathways of erosion. Volumetric surveys involve the field measurement of visible erosion features, often through a mixture of measuring rill or gully lengths and cross sections, at regular intervals, along transects or contours (e.g. (Boardman, 2003; Boardman *et al.*, 1996; Watson & Evans, 1991). Researchers are then able to calculate the volume of soil loss, which can be converted to the rate of soil erosion if the bulk density of the soil is known.

To-date, a number of the national soil erosion monitoring programs carried out in the UK have involved the volumetric survey of visible erosion features within arable land. Additionally, a number of national surveys have been paired with aerial photography or overflight surveys (e.g. Chambers & Garwood, 2000; Evans, 1988; Grieve et al., 1995; Skinner & Chambers, 1996). Aerial photography has had a number of applications, for example Chambers and Garwood (2000) used aerial photography to keep a record of the

erosion events monitored, whereas Grieve *et al.* (1995), used only aerial photographs to quantify areas of erosion, rather than volumes, in upland Scotland. Watson and Evans (1991) compared field surveys with volumetric estimation based on photography of sites in Scotland, with perhaps surprisingly high correlation – though they do note expert opinion is required. However, the combination of aerial photography and ground-based volumetric surveys employed by Evans (Evans, 1988a) and Skinner and Chambers (1996), is perhaps the most effective. Through their use of aerial transects to identify fields within the target areas with visible erosion, prior to carrying out field surveys, they were able to save time and allocate resources efficiently.

On a smaller scale, Boardman's work in the South Downs represents the longest running field-based monitoring scheme in England and Wales (Boardman, 2003; Evans, 2005). Coinciding with a number of muddy flood events in the South Downs, which resulted in a considerable impact upon properties, Boardman *et al*. established a monitoring network within an area of about 36 km^2. Through carrying out regular volumetric surveys and recording topographic information, meteorological data and details of land management, the work has been able to establish that whilst average rates of erosion are low in the area, the occasional storm results in a significant soil loss and fields planted to winter cereals have a particularly high number erosion events; thus providing a significant contribution to the understanding of soil erosion rates in the UK. However, whilst this in-depth understanding exists for the South Downs, the lack of other similar datasets makes mitigation through policy-based programs difficult on a national scale and furthermore, it would be very costly to carry out such a study on a national scale due to the resources required.

While there are many advantages associated with field surveys, particularly when compared to plot studies – field surveys allow natural incidences of soil erosion, under a range of management practices, to be assessed relatively quickly – there are still some shortfalls with the technique. Perhaps most important is the focus on visible erosion pathways and an inability to look at sediment re-distribution patterns and more subtle erosion pathways. The subjective nature of the techniques also leaves room for error, for example within Evans (Evans, 1988a) there are some occasions where the volume of deposition calculated within a field exceeds the volume of erosion calculated. Additionally, targeting fields or regions known to erode introduces a level of bias to the studies, and resultant erosion rates do not,

therefore, provide an accurate representation of rates of soil erosion, both locally and nationally (Brazier, 2004).

2.2.3 Tracers

The use of tracers may allow visible and less visible or subtle erosion pathways and interactions to be quantified. Furthermore, tracers can be used to quantify spatial and temporal changes in soil redistribution, at varying resolutions (Polyakov *et al.*, 2004). Tracers, either naturally occurring or artificially applied, are used to mark (or fingerprint) a soil and develop an understanding of a desired attribute or rate of erosion. There are a number of different markers that have been used as tracers in soil erosion studies, these include: radionuclides (i.e. ^{137}Cs and ^{210}Pb e.g. Porto et al., 2014; Walling & Quine, 1991), magnetics (e.g. Parsons et al., 1993; Ventura et al., 2001), metals (i.e. Aluminium cubes e.g. Govers et al., 1994) and rare earth oxides (REOs) (e.g. Kimoto, Nearing, Zhang, et al., 2006; X. Zhang et al., 2001, 2003). Additionally, the range of tracers available permits the study of both long- and short-term patterns of soil redistribution, over a wide range of scales (Guzmán *et al.*, 2013).

With a particular focus on developing or selecting applied tracers, Zhang *et al.* (2001) suggests a tracer should possess the following properties:

1. be strongly bound with soil particles or easily incorporated into soil aggregates,
2. have great sensitivity in analysis,
3. be easy and inexpensive to measure,
4. possess low background concentrations in soils,
5. not interfere with sediment transport,
6. have low plant uptake,
7. be environmentally benign, and
8. have availability of multiple tracers that are similar in physiochemical properties but are distinct in signature.

Whilst a number of the tracers that have been used to study soil erosion processes match most of these criteria, many are only available in single form (e.g. ^{137}Cs) and consequently are only able to look at patterns of total soil redistribution without conclusive evidence of sediment source(s).

Pryce (2011) classifies tracers into two grades, A- and B-grade, based on response to stimuli. A-grade tracers are described as those that, through having similar or identical physical and chemical properties to the study soil, are expected to have a similar or near identical response to erosion processes, in terms of magnitude and extent. For example, ^{137}Cs, though a complex relationship between affinity, particle size distribution and enrichment ratios exists (see: He & Walling, 1996, 1997), could be considered an A-grade tracer. In contrast, whilst B-grade tracers reflect the magnitude of the erosion agent, they're unable to be used to quantify the extent. For example, without additional modelling, the Aluminium cubes used to study tillage erosion by Govers *et al.* (1994) would only be able to provide an indication of the distance soil is moved following a pass.

The above has highlighted that the tracer technique selected for use within a study is largely determined by the desired outcome. The erosion pathway, or range of pathways, being studied is of particular importance, as is temporal and spatial resolution. Figure 2.5 provides an indication of the distribution of published erosion studies that utilise tracers, grouped by tracing approach and scale (Guzmán *et al.*, 2013). This highlights the relationship between tracer and scale, whereby naturally occurring tracers are more commonly used in landscape scale applications, while artificially applied tracers, such as REOs or magnetite are more commonly used in laboratory-based experiments, reflecting the resources needed for each approach. The following section will detail a few of these methods, with a particular focus on those found to be viable for application to soil erosion work. This will allow for the selection of a tracer technique, or suite of techniques, suitable to studying and quantifying soil erosion, in light of the research aims.

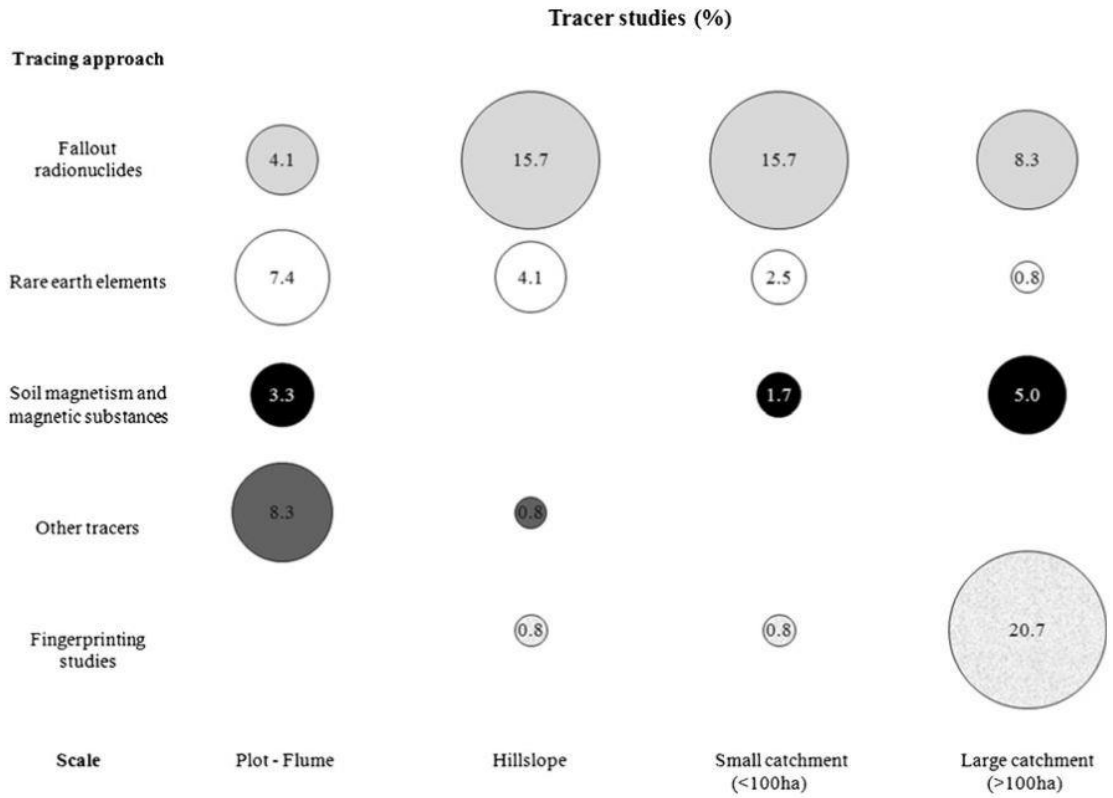

Figure 2.5: Bubble plot indicating the distribution of erosion studies with tracers (from Guzman *et al.*, 2013: Figure 1)

2.2.3.1 Naturally occurring and fallout tracers

The soil at any particular location provides a reflection of the long-term geomorphic processes that have acted over geological time scales (Jenny, 1941). Like soil type, there are a number of naturally occurring or fallout markers that have been successfully used, both in the UK and abroad, for the identification and quantification of soil redistribution patterns over shorter time scales. Additionally, tracers have been used both proximally and *in situ*. Proximal soil erosion studies, quite often based on sedimentation fingerprinting in water bodies, use fluxes of tracer concentrations within cores to determine previous rates of erosion within catchments (Walling, 2005) *In situ* studies typically compare a reference inventory of a particular tracer with that of the targeted site, also representing historical rates of soil redistribution (Walling *et al.*, 1995). Monitoring techniques used *in situ* will be discussed in this section.

Though there are a number of fall-out radionuclides that have been used to capture soil redistribution rates and patterns, such as ^{137}Cs, ^{7}Be and ^{210}Pb (Blake *et al.*, 1999), techniques using ^{137}Cs have had particularly widespread application in the UK (Quine & Walling, 1991; Walling & YuSheng, 2010). ^{137}Cs fall-out resulted primarily from weapons testing in the mid-20th century, though a secondary peak of fall-out did occur as a result of the Chernobyl

disaster. With a half-life of 30.17 years, ^{137}Cs inventories within soil profiles offer an opportunity to capture long-term (c. 50 years) soil redistribution patterns on arable land (Walling & Quine, 1991).

There are two common approaches for using ^{137}Cs fall-out to quantify half-century erosion rates or patterns, namely:

1. The ^{137}Cs inventory within the soil profile for an individual sampling site is compared with a reference ^{137}Cs inventory, collected from a relatively undisturbed area, whereby:
    - Sample ^{137}Cs inventory < ^{137}Cs reference inventory = erosion site
    - Sample ^{137}Cs inventory > ^{137}Cs reference inventory = deposition site
2. The ^{137}Cs inventory does not use an undisturbed reference site, instead the profile inventory from one year is compared to another.

    (Walling & Quine, 1990)

The first technique has had the greatest application within the UK, as the second requires sufficient time between sampling to provide an accurate result given the high level of error associated with deriving ^{137}Cs counts.

Though consistently represented as t ha^{-1} yr^{-1}, results from ^{137}Cs studies are typically reported in three forms: net erosion rate, gross erosion rate and mean erosion rate. Net erosion rate is defined as the total amount of soil leaving the field, gross erosion rate as the total mass of the eroded sediment divided by the area of the field, and mean erosion rate (for the eroding zone) as total mass of eroded sediment divided by the area of the field under-going erosion (Quine & Walling, 1991). Quine and Walling (1991) highlight the importance of selecting an appropriate method for reporting, and suggest that net erosion rates can overshadow gross erosion rates, particularly where sediment deposited within the study area could originate from outside the study area, detailing an example wherein the study area was a 3.2 ha area, encompassing the lowest lying ground within a 27 ha field.

Despite an arguably pivotal role in the development of the understanding of spatial trends of soil redistribution via tillage, there has been some critique of the ^{137}Cs tracer method – as evidenced by a level of polarity within the literature. Proponents of the technique argue that the method can aid in the validation of modelling water-driven erosion pathways, through providing an opportunity to quantify the long-term spatial redistribution of soil;

particularly as diffuse pathways, like tillage erosion, become better understood (Quine, 1999; Walling *et al.*, 2003; Zapata, 2003). This reflects the original aims of the technique: to provide a source of information on average soil redistribution patterns (Walling & Quine, 1991). However, Parsons and Foster (2011, 2013), through critically reviewing the assumptions associated with the ^{137}Cs technique and the approach taken by some researchers in establishing reference inventories, question whether any erosion rate derived from the technique is reliable. Mabit *et al.* (2013) have since responded to the review by Parsons and Foster (2011), arguing that the method can be used to assess magnitude confidently, rather than quantify absolute rates of soil erosion, through rigorously adhering to the assumptions and statistically sound experimental design. More recently, in the context of the findings from their own water erosion studies, Evans et al. (2017) have questioned the validity of the results derived from ^{137}Cs in the UK, to-date. However, whilst there are some issues with the ^{137}Cs technique, lessons learnt from the development can be applied to other (more novel) tracing methods, for example: density of sampling needed, effects of sub-sampling and the impact of tilled-layer.

2.2.3.2 Locally applied tracers

Whilst the use of radionuclide fall-out tracers can, arguably, provide an assessment of long-term patterns of soil redistribution, an inability to trace the local and short-term patterns of soil movement has led to the development of a number of 'applied tracer' techniques. Through not being limited to what is already available within the environment, applied tracers offer the additional advantage of being able to target particular erosion pathways, erosion hotspots or specific variables. Consequently, there is a wide range of tracers that have been developed and applied to soil erosion studies.

Building on Figure 2.5, Table 2.1 lists a number of applied tracers that have been used to study soil erosion, at a range of scales. Metal tracers, such as steel hexagonal nuts (Lindstrom *et al.*, 1992) or Aluminium cubes (Govers *et al.*, 1994; Van Muysen & Govers, 2002), have been incorporated into the plough layer to study soil translocation rates under tillage at the hillslope scale. Lobb *et al.* (1995) also studied tillage erosion, though did so through applying additional ^{137}Cs to a hillslope. A variety of magnetic tracers have been used, for example Parsons *et al.*, (1993, 2010) applied a crushed magnetite source-line to a field plot to study movement in interrill overland flow, initially over a period of 3 rainfall events establishing the feasibility of the method (Parsons *et al.*, 1993) then developing a 16 year understanding of the re-distribution (Parsons *et al.*, 2010). Whereas Ventura *et al.*

(2001, 2002) initially developed artificial magnetic tracers in a laboratory setting (Ventura *et al.*, 2001), before applying them to a depth of 3 cm on connected field-based plots to study redistribution and rates of erosion (Ventura *et al.*, 2001). However, due to the availability of multiple distinguishable forms, rare earths, or more specifically the Lanthanide elements used in the form of rare earth oxides, have recently had increases in application. Rare earth oxides (REOs) have been used to study quantify soil erosion and redistribution patterns at the plot scale (e.g. (Kimoto *et al.*, 2006b; Michaelides *et al.*, 2010; Polyakov & Nearing, 2004; Pryce, 2011; Zhang *et al.*, 2001, 2003), at the field scale (e.g. (Deasy & Quinton, 2010; Polyakov *et al.*, 2004, 2009; Pryce, 2011; Stevens & Quinton, 2008) and at the field-scale over multiple years (Kimoto *et al.*, 2006a).

Table 2.1: Applied tracers used in soil erosion studies.

Tracer	**Examples / References**
Metals	Govers et al., 1994; Lindstrom et al., 1992; Van Muysen & Govers, 2002
Magnetics	Guzmán et al., 2010; Parsons et al., 1993, 2010; E. Ventura et al., 2002; Eusebio Ventura et al., 2001
Radionuclides	Greenwood et al., 2014; D A Lobb et al., 1995
Rare Earths	Deasy & Quinton, 2010; Kimoto, Nearing, Shipitalo, et al., 2006; Kimoto, Nearing, Zhang, et al., 2006; Lei et al., 2006; Matisoff et al., 2001; Michaelides et al., 2010; Polyakov et al., 2009; Polyakov & Nearing, 2004; Pryce, 2011; Senbayram et al., 2015; Stevens & Quinton, 2008; X. Zhang et al., 2001, 2003
Ceramics, Microspheres, and others	Parsons et al., 2014; Plante et al., 1999; Pryce, 2011

Concentration of application, preferential binding and particle size distribution are important considerations associated with the use of applied tracers. For example, Ventura *et al.* (2001) found the magnetic beads used in the study had an armouring effect at higher concentrations. However, it is important to note that, Pryce (2011) found higher levels of uniformity of application when REO concentrations where increased from 50 to 500 times background concentrations, across a range of application methods. Kimoto *et al.* (2006b), found REOs preferentially bound to fine fractions of the soil, highlighting the role of soil texture when tagging and tracing soils, which is important when considering the processes involved with the selective entrainment and deposition of soil classes. Interestingly,

Michaelides *et al.* (2010) found that although REOs preferentially bound with soil classes <125 µm, there was little evidence of leaching from a tagged sandy soil into an underlying clay soil.

As a result of the ability and flexibility to study pre-determined attributes with applied tracers, there is some variability in methods and spatial extent at which they have been applied, broadly fitting into three categories: targeted, partial and full. Stevens and Quinton (2008), through applying REOs at fixed intervals around a tramline within a section of a hillslope, were able to build an understanding of distance travelled to tramlines. However, as they only applied the tracers to the soil surface, they were unable to quantify soil erosion rates. Michaelides *et al.* (2010) through applying 10 REOs to selected areas (partial tagging) of a lab-based, break-in-slope plot, suggest it is possible to quantify soil erosion rates under partial application, at the small-scale and high-concentration of REOs applied within their experiment. Most studies, however, suggest that quantification of soil erosion through the use of tracers requires 'full' application, at greater than 10 times the background concentration (if applicable), ensuring the depth of interaction exceeds the depth of erosion (Kimoto *et al.*, 2006b; Lei *et al.*, 2006; Polyakov & Nearing, 2004; Pryce, 2011; Zhang *et al.*, 2001, 2003).

2.2.1 Fine-scale proximal sensing technologies

Digital terrain models (DTMs) are 3D topographic models with a range of uses in hydrology and geomorphology, where for example they can be used to predict spatial patterns of runoff. DTMs can be utilised in soil erosion as proxies for erosion risk or to quantify volumetric erosion features through the use of DTMs of difference (DoD). DTMs are produced using point based elevation data, collected by a range of proximal sensing technologies, which is plotted on the 'x', 'y' and 'z' axes, in vector format. As shown in Table 2.2 the DTM resolution is in practice controlled by the platform being used and the survey range, which then stipulates the application to soil erosion modelling. It is also important to note that, DTMs created using the highest level of spatial resolution available may not necessarily provide sufficient gains when considering the volume of data produced (Zhang & Montgomery, 1994). Whilst data collected by satellite sensors and aerial LiDAR data has been successfully used to create DTMs in a range of environments, the minimum spatial and temporal resolution that can be obtained is not suitable for on-site erosion investigations, consequently, this section will now look to focus on Terrestrial Laser Scanning (TLS) and Structure-from-Motion Photogrammetry (SfM) (Anderson & Gaston, 2013; Vrieling, 2006).

Table 2.2: Comparison between proximal sensing technology, data resolutions and application to soil erosion using examples.

PS technology	Spatial data resolution	Scale of coverage	Application to erosion studies
Satellite e.g. ASTER GDEM	>30 m	National	Proxy
Airborne LiDAR e.g. Tellus SW	> 1 m	Regional	Proxy or quantifying large gully features
Terrestrial Laser Scanner e.g. Barneveld *et al.* (2013)	> 0.02 m	Field	Mapping surface micro-topography and volumetric soil loss
Aerial SfM e.g. Ouédraogo *et al*. (2014)	> 0.04 m	Field	Mapping surface micro-topography and volumetric soil loss
Ground-based SfM e.g. James and Robson (2012)	<0.05 m	Plot - Field	Mapping surface micro-topography and volumetric soil loss

2.2.1.1 LiDAR and Terrestrial Laser scanning

Light detection and ranging (LiDAR) or as it is more commonly referred to, Laser scanning, uses return times from precision lasers, at a pre-assigned spatial coverage, to build 3D point-clouds of the scanned surface, can provide elevation data at a range of resolutions and levels of vertical accuracy (Telling *et al.*, 2017). Therefore, when considering laser scanning for the application of soil erosion monitoring it is important to note that there are a number of platforms from which laser scanning is operated and within each the point-cloud resolution and accuracy attainable is inherent to the instrument used. For example, Croft *et al.* (2009) were able to attain a sufficiently detailed DTM from a small laser profiling instrument at a 2 mm spatial resolution, on 0.1 x 0.1 m plots, to act as a reference for soil surface roughness, when conducting assessments on the viability of hyperspectral reflectance to assess surface roughness at fine spatial scales. Conversely, on a much larger scale, airborne LiDAR can be used to generate DTMs at the landscape-scale, with recent projects such as Tellus South West creating a Digital Surface Model (DSM) with large spatial coverage (9424 km^2) at 1 m spatial resolution with 25 cm vertical accuracy (Ferraccioli, et al., 2014). Terrestrial Laser Scanners (TLS), however, fit between the two, providing a platform suitable for field- or catchment-scale application (Barneveld *et al.*, 2013; Eltner *et al.*, 2013; Luscombe *et al.*, 2014; Ouédraogo *et al.*, 2014) and are becoming increasingly available to non-specialised consumers.

TLS is an established methodology for the quantification of large scale erosional changes, such as soil erosion within badland environments (Vericat *et al.*, 2014), and is often used as a benchmark for assessing the quality of SfM applications in the geosciences (Glendell *et al.*,

2017; James & Robson, 2012; Smith & Vericat, 2015). However, TLS has only received limited application on arable land, with the focus of studies split between assessments of accuracies for modelling surface roughness (e.g. Barneveld et al., 2013 and Smith et al., 2011) and quantifying soil erosion (e.g. Eltner and Baumgart (2015) and Vinci et al. (2015)). For example, Barneveld *et al*. (2013) assessed TLS application on three different levels of surface roughness - mouldboard ploughed, harrowed (stubble) and seedbed – on three field-sites, finding both DTM resolution and variability in spatial coverage declined with increasing surface roughness. Further assessing the application, Barneveld *et al.*(2013) manually decreased the spatial resolution of the DTMs, finding declining accuracy and precision with decreasing resolution as a result of sub-grid sized roughness elements, highlighting the importance matching DTM resolution with surface conditions. Eltner and Baumgart (2015) presents one of the few studies that specifically attempt to develop TLS application for the quantification of soil erosion on arable land, comparing multi-temporal DTMs to develop an understanding of patterns of soil loss within a Mediterranean field plot. While they were able to quantify soil erosion rates, the study highlighted the difficulty in capturing diffuse erosion and <1.5 cm changes in surface elevations with TLS.

2.2.1.2 Structure-from-Motion Photogrammetry

Structure-from-Motion photogrammetry (SfM-MVS), is a computer vision approach for point cloud and orthomosaic generation, and represents an evolution from traditional photogrammetry techniques. SfM-MVS creates spatial data through the determination of camera extrinsic and intrinsic geometry, and surface structure, through matching pixels, called tie-points, within overlapping imagery collected from close-range or aerial platforms (Micheletti *et al.*, 2015; Smith *et al.*, 2015). SfM-MVS uses ground control points (GCPs) to geo-rectify or scale the modelled surface. The root-mean squared error (RMSE) of independent GCPs can also provide a metric for model accuracy (James and Robson, 2012; 2014). SfM-MVS moves away from traditional photogrammetry through being designed to encourage the use of consumer-grade cameras, thus reducing equipment costs. While the use of consumer-grade cameras has been explored within traditional photogrammetry methodologies it has been to little success due to calibration, processing and software constraints (e.g. Warner, 1995; Chandler *et al*., 2005; Reike-Zapp and Nearing, 2005).

The increasing accessibility of SfM, has resulted in the rapid uptake across the physical sciences resulting in an expanding body of work across a wide range of environments (Smith *et al.*, 2015). The technique has been used to create 3D surface reconstructions at a number

of scales, ranging from a small volcanic hand bomb with RMSE of 110 µm for scaled distances (James & Robson, 2012) to a badland landscape (c. 1km^2) at sub-metre accuracy (Smith & Vericat, 2015). With substantial reductions in data collection times, relative to TLS, SfM provides an interesting platform from which multi-temporal erosion studies can be carried out. Furthermore, aerial SfM has been used to create high-resolution 3D models at the small watershed scale (Ouédraogo *et al.*, 2014) and catchment scale (Anders *et al.*, 2013), wherein erosion features could be identified. Accordingly, SfM has been used to quantify large erosion features and events with results of comparable accuracy to TLS (Castillo *et al.*, 2012; D'Oleire-Oltmanns *et al.*, 2012; Eltner *et al.*, 2014; Glendell *et al.*, 2017; Gómez-Gutiérrez *et al.*, 2014; Smith & Vericat, 2015). However, a linear relationship between error and survey distance has been observed, whereby errors associated with SfM-MVS increase with survey range (Smith *et al.*, 2015). Consequently, if teamed with recent methods development (e.g. James & Robson, 2014; James, Robson, D'Oleire-Oltmanns, et al., 2017; Shahbazi et al., 2015), there is potential to capture fine scale erosion processes, within laboratory environments.

2.3 Summary

This literature review has demonstrated that each of the pathways of soil erosion have different spatial patterns, which are related to the erodibility of the soil, the erosivity of transport agents and the influence of topography on the transport agents. For example, whilst evidence of rilling or gullying is highly visible within the landscape, the removal of soil via overland flow and the variable redistribution of soil via tillage are rarely visible. Consequently, these differences can make accurately quantifying the full magnitude of soil erosion difficult as the processes rarely act in isolation. However, this review has identified that many of the monitoring techniques described were biased towards either diffuse or convergent pathways, as listed in Table 2.3. Furthermore, within each technique, there are additional strengths and weaknesses that must be considered when collecting and/or comparing soil erosion observations.

The need for evidence to answer the policy-driven question "does the United Kingdom have a soil erosion problem?" rationalises the argument for developing a strong process-based understanding of the extent of soil erosion in the UK. This, in turn, requires a directed monitoring strategy, which utilises techniques that act to complement each other. Based on the properties listed in Table 2.3, this could be achieved through the use of tracers in combination with a volumetric technique. Therefore, there is rationale to first, assess the

current understanding of soil erosion in the UK and the performance of existing approaches, before assessing the ability of a novel suite of techniques to capture both convergent and diffuse soil erosion processes. To this end, while field scale assessments provide true conditions, laboratory studies offer a controlled environment that can be used to rigorously assess the performance of techniques.

Table 2.3: Summary of the advantages and disadvantages of the techniques presented in relation the erosion pathways.

Technique	Advantages	Disadvantages	Pathway(s) captured
Plot-based Laboratory (1); Field (2)	Control over conditions[1]; Known hydrological perimeter[1,2]; Capture all soil loss[1,2]	Upscalability[1,2]	Water erosion - diffuse and convergent[1,2]; Isolated processes[1]; Wind erosion
Field surveys Manual volumetric (3); Sediment capture (4); Imagery-based estimates (5)	'True' conditions[3,4,5]; Rapid assessment of multiple sites[3,5]; Understanding of sediment flux[4]; Spatial understanding of soil loss[3,5]	Cannot isolate diffuse and convergent processes[3,4,5]; Difficult to capture all soil loss[3,5]; Requires expert interpretation[5]; Focus on convergent processes[3,5]	Water erosion[3,4,5];
Tracers Naturally occurring (6); Artificially applied (7)	Understanding of patterns of soil redistribution[6,7]; Long-term trends[6]; Tailor to research aims[7]	Requires understanding of original conditions[6]; Analysis costs[6,7]	Water erosion - diffuse [6,7]; Tillage erosion[6,7]; Transport distances[7]
Proximal sensing TLS (8); SfM-MVS (9)	Spatial understanding of soil loss[8,9]; Replicable[8,9]	Equipment cost[8]; Requires understanding of underlying principles[9]	Water erosion - convergent[8,9]; Water erosion - diffuse?

3. WHAT CAN WE LEARN FROM NATIONAL-SCALE GEODATA DESCRIBING SOIL EROSION IN THE UK?

3.1 Overview

In order to address Objective 1, this chapter examines how existing soil erosion data and diverse approaches that measure soil erosion might be utilised to build a national-scale understanding of soil erosion in the United Kingdom. After a brief introduction to soil erosion research in the UK, the steps followed for the collection of soil erosion records are described. The potential magnitudes of soil erosion in the UK are then illustrated, before the analysis of sources of variability. To this end, relationships between environmental controls and rates of soil erosion were explored, and the impacts that different monitoring approaches have had on observations are described.

3.2 Introduction

Inadequate management of cultivated land can result in accelerated soil erosion, leading to reductions in soil profile depth and a decline in soil fertility (Pimentel, 2006). Historically, increased rates of soil erosion can be linked to local and global requirements to intensify agricultural productivity in line with demand (Montgomery, 2007). Consequently, with population growth projected to continue throughout the next century, it is important that there is effective legislation in place to manage food security and the continued urbanisation of green land, and their long-term impacts on soil condition (Amundson *et al.*, 2015; Foley *et al.*, 2005; Gerland *et al.*, 2014; Seto *et al.*, 2011). Whilst unsustainable in the long-term, the impacts of declining soil fertility are unlikely to be felt within a single political cycle, in the UK at least. To this end, without hard and current evidence of soil erosion, little motivation exists for the development of legislation to better manage our soil resource (Evans, 2010), yet arguably, strong policy in this area is long overdue (Brazier *et al.*, 2011).

In the UK, Evans' 1971 paper, in drawing together evidence of soil erosion and highlighting the need for soil conservation (Evans, 1971), marked the start of a new era of soil erosion monitoring (Boardman, 2002; Brazier, 2004). More specifically, there was a shift towards the quantitative assessment of soil erosion, which has been followed by the continued development of soil erosion monitoring techniques (Boardman, 2013). As resources increased, *ad hoc* reports of soil erosion events paved the way for monitoring programs, designed to develop a scientific understanding of the relationship between environmental conditions, land management and soil erosion rates (Evans, 1988a; Harrod, 1998; Quine &

Walling, 1991). As a result, the UK has a rich dataset of soil erosion observations, which have been collected using a wide range of methodologies, across various spatial and temporal scales.

Ironically, although attempts to quantify soil erosion nationally have illustrated that soil erosion can occur in the UK (Evans, 1988a; Harrod, 1998; Walling, 2008), understanding whether or not the UK has a soil erosion problem still remains a question to be answered. Whilst, the recent review by Evans et al., (2017) claims that existing research has shown "that soil erosion was a problem in some areas" (Evans *et al.*, 2017: 50), this was presented without a quantitative definition of what an erosion problem in the UK might be. Furthermore, outside of the often cited 'tolerable' erosion rate of ≤ 1 t ha^{-1} yr^{-1} (Verheijen *et al.*, 2009), the definition of what would constitute an erosion problem in the UK remains problematic in the absence of a comprehensive national-scale study and review of soil erosion rates (Reed, 1979). However, for the purpose of this thesis, accelerated erosion, as defined in Section 2.1 is considered to be a problem if significantly in excess of soil renewal rates of approximately 0.1 kg m^{-2} yr^{-1} or 1 t ha^{-1} yr^{-1}, as presented by Morgan (1985) in the UK context.

Although numerous reviews of existing soil erosion studies have been carried out (e.g. Boardman, 2002, 2006, 2013; Boardman et al., 1990; Brazier, 2004; Evans, 1988b, 1995, 2005, Evans et al., 2015, 2017), to the author's knowledge, there is no single resource that brings all of this work together to facilitate collective development towards a national-scale understanding of soil erosion. Access to empirical measurements is imperative in light of the difficulties of accurately modelling soil erosion in the UK, under high levels of uncertainty (Evans & Boardman, 2016a; Evans & Brazier, 2005). It could be argued, therefore, that this lack of data collation and coherent comparison has resulted in an ineffective top-down approach to soil erosion management, in the UK.

In *lieu* of a national-scale understanding of soil erosion, evaluating the existing state of knowledge on soil erosion in the UK can provide guidance for the heuristic development of both soil management policy and scientific research. The primary aim of this research was, therefore, to identify the extent to which existing data and methodological approaches can be used to develop an empirically-derived understanding of soil erosion in the UK, through:

1. Collating all available, UK-based and empirically-derived soil erosion datasets into a spatially explicit and open-source resource.
2. Developing an understanding of observed magnitudes of potential soil erosion rates.
3. Explore the significance of environmental controls on erosion rates, in a UK setting.
4. Evaluate the impact that monitoring approaches have had on the rates of soil erosion that have been observed.

3.3 Building a national-scale geodatabase of soil erosion observations

Empirical, spatially explicit, and on-site soil erosion observations were sourced from peer-reviewed literature, government-funded project reports and the personal datasets of members of the scientific soil erosion community who were willing to share their data. A critical, underpinning assumption of this work was that all data are of equal value and therefore should be included in the database, regardless of the technique used for erosion measurement. Whilst all techniques are open to criticism (for example see Boardman (2006) and Parsons & Foster (2013)), the approach was taken to ensure that, as far as possible, all data were included in an open access format, so that end users could decide upon the value in future analysis of the data.

Where reported, the following information was recorded for each entry: location; details of the study site (including land use, soil association or type, topography, cropping rotation, climate); information on the study design (including spatial extent, monitoring technique and duration); and soil erosion observations (including rate or volume, erosion process and causes, if known). Preference was given to reporting erosion rates in mean t ha^{-1} yr^{-1}, so that analysis of these data could be standardised across the dataset. The observational unit that was published has also been reported for each entry, to avoid future misrepresentation, due, for example, to conversion from volumetric units via specific bulk densities of the soil. Any additional information that was not contained within the source was collected from open data sources, where available. Soil information freely available on the LandIS website[1] was used to increase the level of detail. Missing location data were extracted from the Ordnance Survey 1:50 000 Gazetteer, and the British National Grid (BNG) reference for the nearest town or village was recorded. To allow the geo-database to be visualised on a 1 km grid and to maintain sufficient anonymity with respect to specific sites of erosion, all coordinates were reported using the British National Grid, the last three digits within each

[1] http://www.landis.org.uk/services/soilsguide/index.cfm

coordinate were removed and replaced with '500' e.g. TL123456 to 512500 Easting, 245500 Northing.

ArcGIS Online was selected to host and visualise the geo-database, following the creation of spatial layers within ArcGIS 10.4. Through the platform, users can select any of the georeferenced datasets to open an attributes box detailing all the collected information, as illustrated in Figure 3.1. Due to the variation in reporting scale, soil erosion observations were split into the following groups for visualisation:

1. Individual site-based data, on a 1 km grid
2. Transect data, e.g. Evans, (1988a)

The web-map is ready to be published and hosted within an open-access 'National Soil Erosion Geodatabase' website on peer-reviewed publication of this paper.

To permit trend analysis and descriptive statistics to be derived for the whole dataset, soil erosion units were standardised to mean t ha^{-1} yr^{-1}. Volumetric observations were converted to t ha^{-1} using the National Soil Inventory representative bulk density information for each individual Soil Series contained within the HORIZON Hydraulics database (© Cranfield University). Where bulk density information was missing for the Soil Association, the mean values for the habitat class reported by Emmett et al. (2007: p.15) were used. Missing soil texture information was extracted from the NATMAP topsoil texture database (© Cranfield University). The NATMAP database groups soil texture classes based on the percentage of sand, silt and clay particles, as demonstrated in Figure 3.2.

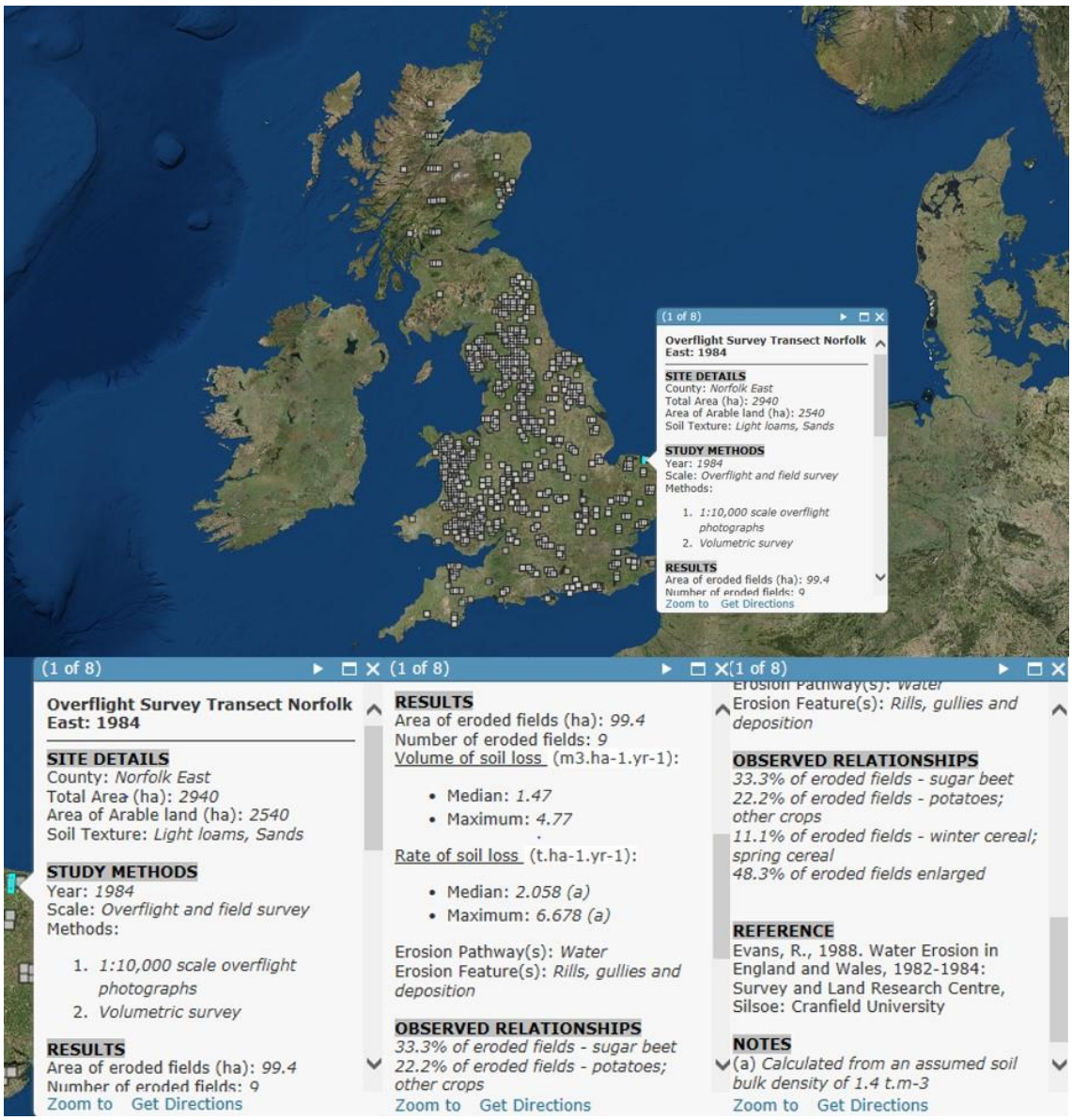

Figure 3.1: Screenshot from the online geodatabase illustrating the spatial distribution of records and an example of the information contained within the interactive dialogue box.

Statistical analyses and figure construction was carried out in R version 3.3.0 (R Core Team, 2016) using RStudio version 0.99.902 (RStudio Team, 2015) and the following packages: ggplot2 (Wickham, 2009), dunn.test (Dinno, 2017), scales (Wickham, 2016a), stringr (Wickham, 2016b) and cowplot (Wilke, 2017). Due to the skewed nature of the results, the non-parametric Independent-Samples Kruskal-Wallis rank sum test was utilised, followed by a pairwise Dunn's test. A critical value of $p \leq 0.05$ was used for statistical significance for the Kruskal-Wallis rank sum tests and a $p \leq \alpha/2$ (i.e. 0.025) for the post hoc Dunn's tests.

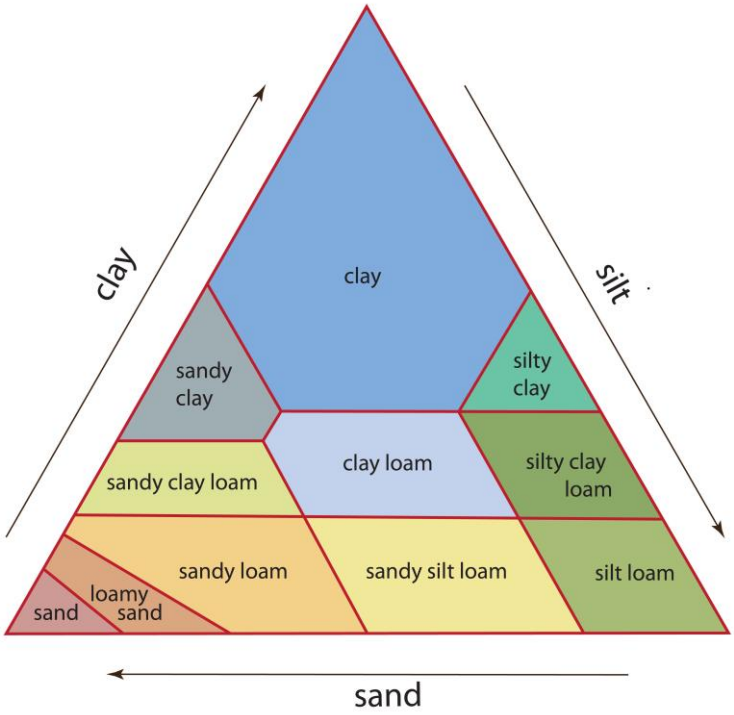

Figure 3.2: Distribution of soil texture classes based on relative percentage of sand, silt and clay particles (© Landis, Cranfield University).

3.4 The occurrence of soil erosion in the UK

The UK has a wealth of soil erosion observations: a total of 1566 individual records were compiled for the database, equating to a density of 1 per 155 km^2, which far exceeds the 1 per 3986 km^2 found in the USA, by García-Ruiz et al. (2015). Of the records held within the database (Figure 3.4), 651 (41.5 per cent) report a presence of soil erosion at the location, with rates ranging from <0.01 t ha^{-1} yr^{-1} to a maximum individual record of 143 t ha^{-1} yr^{-1}, which was reported by Chambers and Garwood (2000) in West Sussex, although the median for the 42 sites studied in the area was only 0.08 t ha^{-1} yr^{-1}. Reporting units were not consistent across the data, reflecting the varied methodologies that have been utilised across soil erosion research. However, the majority of the records could be standardised to mean t ha^{-1} yr^{-1}, with the exception of the upland values. The upland observations included in the database are based on the findings of McHugh et al. (2002) and therefore represent a cumulative eroded volume from a single point in time, rather than a rate of erosion. Consequently, a comparison between upland and the remaining land cover classes was not possible, and has therefore been excluded from this study to avoid distorting the analysis.

Table 3.1: Summary statistics for the records held within the database. *The values reported for the upland environment represent the presence of erosion at a single point in time, rather than annual rates.

Land Cover	N	N (with erosion)	Mean (t ha^{-1} yr^{-1})	Median (t ha^{-1} yr^{-1})	Minimum (t ha^{-1} yr^{-1})	Maximum (t ha^{-1} yr^{-1})
Arable	698	260	1.27	0	0	91.7
Upland*	822	380	55.04	291.2	0	3846.8
Grassland	31	9	0.72	0	0	5.3
Other(s)	15	2	0.44	0	0	6.5

Of the remaining dataset, the arable group had the highest recorded mean erosion values, followed by grassland and other(s), which included a woodland, hop-yard and golf course (Table 3.1). The mean erosion rate for arable results was 1.27 t ha^{-1} yr^{-1}, and the mean for grassland results was 0.72 t ha^{-1} yr^{-1}. There was no significant difference between the grassland and arable results when comparing the distribution of all records ($p = 0.61$) and the distribution of the results with a presence of erosion ($p = 0.26$), as visible in Figure 3.3C and Figure 3.3D. The mean erosion rate for the arable records exceeds the defined 'tolerable' erosion rate, however, the median rate for all cover classes was 0 t ha^{-1} yr^{-1}. The skew towards low value erosion observations is clearly illustrated in Figure 3.3A and Figure 3.3B, which exclude the zero value observations for clarity, and Figure 3.3C. 73.6 per cent of all values were less than or equal to 1 t ha^{-1}, consisting of 65 per cent of upland, 84 per cent of arable and 80 per cent of grassland records. These findings are significantly lower than the median values of 5.2 t ha^{-1} yr^{-1} and 1.8 t ha^{-1} yr^{-1}, for arable and grassland respectively, found by a national ^{137}Cs derived survey conducted by Walling (2008), and lower than the range of median values reported by the Soil Survey of England and Wales (SSEW), which vary between 0.3 and 2.2 t ha^{-1} yr^{-1}, for arable land (Evans, 1988a). It is, however, important to note the monitoring approach used when comparing between these ranges of erosion observations, as discussed further in Section 3.6.

Relative to the mean rates of soil erosion of 4.5 to 38.8 t ha^{-1} yr^{-1} reported across Europe by Verheijen et al. (2009) and the global scale metadata review carried out by García-Ruiz et al. (2015), it could be argued that the UK does not have a severe soil erosion problem. However, there *are* instances where soil erosion has exceeded 'tolerable' rates by one to two orders of magnitude, typically associated with measurements following extreme rainfall events (e.g. Boardman, 1988; Evans & Morgan, 1974). The impact of carrying out ad-hoc studies to assess erosion rates following extreme rainfall events or at sites selected because of observed erosion can, however, also bias perceptions on the extent of a soil erosion problem. This is demonstrated in the cluster of high erosion rates in eastern Scotland visible

in Figure 3.4, which result from a study over two winters, where only fields with significant erosion features were assessed (Watson & Evans, 1991). Consequently, the development of a clear understanding of where the variability in UK soil erosion rates comes from is imperative, particularly given the increased likelihood of large scale rainfall/runoff events with the onset of climate change (Schaller *et al.*, 2016).

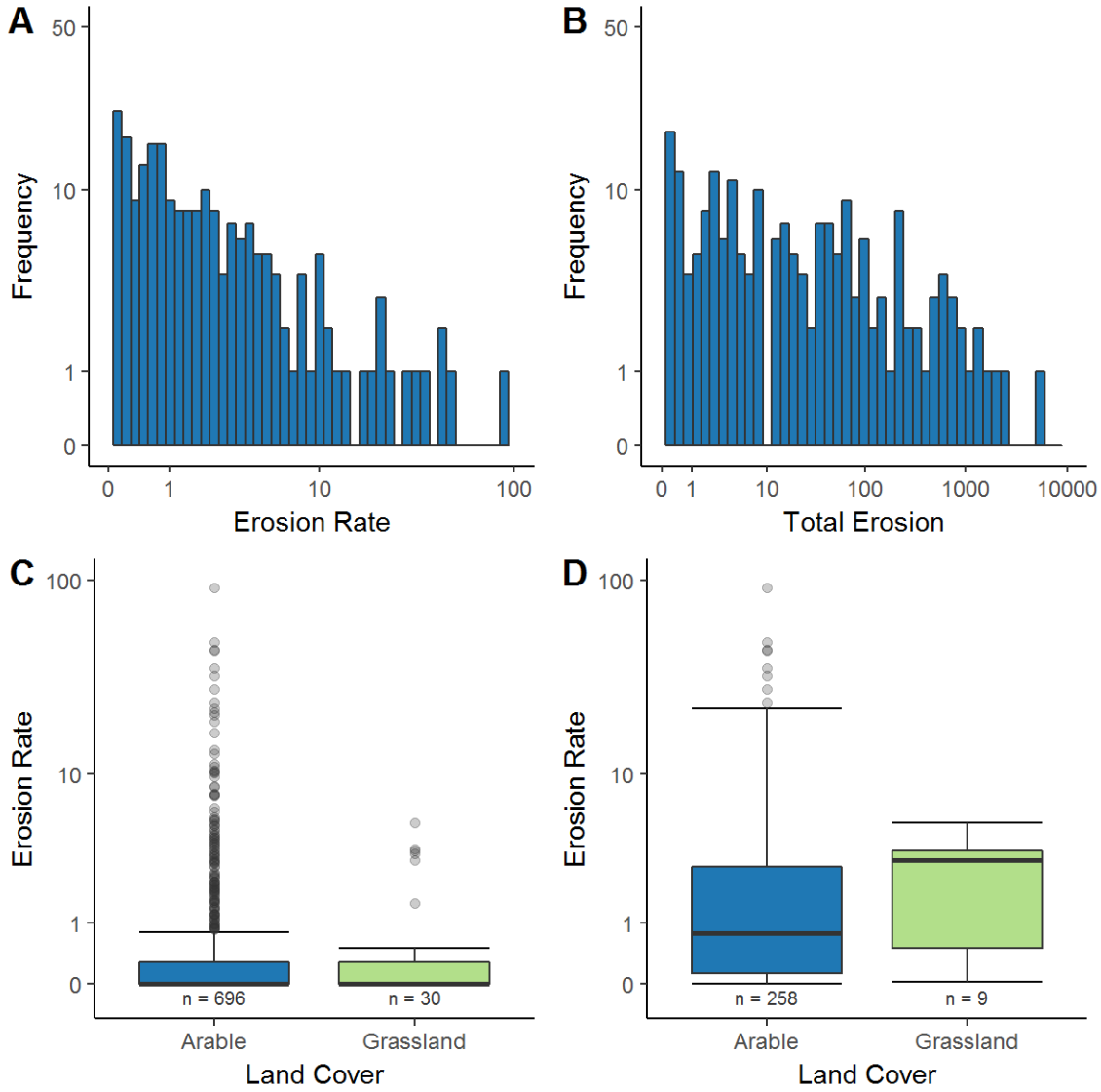

Figure 3.3: Graphical representations of the distribution of erosion records: A) histogram of the frequency of erosion rates (t ha^{-1} yr^{-1}) for arable records with erosion (n = 260), B) histogram of the frequency of total erosion observed (t ha^{-1}), for the 1999 upland observations with erosion visible (n = 206) from McHugh et al. (2002), C) boxplots comparing all arable and grassland observations, and D) boxplots comparing arable and grassland records with erosion.

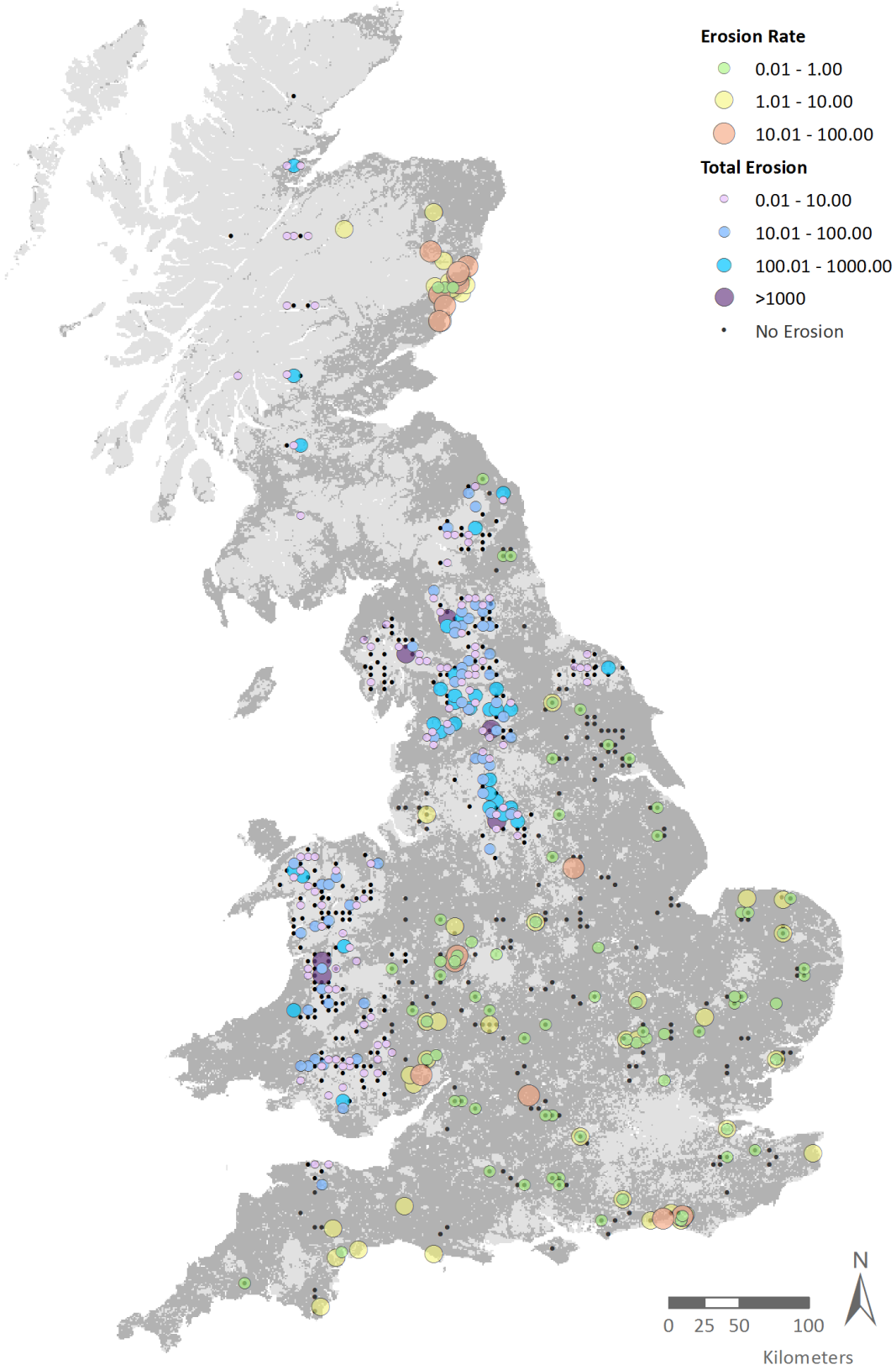

Figure 3.4: Map illustrating the spatial distribution and erosion magnitude of records (t ha^{-1} yr^{-1} for arable and grassland classes, and total t ha^{-1} for upland classes). The darker shading indicates the distribution of arable or improved grassland areas in the UK, based on LCM2000map.

3.5 Understanding the impact of environmental conditions on rates of soil erosion

3.5.1 Soil texture

Soil erosion studies have been carried out across a wide range of soil textures in England and Wales, as visible in Figure 3.5. Of the data included, the correct soil association and texture class was extracted for 381 arable, point-based records (ca. 55 per cent of total). Clay loam was the most common soil texture in the selection, with 173 records, and fine sandy silt loam and loamy medium sand were the least represented, with a single record each. 146 of the records coincided with soil erosion, where loamy coarse sand soils had the highest incidence of soil erosion (100 per cent, n = 6), while coarse sandy silt loam soils had the lowest occurrence of erosion (17 per cent, n = 6), excluding the textures with less than 3 records.

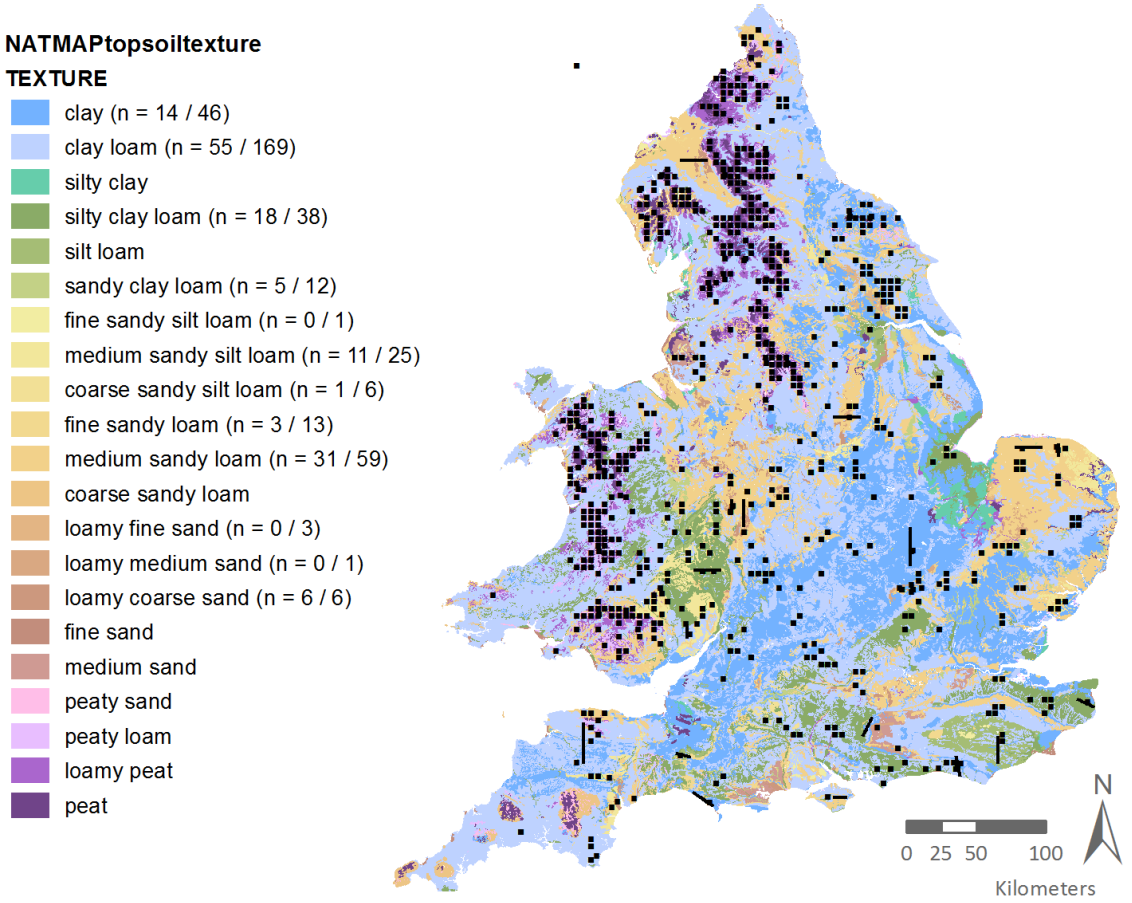

Figure 3.5: The spatial distribution of soil textures in England and Wales, with the locations of soil erosion records held within the geodatabase shown in black. The soil texture information was sourced from the National Soil Map of England and Wales, NATMAP topsoil texture, 1:250,000 © Cranfield University. N values in parentheses indicate the number of sites with erosion (first value) and the total number of studies per soil texture class presented in Figure 3.2.

Figure 3.6 shows the distribution of soil erosion rates within each soil texture class, based on the arable records with a presence of erosion. Pairwise analysis revealed that there was a significant difference between the distribution of the records for the silty clay loam class

(n = 18) and the following texture classes: clay (p = 0.0038, n = 14), clay loam (p = 0.0077, n = 55) and sandy clay loam (p = 0.0143, n = 5). There was also a significant difference between the distributions of results within the loamy coarse sand texture class (n = 6) and both clay (p = 0.0163, n = 14) and sandy clay loam (p = 0.0239, n = 5). The highest erosion rate (91.7 t ha^{-1} yr^{-1}) was found on medium sandy loam soil of the Fyfield4 (571g) association. Based on the erosion risk classification by Evans (1990), where 1 = low risk and 5 = very high risk, Fyfield4 has an erosion risk of 2 (although annotated as 'locally risk of erosion is greater'). From the records with erosion, the loamy coarse sand group had the highest median erosion rate (4.35 t ha^{-1} yr^{-1}), and were all soils classified as a very high risk (5). Of the same subset, the sandy clay loam soils had the lowest median erosion rate (0.6 t ha^{-1} yr^{-1}), whilst all being soils classified as erosion risk 3.

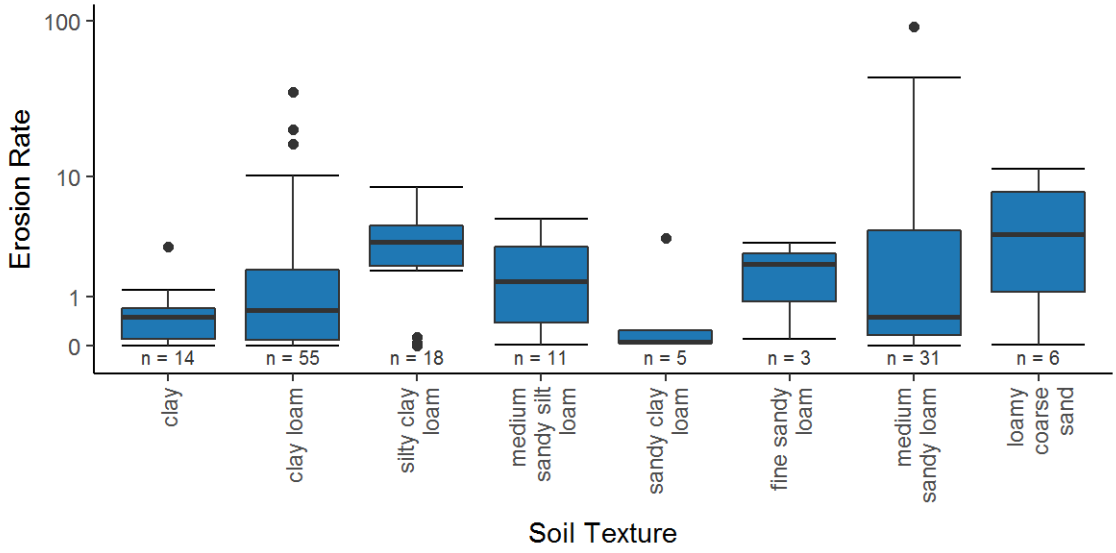

Figure 3.6: Boxplot illustrating the distribution of erosion rates (t ha^{-1} yr^{-1}), on a log scale, within each soil texture class, for arable records with a presence of erosion.

Figure 3.7 further illustrates the relationship between erosion rate and erosion risk, for all arable records (Figure 3.7A) and arable records with a presence of erosion (Figure 3.7B). Of the records held, the greatest number were for erosion risk 3, considered moderate, which had 130 records, followed by risk 2 (n = 112), risk 1 (n = 106), risk 5 (n = 23) and risk 4 (n = 8). For both datasets presented in Figure 3.7, there was a significant difference in the distribution of erosion rates between erosion risk 2 and 3 (p = 0.0003 and p = 0.0052, respectively) and 5 (p = 0.0100 and p = 0.0124, respectively). There was, however, no significant difference between remaining pairs, suggesting that erosion rates do not necessarily correlate with soil erosion risk as prescribed by Evans (1990).

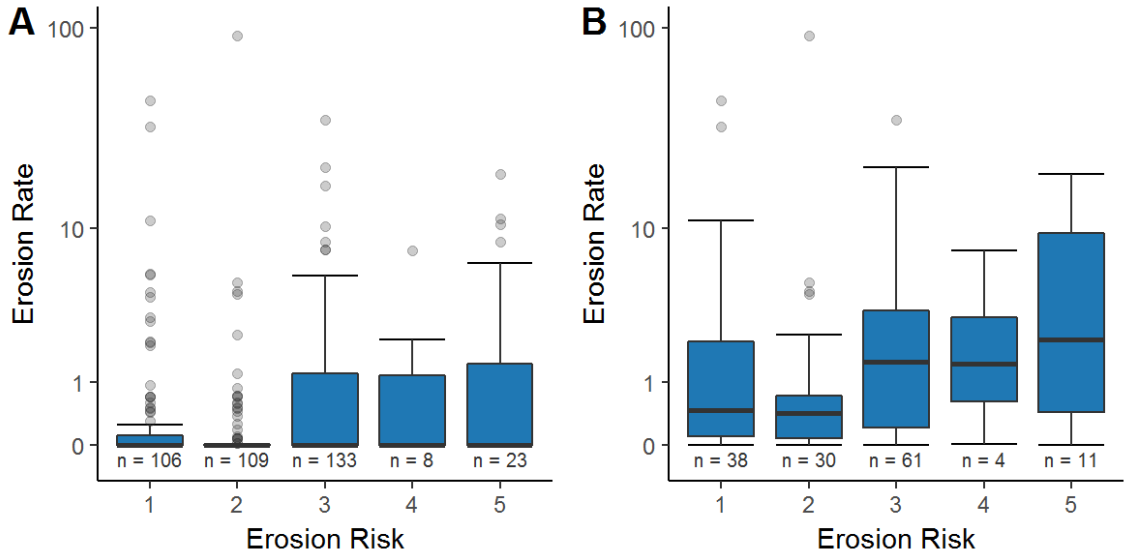

Figure 3.7: Boxplot illustrating the relationship between erosion risk (Evans, 1990b) and erosion rates (t ha^{-1} yr^{-1}) on a log scale for A) all values, and B) records with a presence of soil erosion.

3.5.2 The role of slope

Figure 3.8 illustrates the relationship between slope (%) and erosion rate (t ha^{-1} yr^{-1}), based on n = 627 records. While there is a weak positive correlation between steeper slope and erosion rates (r^2 = 0.23 for arable and 0.012 for grassland), this relationship was only significant for the arable observations (p = <0.05). Furthermore, as Figure 3.8A demonstrates that a wide range of erosion rates can be associated with any slope gradient. Despite slope being considered the greatest influence on soil loss at the European scale (Panagos *et al.*, 2015a), this result is consistent with the findings of García-Ruiz et al. (2015) at the global scale. However, of the studies examined, 74.7 per cent were carried out in localities with a mean slope of less than 10 %, and only 4.5 per cent were from areas with a mean slope greater than 20 %. Therefore, it could be argued that there is a need to build an understanding of rates of erosion at higher slope angles in the UK, as the existing dataset is skewed towards lower angled slopes.

3.5.3 Precipitation

Whilst soil erosion in the UK is frequently linked to large rainfall events (Boardman, 1988; Boardman *et al.*, 1996; Evans & Morgan, 1974), there was a dearth of information within the reporting on precipitation totals or intensities. Furthermore, there was little consistency in the reporting of precipitation across the soil erosion datasets, making robust analysis difficult. A qualitative analysis was carried out for the 45 records that did report the precipitation during the study period, and in some instances the mean annual precipitation for long-term ^{137}Cs-based studies, ranging from a minimum of 140 mm and a maximum of

1049 mm. There was a very weak negative relationship between precipitation and soil erosion observations (r^2 = -0.02), the relationship was not significant. The cluster of erosion observations around 660 mm, resulting from separate studies carried out within the same region and reporting the mean annual rainfall, illustrates the potential variability and influenced the gradient of the overall relationship (Figure 3.8B).

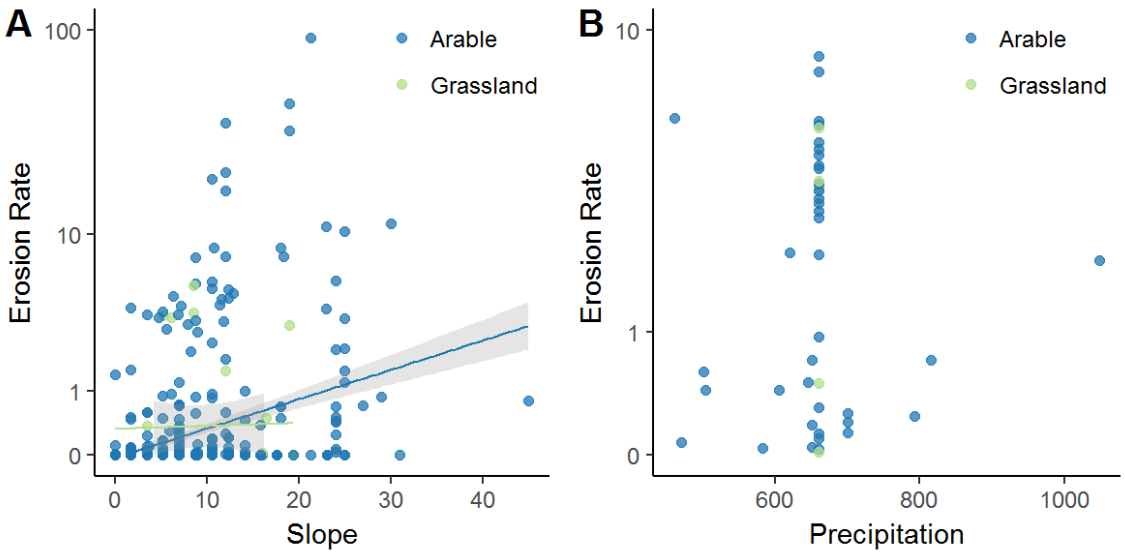

Figure 3.8: Scatter plot illustrating the relationship between erosion rates (t ha^{-1} yr^{-1}) on a log scale and A) slope gradient with 95% confidence intervals shaded, and B) precipitation (mm).

3.6 The relationship between erosion observations and monitoring approaches

Whilst building an understanding of soil erosion primarily requires collecting information from an array of environmental and management conditions, the diverse methodologies used to quantify rates of soil erosion can reveal different information about the processes occurring. Historically, due to their replicability, plot scale studies capturing sediment and runoff leaving a bounded area were used to build an empirical understanding of soil erosion under different land use and soil types, in an experimental setting (Nearing *et al.*, 1999b; Quinton & Catt, 2004). More recently, to minimise the bias created by bounded runoff areas and short slope lengths, hillslope studies have been utilised for the same purpose (Deasy et al., 2009). Both, however, are incredibly resource intensive and, particularly in the instance of bound experimental plots, typically only imitate natural conditions (Boix-Fayos *et al.*, 2006). In the UK at least, there have been numerous efforts to quantify soil erosion *in situ*, with a particular focus on capturing erosion within the bounds of a defined field, under 'natural' management conditions (Bilotta *et al.*, 2008). For example, studies such as the regional overflight surveys carried out by the Soil Survey of England and Wales (SSEW) or the NSI node-based studies by the Soil Survey and Land Research Centre (SSLRC), were

carried out using this approach, and represent some of the most extensive attempts at quantifying soil erosion, on a national scale, to date (Boardman, 2002; Evans, 1988a, 2005; Harrod, 1998).

3.6.1 Scale and soil erosion rates

The spatial extent of empirical soil erosion studies, in particular plot scale studies, is often cited as creating bias within soil erosion models (Parsons *et al.*, 2006). Consequently, to analyse the importance of scale, or more specifically the spatial extent of soil erosion studies, records were grouped into 5 classes: plot (for bounded areas, designed for soil erosion monitoring), hillslope (for unbound areas, designed for soil erosion monitoring), field (for areas naturally defined by constructed field perimeters, such as fences or hedgerows), catchments (for study perimeters defined by a hydrological catchment, extending greater than a single field) and regional (for areas exceeding a single catchment). Field scale studies have been the most common method for conducting soil erosion assessments in the UK to-date (n = 575), and plot scale studies the least common (n = 20). This is reflective of the magnitude of the SSLRC program and the changing nature of soil erosion research (Boix-Fayos *et al.*, 2006).

For the subset of data that included all arable records (Figure 3.9A), there was a significant difference between the distributions of erosion rates collected at field scale and all categories ($p = <0.001$). When considering only arable records with a presence of erosion (Figure 3.9B), there was a significant difference between the field scale observations and plot studies ($p = 0.0193$), hillslope studies ($p = 0.0032$) and catchment studies ($p = 0.0011$). There was, however, no significant difference between all other study extents, highlighting the complexity of scale relationships in soil erosion. Of the subset with erosion recorded, the field scale studies had the lowest median erosion rate (0.48 t ha^{-1} yr^{-1}), while the hillslope studies had the highest median erosion rate (2.95 t ha^{-1} yr^{-1}). As visible in Figure 3.9, plot scale studies had the greatest interquartile variability in erosion rates. Interestingly, the field scale studies had the greatest range of rates observed, capturing the intersection between the ad hoc studies carried out following significant erosion events and the national-scale study carried out by the SSLRC.

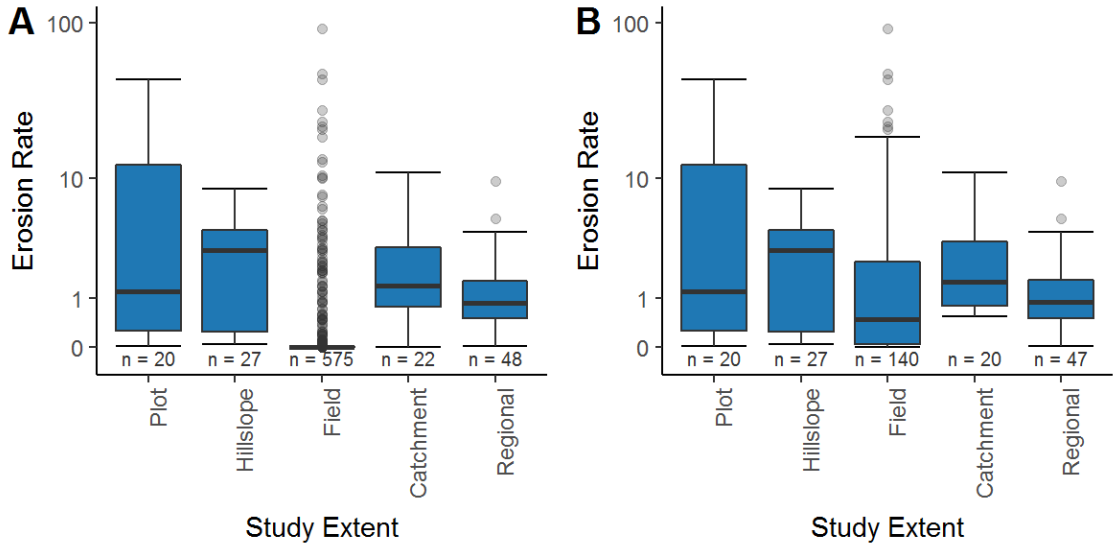

Figure 3.9: Boxplots illustrating the relationship between study extent and soil erosion rates (t ha^{-1} yr^{-1}) on a log scale for A) all arable records, and B) arable records with a presence of erosion.

3.6.2 Monitoring techniques

To assess the impact of the different monitoring techniques on the soil erosion observations, records were divided into three broad assessment categories: volumetric surveys, runoff and sediment capture, and radionuclide or other tracing experiments. The key differences between the techniques are the erosion process(es) captured and the duration for which the observation represents. For example, the very nature of runoff and sediment collection studies (described in Section 2.2.1) allows erosion observations to be derived for set periods of time or singular events, at the control of the researcher. Similarly, volumetric surveys, usually carried out under natural conditions, can be used to calculate soil erosion rates for a defined period if starting conditions are known, typically one arable season as defined by the time the soil surface was prepared. In contrast, the values reported by ^{137}Cs tracing are an average of all active erosion processes since the primary fallout, which is greater than 30 years for all observations in the database, calculated from concentrations within core samples collected at a single point in time. Consequently, ^{137}Cs can be used to quantify all soil redistribution processes (Quine & Walling, 1991), and runoff and sediment collection approaches can capture all soil leaving a known area. However, traditional volumetric surveys are only useful for quantifying soil loss via convergent erosion processes, namely, rills and gullies.

Volumetric surveys were the most common, representing 92 per cent of all records, followed by the radionuclide group, which consisted solely of ^{137}Cs derived results. Runoff and sediment collection was the least common methodology, consisting of 3 per cent of all

records, reflective of the resource intensive nature of the technique. Of the arable records in the subset of data with a presence of erosion (Figure 3.10B), the ^{137}Cs surveys yielded the highest median erosion rates at 3.12 t ha^{-1} yr^{-1}, while the runoff and sediment collection studies had the lowest median erosion rate (0.25 t ha^{-1} yr^{-1}). The number of significant outliers for the volumetric survey group reflects the selection of volumetric surveys to rapidly quantify large-scale erosion events, typically through transects, as implemented by Evans and Morgan (1974) in south Cambridgeshire following a single rainfall event. In this instance, the authors reported a loss of 112.5 tonnes of soil over an area of 34.4 ha. Pairwise comparisons found a significant difference between the distributions of the erosion rates measured by volumetric surveys and both other categories (p = <0.001), for the all observations subset (Figure 3.10A). However, when comparing the distribution of results for the records with a presence of erosion (Figure 3.10B), the ^{137}Cs and both volumetric surveys (p = <0.001) and sediment and runoff collection (p = <0.001).

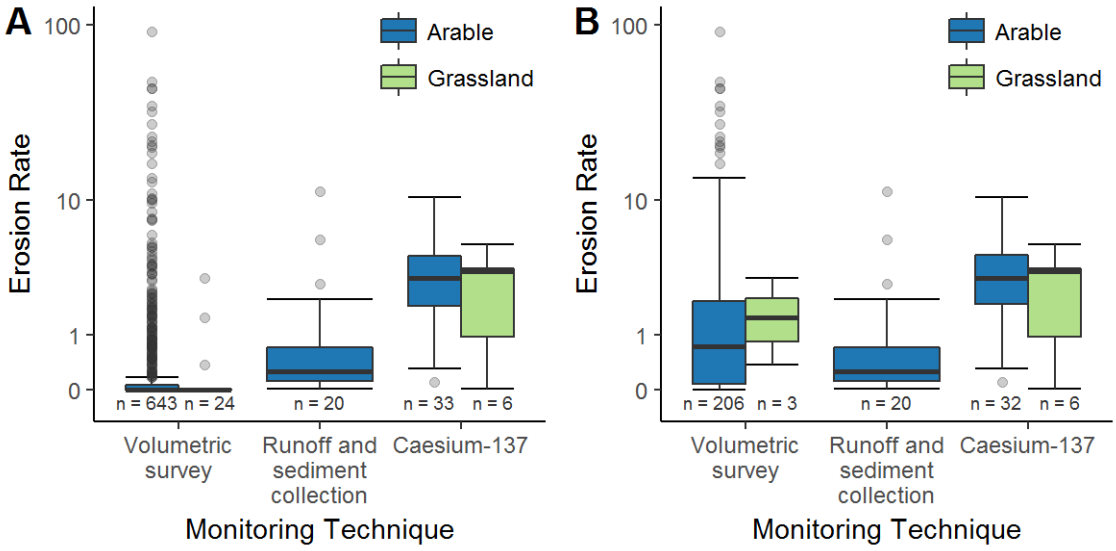

Figure 3.10: Boxplot illustrating the relationship between erosion rates (t ha^{-1} yr^{-1}) and the monitoring technique employed for the study, for A) all arable and grassland records, and B) arable and grassland records with a presence of erosion.

Given ^{137}Cs can be utilised to quantify all pathways of soil erosion, it is not unreasonable that the ^{137}Cs results were an order of magnitude higher than other results, particularly in the context of the 3 and 70 t ha^{-1} yr^{-1} range of soil loss for tillage erosion reported by Van Oost et al. (2006). Furthermore, it is important to consider that a mean surface lowering of 1 mm over an area of 1 ha, almost invisible to the naked eye and virtually impossible to quantify using volumetric transect surveys, would equate to a soil loss of 13 t, based on a bulk density of 1.3 g cm^3, which exceeds the tolerable rates of erosion by an order of magnitude. Differences resulting from monitoring technique are also evident in the

comparison between erosion rates for locations that have been studied with different techniques (Brazier, 2004). These findings highlight the need for caution when drawing conclusions from erosion rates collected using varying methodologies, and the validity in conducting soil erosion assessments using a unified approach.

3.6.3 Site selection

Records were grouped into the following categories based on the rationale for site selection for the soil erosion assessment: sites known to erode, sites predicted to erode or perceived as 'high-risk', sites based on sampling grid design, sites selected on statistically-based design, and others (which includes experimental farms). The distribution of the results within each category are presented in Figure 3.11. In the UK, there were no statistically unbiased soil erosion assessments. 14.1 per cent of erosion records fell into the 'predicted to erode' group, 8.1 per cent in the 'known to erode group' and 77.2 per cent in the sampling grid. However, while only 17.7 per cent of the sampling grid records report a presence of erosion, 99 per cent of the sites selected based on a predicted likelihood of erosion and 96 per cent of the known to erode site report soil erosion. Perhaps unsurprisingly, this highlights that if erosion is monitored at sites known/predicted to erode, there is a greater likelihood of observing accelerated soil erosion.

The distribution of erosion rates was significantly different between the sampling grid records and both the sites known and predicted to erode ($p = <0.001$), across the whole dataset (Figure 3.11A). However, when considering only the records with erosion observed, there was a significant difference in the distribution of all groups (Figure 3.11B). Whilst, the predicted to erode and sampling grid sites were similar in frequency, with 98 and 94 records respectively, the range of erosion rates within the sampling grid group is much smaller, with a greater number of outliers (9.6 per cent, compared with 3.1 per cent). Furthermore, the median erosion rate for the 'known to erode' results was an order of magnitude higher than the 'sampling grid' median, with values of 1.1 and 0.08 t ha^{-1} yr^{-1} respectively. The impact that site selection can have on skewing the understanding of soil erosion is further demonstrated in Figure 3.11A, which utilised all arable and grassland records. Unlike the median values for the known to erode and predicted to erode categories (2.97 and 1.06 t ha^{-1} yr^{-1} respectively), the median values for the sampling grid data set was 0 t ha^{-1} yr^{-1}, based on 552 records. This illustrates that even grouped erosion observations from localities with a known history or high likelihood of soil erosion occurrence cannot be used to build a picture of national-scale soil erosion rates. They are, however, useful for building

an understanding of potential magnitudes of soil erosion, particularly in light of the high costs associated with conducting large-scale soil erosion studies (Brazier *et al.*, 2016).

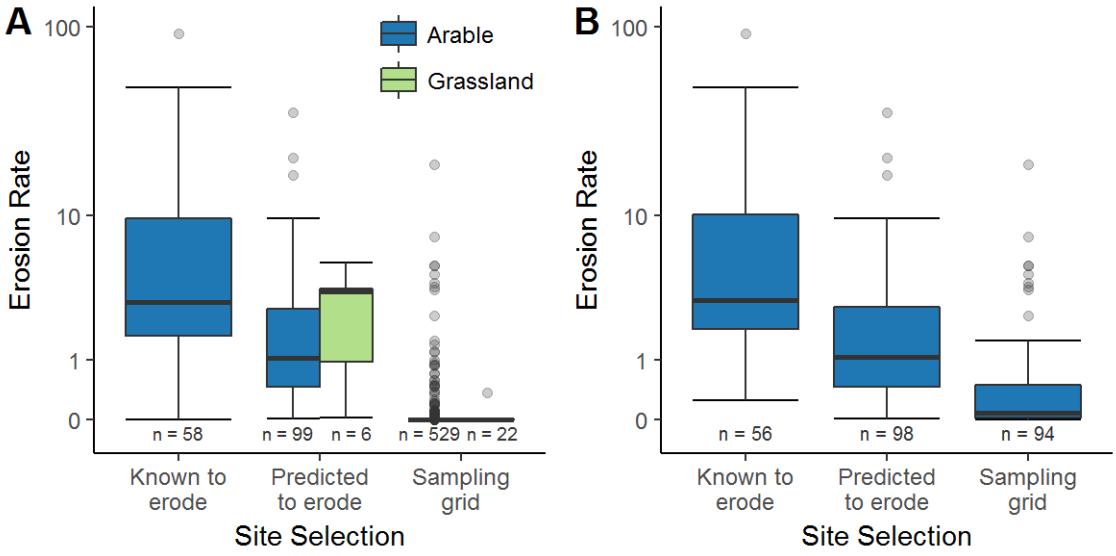

Figure 3.11: Boxplot illustrating the relationship between erosion rate (t ha^{-1} yr^{-1}) and the criteria used for selecting the study location, for sites with a presence of erosion, for A) all arable and grassland records, and B) arable and grassland records with a presence of erosion.

3.7 Towards a national-scale understanding of soil erosion in the UK

Through collating all readily available and empirically-derived soil erosion data from UK-based studies into a geodatabase, this exercise has clearly identified that the UK does indeed have a rich history of soil erosion research, which can be used to describe potential magnitudes of soil loss, in the context of the underlying methodological assumptions. Whilst the median soil erosion rate for all land use groups was 0 t ha^{-1} yr^{-1}, soil erosion does occur in the UK and 16 per cent of arable records had soil loss in excess of the 'tolerable' 1 t ha^{-1} yr^{-1}, and in ca. 20 instances, soil loss was greater than 10 t ha^{-1} yr^{-1}. When compared to erosion rates reported for other European countries by Verheijen et al. (2009), soil erosion in the UK might be interpreted as not presenting a serious problem. However, as the records within the database do not present a statistically unbiased national-scale understanding of current and historic rates of soil erosion, it could be argued that we still do not understand what constitutes an acceptable level of soil erosion for the UK (Reed, 1979). It is also important to note that a rate of 1 t ha^{-1} yr^{-1} may not actually be tolerable, or indeed sustainable, given the low soil formation rates typical of temperate soils (Foth, 1990; Jenny, 1941). Consequently, it is imperative that future studies are designed to permit the definition of tolerable rates of erosion to be constructed for the UK, while building on the present state of knowledge.

Analysis has revealed that the relationship between soil erosion rates and the environmental controls are variable. It has also highlighted the need for standardised reporting of environmental controls within all publications in order to allow post-hoc analysis and integration into modelling. This study has identified that soil erosion in the UK is not limited to the 'high' or 'very high' risk soils (per Evans, 1990). Therefore, a representative sample of all risk classes is necessary. However, based on the 1 km^2 data, there has been an over representation of soils at moderate risk of soil erosion, relative to the other soil risk classes, to-date. Similarly, while increased slope did have a weak positive relationship with erosion rates, consistent with the findings of García-Ruiz et al. (2015), the results revealed that rates can vary by an order of magnitude in fields of the same gradient. The weak correlation found between environmental factors and erosion rates is also consistent with the difficulty of modelling soil erosion in the UK (Evans & Boardman, 2016a; Evans & Brazier, 2005). Therefore, this research presents a strong argument for the improved validation of soil erosion models, and in turn, the usefulness of collating soil erosion observations into an open access geodatabase both for this purpose and to guide the future structure of soil erosion monitoring programs.

Building a sound understanding of soil erosion also requires the quantification of soil loss via all erosion processes, under a range of environmental conditions which capture the annual and inter-annual temporal variability of erosion rates across the UK landscape. However, through primarily employing volumetric surveys for quantifying soil loss, the bulk of soil erosion research in the UK has focussed on visible erosion processes or pathways, namely, rilling and gullying. Although there is on-going discussion surrounding the merits of ^{137}Cs fallout for tracing soil redistribution patterns (Mabit *et al.*, 2013; Parsons & Foster, 2013), the significant difference in distribution between the volumetric survey and ^{137}Cs results brings to light the importance of quantifying less-visible erosion processes, such as sheet wash. However, at present there is no clear and quantitative understanding of rates of soil loss derived from sheet wash in the UK, for example, leaving ambiguity and conflicting schools of thought amongst the research community (Evans & Boardman, 2016a, 2016b; Panagos *et al.*, 2016). Similarly, the results provide evidence that grassland environments can erode at an accelerated rate, and one in three records had evidence of soil erosion, however, improved grassland studies represented only 31 of the 1566 total studies, despite covering over 55,000 km^2 in the UK (LCM2000).

With the exception of the work carried out along the NSI sampling grid by the SSLRC (Harrod, 1998; McHugh et al., 2002), it was found that all other soil erosion research in the UK has been carried out in localities with a known propensity for soil erosion. This sampling bias, when compared to the distribution of soil erosion rates found by the sampling grid approach, had a significant impact on the distribution and magnitude of results. Whilst this has biased the current understanding of soil erosion in the UK towards localities known to erode, the intersection between these groups of studies illustrates the highly variable nature of soil erosion rates in the UK. Consequently, although these studies do provide an insight into potential magnitudes of erosion in the UK, caution must be taken when drawing conclusions about national-scale erosion rates from the results.

The majority of soil erosion observations in the UK are at least 20 years old. Furthermore, with the exception of the ^{137}Cs studies, most erosion rates are collected over periods of less than 4 years. However, Boardman (2003) through reporting on a 10 year study in the South Downs, illustrated that median erosion rates can vary by an order of magnitude and 89 per cent of soil loss can occur within a 3 year period. Accordingly, many of the existing studies are thus unable to describe seasonal or inter-annual variability and the importance and frequency of extreme erosion events, such as the aforementioned events described by Chambers and Garwood (2000) and Evans and Morgan (1974), in West Sussex and Cambridgeshire, respectively. Whilst ^{137}Cs can be used to determine long-term pattern and rates of soil erosion, without repeat measures to provide up-to-date inventories, it cannot be used to quantify contemporary responses to policy measures, such as the impact described by Evans (2010), or changes resulting from climate change. Volumetric surveys, rapidly deployed using the visual estimation approach employed by Evans (2017) have been suggested as an option by the same author for longitudinal monitoring studies, however, outside of specialist application, this is not a robust approach and will not capture diffuse erosion processes.

Whilst previous reviews have argued that existing studies have sufficiently quantified water erosion in the UK, giving "*a consistent picture of the extent, frequency and rate of erosion*" (Evans *et al.*, 2015: 10), this chapter, through providing an independent review of existing studies, has illustrated that this is not the case. Furthermore, the majority of soil erosion observations not only predate current policy, but also measure only visible pathways of erosion (in most cases) and therefore undermine confidence in any resultant understanding

of changes to erosion rates affected by land use change. Accordingly, it is argued that there is a need for a refined national-scale assessment of soil erosion in the UK. In light of the short-comings highlighted in this study, future studies should be replicable and robust, meeting the following criteria:

1. Unbiased statistical sampling design (as opposed to monitoring erosion where it is known to occur).
2. Including a representative range of environmental conditions from upland to lowland land covers.
3. Quantifying both visible and less-visible erosion pathways.
4. Capturing the seasonal and inter-annual variability of erosion rates.
5. Representing a selection of land use categories, including emerging land use under changing climates.
6. Standardising erosion measurements to ensure that results are comparable nationwide as the same (and best) techniques are deployed.

The analysis of national-scale geodata describing soil erosion has identified the potential magnitudes of soil erosion in the UK. However, it has also highlighted the costs associated with an *ad hoc* approach to soil erosion monitoring and the inconsistent publication of the findings. Whilst existing monitoring strategies have provided a useful insight into some of the relationships between environmental controls and rates of soil erosion, if their scope is limited by insufficient reporting, or inconsistent sharing of raw data for future analysis, the resource intensive nature and/or bias towards a single erosion process hinders their suitability for future national-scale monitoring programs. To this end, there is a real need to identify and develop unified monitoring techniques, which are capable of meeting the above-listed requirements across changing spatial extents and magnitudes of erosion. Although caution must be employed when comparing rates of erosion across different scales (Parsons *et al.*, 2006), using a standardised workflow, sharing data in an open access format as demonstrated, and thus producing a consistent unit of measure across the soil erosion community, will provide a robust platform from which a national-scale understanding of soil erosion can evolve.

4. EXPERIMENTAL METHODS

4.1 Overview

The previous chapter has highlighted the need for the development of new approaches to soil erosion monitoring, these should be capable of quantifying both visible and non-visible pathways of erosion. Consequently, this chapter details the methods used for the application of a selection of alternative methods that were used to quantify water erosion features in order to meet Objectives 2 and 3, where the methods used were not specific to the needs of an individual chapter. This chapter first outlines the experimental setup and conditions employed, including the tagging of experimental soils with Rare Earth Oxide (REO) tracers, and then lists the protocols followed for the creation of point clouds, using Terrestrial Laser Scanning (TLS) and Structure-from-Motion photogrammetry (SfM) techniques. The methods have been applied based on best practice at the time of application, however, some methods development was appropriate to allow for the small spatial extent of the study areas.

4.2 Spatial scales and experimental setup

To assess the suitability of the selected techniques across changing magnitudes and patterns of soil erosion, experiments were conducted at two different scales, described herein as 'plot' and 'flume', as detailed in Table 4.1. The soil erosion experiments were carried out within the University of Exeter Sediment Research Facility, affording further control over the conditions of the experiment and thus the active erosion process(es). The experimental hall is equipped with a network of pipes that, together with interchangeable Lechler full cone axial flow nozzles, two pumps and a water tank, form a large indoor rainfall simulator.

Table 4.1: Outline of the basic properties of the plots and flumes used, where dimensions represents the volume filled with soil. The bottom of the flume was filled with 8 cm of sand.

	Dimensions						
Experimental Scale	Length (m)	Width (m)	Depth (m)	Volume (m^3)	Soil mass (kg)	Soil ρb (g cm^{-3})	Replicates
Plot	0.5	0.3	0.075	0.012	14.4	1.3	4
Flume	3	1	0.12	0.39	540 (+/- 5kg)	1.4	3

The four plots were constructed from treated rough sawn timber, with a base constructed of ridged 20 mm galvanised wire mesh overlain with permeable polyester ground cover, to allow water to infiltrate through the soil profile. The downslope end of the plot was fitted with a removable plot wall and a gutter in order to allow sediment to leave the plot during the sheetwash and rilling experiments, as visible in Figure 4.1A. The upslope end and

sidewalls of the plots and flumes exceeded the top of the soil surface by at least 0.08 m to minimise soil loss via splash erosion. The flume experiments were carried out within a pre-existing 3 x 3 m fiberglass flume, which was divided into the three flumes, using 18 mm exterior plywood, as demonstrated in Figure 4.1B. The base of the flume contained nine freely draining holes per square metre, and was covered with a permeable polyester ground cover then 0.08 m of sand and a second layer of ground cover. Housing gutters with polyethylene skirts were attached to the downslope end to allow sediment to leave the flume.

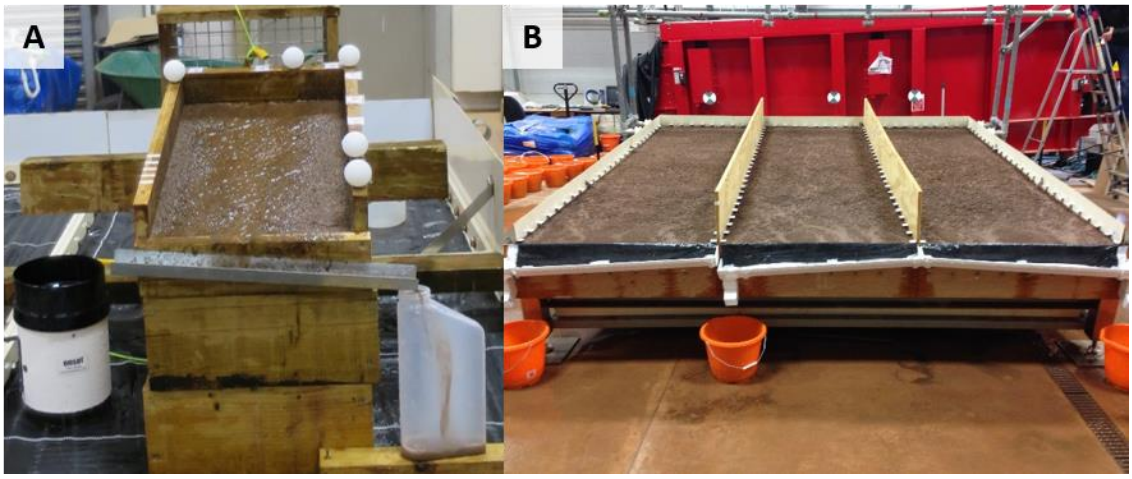

Figure 4.1: Experimental setup for the A) plot-scale rilling experimental runs and B) flume rainsplash and compaction experimental run.

4.3 Preliminary characterisation work

4.3.1 Rainfall uniformity

Lechler full cone axial flow nozzles, type 460.648.30.CC, were fitted and engaged in the locations shown in Figure 4.2. By channelling water into the centre of the nozzle, the axial flow nozzles produce an even distribution of water, at a 60 degree spray angle. To build a spatial and temporal understanding of rainfall inputs, two 0.5 x 0.3 m plots, lined with plastic and fitted with a drainage funnel, thus acting as large rain gauges, were positioned under the rainfall simulator for a rainfall experiment. Rainfall was collected at 5 minute intervals, until the rainfall intensity was uniform for a minimum of three replicates for both experimental scales. To build a spatial understanding of the rainfall intensity for the flume experiments, a large rain gauge was placed in the centre of the top and bottom third of each flume, simultaneously. The experiment revealed that the design of the rainfall simulator results in rainfall intensities that are spatially variable but temporally constant, consequently, each flume was subject to different rainfall intensities. This enabled an opportunity to test the accuracy of the techniques across changing magnitudes and of soil loss. To provide a reference during the experimental runs, a HOBO automatic tipping bucket

rain gauge (Onset, Bourne USA) was positioned within the rainfall zone, and programmed to record rainfall at 0.2 mm increments. The tipping bucket rain gauge was also in place during the rainfall experiment to allow the spatial variable intensities to be calibrated with a single monitoring location.

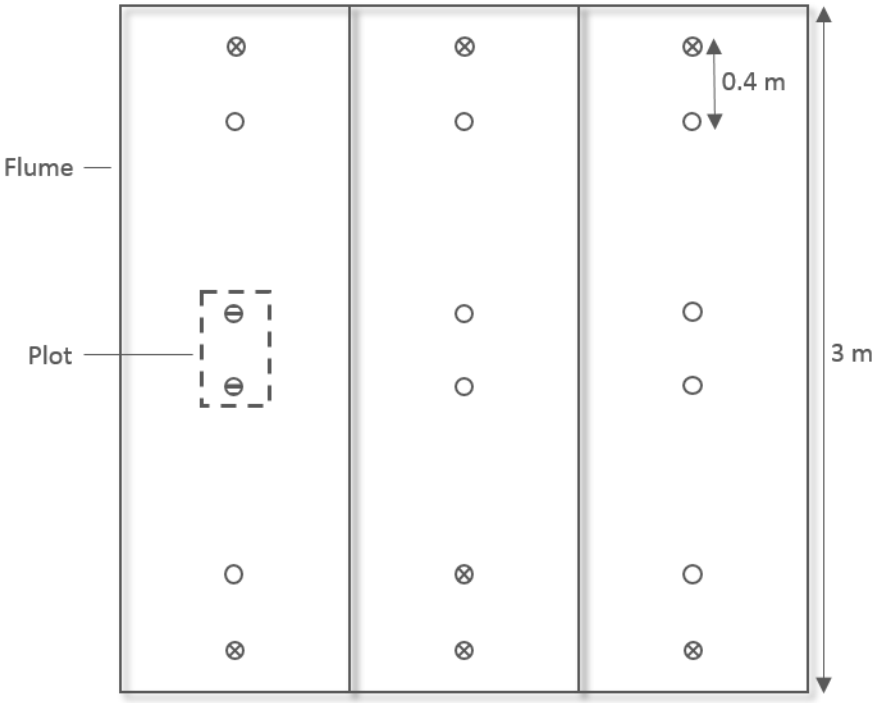

Figure 4.2: Schematic diagram illustrating the set-up of the rainfall nozzles in relation to the experimental areas. Dashed circles indicate the nozzles engaged for both the plot and flume scale experiments, open circles the nozzles engaged for only the flume scale experiments, and the crossed are nozzles that were not engaged.

4.3.2 Soil particle size distribution

The soil particle size distribution (PSD) was characterised for air dried sub-samples of each soil by sorting a sub-sample into 6 classes at one φ (Wentworth phi) intervals, namely, >1000, 1000 > 500, 500 > 250, 250 > 125, 125 > 63, <63 µm, using a mechanical dry sieving stack (Retsch AS200) for 10 minutes. A minimum size threshold of <63 µm was considered appropriate for an undispersed assessment of soil PSD (Cunliffe *et al.*, 2016), and for the requirements of the experimental design.

4.4 Soil surface conditions

4.4.1 Experimental soil

A screened, sandy loam topsoil was sourced from a local supplier (HCT Turf) for the plot and flume experiments. The soil was selected due to the erodible nature of sandy soils (as highlighted in Section 3.5.1), and furthermore, a loamy soil texture provides an interesting platform for assessing the impact of the preferential binding of REOs to finer soil particles (Kimoto et al., 2006; Michaelides et al., 2010). Logistical constraints necessitated the soil

being sourced in separate batches for the plot and flume experiments, which resulted in slightly different soil types being used for each experimental scale, as listed in Table 4.2.

Table 4.2: PSD of soil used in plot and flume experiments, based on three replicates.

		Plot		Flume	
Texture	Grain size (µm)	Percentage (% total mass)	Std. Dev.	Percentage (% total mass)	Std. Dev.
Fine Gravel	> 2000	17.1	4.1	24.5	4.6
Very Coarse Sand	2000 > 1000	11.8	0.5	11.5	1.2
Coarse Sand	1000 > 500	12.4	0.2	11.4	1.1
Medium Sand	500 > 250	14.7	1.0	22.9	0.5
Fine Sand	250 > 125	17.0	1.3	19.4	0.3
Very Fine Sand	125 > 63	14.5	1.4	7.3	0.8
Silt and Clay	<63	12.6	1.0	3	2.1

4.4.2 Soil preparation – Rare Earth Oxide tracers

Rare earth oxides (REO) were selected as tracers in order to aid in the identification of active soil erosion processes, sediment source and sediment transport distances, in line with Objective 3. The REOs used for the experiments were: Lanthanum oxide (La_2O_3), Praseodymium (Pr_6O_{11}), Gadolinium (Gd_20_3), and Neodymium (Nd_20_3). To capture the transition between sheetwash and rilling, and the relative contribution of inter-rill and rill erosion, the soil was tagged in the following layers from the top: 0 – 5 mm, 5 – 15 mm, >15 mm, for the plot scale experiments, as illustrated in Figure 4.3A. The length of the flumes also afforded an opportunity to capture sediment transport distances. Therefore, the top 10 mm was divided into three sections and each tagged with a different REO, above a 70 mm layer of Lanthanum oxide (La_2O_3) tagged soil, as shown in Figure 4.3B.

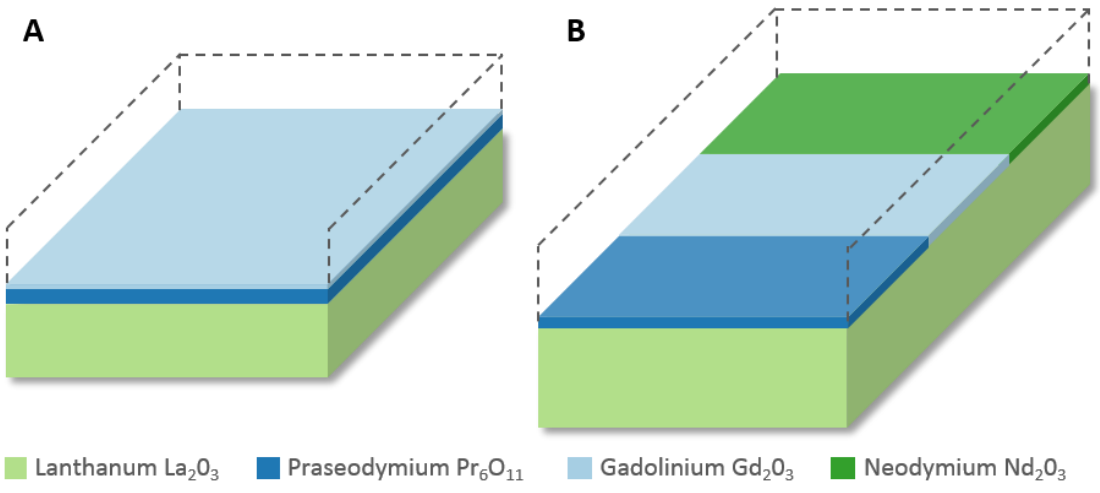

Figure 4.3: Schematic diagram illustrating the REO tagging design for the plots (A) and flume (B)

Previous field and laboratory scale erosion studies have applied REOs at approximately 10 times background concentrations (e.g. Polyakov & Nearing, 2004; Senbayram et al., 2015; Stevens & Quinton, 2008), however, Pryce (2011) found increased uniformity of application and recovery rates with higher application concentrations. Furthermore, the high rates of application used by Michaelides et al. (2010) i.e. 500 to 2000 times background concentrations, allowed for the successful quantification of soil erosion rates from a partially tagged soil using sediment and core samples. However, applying REOs at 500 or greater times background concentrations is not practical at the field scale due to the quantities of REOs needed. Consequently, to test a field-appropriate methodology, the soils used in the experiments were tagged with REOs to at least 100 times the background concentration. The soil profile was tagged to the maximum soil loss depth, as illustrated in Figure 4.3, in order to reduce the impact that lower tagging concentrations can have on recovery rates.

The soil was sieved to 6 mm for the plot studies and 8 mm for the flume studies (Armstrong *et al.*, 2011; Kimoto *et al.*, 2006b; Polyakov & Nearing, 2004) and tagged at maximum soil moisture content (SMC) of 8 %, using a clean 134 L cement mixer (32 rpm, Screwfix). While previous studies have tagged soil at a SMC of ca. 15 % (e.g. Michaelides et al., 2010; Zhang et al., 2003) it was found that this led to the formation of large aggregates during a preliminary test, which would have decreased the uniformity of the tracer application. To increase the mass being mixed into the soil, and in turn the final homogeneity of the tagging, a randomly selected 200 g of soil was thoroughly mixed by hand with the mass of REO listed in Table 4.3 for the plot scale experiments, and 500 g with the mass of REO listed in Table 4.4 for the flume experiments. The tagged soil was then transferred to the cement mixer, where 200 g of untagged soil was added every three full rotations and manually riffled every 1 kg, until all the soil was tagged. For the plot studies, the soil for all five plots was tagged in one batch for each REO, excluding the La_2O_3 layer, which was tagged in two batches due to the larger tagged mass required. The La_2O_3 layers of the flume studies were tagged in 12 equal batches per flume, while each subsequent REO was tagged in one batch per flume. A random 50 g composite of each tagged soil was saved for analysis.

Table 4.3: Summary of mass of REO tracers used for plot scale experiments.

		Per plot		Total	
Rare Earth Oxide	Tagging depth (cm)	Tagged mass (g)	REO mass (g)	Total tagged mass (Kg)	Total REO mass (g)
Gd_2O_3	0.5	900	15.3	4.5	76.5
Pr_6O_{11}	1.0	1800	21.6	9	108
La_2O_3	6	11700	35.1	58.5	175.5

Table 4.4: Summary of REO tracers and soil used for flume scale experiments.

			Per flume		Total	
Rare Earth Oxide	Tagging depth (cm)	Tagging length (cm)	Tagged mass (kg)	REO mass (g)	Total tagged mass (kg)	Total REO mass (g)
Gd_2O_3	1.0	100	13.8	207	41.4	621
Pr_6O_{11}	1.0	100	13.8	207	41.4	621
Nd_2O_3	1.0	100	13.8	207	41.4	621
La_2O_3	7	300	290 (2.6)	1452 (13)	871	4355
Blank	4.5	300	181 (8.5)	-	543	-

4.4.3 Soil bed preparation

Emmett et al. (2007) report an average bulk density (ρ_b) of 1.23 g cm^{-3} for arable land in the UK, and soil was laid at ρ_b 1.3 g cm^{-3} for the plot scale experiments, aligning the work with similar previous studies (e.g. Armstrong et al., 2011; Polyakov & Nearing, 2004) and creating a 'realistic' soil bulk density for arable UK soils. For the flume scale work, the soil was placed with a target ρ_b 1.4 g cm^{-3}, in an attempt to mitigate the high level of rainsplash compaction and subsidence found in the plot scale experiments. To achieve the target bulk density, the side-walls of the plots and flumes were marked along all sides to the fill height. At the plot scale, each tagged soil was then evenly applied in 600 g increments and smoothed every 1800 g, using a bricklaying trowel, to maintain even layering and a consistent bulk density throughout the soil profile. The flume was filled in 1 kg increments and smoothed every 3 kg. Given the complexity of applying a 5 mm layer of soil, the soil for the upper layer of the plots was applied in 100 g increments.

4.4.4 Experimental runs

To ascertain the efficiency of each technique when quantifying soil loss, relative to changes in structural complexity associated with different erosion pathways, it was necessary to create hydrological conditions that promoted the development of the different soil surface conditions typically associated with water erosion, namely:

1. Compaction and rainsplash
2. Sheetwash erosion
3. Rill erosion

This was achieved through a reductionist approach for the plot scale studies, whereby each soil surface condition was achieved in separate experimental runs, sequentially conducted on each plot.

For plots the plot scale experiments, the slope gradient and rainfall intensity was the same for both the sheetwash and rilling experiments, while the duration of the rilling experiment was varied to created different size erosion features. To promote the formation of a rill feature, the plot scale experiments included a single run-on source for Event 3, as listed in Table 4.5 and visible in Figure 4.1A. A period of three hours was allowed between each event. The plots were covered with a waterproof tarpaulin for 5 minutes after the rainfall was switched on, in order to allow the simulator to reach a constant rate.

Table 4.5: Outline of the basic experimental conditions for each plot experiment. Rainfall is correct to +/- 5 mm hr^{-1} and run-on varied by +/- 50 mL min^{-1}.

	Event 1 Compaction and Rainsplash			**Event 2 Sheetwash**			**Event 3 Rilling**			
Plot	Slope (%)	Rainfall (mm hr^{-1})	Duration (mins)	Slope (%)	Rainfall (mm hr^{-1})	Duration (mins)	Slope (%)	Rainfall (mm hr^{-1})	Run-on (mL min^{-1})	Duration (mins)
2	0	75	20	21	75	30	21	75	700	30
3	0	75	20	21	75	30	21	75	600	10
4	0	75	20	21	75	30	21	75	700	15
5	0	75	20	21	75	30	21	75	700	20

The flume scale experiments were designed to create a more complex series of erosional features, better aligned with natural conditions. Due to the layout of the experimental set-up, as shown in Figure 4.1B, each flume event was carried-out concurrently, under the conditions listed in Table 4.6. Event 1 was stopped when ponding had occurred across all plots, and two hours was then allowed between events. Following the compaction and rainsplash experiment, the flumes were elevated to 9 %, this was the maximum gradient attainable using the kit. The flumes were covered with a waterproof tarpaulin at the start and finish of each event to allow for constant rainfall intensity to be reached before the experiment began and to minimise runoff at the completion of the experimental period.

Table 4.6: Outline of the basic experimental conditions for each flume experiment, where rainfall intensity is +/- 25 mm hr^{-1}

	Event 1 Compaction and Rainsplash			Event 2 Sheetwash and Rilling		
Flume	Slope (%)	Rainfall (mm hr^{-1})	Duration (mins)	Slope (%)	Rainfall (mm hr^{-1})	Duration (mins)
1	0	110	10	9	90	66
2	0	150	10	9	120	66
3	0	140	10	9	110	66

4.5 Sediment flux

To provide a true picture of total soil loss and to contribute to the understanding of soil erosion processes, all runoff and sediment leaving the plots or flumes was captured on timed intervals. 1 litre bottles and 12 litre buckets were used to collect all runoff from the plots and flumes, respectively (as visible in Figure 4.1). These were changed at 2 minute intervals for the plot sheetwash experiment, 1 minute intervals for the plot-scale rilling experiment, and 2 minute intervals for the flume-scale experiment. Following the experiments, all samples were covered and left to settle for at least 48 hours before the volume of each was recorded. The water was then carefully poured off the sediment, which was then recovered and dried at 60 ˚C for 48 hours. Following drying, all sediment samples were weighed and then characterised using the methods described in Section 4.3.2. Due to the small-scale nature of the experiments, this was reported in the format of sediment flux, a unit of mass (g) per unit volume (L), rather than sediment yield which has reference to a unit of area (Parsons *et al.*, 2004).

4.6 Terrestrial Laser Scanning

Often considered the benchmark for collecting spatial data (Glendell *et al.*, 2017; James & Robson, 2012; Smith & Vericat, 2015), terrestrial laser scanning (TLS) technology has developed to allow a non-expert user to derive highly accurate (+/- 2-5 mm) 3D spatial information for use in a geomorphology setting. Consequently, TLS was selected to meet Objective 2, providing a platform to quantify soil erosion and acting as a reference to assess the spatial accuracy of the SfM approach described in Section 4.7. Using LiDAR technology, the instrument used for the experiments was a pulse-based scanner, employing 'time-of-flight' to derive repeat measures of distance to the soil surface. The main source of complexity and thus systematic error can arise through the 'stitching' of multiple scans into a singular point cloud (Ouédraogo *et al.*, 2014). Therefore, to avoid the introduction of user and systematic error, all experimental surfaces were captured with a single scan.

Each plot was scanned immediately before and 1 hour after each event, with a Leica Geosystems ScanStation P20. The instrument uses an 808 nm (invisible) and 658 nm (visible: red) wavelength laser with a beam diameter of ≤ 2.8 mm, and a 3D positional accuracy of 3 mm at 50 m and 6 mm at 100 m. To minimise shadows and occlusions caused by a single viewpoint the scanner was positioned oblique to the soil surface. Whilst increasing the angle of incidence can increase the scan noise levels, this was minimised through reducing the distance between the TLS and the scanned surfaces (Soudarissanane *et al.*, 2009). A 'scanning station' was created to ensure the distance (2 – 2.5 m) and angle of incidence (34 – 40 degrees) was the same for all iterations. The scanner was set to highest possible quality and resolution combination, consequently, each point was derived from the mean of 16 returns and the scan resolution was approximately 0.16 mm (based on 1.6 mm at 10 m). The true Ground Sampling Distance (GSD) was calculated from the final point cloud density (PD), where $GSD = PD^{-0.5}$. To minimise the impact of any small discrepancies in the placement of the plots within the scanning station, six 35 mm, matt-white plastic spheres were affixed to the plots to aid alignment of the point clouds in during processing, for change detection.

4.7 Structure-from-Motion Photogrammetry

Through the use of consumer grade cameras, Structure-from-Motion Multi-View-Stereo Photogrammetry (SfM MVS) can be utilised to produce ultra-fine scale spatial data within field and laboratory environments. SfM MVS generates 3D point clouds through three stages of image processing using specialist open-source or commercially available software tools or packages such as Agisoft PhotoScan, VisualSFM or Pix4D. First, tie-points between images are found and used to create an estimate of 3D structure, then a self-calibrating bundle adjustment process fine tunes the model through estimating camera extrinsic and intrinsic geometry and adjusting tie-point positions (James *et al.*, 2017b; Micheletti *et al.*, 2015; Smith *et al.*, 2015). Within the software, scaling and subsequent accuracy assessments are then carried out through the use of 'ground control points', whereby the highest level of reconstruction certainty and in turn the *effective* detection limits for spatial change is controlled by the accuracy of the control. The final, optional, stage involves the construction of dense point clouds through Multi-View-Stereo (MVS) processing.

The estimation of camera intrinsic geometry as part of the bundle optimisation process, within a standard SfM MVS workflow, produces a lens calibration specific to the individual camera and lens configuration. Consequently, constructing precise and spatially accurate

SfM MVS point clouds requires the careful control over camera and image network geometry. However, calibrating lens parameters prior to the collection and processing of experimental imagery reduces the need for multiple images, of varied extrinsic geometry (Eltner *et al.*, 2017; Shahbazi *et al.*, 2015). As a result, the geometry of experimental imagery only needs to provide coverage of the area of interest, from a minimum of two viewpoints, similar to traditional photogrammetric studies. This allows for the use of a fixed imaging station, increasing the replicability of the overall workflow, could permit the collection of time-lapse imagery in future applications. Similarly, calibration of the cameras separate to the experimental imagery can reduce the doming associated with capturing sequential nadir imagery (James & Robson, 2014). Therefore, this was the approach to SfM MVS taken for this study. The sections below detail the data collection and processing steps followed for the creation of ultra-fine scale (<0.5 mm/pixel) point clouds via SfM MVS, in line with Objective 2.

4.7.1 Camera properties

Three Canon 600D digital SLR cameras with Canon EF-S 18-55 III lenses, were used for the plot and flume scale experiments using the set ups illustrated in Figure 4.6 and Figure 4.7, respectively. While it is common practice to use a prime or fixed lens for ground-based SfM MVS (e.g. Glendell et al., 2017; James & Robson, 2012), a secondary aim was to build a low-cost workflow for creating high-resolution DTMs for small-scale erosion projects. As a result, the standard-issue zoom-lens' that came with the Canon 600D cameras were used for the work presented in this thesis. Once the cameras were sufficiently focused on their subject, both the focus and zoom were taped in place with electrical tape and splints for extra support, to mitigate any avoidable changes to the intrinsic lens geometry during the experiments. While shutter speed was set to auto, the remaining camera operative settings were kept consistent between the plot and flume scale experiments. ISO was set to 200, aperture was F8.0, exposure was adjusted to -2/3 and the highest resolution JPEG format (18MP) was selected. The focal length of each camera was adjusted to 21 mm for the plot experiments and 18 mm for the flume scale experiments.

4.7.2 Ground control points

Due to the scale and location of the experiments it was not possible to use a real-world coordinate system, scaling and checks on control were therefore achieved through the use of scale bars and the creation of unique coordinate systems. For the plot scale work, this was achieved through the use of a 'control frame', which consisted of a three-tiered frame of rigid steel, as illustrated in Figure 4.4A, with 18 markers affixed to each layer of the frame,

54 in total. For the flume scale work, markers were affixed to 3 sides of the flumes on small metal brackets with a water resistant epoxy glue, approximately 0.12 m apart and thus equating to 59 per flume, as visible in Figure 4.1B.

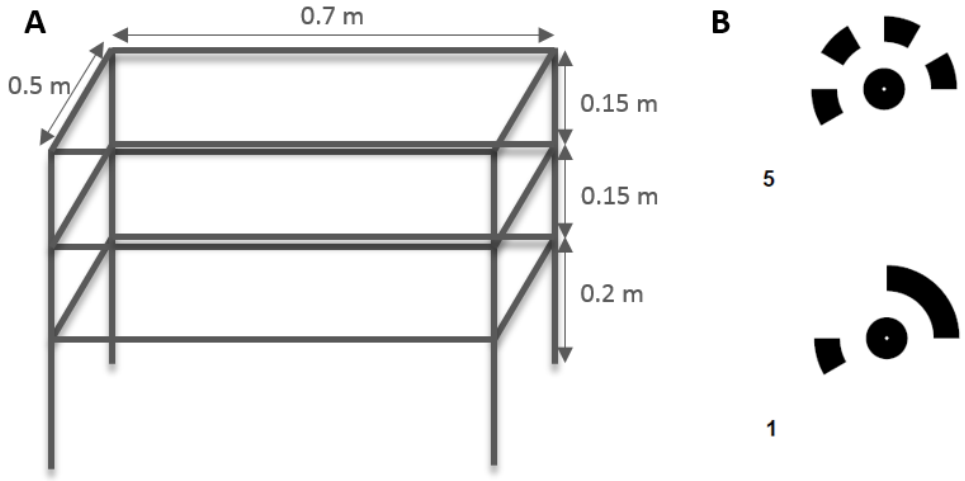

Figure 4.4: A) Schematic diagram of the control frame used for calibration and the plot scale experiments, B) example 12-bit markers printed from PhotoScan (Agisoft LLC).

To allow for automated detection of control points, 12-bit coded markers, generated by PhotoScan, were used (see Figure 4.4B). While the PhotoScan 'PS 1.1 Coded Targets and Scale Bars' user manual suggests users keep the central circle below 30 pixels, comparisons between 0.5, 1, 2 and 4 mm radius markers found that although the 0.5 and 1 mm markers met this criteria, they had a lower detection rate than the 2 and 4 mm markers. While it is possible to manually identify markers within the imagery, this would have decreased the positional accuracy of marker locations significantly below that achievable with automatic detection. Consequently, the 2 mm markers were used, which equated to approximately 254-452 pixels per marker. The horizontal distance between all markers was measured with Digital Vernier Calipers (Silverline – 380244). To provide control in the z axis, the vertical distance between pairs of markers on the control frame was also measured. While the manufacturer suggested the calipers had an accuracy of +/- 0.01 mm, in the context of human error, an accuracy of 0.5 mm was assumed to be more realistically attainable.

4.7.3 Lens calibration imagery

A set of calibration imagery was collected for each camera prior to running each group of events, i.e. once for each plot and once for the flume experiments. A flat 'calibration board' was positioned within the control frame during the acquisition of camera calibration photos to provide additional control within the centre of the shot and region of interest, as visible in the centre of Figure 4.5B. The calibration board was configured using a difference selection of the 2 mm radius 12-bit markers, which were placed on a 5 (x) by 6 (y) grid

(n = 30), approximately 60 mm apart. The distances between all adjacent points were measured with the digital calipers, and a subset were converted to coordinates to provide a local coordinate system. As convergent imagery from each camera is particularly important for the calibration of cx and cy lens parameters (Nouwakpo *et al.*, 2014), ca. 30 images of the control frame were collected with each camera, following the configuration presented in Figure 4.5A.

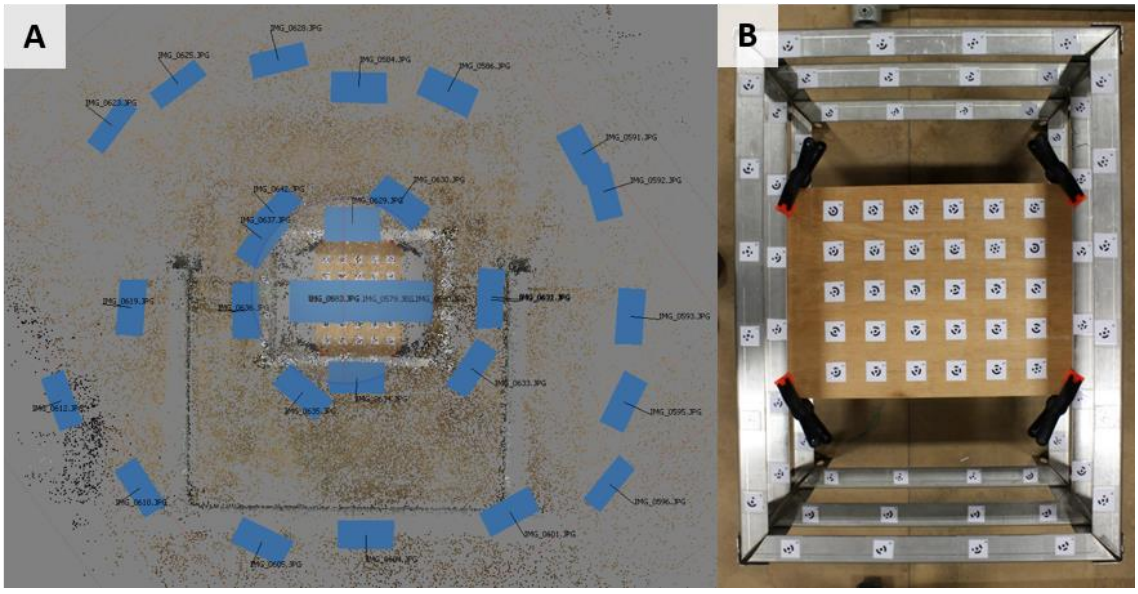

Figure 4.5: a) example geometry of image network surrounding the control frame, and b) the control frame and board used for calibration.

4.7.4 Experimental imagery

Imagery of the soil surfaces were collected immediately before and 1 hour after each experimental run, for both the plot and flume scale experiments. To create a replicable workflow and to reduce the data collection and processing times, the three cameras were mounted 0.18 m apart on a fixed and rigid aluminium bar. The central camera was nadir to the soil surface, and the outer cameras were angled at 13 degrees for the plot scale work and 10 degrees for the flume, consistent with the work of Heng et al. (2010), thus creating 100 % overlap within the area of interest between all cameras. For the plot scale experiments, an imaging station was built, as illustrated in Figure 4.6. Each plot was carefully positioned within the control frame, where the cameras were situated 87 cm above the soil surface, resulting in a GSD of 0.175 mm per pixel. Once in position, all three cameras were triggered simultaneously using a modified remote, and only a single image was collected from each camera for every surface reconstruction.

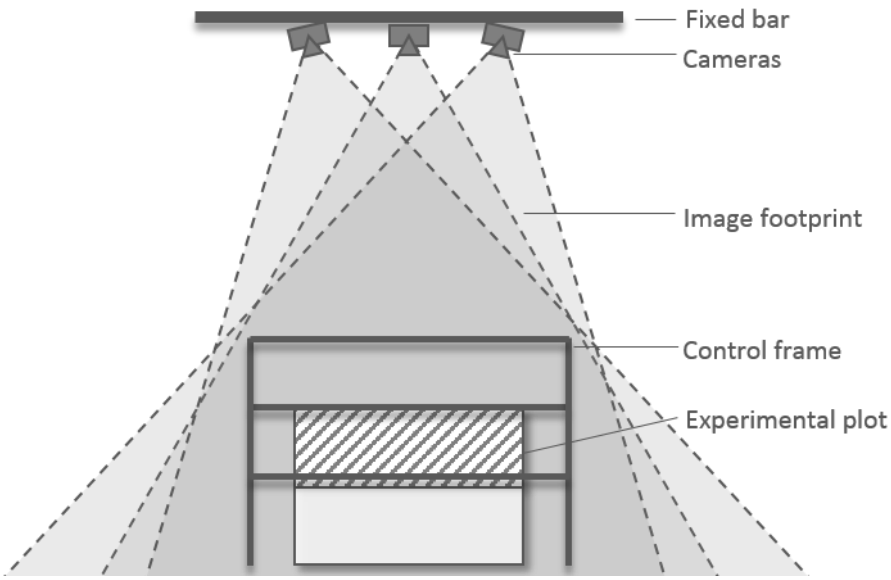

Figure 4.6: Schematic diagram illustrating the set-up of the imaging station used to collect experimental images for the plot scale experiments.

At the flume scale, it was not possible to capture the full soil surface with sufficient overlap and a comparable GSD using a setup similar to the plot scale. The camera bar was therefore mounted 90 cm above the soil surface on a gantry that ran the length of each flume. As visible in Figure 4.7, this created 100 % overlap of the soil surface by all three cameras when triggering the three cameras simultaneously. The gantry was then moved down each flume, collecting imagery from all three cameras on 10 cm intervals, creating ca. 86 % forwards overlap between sequential pairs. A total of 81 images were collected for every surface reconstruction, 27 images per camera, with a mean GSD of 0.21 mm per pixel.

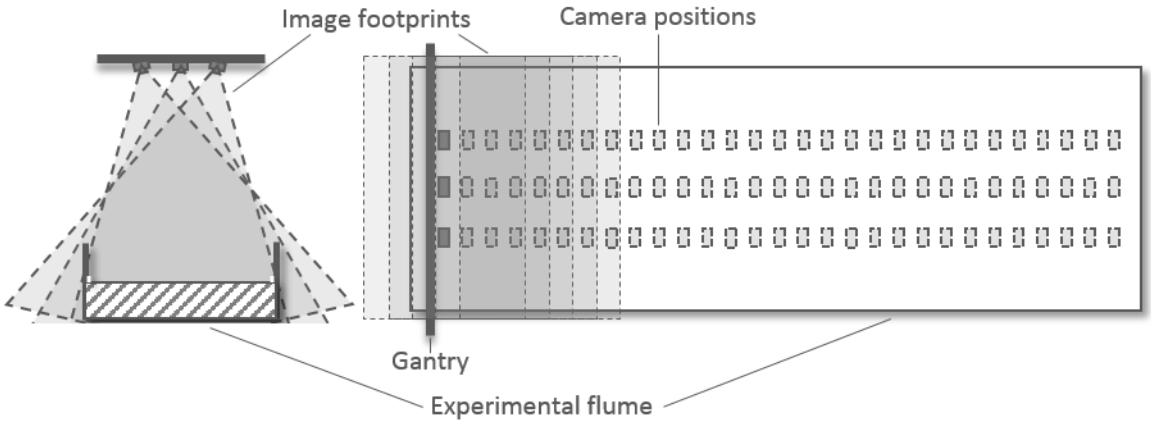

Figure 4.7: Schematic diagram showing the set-up used to collect experimental imagery for the flume scale experiments.

4.7.5 Data processing

Figure 4.8 provides a simple overview of the workflow that was followed for processing the above-described imagery using Agisoft PhotoScan Professional version 1.2.6 (referred to

herein as PhotoScan). Processing was broken into two distinct stages: camera calibration and dense point cloud construction, as detailed in the sections below.

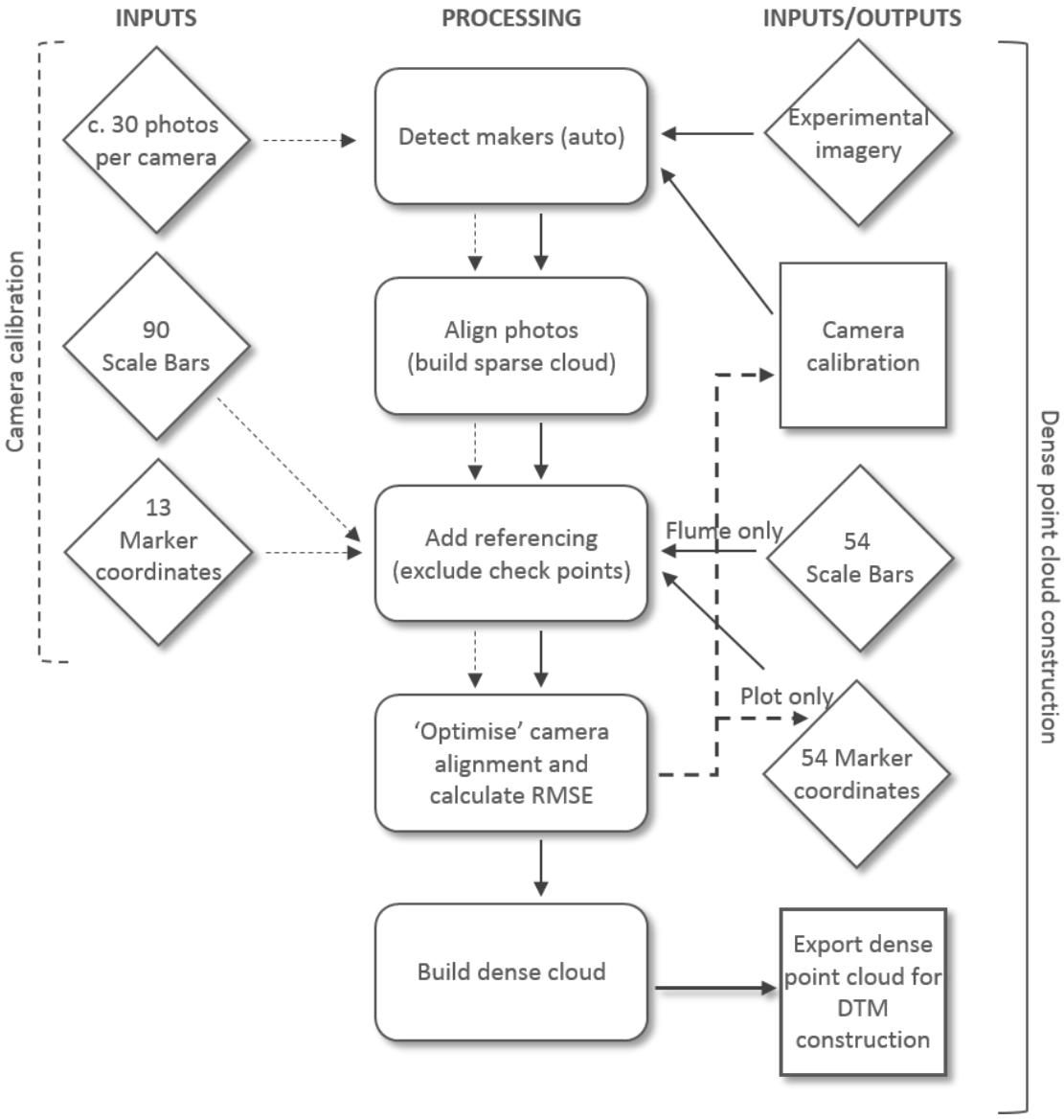

Figure 4.8: Workflow for the production of georeferenced dense point clouds using PhotoScan. Dashed lines indicate the calibration phase, while solid lines the processing for dense point clouds.

4.7.5.1 Camera calibration

For each iteration, the calibration images (described in section 4.7.3) from each camera were loaded into PhotoScan as a single 'chunk', and the images from each of the three cameras were placed into three separate camera calibration groups. The images were then assessed for quality using the PhotoScan 'estimate image quality' tool, and any photo with a quality of less than 0.5 was disabled, per guidance in the 'Agisoft PhotoScan User Manual, Professional Edition, v. 1.2'. The 12-bit markers were then (auto)detected in each of the images using the software's 'Detect Markers' function. SfM was then carried out using the 'Align Photos' function, using the 'high' accuracy setting with no tie point limit set. Any

obviously erroneous point were then removed from the resultant sparse cloud. The distance of 90 scale-bars and the coordinates for 13 markers on the control board were then added using a python script, in the case of the former, to avoid user errors. 10 scale-bars and 5 markers were excluded from the processing for independent error evaluation. The values 'marker accuracy (m)', 'scale bar accuracy (m)', 'marker accuracy (pix)' and 'tie point accuracy (pix)' were adjusted to match the reported values for the 'pix' fields and 0.5 mm for the 'm' fields. 'Optimisation' or bundle adjustment was then carried out using the following internal orientation parameters: cx, cy, k1, k2, k3, b1, b2, p1 and p2. The calibration file for each camera and the estimated coordinates for each marker on the control frame were then exported for use in the dense point cloud construction.

4.7.5.2 SfM MVS processing

The experimental images for each surface were loaded into PhotoScan and grouped according to camera. The camera calibration for each camera was then imported. As above, the 12-bit markers were auto-detected in each image prior to camera alignment and tie point matching. Obviously erroneous points were then removed from the sparse cloud. For the plot scale experiments, the 54 marker coordinates exported from the calibration processing were then loaded and assigned an accuracy of 1 mm. For the flume scale experiments, the scalebar distances between every pair of markers were imported using a python script, which were assigned an accuracy value of 0.5 mm. Any markers (and subsequent scalebars in the case of the flume work) that appeared in only 1 image were removed. To provide an assessment of model accuracy, at the plot scale, all markers present in ≤2 images were used as a check point (12-15), while at the flume scale 15 % of the total number of scalebars were used a checks. Bundle adjustment was then carried out using the following internal orientation parameters: cx, cy, k1, k2, k3, b1, b2, p1 and p2. The bounding box for each area of interest was then checked before dense cloud construction (MVS). Dense clouds were built using mild depth filtering and the 'ultra-high' quality setting for the plot experiments and the 'high' quality setting for the flume experiments. The dense clouds were then exported as an ASCII text file.

5. TESTING A SUITE OF INNOVATIVE SOIL EROSION MONITORING TECHNIQUES

5.1 Overview

This chapter responds to Objective 2: Test a suite of innovative soil erosion monitoring techniques and identifies those best suited to a cost-effective, replicable and robust assessment of soil erosion within laboratory environments. Consequently, this chapter aims to improve the understanding of both the strengths and limitations of Terrestrial Laser Scanning (TLS) and Structure-from-Motion Multi-View Stereo (SfM-MVS) approaches when quantifying soil erosion following simulated rainfall events. This is achieved through first building an understanding of the resolution of information attainable through each technique. DTMs of Difference (DoDs) are then used to assess the ability of each technique to quantify volumetric soil loss in relation to empirical soil loss observations. Through the use of two experimental scales (plot and flume) and varying the hydrological and experimental conditions, this chapter has allowed for exploration of the robustness of TLS and SfM-MVS approaches across common applications and changing magnitudes of soil erosion and spatial complexity.

5.2 Introduction

If global rates of soil erosion continue to exceed rates of soil formation (Montgomery, 2007; Verheijen *et al.*, 2009), there will be serious implications for food security (Pimentel, 2006), increasing pressure on an already fragile climatic system (Regnier *et al.*, 2013). Unfortunately, when using existing data on soil erosion observations alone, it is challenging to build a clear understanding of local, national and global rates of soil loss, due to the large variability within the observed rates (García-Ruiz *et al.*, 2015). Furthermore, it is difficult to ascertain from existing data if the wide range of rates present are reflective of natural variability or an artefact arising from discrepancies between study scales, monitoring techniques and reporting units (as discussed in Chapter 3). While modelling provides an alternative platform for the prediction of national soil erosion rates, robust model development requires validation with sound empirical data collected across a wide range of environmental conditions and study scales (Brazier *et al.*, 2000). There is therefore a real need for a unified approach to the quantification and monitoring of soil erosion, which is suitable for application across varied research needs.

The prevailing methods for quantifying soil erosion empirically can be grouped into three broad categories: tracers, sediment capture and volumetric surveys. Soil tracers, either naturally occurring or artificially applied, are particularly useful for identifying patterns of soil redistribution, and can be used to quantify soil erosion when a stable baseline is available (Guzmán *et al.*, 2013; Quine & Walling, 1991). Both applications require the collection of sediment or spatially distributed soil samples, of which the collection and processing requires a substantial resource investment for applications beyond laboratory plot and field scale assessments (Brazier *et al.*, 2016). Total sediment capture requires the collection of runoff and sediment leaving a known area, and can provide a true measure of soil loss and an understanding of temporal variability (Nearing *et al.*, 1999b; Quinton & Catt, 2004). Due to the resource intensive nature of collecting and analysing all sediment, full sediment capture is only practical in studies with a small spatial or temporal extent i.e. erosion plots (Deasy *et al.*, 2011; Parsons *et al.*, 2006). Volumetric surveys quantify soil loss through the measurement of erosion features' lengths and cross sections, at regular intervals for both lab and field environments (Boardman, 2003; Boardman et al., 1996; Jester & Klik, 2005). In order to reduce the time-resource needed for conducting such studies across multiple fields or regions, some practitioners have adopted an approach of estimating volumes of soil loss and deposition from ground-based or aerial imagery, utilising substantial expertise and experience in the field as quality control (Evans, 1988a; Watson & Evans, 1991). Nevertheless, both existing volumetric approaches are heavily biased towards quantifying visible and convergent erosion features, namely, rills and gullies, and thus potentially underestimate the magnitude of diffuse erosion processes. Accordingly, an argument exists for the development and application of alternative methodologies for the accurate and replicable assessment of soil erosion processes, across a range of spatial scales.

Over the past decade, point cloud based, proximal sensing technologies, Terrestrial Laser Scanning (TLS) and more recently Structure-from-Motion Multi-View Stereo (SfM-MVS) have become popular tools for collecting fine-grain (< 1 m) topographic data (Smith *et al.*, 2015; Telling *et al.*, 2017), and the collection and interpretation of multi-temporal datasets present an exciting alternative to traditional volumetric surveys of soil erosion, suitable for application across a range of spatial extents (Smith & Vericat, 2015; Vericat *et al.*, 2014). TLS platforms utilise time-of-flight return information from high-precision, pulse-based lasers to automatically generate 3D models of surface topography, at user-defined intervals, from

static locations. Often considered the benchmark for collecting point cloud based spatial data (Glendell *et al.*, 2017; James & Robson, 2012; Micheletti *et al.*, 2014), the resolution and quality of information collected via TLS is primarily limited by the equipment capabilities, survey range, surface properties and footprint of the laser (Barneveld *et al.*, 2013; Ouédraogo *et al.*, 2014). Spatial data resulting from SfM-MVS is created through the simultaneous determination of camera extrinsic and intrinsic geometry, and surface structure, through the matching of pixels from consumer-grade camera imagery, and thus also presents a significant reduction in financial outlay (Eltner *et al.*, 2016; Smith *et al.*, 2015). Producing accurate point clouds through SfM-MVS requires careful consideration of the geometric needs of the post-processing steps prior to the collection of raw imagery, the inclusion of reference points to provide scale and orientation, and the need for error analysis (Eltner *et al.*, 2017; James *et al.*, 2017a, 2017b; James & Robson, 2014; Nouwakpo *et al.*, 2014).

To-date, published research provides examples of the successful quantification of large erosion events and features, to centimetre accuracy in field settings and decimetre accuracy at the catchment scale (Castillo *et al.*, 2012; Eltner *et al.*, 2014; Eltner & Baumgart, 2015; Glendell *et al.*, 2017; Kaiser *et al.*, 2014; Ouédraogo *et al.*, 2014; Smith & Vericat, 2015; Vericat *et al.*, 2014). The accuracy and level of change detectable through each technology is dependent on the quality of data acquisition, the survey range (i.e. the distance between the sensor and the soil surface), and the roughness of the surface. For example, the accuracy of TLS has been shown to decrease with increasing surface roughness (Barneveld *et al.*, 2013), and Smith and Vericat (2015) illustrated a linear increase in errors associated with SfM MVS with survey range, for ranges >1 m. While examples of SfM-MVS application in laboratory or similar settings (i.e. survey range <1 m) do exist (Guo *et al.*, 2016; Morgan *et al.*, 2017; Nouwakpo *et al.*, 2014; Prosdocimi *et al.*, 2017), they are arguably immature in their application, and to the authors' knowledge, there are no examples of the quantification of soil erosion via diffuse *and* fluvial pathways, within a controlled laboratory environment. Similarly, while TLS is frequently used as a benchmark to assess the quality of SfM MVS reconstructions, within both field and laboratory settings (Glendell *et al.*, 2017; Morgan *et al.*, 2017), the strengths and limitations of the technique are yet to be fully explored in a controlled setting, where evaluation against actual soil erosion observations can be undertaken.

The following body of work builds on the understanding of the strengths and limitations of TLS and SfM MVS methodologies and identifies which is best suited for a cost-effective, replicable and robust assessment of soil erosion within the laboratory environment. This is achieved through application of TLS and SfM-MVS, in the presence of diffuse and convergent erosion processes, addressing the following objectives:

1. Identify the resolution of information attainable through each technique, under different experimental conditions.
2. Numerically compare the use of point cloud technologies for the volumetric quantification of soil loss.
3. Explore the roles changing soil erosion magnitudes and spatial complexities have on the accuracy of erosion quantification.

5.3 Research methods

5.3.1 Experimental conditions

To compare and contrast the suitability of TLS and SfM MVS, soil erosion events were simulated at two experimental scales, 0.15 m^2 and 3 m^2, referred to herein as 'plot' and 'flume' scale, respectively. For clarity, the each plot or flume has been numbered, and will be referred to henceforth using P2, P3, P4 or P5 for the plots and F1, F2, and F3 for the flumes. The boxes were filled with sandy loams, screened to 6 mm for the plots and 8 mm for the flume, as detailed further in Section 4.4. Each plot or flume was then subject to a series of sequential hydrological events, each designed to produce different erosion processes, as described in Section 4.4.4. To minimise repetition the hydrological events have been coded as E1 for the compaction and rainsplash event, E2 for the sheetwash (or general erosion event, in the case of the flume experiments) and E3 for the plot scale rilling event, which included a single runon source to promote rill development.

5.3.2 Runoff and sediment collection

To test the efficiency of both SfM-MVS and TLS for the identification of volumetric change and the assessment of soil erosion rates, all sediment and runoff leaving the plots and flumes was collected to provide a true reference for soil loss, as detailed in Section 4.5.

5.3.3 TLS point clouds

Each plot was scanned immediately before and 1 hour after each event, from the same location (+/- 1 cm positional accuracy in the location of the TLS system) to ensure the angle of incidence between the laser and soil surface, and scan distance (2 – 2.5 m) was the same for all iterations. The platform and settings used are described in Section 4.6.

5.3.4 SfM-MVS point clouds

For both experimental scales, SfM-MVS point clouds were derived immediately before and 1 hour after each event, using three distinct steps, namely: lens calibration, collection of experimental image data, and SfM-MVS processing in specialised software (see Section 4.7). Three Canon 600D digital SLR cameras with Canon EF-S 18-55 III lenses were used for stages one and two. The image data were then processed within Agisoft PhotoScan Professional version 1.2.6 (referred to herein as PhotoScan).

5.4 Precision and replicability of the SfM-MVS methods

As SfM-MVS relies on the computation of tie-points and camera intrinsic and extrinsic geometry through largely 'black box' software, analysis was carried out to build an understanding of the precision of the methods used for the experiments.

To assess the precision of the automated marker placement, one set of 'calibration imagery' (as described in Section 4.7.3) was processed three times using the same settings. A total of 83 images of the calibration frame and board, collected using the three experimental cameras, were loaded into PhotoScan. The coded markers present within each image were then automatically detected using the software's 'Detect Markers' function. Following tie-point matching and the initial estimation of camera geometry, the coordinates for 13 control points and the scalebar distances between 54 pairs of markers were imported into PhotoScan, using a python-based script in the case of the latter to mitigate operator errors. 'Optimisation' or bundle adjustment was then carried out across the following internal orientation parameters: cx, cy, k1, k2, k3, b1, b2, p1 and p2. The estimated marker coordinates for the remaining 87 markers were then exported and compared using a one-way ANOVA. Despite a relatively high reprojection error (1.18 pix), there was no significant difference between the x, y, and z determined coordinates for all replicates ($F(2,267) = <0.001$, $p = 1.0$).

The RMSE of ground control points (GCPs) can indicate how well the modelled point cloud matches independent validation measurements and RMSE measures are automatically calculated during the bundle adjustment process within PhotoScan. Consequently, the RMSE of GCPs are frequently presented as a metric for reporting the uncertainties associated with SfM-MVS point clouds. As GCPs are also used to provide constraint and scaling during the bundle adjustment processes, a truly valuable understanding of model performance can only be achieved through the RMSE of GCPs kept independent from the

model construction. In PhotoScan, these independent markers are called 'check points' rather than 'control points', and will be referred to herein as such. Check points also provide a platform for interpreting the appropriateness of the precision applied to model parameters, such as those identified as 'marker accuracy' and 'tie point accuracy' in PhotoScan (James *et al.*, 2017a).

As described in Section 4.7.2, a total of 54 GCPs were used for the plot scale experiments and 59 GCPs for the flume experiments, equating to 154 per m^2 and 20 per m^2, respectively. 22- 28% of the GCPs were allocated as check points for the plot scale work. For the flume experiments, the GCPs were used to make scalebars based on the distances between pairs of GCPs, of which 15% were kept independent. The RMSE for both the control and check points for the plot experiments are presented in Table 5.1. Table 5.2 presents the RMSE values for the scalebars used in the flume experiments. Despite taking a standardised approach to SfM-MVS data acquisition and processing, different RMSE values were achieved both across and within each plot or flume, ranging from 0.14 to 0.43 mm for the plot check points, and from 0.13 to 0.27 mm for the flume scalebars.

Table 5.1: RMSE values of the control and check points for each plot SfM-MVS point cloud.

	Reference	RMSE (mm)			
Plot	use	E0	E1	E2	E3
2	Control	0.13	0.15	0.11	0.11
	Check	0.24	0.23	0.14	0.17
3	Control	0.15	0.19	0.15	0.15
	Check	0.32	0.36	0.25	0.27
4	Control	0.12	0.24	0.23	0.28
	Check	0.18	0.33	0.35	0.40
5	Control	0.14	0.15	0.13	0.28
	Check	0.16	0.16	0.16	0.43

Table 5.2: RMSE values of the control and check scalebars for each flume SfM-MVS point cloud.

	Reference	RMSE (mm)		
Flume	use	E0	E1	E2
1	Control	0.14	0.16	0.16
	Check	0.13	0.16	0.13
2	Control	0.14	0.15	0.13
	Check	0.13	0.17	0.18
3	Control	0.17	0.21	0.36
	Check	0.18	0.15	0.27

The RMSE of the check points was consistently higher than that of the control points for the plot experiments, suggesting that the precision values used for the control points could have been increased to allow the photogrammetry to have a greater influence over the model

construction. This is not an uncommon, if rarely reported, situation based on values in the literature and further highlights the need for reporting full GCP RMSE information for better transparency in the presentation of model quality/precision (James *et al.*, 2017a; Smith & Vericat, 2015). It is important to note that when the RMSE values are transformed into relative precision ratios, where RMSE values are calculated relative to survey range (James & Robson, 2012), the values gained from this experiment ranged from 1:2000 to 1:6200, and fell well below the ranges achieved within existing studies (Smith *et al.*, 2015). Consequently, it was decided, however, that the RMSE achieved for these experiments was sufficient to meet the aims of the study. For further transparency, a detailed breakdown of the errors calculated for the plot SfM-MVS point clouds are provided in Supplementary Table 8.2 and Table 8.3.

Whilst the RMSE of check points is a common approach to reporting uncertainties associated with SfM MVS point clouds (Eltner *et al.*, 2016; Smith *et al.*, 2015), it doesn't provide detailed information on the spatial distribution of precision within the SfM-MVS model. To this end, James et al. (2017b) present a unique methodology for assessing the 3 dimensional precision of SfM tie points, through implementing a Monte Carlo-based approach to the bundle adjustment process. This method of precision analysis is particularly useful when studies have a large spatial extent and GCP placement is limited, and when the survey area has numerous artefacts, such as variable vegetation cover and complex terrain. For laboratory scale experiments, the analysis provides an understanding of the variability within the area of interest (AOI), where GCP distribution is often restricted by the experimental design. Accordingly, to provide a more thorough review on the performance of the SfM-MVS approach adopted, the precision analysis presented by James et al. (2017b) was trialled for two plot scale surface models and one of the flume surface models.

The precision of the models was determined through 4000 Monte Carlo iterations, and based on the sparse point clouds produced by PhotoScan. P5E2 and P5E3 were selected to capture the full range of precision values within the plot scale models. Table 5.3 presents the properties of the models used and the estimated dimensionless precision for each to provide a platform for comparisons of model quality. The 'georeferenced' values take into consideration the georeferencing included in the model i.e. the GCPs, while the 'shape only' values indicate the performance of photogrammetric element of the model, irrespective of the precision of the GCPs. Of the plot scale results, P5E2 had the highest precision, which is

consistent with the relationship between the two models' check point RMSE values. Whilst the range of the georeferenced precision was comparable to the check point RMSE values for the plots, the results suggest the check point RMSE slightly under-estimate the error within the P5E2 model, while over-estimating the P5E3 error. The 'shape only' precision was better than the georeferenced precision and ranged from 1:7050 to 1:11200, suggesting the photogrammetric approach taken was strong, but limited by GCP precision. For the flume scale model, the 'georeferenced' precision calculated by the precision analysis does not necessarily reflect true georeferenced precision, as the model was referenced using 2 dimensional scalebars rather than georeferenced GCPs. The 'shape only' precision however, suggests that the overall model precision was in line with that of P5E2. In all instances, the greatest error was in the 'z' axis, consistent with James et al. (2017b). Figure 8.1, Figure 8.2 and Figure 8.4 in the Supplementary Material provides the full reports for transparency.

Table 5.3: Properties and results for the models used for the precision analysis.

				Dimensionless precision	
Model	Number of points	Check point RMSE (mm)	Dimensionless RMSE	'Georeferenced' RMSE	'Shape only' RMSE
P5E2	6428	0.16	1:5500	1:3760	1:11200
P5E3	7049	0.43	1:2140	1:3220	1:7050
F2E2	31265	0.17	1:5222	1:1040	1:10500

To understand if there were any spatial trends in point precision, Figure 5.1 and Figure 5.2 were constructed and present the spatial distribution of the 'z' axis precision for each model, based on the mean precision within a 5 and 10 mm grid cell, for the plot and flume assessments, respectively, interpolated using Surfer. Precision increased slightly in the centre of the AOI for both the plot and the flume georeferenced precision models. However, for the plot scale 'shape only' precision estimates, there wasn't any spatial pattern in the results, and decreases in precision were not associated with any physical features within the plots (Figure 5.1). The 'shape only' precision decreased at either end of the flume where the amount of image overlap was the smallest, consistent with the edge effects found with UAV surveys (James & Robson, 2014)(Figure 5.2B).

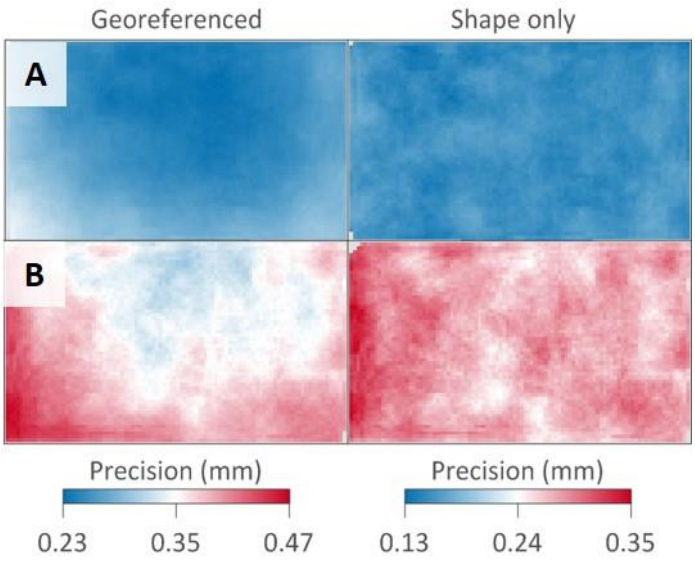

Figure 5.1: 'z' axis precision for A) P5E2 and B) P5E3, based on the mean precision of the tie points within in a 5 mm grid cell.

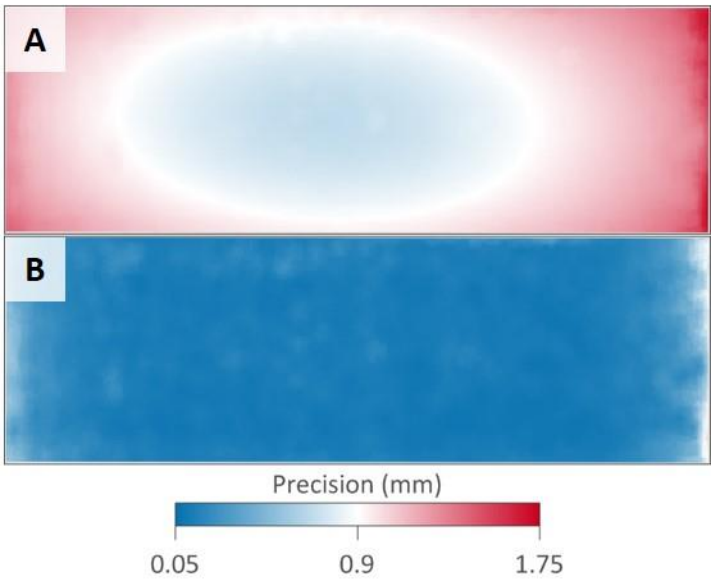

Figure 5.2: 'z' axis precision for F2E2 A) georeferenced and B) shape only, based on the mean precision of the tie points within in a 10 mm grid cell.

5.5 Predicting volumes of soil loss

The final point clouds, from both platforms, were loaded into CloudCompare version 2.6.1 (http://www.danielgm.net/cc/) for cropping and co-registration. While examples within SfM-MVS literature have used CloudCompare's iterative closest point function to co-register datasets (Glendell *et al.*, 2017), when compared to manually selecting matching pairs of points, it was found that the former lead to RMSE values at least an order of magnitude greater than the latter. Consequently, 6 – 8 pairs of stable matching points were selected to align each point cloud with the point cloud for the first time-step for each plot or flume. For the SfM-MVS point clouds the centre of the coded markers positioned on the perimeter of

each plot and flume (visible in Figure 4.1) were used. For the TLS clouds, the six 35 mm, white balls positioned on the perimeter of each plot were used for co-registration. Following co-registration the point clouds were trimmed to the perimeter of the soil surface to avoid including artefacts in the calculations. All iterations of each plot or flume were then trimmed simultaneously, to eliminate discrepancies in the final cloud size and shape.

The co-registered point cloud data were then interpolated into Digital Terrain Models (DTMs), using the 'gridding' function within Surfer (Golden Software LLC, version 13.5). Kriging was selected as the method for interpolation, which the software implements with a combination of weighted averaging (i.e. the point closest to the grid node has more weight in determining the z value) and exact interpolation, when the grid point hits a raw data point, using a linear variogram. To test the impact of DTM resolution on the accuracy of volumetric calculations, DTMs were constructed at 5, 10 and 20 mm resolution for the TLS point cloud data, and at a 0.5, 2, 5, 10 and 20 mm resolution for the SfM-MVS point cloud data, for the plot scale experiments. All flume point cloud data were processed to produce DTMs at 5 mm resolution.

The predicted volume of soil loss was then calculated as the volumetric difference between sequential DTMs, following the creation of DTMs of Difference (DoD) for each pair within a plot or flume experimental series, using Surfer's 'Grid>Math' function. As an example, the most basic forms of the TLS- and SfM-MVS-based DoD, where only the elevation changes between the DTMs were calculated, are illustrated in Figure 5.3A and B. However, to ensure that changes between DTM pairs were significant, sources of error were combined to determine a cell-by-cell minimum 'level of detection' (LoD), consistent with the approach of Smith & Vericat (2015) following the work of Brasington et al. (2003) Lane et al. (2003) and Wheaton et al. (2010)**.** Three potential sources of error were identified for the volumetric calculations: within the point clouds, the interpolation into DTMs and the co-registration of pairs of point clouds. For the TLS data, the error within the point clouds was calculated using the 3D positional accuracy supplied with the equipment i.e. 3 mm. The error associated with the SfM MVS point clouds were calculated using the RMSE of check points for the plot scale experiments and the error associated with the check scalebars at the flume scale (see Table 5.1 and Table 5.2). To quantify the error associated with the interpolation of the DTMs, the standard deviation of the elevation (σ_z) for all points within each grid cell was calculated using Surfer's 'Z moment Statistics' function, which was then translated into a grid

representing the cell-by-cell information. Finally, the registration error was considered to be the RMSE of the matching pairs described above, as calculated by CloudCompare. The LoD was calculated for each DoD using Equation 5.1, which builds on the LoD equation presented by Lane et al. (2003):

$$LoD_i = \pm t\,[\varepsilon_{PC1}^2 + \varepsilon_{DTM1i}^2 + \varepsilon_{PC2}^2 + \varepsilon_{DTM2i}^2 + \varepsilon_{REG}^2]^{1/2}$$

Equation 5.1: Level of Detection for volumetric estimations between point clouds.

Where, LoD_i is the LoD for the *i*th grid cell, *t* is the critical t value for the given confidence interval and ε is the error associated with each metric. DTM error was the σ_z for the *i*th grid cell in each DTM, i.e. DTM_1 and DTM_2. Point cloud error for each cloud (i.e. PC_1 and PC_2) was applied uniformly across the surface for both the TLS and SfM-MVS data, as the TLS error is inherent to the equipment and the analysis carried out in Section 5.4 did not reveal any significant spatial trends in the precision of the experimental tie points (Figure 5.1). Co-registration error (*REG*) was also assumed to be uniform, and consequently a single value was used for the entire DoD. In this instance, a confidence interval of 95% was used (t = 1.96), and the LoD was used to filter any change in the DoD that was less than the LoD for that particular pair of cells i.e. if the change detected was -15 mm and the LoD was ±2 mm, the change calculated was -13 mm, and any changes less than ±2 mm were discarded (based on a dimensionless calculation of change). Figure 5.3 has examples of the cell-by-cell calculated LoD for a 5 mm resolution SfM-MVS DoD (Figure 5.3C) and a 5 mm resolution TLS DoD (Figure 5.3D), where the greatest uncertainty is visible along the edge of the rill.

The LoD was implemented using Surfer's 'Grid>Math' function through the following nested 'if' logical expression:

$$PV_i = If\begin{bmatrix} LoD_i > ((DTM_{2i} - DTM_{1i})^2)^{\frac{1}{2}}, \\ TRUE = 0, \\ FALSE = If\begin{bmatrix} (DTM_{2i} - DTM_{1i}) < 0, \\ TRUE = (DTM_{2i} - DTM_{1i} + LoD_i), \\ FALSE = (DTM_{2i} - DTM_{1i} - LoD_i) \end{bmatrix} \end{bmatrix}$$

Equation 5.2: Nested if logic for determining predicted volume change using LoD.

Where, PV_i is the predicted volume change for the *i*th grid cell, LoD_i is the level of detection for the *i*th grid cell as defined in Equation 5.1, DTM_{2i} is the elevation for the *i*th grid cell for the 'after' surface and DTM_{1i} is the elevation for the *i*th grid cell for the 'before' surface. Supplementary Material Figure 8.5 presents a full description and functional translation of the expression, for use in Surfer v. 13.5. The process creates a DoD (Figure 5.3E and F) whereby volume change can then calculated using a 'z' = 0 grid. The trapezoidal rule is used

to determine areas of positive (cut) and negative (fill) change, and the predicted volume of soil loss for each event was assumed to be the difference between the two.

To provide a metric for the overall performance the predicted volume change of each technique versus the observed soil loss, the volume measurement error was quantified using Equation 5.3 (Castillo *et al.*, 2012; Glendell *et al.*, 2017). Where E_v is the relative volume measurement error (%), V_p the volume of soil loss predicted using the technique (cm^3), and V_o is the observed volume of soil loss calculated using the mass of exported sediment (cm^3).

$$E_V = \frac{(V_p - V_o)}{V_o} \times 100$$

Equation 5.3: Volume measurement error (%)

To identify significant differences between predictions at different grid resolutions, a non-parametric Independent-Samples Kruskal-Wallis rank sum test was utilised, followed by a pairwise Dunn's test. A critical value of $p \leq 0.05$ was used for statistical significance for the Kruskal-Wallis rank sum tests and a $p \leq \alpha/2$ (i.e. 0.025) for the post hoc Dunn's tests.

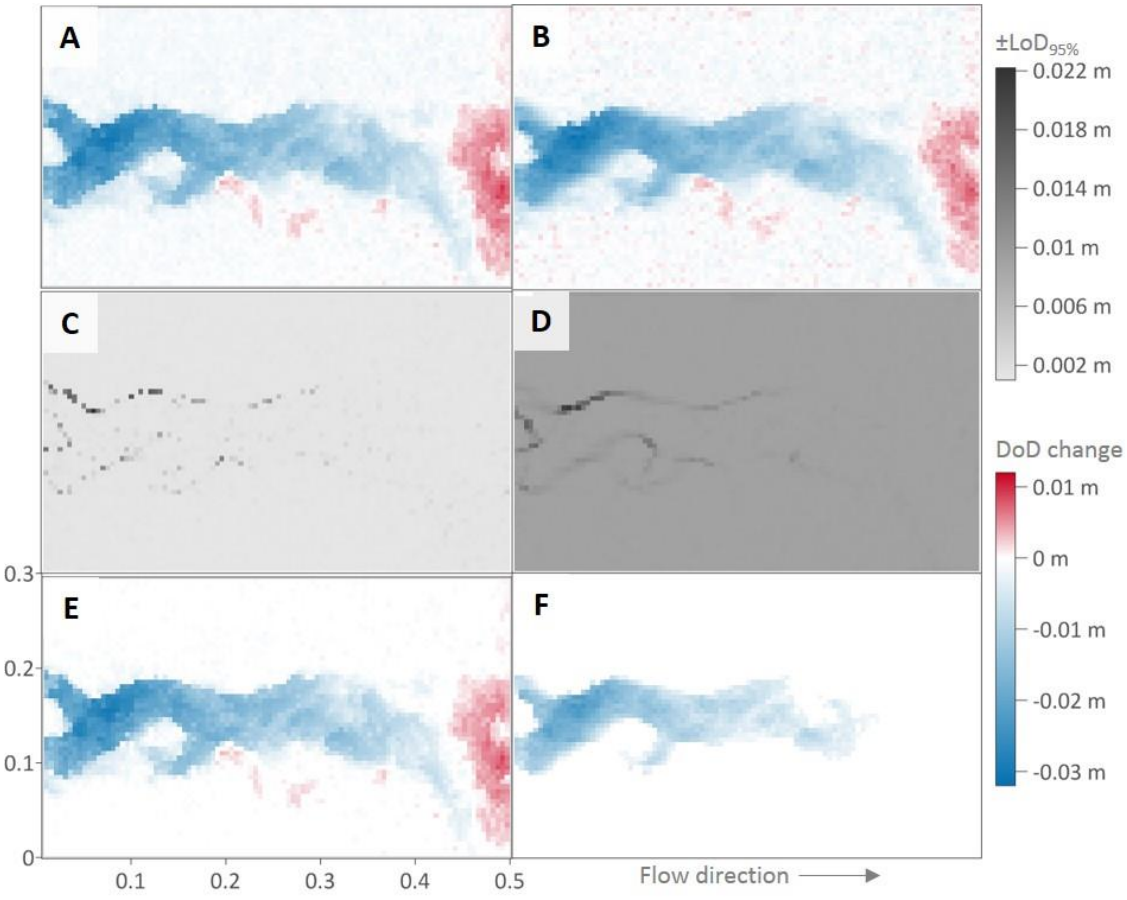

Figure 5.3: Illustration of the application of a cell-by-cell LoD to the prediction of elevation change for P5E3, where, A) and B) are the original DoDs processed from SfM-MVS and TLS point clouds, respectively, C) and D) are the 95% confidence intervals LoD for the SfM-MVS and TLS DoDs, respectively, and E) and F) are the LoD filtered DoDs for the SfM-MVS and TLS clouds, respectively.

5.6 Results

5.6.1 Sediment yields

The sediment yield across the plot and flume scale experiments ranged between 14.59 g and 5705.6 g per event, which is equivalent to volume changes between 11.2 to 4075.4 cm^3 (Table 5.4). At the plot scale, total sediment yield ranged between 14.59 and 31.3 g for E2, and 274.58 and 714.37 g for E3. For the E3 events, this equated to a calculated maximum volume change of 549.5 cm^3 on P2 and a minimum change of 274.58 cm^3 for P3, which related to the duration of the experiments. For the E2 events, the largest calculated change was 24.1 cm^3, for P4, which when averaged over the area of the plot equates to a mean denudation of 0.016 cm. There was no visual evidence of rilling or nick-point formation during all plot scale E2 experiments, consistent with sheetwash erosion being the dominant erosion process (as visible in Figure 5.8A-C). In all instances, the addition of a runoff source (E3) led to the formation of a rill feature and soil loss an order of magnitude greater than E2 (Figure 5.8A-C). The total sediment yield from the flume experiments ranged from 2715.3 g on F1 and 5705.6 g F2, or 1939.5 and 4075.4 cm^3, which is consistent with higher rainfall intensity present over F2.

Table 5.4: Summary of sediment collected (g) during each plot and flume experimental run and the calculated volume (cm^3) based on ρb 1.3 g cm^{-3}.

	E1		E2		E3	
Plot	Sediment (g)	Volume (cm^3)	Sediment (g)	Volume (cm^3)	Sediment (g)	Volume (cm^3)
P2	0	-	14.59	11.2	714.37	549.5
P3	0	-	22.48	17.3	274.58	211.2
P4	0	-	31.3	24.1	507.09	390.1
P5	0	-	25.22	21.0	589.21	491.0
Flume						
F1	0	-	2715.3	1939.5		
F2	0	-	5705.6	4075.4		
F3	0	-	3914.1	2795.8		

5.6.2 Plot experiments

5.6.2.1 Terrestrial Laser Scanning

The TLS mean point density was 359 per cm^2 and the mean GSD was 0.53 mm/pixel, over the surface area of the plots. DoDs were produced for E2 and E3 at 5, 10 and 20 mm resolution, which were used to predict the volumes of change reported in Table 5.5. In all instances the LoD was greater than the elevation change detected following the sheetwash event (E2), resulting in zero soil loss being predicted. For E3, volumetric predictions ranged

from a minimum of 72.9 cm^3 on P3 to a maximum of 346.4 cm^3 on P2, both were predicted with the 20 mm resolution DoD. There was no significant difference between the volumes predicted with the 5, 10 and 20 mm grids (p = 0.99).

Table 5.5: Summary table showing the point density of the raw TLS point clouds and the volume of change predicted (cm^3) following each experimental run at 5, 10 and 20 mm resolution. The calculated volume of observed sediment loss is included for reference.

Event	Plot	Point density (points/cm^2)	Sediment volume (cm^3)	Predicted soil loss detected at DoD resolution (cm^3)		
				5 mm	10 mm	20 mm
E2	P2	360	11.2	0	0	0
	P3	360	17.3	0	0	0
	P4	357	24.1	0	0	0
	P5	355	19.4	0	0	0
E3	P2	354	549.5	344.7	339.3	346.4
	P3	356	211.2	76.2	75.7	72.9
	P4	352	390.1	183.2	180.5	167.5
	P5	349	453.2	187.9	188.3	175.8

The volume of soil loss predicted for E3 using the TLS point clouds was less than the observed volume for all plots (Figure 5.4A). As the LoDs for the sheetwash experiment (E2) were greater than the elevations changes detected, the mean relative measurement error was -100% for all plots. With the exception of P2E3, the 5 mm DoD had the lowest relative measurement error, while the 20 mm DoDs had the greatest measurement error. The relative measurement error for the 5 mm rilling event (E3) DoDs ranged between -37 and -64%. There was, however, a positive linear correlation between the predicted and observed volumes of soil loss following E3 (R^2 = 0.8877, based on 5 mm resolution, where n = 4), as visible in Figure 5.4B.

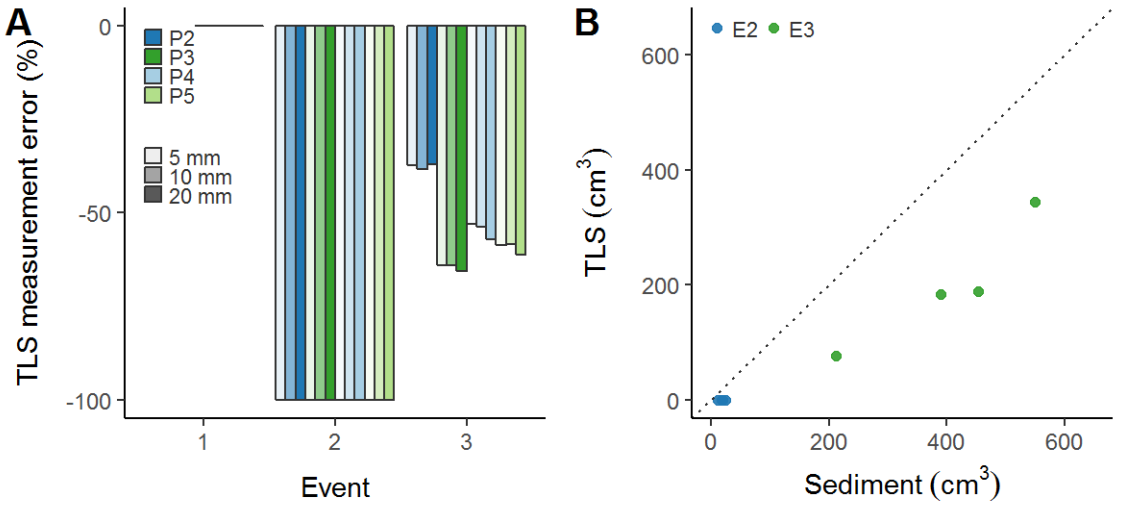

Figure 5.4: Graphical illustration of the distribution of results for the TLS predictions, showing A) the TLS relative measurement error (%) for all grid resolutions, and B) the relationship between the TLS predictions from a 5 mm DoD and sediment observations (cm3), where the dotted line represents a 1:1 relationship.

Any possible positive changes in surface elevation resulting from sediment deposition, as visible in Figure 5.3B, were filtered out by the LoD. Decreases in elevation resulting from sheetwash, which was visible during E2 and E3 across all plots throughout the experiments, were not quantified with any of the TLS DoDs. As a result, the predictions of volumetric changes were limited to soil loss from within the rill features, across all plots and DoD resolutions, as shown in Figure 5.5 and Figure 5.6. Based on the 5 mm resolution DoD, the greatest depth of elevation change, and therefore soil loss from within a rill, was 4.4 cm on P2, while P5 had the shallowest rill feature detected (2.4 cm). Detail on the complexity of the structure of the rill formation was reduced with increasing grid cell resolutions, however, the overall shape could still be resolved from the 20 mm DoDs (Figure 5.6). The soil surface microtopography could not be resolved using the even the most fine resolution TLS-based DTM, or DoD, as visible in Figure 5.5.

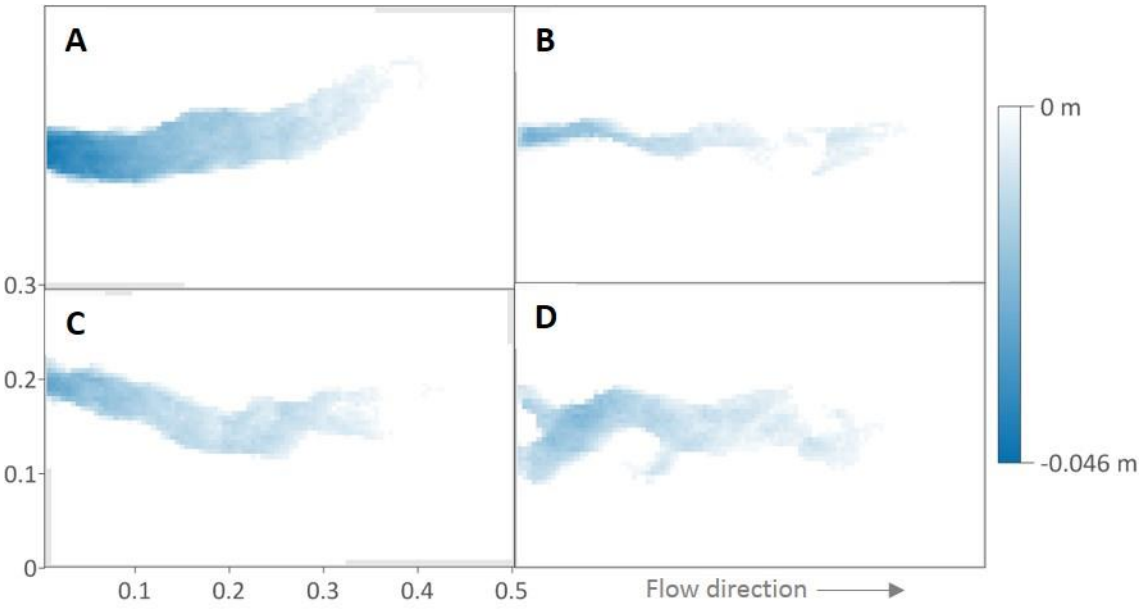

Figure 5.5: 5 mm resolution DoD showing changes in surface elevation following the rilling event (E3), for Plot 2 (A), Plot 3 (B), Plot 4 (C), and Plot 5(D). White represents areas with zero change detected.

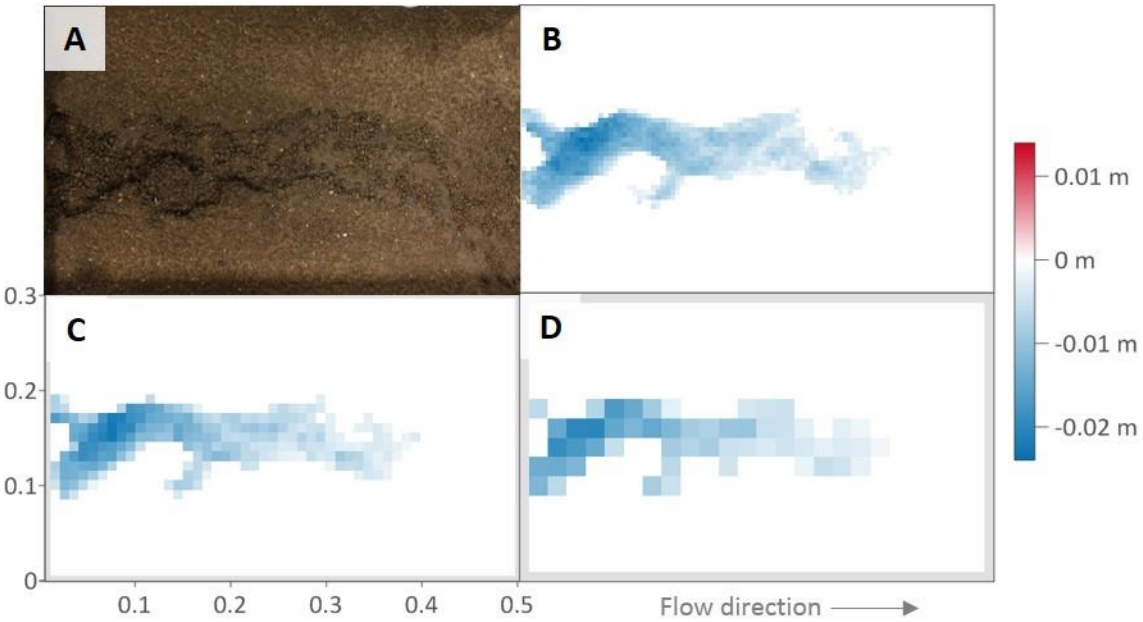

Figure 5.6: A true colour photo of P5 following E3 (A) and DoDs for the same at the following grid resolutions B) 5 mm and C) 10 mm and D) 20 mm. White represents areas with zero change detected.

5.6.2.2 Structure-from-Motion Multi-view Stereo

The mean point density of the SfM-MVS clouds was 3496 points per cm^2 and the mean GSD was 0.17 mm/pixel. The point clouds were interpolated into 0.5, 2, 5, 10 and 20 mm DTMs to create the DoDs for the prediction of changes in surface elevation following E1, E2 and E3. The predicted volumes of soil loss, for all iterations, are listed in Table 5.6, and examples of the DoDs are provided in Figure 5.8 and Figure 5.9. The SfM-MVS approach detected changes in the surface elevation across all plots and grid resolutions. The minimum change predicted was 81.0 cm^3, which was for P5E1 at 20 mm grid resolution, and 647.2 cm^3 for P2E3 at 2 mm resolution, was the greatest predicted volume of change. The predicted soil loss for the rainsplash and compaction events (E1) ranged from a minimum of 81.0 cm^3 (P5 – 20 mm resolution) to a maximum of 152.3 cm^3 (P3 – 0.5 mm resolution). Following the sheetwash experiment (E2), the SfM-MVS approach predicted volumetric changes ranging between 92.6 cm^3 (P5 – 0.5 mm) and 303.7 cm^3 (P4 – 0.5 mm). The predicted volume of soil loss ranged from 257.3 (P3 – 2mm) to 647.3 cm^3 (P2 – 2mm) for the rilling experiments (E3). There was no significant difference between the volumes predicted for all grid resolutions ($p = 0.99$).

Table 5.6: Summary table showing the point density of the raw SfM-MVS point clouds and predicted volume of soil loss for each event, at 0.5, 2, 5, 10 and 20 mm grid resolutions. The calculated volume of observed sediment loss is included for reference.

Event	Plot	Point density (points/cm^2)	Sediment volume (cm^3)	Predicted soil loss at DoD resolution (cm3)				
				0.5 mm	2 mm	5 mm	10 mm	20 mm
E1	P2	3562	-	128.2	127.9	128.6	128.1	125.2
	P3	3540	-	152.3	151.1	149.6	145.0	135.7
	P4	3491	-	98.9	98.7	99.5	99.9	98.1
	P5	3556	-	85.9	85.9	85.3	85.5	81.0
E2	P2	3528	11.2	218.4	218.6	218.3	219.1	215.6
	P3	3494	17.3	103.4	103.4	103.5	102.6	103.8
	P4	3490	24.1	303.7	303.7	303.2	297.9	299.7
	P5	3470	19.4	92.6	92.7	93.5	92.8	95.0
E3	P2	3596	549.5	646.7	647.2	644.1	631.0	635.0
	P3	3552	211.2	258.3	257.3	259.8	263.6	260.1
	P4	3539	390.1	386.4	386.9	383.0	378.2	375.0
	P5	3592	453.2	393.7	394.2	393.4	389.0	370.1

The predicted volume of soil loss calculated by SfM-MVS was greater than the observed amount in all instances, for both the compaction and rainsplash events (E1) and the sheetwash events (E2), as shown in Figure 5.7. The relative measurement error was, however, an order of magnitude less for E1, which ranged from 86 to 152% for the 0.5 mm DoD. The relative measurement error was the greatest for E2, which ranged from 377 to 1850% for the 0.5 mm DoD (Figure 5.7A). The predicted volume of soil loss for the rilling experiment had the lowest range of measurement error (ranging between -1 and 22%, for the 0.5 mm DoD). Whilst increasing predicted volume of soil loss did not correlated with increases in observed volumes for E2, the predicted volumes of soil loss for the E3 events were correlated with observed volumes ($R^2 = 0.83$, n = 4) as visible in Figure 5.7B.

The maximum negative elevation changes resolved by the SfM-MVS DoDs for 'rainsplash and compaction' (E1) and 'sheetwash' (E2) experiments ranged from -3.6 to -5.5 mm and -3.9 to -7 mm, respectively, based on the 0.5 mm DoDs shown in Figure 5.8. The maximum rilling depth identified was 5.45 cm on P2, which was the longest running rilling event, while the minimum rill depth was 3.22 cm, for P5. There were areas of positive surface elevation change also detected for all plots following E3. These ranged from a minimum increase of 5 mm on P3 to a maximum of 9.2 mm on P5. The most significant areas of positive elevation change resulted from areas of sediment deposition from the primary rilling feature (Figure 5.9 and Figure 5.8).

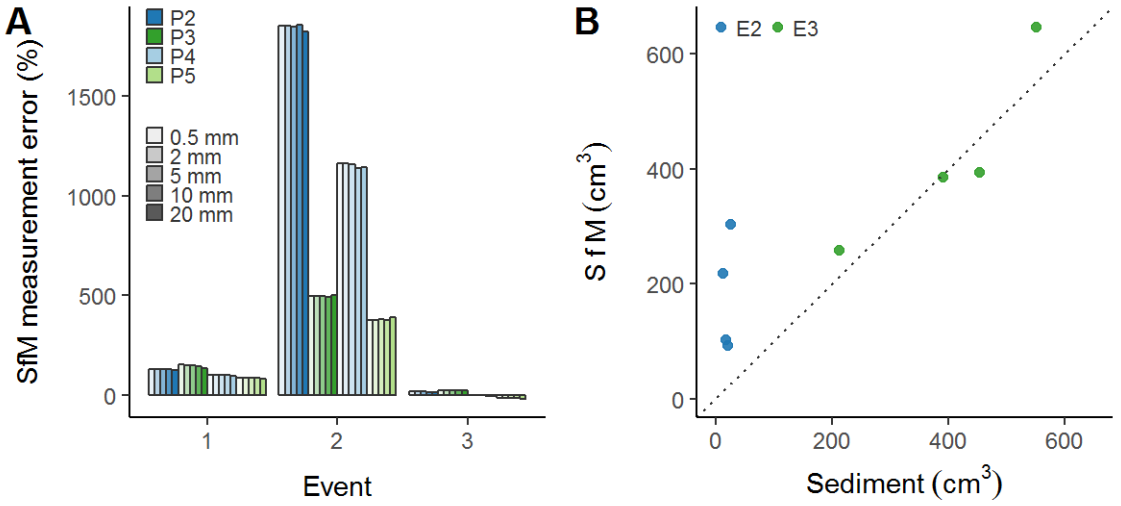

Figure 5.7: Graphical illustration of the distribution of results for the SfM-MVS predictions, showing A) the SfM-MVS relative measurement error (%) for all grid resolutions, and B) the relationship between the SfM-MVS predictions from a 0.5 mm DoD and sediment observations (cm^3), where the dotted line represents a 1:1 relationship.

The SfM-MVS derived DoD could be used to visually identify patterns and changes in the surface structure following the different events. Smaller depositional features, such as a secondary area of deposition located 0.2 m from the top of P5E3, associated with a depositional area from earlier in the evolution of the central rill, could be identified using the 0.5, 2, 5 and 10 mm DoDs as visible in Figure 5.9 and Figure 5.8F. The elevation changes predicted for the sheetwash and rilling experiments could be used to resolve the features visible in the raw imagery. This included the lowering of the soil surface around aggregates during E2 and the presence of large aggregates in the bottom of the rill, as visible in Figure 5.8E and F.

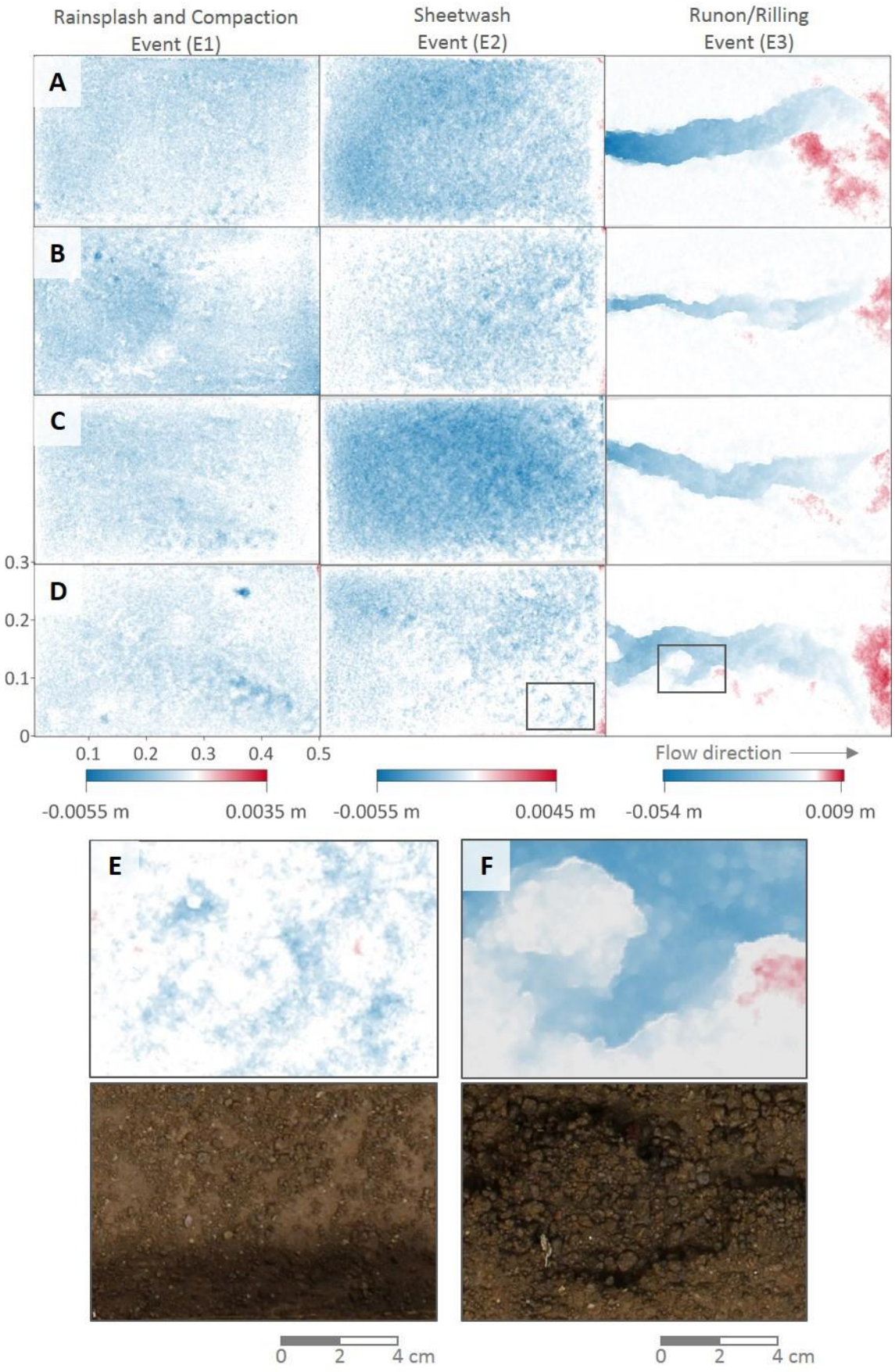

Figure 5.8: 0.5 mm resolution DoD showing changes in surface elevation following E1, E2 and E3, for Plot 2 (A), Plot 3 (B), Plot 4 (C), and Plot 5(D). E) and F) show the same DoD and the original nadir image for the areas identified in D. Where, white represents areas with zero elevation change, blue indicates areas of elevation decreases and red areas of increased surface elevation.

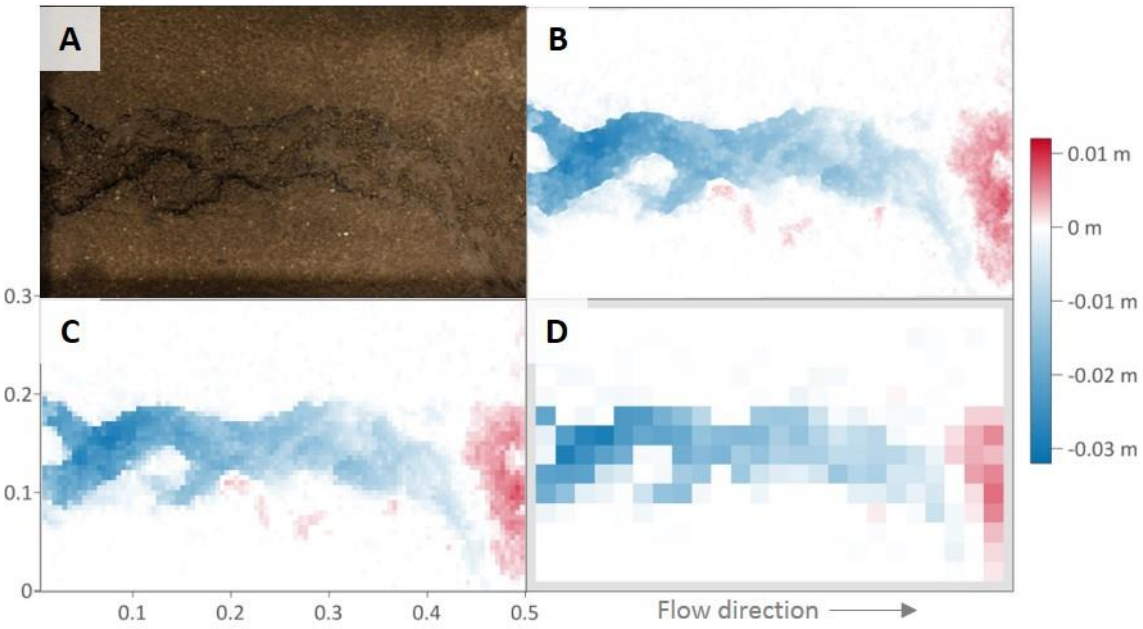

Figure 5.9: A) True colour SfM-MVS point cloud of Plot 5, after the rilling event (E3), and DoD for surface elevation change between E2 and E3, after application of LoD, at B) 0.5 mm, C) 5 mm, and D) 20 mm grid resolution. Where, white represents areas with zero elevation change, blue indicates areas of elevation decreases and red areas of increased surface elevation.

5.6.3 Flume experiments

At the flume scale, the mean point density was 803 points per cm^2 and the mean GSD was 0.21 mm/pixel. 5 mm resolution DoDs were created for each event and compared to the calculated volume of sediment, as listed in Table 5.7. The change in surface elevation from the rainsplash and compaction event (E1) ranged between an increase of 2.4 cm^3 on F2 to decrease of 292.1 cm^3 on F3, and was thus not related to the rainfall intensity. The volume of change detected following E2, when the plot was raised to a 9 % gradient, ranged between a maximum of 6591.2 cm^3 on F1 and a minimum of 1762.4 cm^3 on F3, which was again not related the intensity of the rainfall. However, based on the volume calculated from the sediment, the error was also the highest for F1E2, equating to an over-estimation of soil loss by over 240 %. The DoD calculation was the closest to the volume of sediment for F2, which had an error of -25 %.

Table 5.7: Summary table showing the point density of the SfM-MVS point clouds and the volume of change detected following each experimental run based on 5 mm DoD. Error is the relationship between sediment and DoD calculations.

Event	Flume	Point density (points/cm^2)	Volume of soil loss (cm^3)		Measurement error (%)
			Sediment	SfM Predicted	
E1	1	791	-	196.8	100
	2	775	-	+2.4	100
	3	808	-	292.1	100
E2	1	821	1939.5	6591.2	240
	2	825	4075.4	3073.9	-25
	3	824	2795.8	1762.4	-37

Figure 5.10A is a screen capture of the dense SfM-MVS point cloud of the soil surface in F2 following E2, and illustrates the level of detail present within the SfM-MVS point cloud, while Figure 5.10B is the 5 mm DoD interpolated from the point cloud. The DoD captured the features visually identified within the soil surface, including the formation of small rills up to 1.25 cm in depth and the deposition feature at the exit of the flume, showing accumulations of soil up to 1 cm in depth. In contrast, while Figure 5.11A clearly illustrates the level of detail present within the point cloud for F1 following E2, the bulk of the changes in surfaces elevation identified with the 5 mm DoD in Figure 5.11B, are not consistent with the features visibly present. Visual inspection of the aligned surfaces revealed an inverse 'doming' of the F1E2 surface, despite all surfaces being processed with the same workflow. Nevertheless, the DoD does capture the depositional area some of the small rills observed, and the protective barrier created by a strut 6 cm below the soil surface (c. 1 m from the left-hand side) in the flume. Furthermore, despite the inverse doming of the E2 surface, which should have resulted in the elevation changes being underestimated throughout the centre of the flume, there were some areas of positive or zero elevation change, which indicates that swelling of the soil resulted in elevation changes greater than the magnitude of the doming. The strip of lowering visible at the upper end of both flumes is an artefact related to large droplets forming on the equipment used to capture the imagery.

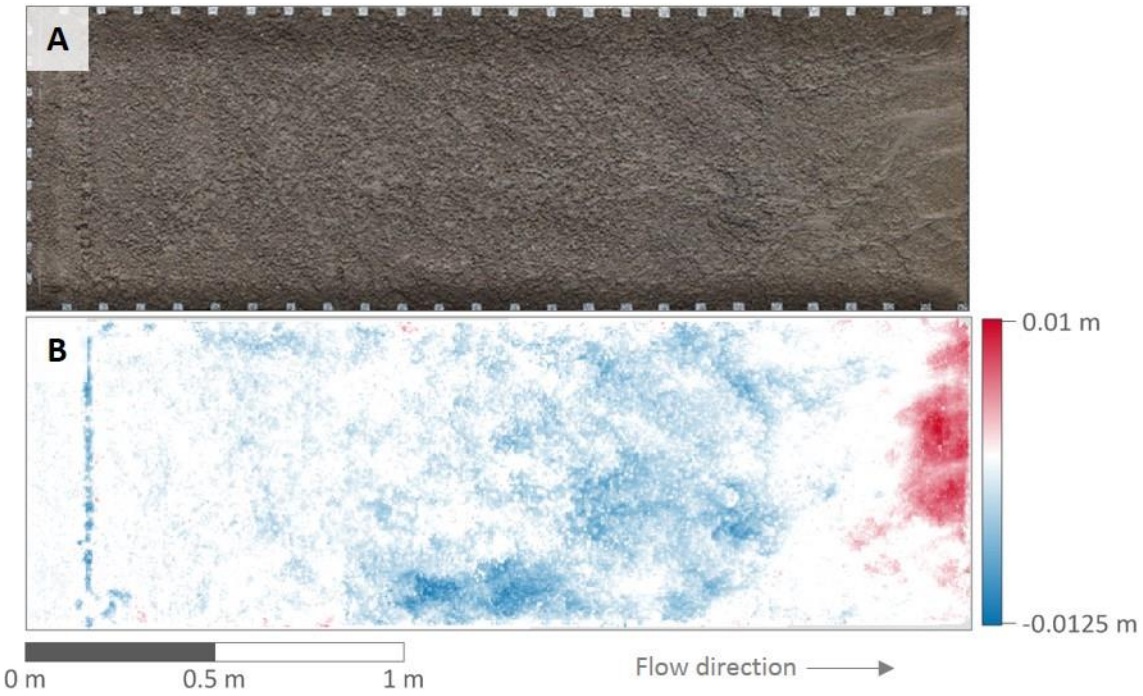

Figure 5.10: A) True colour SfM-MVS point cloud of F2, after E2, and B)DoD for total surface elevation change at 5 mm resolution. Where, white represents areas with zero elevation change, blue indicates areas of elevation decreases and red areas of increased surface elevation.

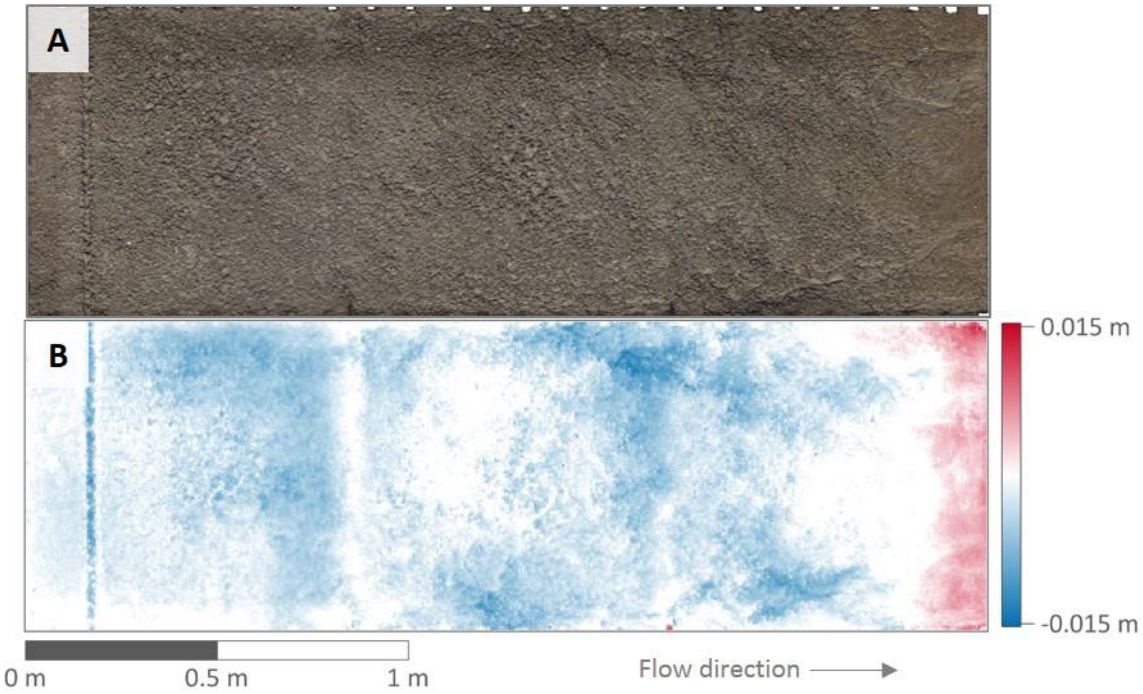

Figure 5.11: A) True colour SfM-MVS point cloud of F1, after E2, and B)DoD for total surface elevation change at 5 mm resolution. Where, white represents areas with zero elevation change, blue indicates areas of elevation decreases and red areas of increased surface elevation.

5.7 Discussion

Capturing ultra-fine grain (<1 cm) topographic data using modern, user-friendly technologies has the potential to revolutionise the quantification of soil erosion within laboratory environments. Accordingly, this study compared the application of two point cloud technologies with true soil loss observations to determine which was the most suited to future laboratory-based assessment of soil erosion processes. Soil erosion experiments were carried out at two spatial extents, 0.15 and 3 m^2, called 'plot' and 'flume', respectively. These were selected to reflect some of the scales commonly used within laboratory-based soil erosion studies (e.g. Armstrong et al., 2011; Gómez & Nearing, 2005; Michaelides et al., 2010; Pryce, 2011; Ventura et al., 2001). Varying the experimental conditions in accordance with the experimental design resulted in different erosion processes and magnitudes of soil loss. Soil loss during the plot scale sheetwash events (E2) ranged from 14.6 to 31.3 g, which is equivalent to a mean lowering of 0.07 to 0.16 mm, based on a bulk density of 1.3 g cm^3. The inclusion of a single source of runon for the plot scale rilling experiment (E3), lead to the formation of rill features, which ranged in maximum depth from 30 to 55 mm. The flume scale sheetwash/rilling experiments (E2) resulted in soil losses between 2.7 and 5.7 kg, where increased rainfall intensities lead to greater soil losses. Were the soil losses from the flume scale experiments to be uniformly applied over a 1 ha area, (with the obvious assumptions that this rudimentary 'upscaling' involves), it would equate to 9 - 19 t of soil

loss, while the soil losses from the plot sheetwash experiments would equate to approximately 0.97 - 2.08 t of soil loss.

5.7.1 Model spatial resolution

Of the two point cloud techniques presented in this study, the SfM-MVS approach delivered the finest resolution topographic information. The plot scale point clouds had a mean GSD of 0.17 mm/pixel, and the flume point clouds a mean GSD of 0.21 mm/pixel. As the GSD achievable with SfM-MVS is directly related to sensor size and survey range (James & Robson, 2012), the inclusion of convergent imagery covering a larger AOI within the field of view resulted in the greater GSD for the flume scale experiments. The TLS produced raw point cloud data with a mean GSD of 0.53 mm, however, this was <20% of the beam diameter (≤ 2.8 mm at the front window). This resulted in approximately 4 mm of visible noise within the TLS clouds, consistent with the observations of Lichti and Jamtsho (2006), who suggest an optimal sampling interval of 86 % of the beam diameter. The GSD of the SfM-MVS point clouds allowed aggregates greater than ca. 2 mm in diameter to be resolved, as visible in Figure 5.9 and Figure 5.10. The identification of individual aggregates was not possible with the TLS point clouds, consistent with Hodge et al., (2009) who found that beam diameter controlled the minimum grain size that could be resolved. The highest resolution DTM that could be confidently interpolated from the point clouds was 0.5 mm and 5 mm, for the SfM-MVS and TLS clouds, respectively.

While GSD is important, measurement precision, particularly in the 'z' axis, limits the precision with which point clouds can resolve surface topography and the potential magnitude of surface elevation change that can be detected using DoDs. In the first instance, measurement precision is inherent to the application of the technology. The TLS vertical precision was assumed to be 3 mm, as defined by the hardware specifications, and was therefore an order of magnitude less than the vertical precision achieved using the SfM-MVS approach, as defined by the RMSE of the check points or scalebars. The dimensionless precision ratios of the plot scale check points ranged between ranged from approximately 1:2000 and 1:6200 and were consistent with the magnitudes found by the precision analysis trial (1:3760 and 1:3220). These represent a significant improvement on the ca. 1:600 reported in other physical geography applications of SfM-MVS (Smith *et al.*, 2015). Furthermore, when compared to the more recent field application by Prosdocimi et al. (2017) where image data were captured from a similar survey range (1 m) and a spatial

extent (0.25 m^2) to the plot scale work, based on the RMSE of the check points the precision achieved in this study represent an order of magnitude improvement.

The trialled precision analysis suggested that there was scope for further improvements in SfM-MVS point clouds precision, through better constraint of the model (James *et al.*, 2017a, 2017b). Typically, this can be achieved through either collecting imagery with greater variations in extrinsic geometry i.e. the inclusion of greater number of camera orientations from each camera (James & Robson, 2014) or a better distribution and precision of GCPs coordinates (James *et al.*, 2017a). The 'shape only' precision for the plot scale suggests that while the consideration of the photogrammetric requirements was sound, the collection of more precise GCP information could have improved the 'georeferenced' precision (James *et al.*, 2017b). However, at 0.5 mm, it could be suggested that the GCP precisions achieved were already at the limit of that practically achievable at this scale. While the georeferenced flume results are in effect meaningless, as the point clouds are only scaled using the scalebars, the slight increase in precision towards the centre flume indicate that areas with the greatest amount of overlap over the control had the greatest overall precision i.e. in the centre of the flume all GCPs were visible in ≥20 images (as visible in Figure 5.2). Furthermore, the linear image acquisition and use of scalebars rather than georeferenced GCPs did have a significant impact on the accuracy of the flume experiments, where despite the pre-calibration of the experimental cameras, doming consistent with that reported by James and Robson (2014) for linear imagery acquisition, was present in some point clouds. Accordingly, better quality models of flume scale experiments could be achieved through the use of georeferenced markers and the collection of additional convergent imagery along the length of the flume, rather than just across the flume width-ways.

5.7.2 Calculated mass of soil loss

When the errors from the point clouds were incorporated into LoDs in combination with the uncertainties associated with co-registration and DTM interpolation, the TLS data had greater LoDs than the SfM-MVS, as visible in Figure 5.3. As a result, elevation changes following the sheetwash (E2) events and areas of sediment deposition following the rilling event (E3), for example, could not be detected with the TLS method, while such changes could be resolved using all of the SfM-MVS DoDs. Implementing a less conservative approach to the determination of a LoD for the TLS clouds, such as removing the errors associated with the individual point clouds, would have allowed positive changes in surface elevation to be resolved. However, while this is common in field scale applications (Smith &

Vericat, 2015), where DTM σ_z is likely to be the most significant cause of DoD uncertainty, under the experimental conditions presented herein this would not be appropriate because of the magnitude of changes and topographic variability. It is important to note, however, that the noise created by sampling at less than the beam diameter may have also had an impact on the magnitude of uncertainty related to σ_z for the TLS DoDs. Conversely, MVS processing reduces noise within the SfM-MVS point clouds, and thus potentially lowered the σ_z for each grid cell (James & Robson, 2012), particularly at the finer grid resolutions where a single grid cell would have rarely captured any topographic variability.

Experimental observations by the author suggest that the rainsplash and compaction events (E1) resulted in a lowering of the soil surface, at both the plot and flume scale, consistent with the breakdown of aggregates and the lowering of the soil surface due to consolidation (Ghadiri & Payne, 1977; Kinnell, 2005; Römkens *et al.*, 2002). While, it was not possible to detect changes in surface elevation following the plot scale rainsplash and compaction events (E1) using the TLS DoDs, SfM-MVS did detect the lowering of the soil surface, for both the plot and flume events. Following E1, the greatest surface lowering was on P5, where an isolated 5.5 mm of compaction was detected in a location where a screw had been dropped by a maintenance team prior to the experiment. While care had been taken to return the surface to the original condition, rather than simply displacing the soil, the screw had evidently created changes to the structure of the soil profile at depths greater than the top 5 mm, and invisible to the eye (Figure 5.8). Based on the 0.5 mm DoDs, following E1 median surface lowering ranged from 0.54 mm on P5 to 1.07 mm on P3, and dominated the areas between the large (>4 mm) aggregates. There was significantly less lowering identified with the SfM-MVS predictions following the flume scale experiment, which suggests that increasing the bulk density by 0.1 g cm^{-3} did reduce compaction effects.

The magnitude of the LoD for the TLS DoDs meant it was also not possible to calculate elevation changes following the sheetwash events (E2) on the plots using the TLS data. Whilst elevation changes detected using SfM-MVS were greater than the LoD, the relative measurement error for the SfM-MVS E2 predictions ranged from 377 to 1850 %, for the plot scale experiments. This results suggests that further consolidation of the soil profile may have occurred during the sheetwash experiment, and could indicate that further saturation of the already moist soil lead to further aggregate disintegration or deformation (Bryan, 2000). Median surface lowering across the plots was between a minimum of 0.53 mm on P5

and a maximum of 2.3 mm on P4, which is less than the 4.2 mm of soil consolidation found by Rieke-Zapp and Nearing (2005). Based on the largest 'measurement error' at the plot scale, total consolidation resulted in a mean bulk density increase of 0.04 g cm^3. Patterns of soil loss present within the DoDs matched visual observations during the rainfall events, and suggest that during the experiment networks of aggregates, shifted downslope by the moving water created shallow flow paths (Figure 5.8E). This is consistent with the observations of Slattery and Bryan (1992) who suggest that these changes in the surface can facilitate the development of higher velocity flows.

For the plot scale rilling experiments (E3), there was a strong linear relationship between the volumes of soil loss predicted by the TLS and SfM-MVS DoDs (R^2 = 0.9913, based on n = 4). Furthermore, there was a strong correlation between the predicted and observed volumes of soil loss using both techniques, (R^2 = 0.8877 and R^2 = 0.83, for TLS and SfM-MVS, respectively). However, in all instances, the TLS DoDs underestimated soil loss, and detected smaller changes in elevation relative to the SfM-MVS clouds. For example, the maximum negative elevation change detected by the 5 mm TLS DoD was 44 mm on P2, while SfM-MVS detect a negative change of 54.5 mm for the same rill feature. This highlights that while TLS can provide a useful spatial indicator of relative SfM-MVS performance in laboratory environments, as used by Morgan et al. (2017), caution must be taken when TLS is used to quantify or indicate the accuracy of techniques for soil erosion monitoring. There was no significant difference found between the volumes of soil loss predicted by both techniques with changing DTM resolutions. However, comparisons between the maximum predicted eroded volume and the minimum for the same DoDs ranged between 2 and 8.6% for TLS and 2.4 and 6.1% for SfM-MVS. Finally, if considered in the same light as the sheetwash experiments, the lower relative measurement errors in the SfM-MVS E3 predictions indicate a stabilisation of the non-erosional processes, such as aggregate breakdown and compaction, within the soil profile.

5.8 Conclusions

Through applying SfM-MVS and TLS alongside sediment-based observations of soil loss, under changing experimental conditions, this chapter has presented a novel assessment of the strengths and limitations of both techniques. There was a strong correlation between the volume of soil loss predicted by both techniques and the sediment-based observations for the plot scale experiments rilling experiments. However, the TLS predictions consistently underestimated soil loss and applying a conservative LoD meant that decreases in surface

elevation from compaction and sheetwash and the positive elevation changes associated with the deposition of sediment, could not be detected using TLS-derived DoDs. Conversely, positive and negative elevation changes were detected using the SfM-MVS DoDs across all experiments, although only predicted soil losses from the rilling experiment correlated with the sediment-based observations. Accordingly, this study has also illustrated that changes in surface elevation during soil erosion experiments do not always correlate with soil losses, particularly when the magnitude of changes resulting from changes to the soil bulk density exceed the changes related to soil loss. However, the comparison between known rates of soil loss and the volumes of change predicted using SfM-MVS has revealed the technique's potential for elucidating further information about changes in soil physical properties during erosive events. The use of an imaging station and pre-calibrated camera models reduced data collection and processing times, while producing high-precision point clouds for plot scale experiments, and thus offered a replicable and robust methodology. The accuracy of the SfM-MVS-based soil loss predictions following the flume experiments were limited by artefacts consistent with the processing of linearly acquired imagery. However, the precision of the tie points based purely on the photogrammetric processing indicate that for future studies the inclusion of precise, georeferenced GCPs would lead to improvements to the replicability and confidence in flume-scale SfM-MVS applications, using a similar set up. Accordingly, this study has identified that of the two point cloud based, proximal sensing technologies assessed herein, SfM-MVS would be the most suited to future assessments of soil erosions within laboratory environments.

6. USING REO AND SFM BASED TECHNIQUES TO IDENTIFY SOURCE APPORTINMENT OF SOIL EROSION AT LABORATORY SCALES

6.1 Overview

Addressing Objective 3, this chapter uses both REO tracers and SfM point clouds to elucidate retrospective information about sediment sources under changing soil erosion conditions, within a laboratory environment. This is achieved through taking a stratified approach to tagging with REO tracers and building on the SfM-MVS results delivered in the previous chapter. The results section uses REO tracer concentrations and SfM-based volumetric techniques to quantify soil source apportionment at two experimental scales. The discussion then explores the information content of the different techniques through describing the changes in source apportionment under different soil erosion conditions.

6.2 Introduction

Rainfall striking a bare soil surface with sufficient energy can loosen soil particles and cause soil aggregates to disintegrate into smaller, more mobile, fragments (Kinnell, 2005). These particles can then become entrained within the water droplet and transported with the upward force or refraction of the water (Long *et al.*, 2014). Alternatively, the downward force of the raindrop can act to compact and consolidate the soil surface, creating a seal or crust, and reducing infiltration (Berger *et al.*, 2010; Evans & Morgan, 1974; Le Bissonnais *et al.*, 2005). When infiltration capacity is exceeded, shallow flows of water can transport the loosened soil particles downslope, as sheetwash erosion (Kinnell, 2005; Morgan, 1995). Should sufficient energy be reached, the moving water can become convergent, increasing erosivity of the water, resulting in soil transportation downslopes as rill erosion (Bryan & Poesen, 1989).

Soil erosion via water can therefore be divided into diffuse and concentrated processes, which have different impacts on the landscape and relative contributions to the total soil lost from the landscape. With less erosive energy, diffuse erosion is primarily associated with the relatively uniform transport of fines (Armstrong *et al.*, 2011). In contrast, rill erosion shows less evidence of size selectivity and leaves visible evidence of concentrated flow pathways (Alberts *et al.*, 1980). Furthermore, soil particles and aggregates can be transported variable distances either in suspension or in a series of 'jumps' along the soil surface, an understanding of which is of importance to model development (Wainwright *et*

al., 2008b). Consequently, accurately describing soil loss via each process requires employing monitoring techniques capable of spatially quantifying the magnitude of both processes.

Tracers, or more specifically sediment tracers, either naturally occurring or artificially applied, are used to mark (or fingerprint) a soil in order to develop a spatial understanding of the sources of eroded sediment (Guzmán *et al.*, 2013). Accordingly, REOs have been used in laboratory studies to identify sediment sources during erosion experiments (Kimoto *et al.*, 2006b; Michaelides *et al.*, 2010; Polyakov & Nearing, 2004; Pryce, 2011; Zhang *et al.*, 2003). However, gaining a high resolution spatial understanding of source apportionment requires the use of multiple unique REOs, such as the ten used in the study presented by Michaelides et al. (2010) in their study of sediment movement over a break-in-slope. Furthermore, while applications thus far have illustrated their strength for quantifying transport distances, the potential for REO tracers to elucidate information on the relative contributions of diffuse and convergent processes, has yet to be fully explored.

Chapter 5 has illustrated that SfM can be used to derive a spatially explicit understanding of elevation changes resulting from soil erosion experiments in laboratory environments. Consequently, this chapter will build on this work through applying both REO tracers and SfM point clouds to source apportionment, to elucidate retrospective information about soil sources during erosion experiments, in line with objective three. To this end, the main aim of this piece of work is to apply REO tracers and SfM-based volumetric techniques to understand soil source apportionment at two discrete scales – plot and flume, as described below. The discussion will then explore the application and value of the information through describing the changes in source apportionment under different soil erosion conditions within laboratory environments.

6.3 Methods

6.3.1 Experimental conditions

Soil erosion events were simulated at two experimental scales, 0.15 m^2 and 3 m^2, referred to herein as 'plot' and 'flume' scale, respectively. The boxes were filled with sandy loams, screened to 6 mm for the plots and 8 mm for the flume. The soil was tagged with REO tracers, as detailed further in Section 4.4.2 and illustrated in Figure 6.1. The REOs used for the experiments were: Lanthanum oxide (La_2O_3), Praseodymium (Pr_6O_{11}), Gadolinium (Gd_20_3), and Neodymium (Nd_20_3), which will be referred to herein using their element only

i.e. La, Pr, Gd and Nd, respectively. To enable the production different erosion processes, each soil surface was subjected to sequential hydrological events, as described in Section 4.4.4.

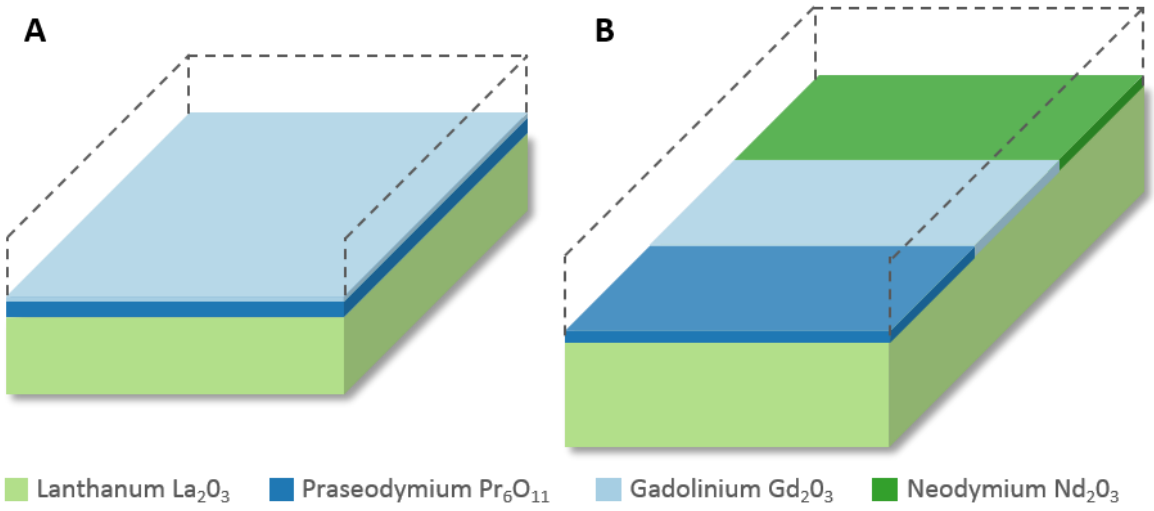

Figure 6.1: Schematic diagram illustrating the REO tagging design for the plots (A), where the tracer changes 0 – 5 mm, 5 – 15 mm and >15 mm into the soil profile, and the flume (B), where the upper segments were tagged to a depth of 10 mm and change every 1 m from the top of the flume.

6.3.2 Runoff and sediment collection

All sediment and runoff leaving the plots and flumes was collected, as detailed in Section 4.5. The particle size distribution of the sediment samples was analysed using the methods defined in Section 4.3.2. The enrichment ratio for exported particle size fractions was determined through comparing the relative portion of each particle size fraction within the exported sediment with the original soil, and was calculated to identify preferential transportation of fractions. Enrichment ratios greater than 1 indicate the preferential transport of a particle size fraction.

6.3.3 REO analysis

REO concentrations were determined using an ICP-OES following a heavy metal digest via aqua regia. To carry out the heavy metal digest 0.25 g of sediment was transferred into a 100 mL glass beaker. 3 mL of concentrated nitric acid (HNO_3) was then added to each beaker, before being warmed to dryness using a hotplate. A further 3 mL of concentrated HNO_3 and 0.5 mL of concentrated hydrochloric acid (37%) (HCl) was then added to each beaker. The beakers were then warmed until the appearance of brown nitrogen dioxide fumes, or dryness if the fumes were not observed due to the low presence of organic matter. The beakers were removed from the hotplate and allowed to cool. The remaining sediment was washed through Whatman #42 ashless filter papers into 25 mL volumetric flasks and

made up to 25 mL, using distilled water. Prior to analysis the samples were diluted to the range of ICP-OES detection.

It was assumed that the extraction efficiencies were uniform for all REOs. It was also assumed that enrichment i.e. the preferential transportation of unbound REO particles, was uniform. Thus, the mass of soil loss from each tagged zone was calculated from the relative REO concentrations, as identified by the ICP-OES, using the proportional method (Polyakov & Nearing, 2004). REO analysis was carried out on the bulked sediment for the plot experiments and every second sample for the flume experiment. To determine the total contribution from each tagged zone on the flume was calculated from a linear relationship between samples. The approach accounted for 99.8% of the total sediment yield.

6.3.4 Structure-from-Motion Multi-view-Stereo data

SfM-MVS point clouds were derived from three distinct steps, namely: lens calibration, collection of experimental imagery, and SfM-MVS processing, using three Canon 600D digital SLR cameras with Canon EF-S 18-55 III lenses and processed within Agisoft PhotoScan Professional version 1.2.6 (referred to herein as PhotoScan), as described in Section 4.7. The point clouds were used to build DoDs at 0.5 mm resolution for the plots and 5 mm resolution for the flume, using the methods presented in Section 5.5. Whilst in the previous chapter soil loss was calculated as a function of both the negative and positive volumes of change, the soil loss presented herein represent the negative and positive volumes of change independently, as appropriate.

To match the extent of REO tagging within the flume, the point cloud was first segmented into 1 m sections along the flume in CloudCompare before being converted to DTMs and DoDs using the methods described in Section 5.5. Sectioning was carried out to allow volumetric estimations to be calculated for each section independently. As each segment could be aligned individually, reducing the magnitude of alignment error caused by any doming in the model, thus reducing the minimum LoD when compared to that presented in Chapter 5. The plot-scale SfM-MVS DoDs were used to identify the total volume of change from each different REO tagged layers i.e. 0 – 5 mm, 5 – 15 mm, and >15 mm. To allow for comparison with the REO-based calculations, volumes were then converted to a mass of soil loss using the bulk density of the initial soil mass i.e. 1.3 g cm^{-3} for the plots and 1.4 g cm^{-3} for the flume.

6.4 Results

6.4.1 Plot scale experiments

6.4.1.1 Runoff and sediment flux

During the sheetwash events (E2), runoff and sediment flux reached a steady state after approximately 10 minutes, across all plots (Supplementary Material Figure 8.6). The maximum discharge rate was 0.0023 L s^{-1} on P4 after 20 minutes, and the greatest sediment concentration was 11.97 g L^{-1}, which was also on P4, 30 minutes into the event. P3 and P5 experienced a decline in sediment concentration from the 20th minute of the event. Conversely, whilst discharge reached a steady state after two minutes for all plots during the rilling experiment (E3), sediment concentration did not reach a steady state (Supplementary Material Figure 8.7). The inclusion of a runon source increased runoff by an order of magnitude, accordingly, the maximum discharge rate was 0.013 L s^{-1}, which was after 15 minutes on P4, and the highest sediment concentration was 109.6 g L^{-1} on P4, 6 minutes after the event began. With the exception of P3, sediment concentrations declined after 5 minutes.

There was a significant difference between the PSD of the bulked sediment from E2 and E3, for all classes bar the silt and clay fraction (<63 µm) (ANOVA, $F(1,6) = 6.891$, $p = 0.039$). Furthermore, there was a preferential transportation of the medium to fine sand particles (500 > 125 µm) and the silt and clay fraction (<63 µm) during the sheetwash experiment (E2). In contrast, for the rilling experiment (E3) there was only evidence of preferential transport of the silt and clay fraction. Across all events, the fine gravel fraction (>2000 µm) was under-represented within the exported sediment. The export of both the fine gravel and very coarse sand fraction (>2000 and 2000 > 1000 µm) did, however, increase with event magnitude.

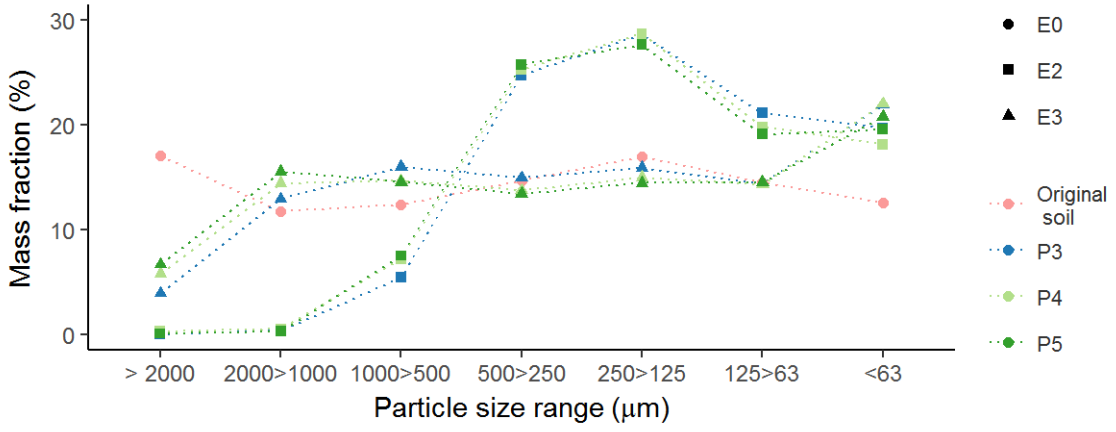

Figure 6.2: PSD for bulked sediment samples following experimental runs two and three, presented as mass faction (%) for each φ interval.

6.4.1.2 REO tracers

The REO-derived calculations indicate that the top 5 mm of soil within the plots was the primary source of sediment during the sheetwash experiment (E2), accounting for over 99 % of all soil loss, as visible in Figure 6.3A. The mass of soil exported from the top layer of soil ranged from a minimum of 20.04 g on P3, to a maximum of 28.26 g on P4. During E2, a maximum of 0.28 g of soil was exported from the second soil layer (5 – 15 mm), which was on P4. Based on the relative REO concentrations, the top 5 mm of the soil profile was also the main source of sediment during the rilling experiments (E3), as shown in Figure 6.3B. Soil loss from the top layer ranged from a minimum of 114.0 g on P3 to a maximum of 228.9 g on P5, accounting for between 39.1 and 41.5 % of the total sediment yield. The middle layer contributed 30.6 to 40.4 % of the total sediment yield. Accordingly, soil from the depths greater than 15 mm contributed the least to the total sediment yield. The relative contribution from depths >15 mm increased with event magnitude, and ranged from a minimum of 18 % on P3 to a maximum of 29.4 % on P5.

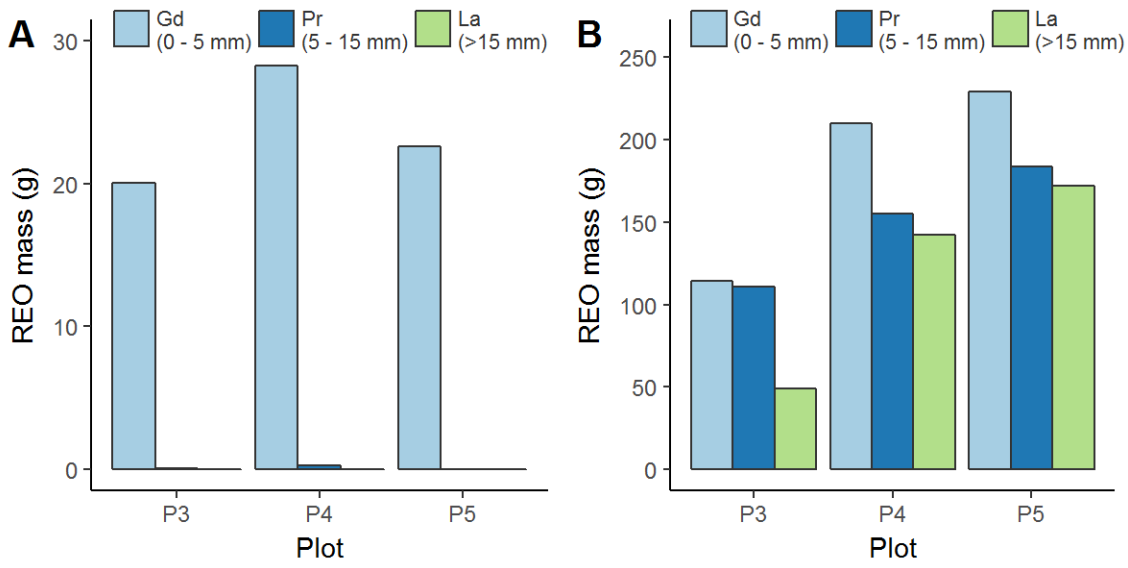

Figure 6.3: Calculated contribution from each tagged layer in the soil profile based on REO concentrations in the bulked sediment samples for A) the sheetwash events (E2), and B) the rilling event (E3). Note the different y-axis scales.

6.4.1.3 Structure-from-Motion photogrammetry

The SfM-derived calculations show that the top 5 mm of the soil was the primary source of soil loss during E2, accounting for over 99.9 % of the total changes identified (Figure 6.4A). The magnitude of soil loss from the top 5 mm of the soil profile ranged from a minimum of 120.4 g on P5 to a maximum of 394.8 g on P4. The SfM DoD found that elevation changes did exceed 5 mm on P4, however, these only equated to a soil mass of 0.02 g, or a 0.005 % of the total.

The SfM DoD indicates that soil was eroded from all three layers of the soil profile, across all plots, during the rilling experiments (E3), as visible in Figure 6.4B. The volumetric predictions show that the top 5 mm of the soil profile was the also greatest source of sediment during E3, for P3 and P4, contributing 60.3 and 46.6 % to the total sediment yield, respectively. Conversely, for P5, the 5 – 15 mm layer had the greatest soil loss, accounting for 44.6 % or 245.7 g of the total. The SfM DoDs show that the magnitude of soil loss from depths greater than 15 mm increased with event duration. Accordingly, the calculated mass from this section was the greatest for P5, equating to 73.4 g and 13.3 % of the total. The mass of soil transported but deposited in a fan within the plot (calculated from net positive elevation changes) ranged from 39.0 g on P5 to 7.8 g on P4, and was therefore not related to event duration.

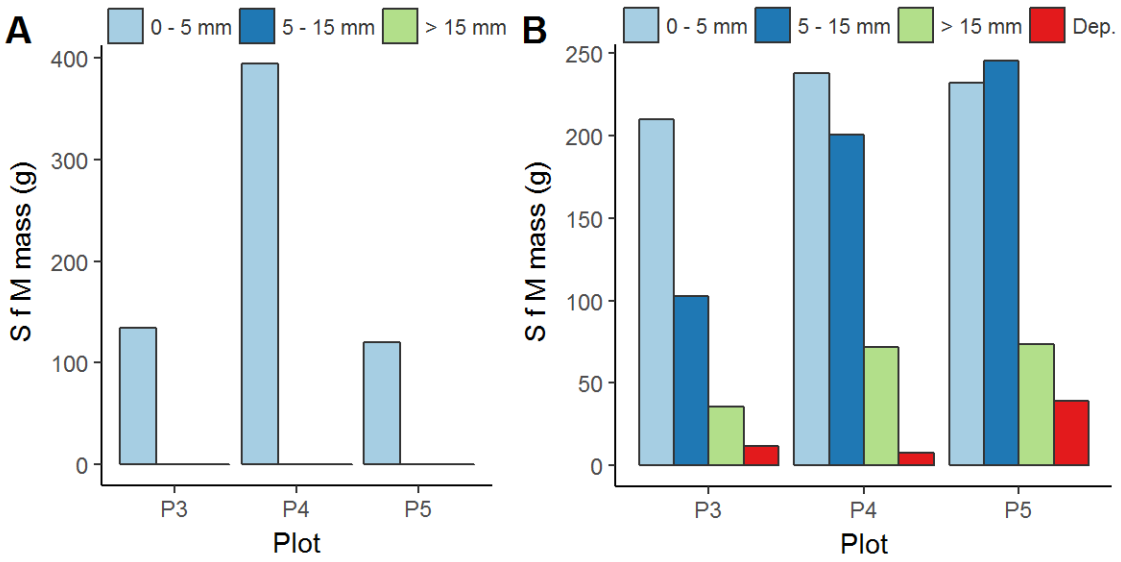

Figure 6.4: Calculated contribution from each tagged layer in the soil profile based on SfM-derived elevation and volumetric change for A) event 2, and B) event 3, where 'Dep.' represents the positive change resulting from sediment deposition. Note the different y-axis scales.

Figure 6.5 demonstrates the spatial extent of elevation changes within the three layers presented in Figure 6.4, following E3, for P3 and P5 for contrast. The spatial extent of the elevation changes indicates that the rilling feature was the greatest source of sediment material during E3. Negative elevation changes covered 79 % of the surface of P3 and 64 % of P4, and were not limited to the rill. Negative elevation changes covered 41 % of the surface of P5, and were primarily limited to the rill. All elevation changes 5 – 15 mm into the soil profile were confined to the rill. Elevation changes greater than 15 mm were limited to the upper 25 cm of the plot length, as visible in the right-hand side of Figure 6.5.

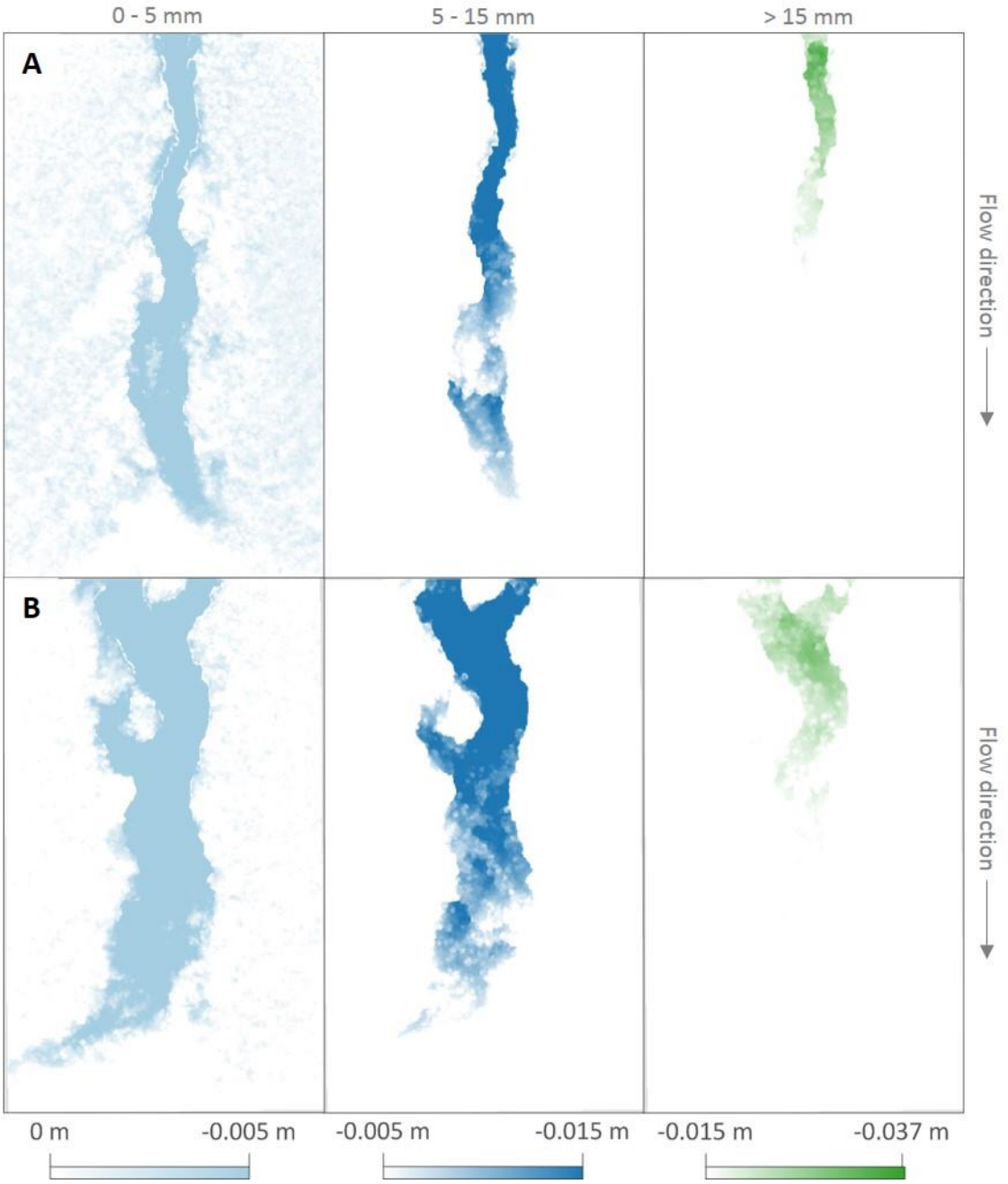

Figure 6.5: SfM-derived 0.5 mm DoD for P3 (A) and P5 (B) following E3, showing the area and magnitude of negative elevation changes in layers consistent with the REO tagging of the 0.3 x 0.5 m plots.

6.4.2 Flume scale experiment

An approximate steady state of runoff, where variance with the 5 subsequent samples was <0.0006 %, was reached after 34 minutes (Figure 6.6A). There was however an on-going slight increase in discharge from this point, ranging from 0.094 L s^{-1} at 34 minutes to 0.096 L s^{-1} at 66 minutes. An approximate steady state of sediment concentration was reached after 16 minutes. The mean steady state sediment concentration was 11.4 g L^{-1} (±1.02). There was a final peak in sediment export at minute 58, where sediment

concentration was 14.4 g L^{-1}, as visible in Figure 6.6B. The total sediment yield for the experiment was 3914.04 g.

Analysis of the PSD of the bulked sediment yield (Supplementary Material Figure 8.8) and the enrichment ratios of the individual sediment samples (Figure 6.6C) show that the fine gravel fraction (>2000 µm) and the coarse sand fraction (2000 > 1000 µm) were under-represented in the sediment transport. As a result, there was evidence of the preferential transport of the fractions finer than 1000 µm, most notably the silt and clay fraction (<63 µm), which had an enrichment ratio of 3.4 in the bulked analysis. The concentration of the <63 µm fraction was the greatest in the initial sediment sample, representing an enrichment of 12.2 (not visible in Figure 6.6C due to scaling). The 500 > 250 µm and 250 > 125 µm fractions, the fine and medium sands, were the most eroded. Whilst this is consistent with the PSD of the original soil (Supplementary Material Figure 8.8), both fractions had a cumulative enrichment ratio of 1.2.

The REO concentrations in the sediment samples indicated that the Gd-tagged portion of the soil, the upper 10 mm of soil profile 1 - 2 metres from the top of the flume, was the greatest source of exported sediment, as shown in Figure 6.7A. Based on the REO-based calculations, a total of 2395.5 g of soil was exported from this section (61.2 %), in contrast with 1038.3 g (26.5 %) from the Pr-tagged section (2 - 3 m from the top of the plot, closest to the exit) and 334.3 g (8.5 %) from the Nd-tagged section (0 - 1 m from the top of the plot). The maximum concentration of sediment from any one section was 9.6 g L^{-1}, which was from the Gd-tagged section (Figure 6.6D). Furthermore, the relative contribution of sediment from the Gd-tagged zone increased throughout the experiment (Figure 6.6E). Similarly, the relative amount of soil from the Nd and La sections increased throughout the experiment. The Nd section contributed 5 % of the sediment flux in the 4th minute, increasing to a maximum 10 % at the 66th minute. Conversely, the contribution of sediment from the Pr section, whilst greater than that from the Nd section overall, decreased throughout the experiment. There were two slight spikes in La contribution, which were 38 and 50 minutes into the erosion event, and 5.1 and 5.3 % of the sediment flux, respectively. The La-tagged soil apportionment increased to a maximum of 7.5 % of sediment flux, and contributed 3.6 % (140.5 g) of the total sediment yield.

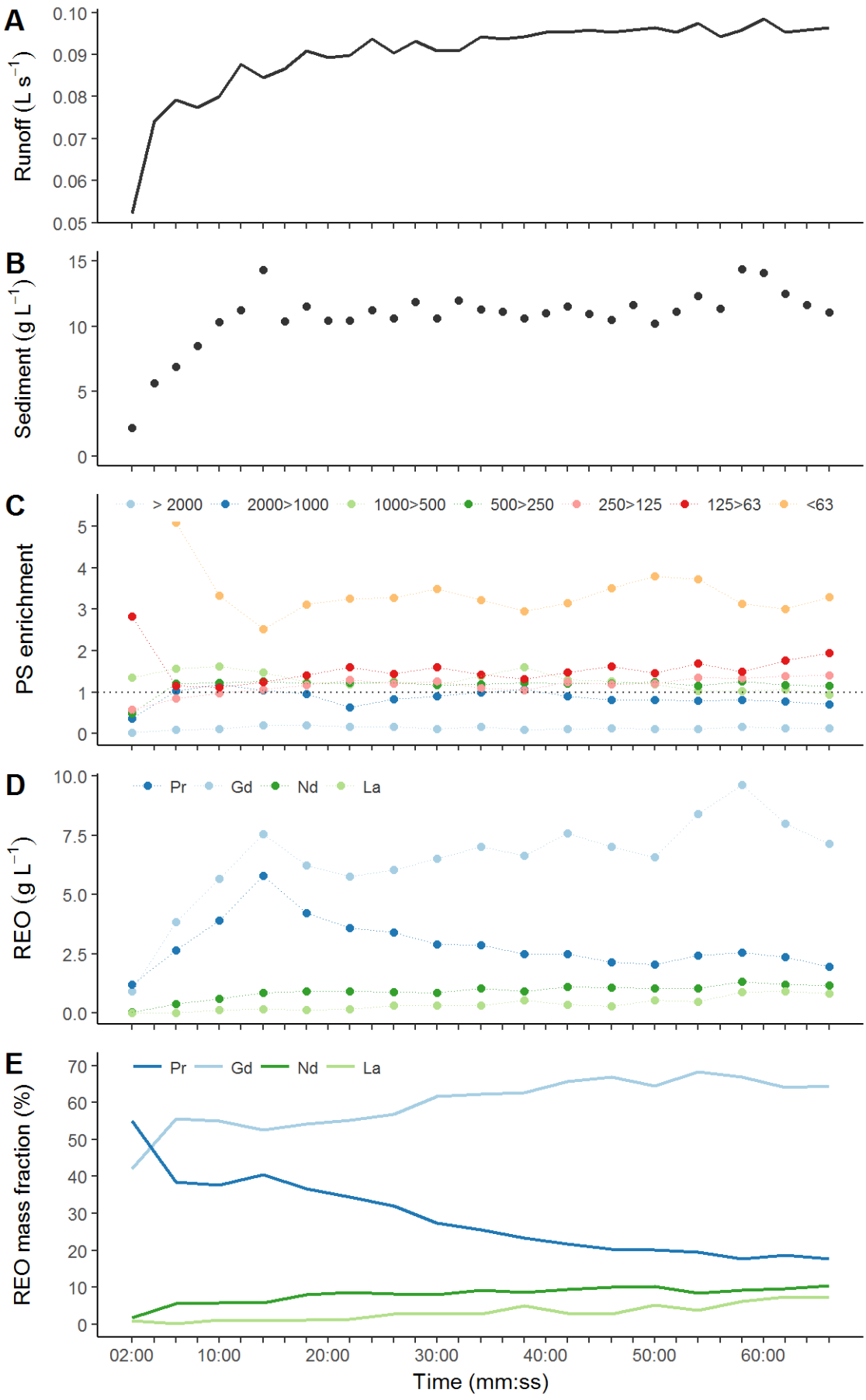

Figure 6.6: Summary of discharge (A), sediment concentration (B), Enrichment of particle size fractions (C), REO-based concentrations calculated from the sediment samples (D), and REO-based sediment apportionment (E), for Flume 3 through time during Event 2.

Figure 6.7 presents the predicted mass of soil lost from each section, based on the REO concentrations (Figure 6.7A) and the SfM DoDs (Figure 6.7B). Based on the total negative elevation changes within the different tagged sections, the SfM DoD found that the Gd-tagged portion experienced the greatest soil loss, representing 58.7 % of the total. The Nd-tagged section represented 12.9 % of the total negative changes and the Pr-tagged area, closest to the exit, represented 28.3 %. Accordingly, the SfM-derived calculations of soil loss from each section were strongly correlated with the REO-derived estimations of apportionment (R^2 = 0.981). However, the SfM DoDs overestimated the total mass of soil loss from each section, except the La tagged layer. The areas identified within the SfM DoD as having negative elevations changes greater than 10 mm were consistent with visual observations during and after the experiment, which are coloured green on Figure 6.8. However, the DoD changes underestimated the soil loss from the La section, according to the sediment REO concentrations. The mass of soil transported but deposited in the Pr-tagged section of the flume, based on positive elevation changes, was 975.4 g.

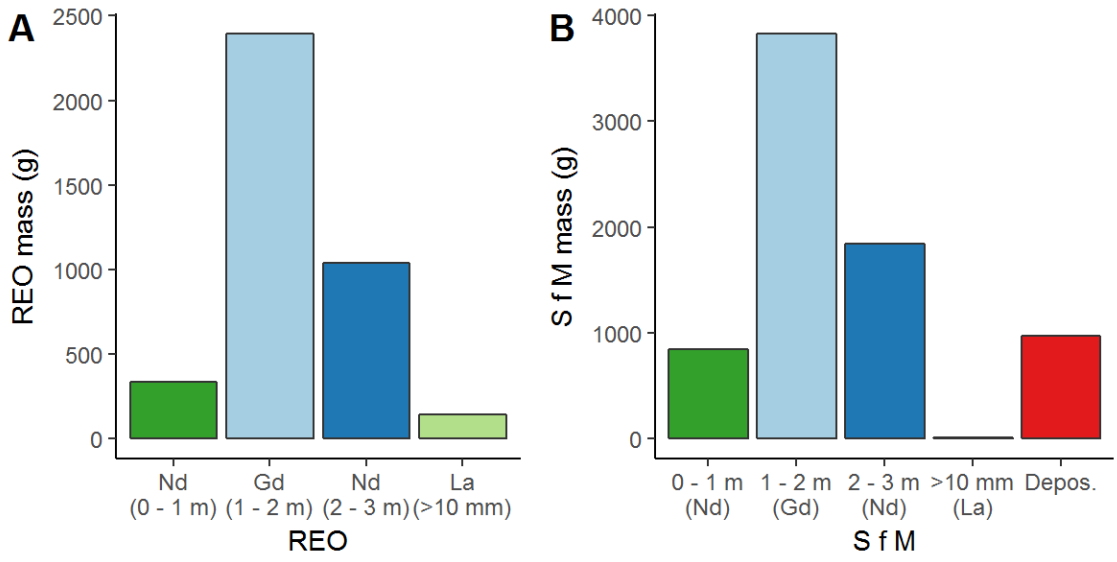

Figure 6.7: Calculated contribution from each section in the flume based on REO concentrations in the bulked sediment samples (A) and SfM elevations changes within each section (B) where 'Depos.' indicates the mass calculated from positive elevation changes at the lower end of the flume. Note the different y axis scales.

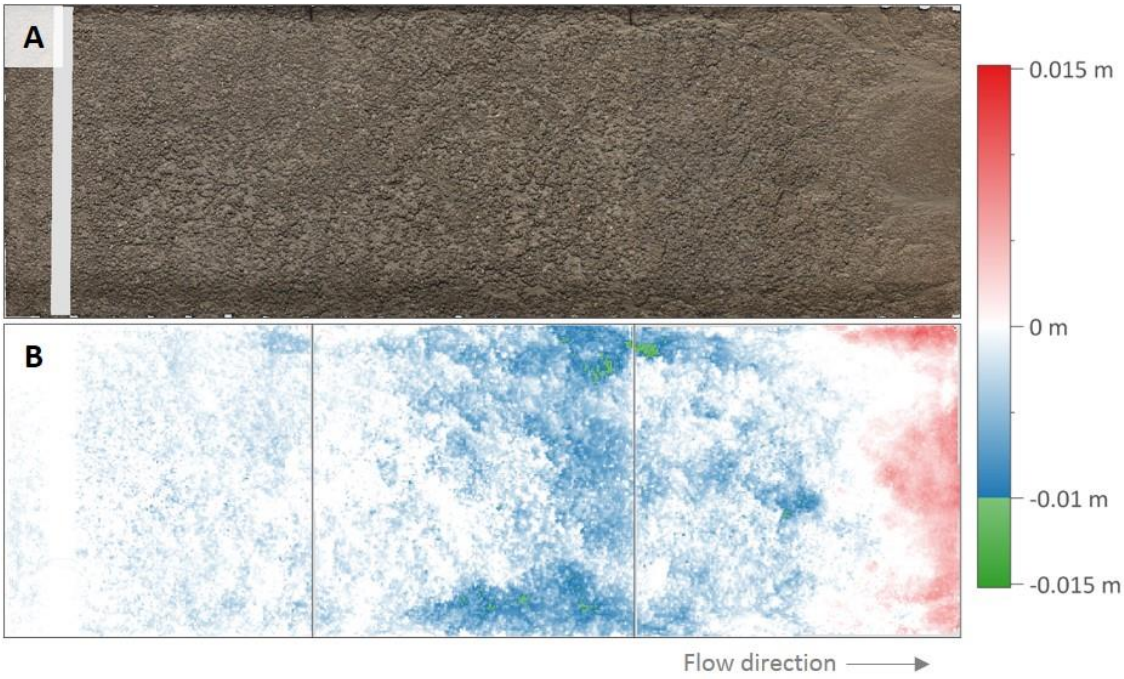

Figure 6.8: SfM based raw point cloud showing the surface of Flume 3 following the erosion experiment (A), and the SfM-derived DoD, illustrating the spatial distribution of elevation changes (B).

6.4.3 REO versus SfM-MVS Calculations

As presented in Section 5.6.2.2 of the previous chapter, the predicted soil loss resulting from the plot scale sheetwash were overestimated by SfM-MVS, ranging from a 377 – 1850 % overestimation of soil loss. Following E3, the SfM-MVS approach overestimated the mass of soil loss from the top 5 mm on all plots, ranging from maximum of 83.8 % on P3, to a minimum of 1.3 % on P5, relative to the REO. Similarly, in all instances the SfM-MVS calculations underestimated the mass of soil exported from depths greater than 15 mm (the La tagged section), ranging from a minimum of -28.2 % on P3 to a maximum of -57.3 % on P5. Conversely, the relative error of the predicted mass of soil loss between 5 and 15 mm into the soil profile was underestimated by -7.6 % for P3, and overestimated for both P4 and P5, by 29.3 and 33.6 %, respectively. The total relative measurement error of the SfM-MVS approach for the plot scale experiments, taking into consideration the mass of soil deposited, ranged between -0.95 and 22.4%. For the flume results, when compared to the REO calculations, the relative measurement error of the SfM-MVS-based calculations was 77.5 %, 59.8 %, 152.4 % and -94.7 % for the Pr, Gd, Nd and La sections, respectively. Taking into consideration the mass of soil deposited, this resulted in a total relative measurement error by SfM-MVS of 41.9 %.

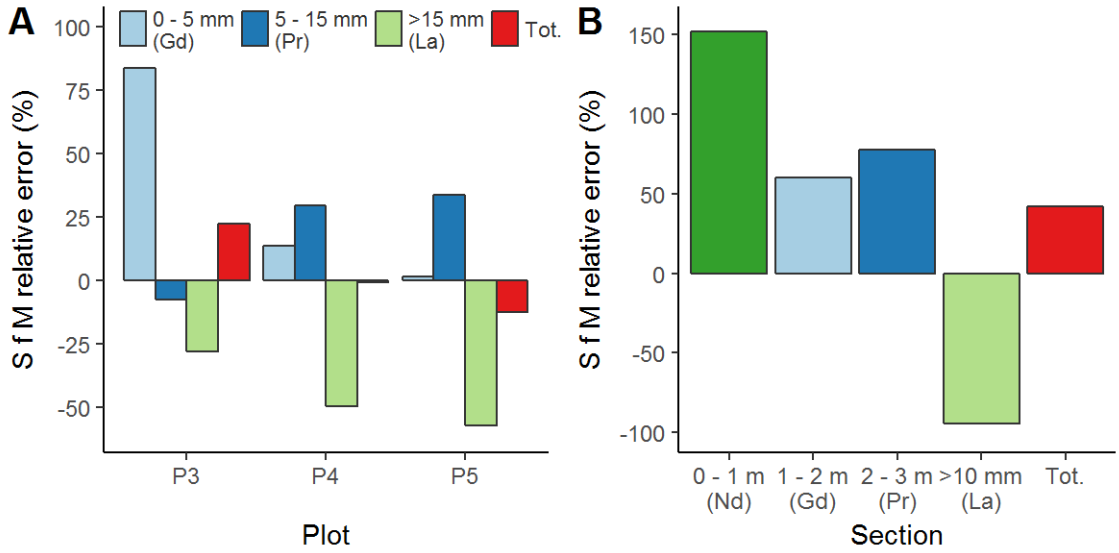

Figure 6.9: The relationship between mass calculated by REO and SfM, presented as the relative error of the SfM predictions when compared to the REO results. Tot. indicates the total measurement error, including the estimated mass of deposited sediment.

6.5 Discussion

6.5.1 Plot scale erosion experiments

The first erosion experiment on the plots, E2, resulted in the preferential transport of fine sediment (<500 µm) across all three plots (Figure 6.2), consistent with the sheetwash erosion described by Armstrong et al. (2011). E2 thus presented an appropriate platform to assess the suitability of both techniques for the quantification of diffuse water erosion. Discharge and sediment concentration reached a steady state across all plots, however the decline in sediment concentration following 20 minutes of runoff on P3 and P5 suggests that there was a depletion of readily available material during the final third of the experiments. While this could have been caused by an exhaustion of the finer sediment fractions, sealing of the soil surface by particles dispersed by the slaking of aggregates presents a more likely explanation (Le Bissonnais *et al.*, 2005), as a smoothing between the remaining aggregates was visible on the soil surface. Conversely, following a temporary decline, sediment concentrations increased towards the end of E2 on P4. Furthermore, whilst both the REO and SfM calculations indicate that sediment was only sourced from the top 5 mm of the soil profile for P3 and P5 during E2, both techniques also indicate that there was some transportation of sediment from depths greater than 5 mm on P4. As the top layer of the soil had an initial air-dried mass of 900 g, this suggests that the ingress into the second layer was due to a breach in the surface seal caused by increased sheer stress, rather than the exhaustion of the top layer of the soil profile (Morgan, 1995). Interestingly, while the SfM DoDs overestimated the total mass of sediment exported via sheetwash from the plots, the

mass of sediment apportioned to depths greater than 5 mm was underestimated when compared to the REO results. This suggests that there was some deposition of sediment within the feature, and indicates that there was not yet sufficient energy within the system for convergent flow paths to form (Slattery & Bryan, 1992).

The introduction of a single runon source for E3 lead to the formation of a rill on all three plots. Changing the hydrological event duration and magnitude resulted in rills of varied spatial extent, and was thus ideal for testing the application of the techniques on laboratory-scale convergent soil erosion features. Consistent with erosion from convergent features, there was less evidence of size selectivity in the sediment (Figure 6.2) (Alberts *et al.*, 1980). Coarse-grain sediment (>2000 µm) was, however, under-represented relative to the PSD of the original soil. Accordingly, large aggregates (>2000 µm) were visible in the bottom of the rills on all plots, which were also resolved using the 0.5 mm DTMs and DoDs constructed from the SfM point clouds. With the exception of P3, which was subjected to the smallest hydrological event, sediment concentrations declined after 5 minutes, indicating that following the cutting of the rills, the systems were detachment limited on P4 and P5. Despite this, the sediment PSD and aggregates deposited within the rill shows that there was insufficient erosive energy within the system to carry the larger aggregates out of the plot.

The REO tracer concentrations in the exported sediment show that the top 5 mm of the soil profile was a significant source of sediment during E3, accounting for between 39.1 and 41.6 % of exported sediment. Thus, in accordance with the rationale behind the tagging design (Section 4.4.2), the results could be interpreted to indicate that sheetwash was also a significant route of soil loss during the E3. However, through providing a detailed spatial representation of elevation changes, the SfM DoDs allowed further information on the distribution of soil erosion in the top 5 mm of the soil profile to be elucidated following the event. The P3 SfM DoD, for example, shows that soil losses to a maximum depth of 5 mm covered 79 % of the soil surface during E3, of which 67 % was outside of the area of the rill, thus confirming that sheetwash also contributed to soil loss (Figure 6.5). Similarly, the P4 SfM DoD also provided evidence of soil loss via sheetwash outside of the rill, with soil losses outside of the rill covering 49 % of the soil surface. Unlike the other two plots, the spatial extent of elevation changes on the P5 SfM DoD suggests that soil loss from the top 5 mm was primarily limited to the rill (as visible in Figure 6.5). Furthermore, while elevation changes within the rill exceeded 5 mm across all three plots, elevation changes outside of

the rill reached a maximum depth of ca. 2 mm, indicating that despite sheetwash occurring on the plots, most of the sediment exported from the top 5 mm on P3 and P4 was indeed exported from within the direct spatial extent of the rill.

Informed by the spatial distribution of the elevation changes identified with the SfM DoDs (Figure 6.5), all soil loss from depths greater than 5 mm were sourced from within the rills. Accordingly, the REO calculations show that soil loss from within the rill, at depths greater than 5 mm, contributed between 58.4 and 60.9 % of the total mass eroded from the plot. Although the two combined layers represent a greater sediment source than the top 5 mm of the soil profile, the REO tracers have illustrated that the total exported mass apportioned to each individual layer was less than that of the top 5 mm, despite a greater initial resource. Furthermore, of the two layers, both the REO and SfM calculations illustrated that the 5 to 15 mm layer was the great source of sediment. This indicates that transport efficiency declined as the rill matured, which is consistent with the reductions in sediment concentration (shown in Supplementary Material Figure 8.7). Furthermore, as the SfM calculations under-estimated the mass of exported sediment apportioned to depths greater than 15 mm, while over-estimating the losses between 5 and 15 mm for P4 and P5, this provides evidence that sediment from all layers was deposited within the rill. Conversely, for the smallest rill, P3, the SfM technique under-estimated soil losses from both layers greater than 5 mm and only over-estimated soil losses from the top layer.

It is also important to consider the total relative measurement error of the SfM approach, as discussed in Chapter 5, in the context of the REO results as shown in Figure 6.9. While there was a strong correlation between the total mass calculated by SfM and the exported mass for P4, SfM over-estimated the mass of soil loss on P3 by 22.4 % while under-estimating soil loss on P5 by 12.5 %. For P3, this was most reflected in the over-estimation of the top layer, and thus most likely resulted from the overall deformation of the soil surface via slaking. Conversely, the under-estimation of soil loss on P5 could have resulted from an uplifting of the soil profile cause by swelling, or an inappropriate application of the LoD model to the DoD calculations are possible explanations for the under-estimation of soil loss on P5 by SfM.

6.5.2 Flume scale erosion experiment

A single erosion experiment was carried out on the flume, which resulted in a mean surface lowering of 1.4 mm. Observations during the rainfall event indicated that sediment was

transported in flows more consistent with interrill erosion than rill, although some small convergent features were visible towards the end of the experiment. Following the experiment, qualitative observations suggested that surface lowering was primarily situated around large aggregates on the soil surface, which was also visible in the SfM point cloud and DoDs (Figure 6.8). Unlike the plot scale sheetwash experiments, the bulked PSD of the exported sediment was not significantly different to the PSD of the original soil (Supplementary Material Figure 8.8). However, there was a mean enrichment of 3.9 for the <63 µm fraction throughout the experiment, and sediment fractions between 500 and 125 µm represented over 50 % of the total yield. This is consistent with the plot scale sheetwash experiment (Figure 6.2), however, unlike the plot experiments, sediment concentrations did not decline with time, suggesting that there was not an exhaustion of material or similar level of sealing on the soil surface. These findings thus highlight the vulnerability of the soil used in the flume experiments to sheetwash, and agree with the findings presented in Chapter 3 (see Figure 3.6).

Analysis of REO concentrations within the exported sediment revealed that the middle section of the flume, which was tagged with Gd (1 – 2 m from the top) was the primary source (Figure 6.7). This is consistent with the findings of Polyakov and Nearing (2004), who were working with a 4 metre long flume. For the first time-step, however, the section of the flume nearest to the exit (tagged with Pr) was the dominant soil source, contributing 60 % of the total sediment yield and the mid-section contributed 40 %. While the mid-section of the flume was the primary source of exported sediment for all subsequent samples, the sediment concentrations from both the mid-section and the section nearest the exit continued to increase for the first 14 minutes of the experiment, matching increasing discharge. However, after steady state was reached, the amount of sediment exported from the final metre of the flume decreased for the remainder of the experiment. This also coincided with a gradual increase in sediment sourced from the section furthest from the flume exit, tagged with Nd, indicating that sediment travel distances did reach at least 2 m during the experiment. The results therefore demonstrate that as the flow pathways became more connected along the length of the flume, the carrying capacity that remained after the mid-section of the flume decreased, which suggests that some sediment was transported in suspension.

Given the dominance of sheetwash erosion during the experiment, only 3.6 % of the sediment was sourced from within the La-tagged mass. The patterns of soil loss identified by the SfM DoD for negative elevation changes greater than 10 mm were, however, visually consistent with the features typical of rill initiation as found by Bryan and Poesen (1989), for example. This suggests that the flow rate of the moving water had reached critical sheer stress, and should the experiment have run for longer suggests the rills would have continued to develop. However, while the SfM DoD over-estimated soil loss from all three sections along the flume length, losses from the La-tagged soil were underestimated. This suggests that there could have been some back-filling of the rills with sediment transported from upslope, consistent with the theory that most sediment is moved downslope in a series of short movements (Wainwright *et al.*, 2008b). Indeed, the Nd-tagged section had the greatest relative error between SfM and REO calculations, identifying a potential source of the deposited sediment. However, unlike the plot scale experiments, visual inspection of the SfM MVS DoD and point clouds illustrate that the soil surface within the convergent features was smooth, rather than covered with large aggregates, indicating that deposited material primarily consisted of disaggregated soil particles.

6.6 Conclusions

This study has presented two different approaches to elucidating retrospective information about sediment sources under changing soil erosion conditions, within a laboratory setting. The sediment apportionment and story presented by both techniques was consistent with experimental observations, such as identifying the presence of convergent flow paths, changing transport efficiencies, and deposition within rills. Thus this study has confirmed that the application of both methods can provide useful retrospective information on soil erosion processes and sediment sources, in addition to that which can be gleaned from runoff and sediment fluxes alone. Through presenting a stratified and spatial understanding of source apportionment, the study was also able to reveal information about the relative contribution of different soil erosion processes within the experiments. Furthermore, the REO tracers were able to confirm that the depths of change identified by the SfM-MVS DoD were not artefacts caused by SfM-MVS processing, and increasing the confidence in SfM approaches for assessing non-erosive changes to soil structure.

Aside from examining the application of REO tracers and SfM-MVS derived DoDs to assessments of source apportionment, the study has aligned with the broader soil erosion discourse. Through illustrating the dominance of soil fractions between 125 and 500 µm

(fine and medium sands) within the eroded sediment, at both scales and from two different soils, the experiments have further highlighted the vulnerability of sandy loams to soil erosion, even in the absence of rilling. The combination of REO tracers and SfM-MVS has identified that during soil erosion events sediment in both aggregate and particle form is deposited within the convergent features, even when the rill extended the full length of the soil surface, as with the plot experiments. Accordingly, this study has confirmed that while some sediment is transported in suspension across the full length of the soil surface, sediment can also move as a series of shorter movements both within (as sediment redistribution) and beyond (as soil loss) the plot or flume.

7. DISCUSSION AND CONCLUSIONS

As we move towards a national-scale understanding of soil erosion in the UK, this thesis aimed to explore some of the multiple techniques available for developing an understanding of soil erosion in the UK. To that end, this thesis has presented three novel pieces of research; each designed to answer the specific objectives set out in Section 1.2 to 1.4. The first research chapter (Chapter 3) collated the existing body of UK-based soil erosion research into a geodatabase, before determining the extent to which these existing data and methodological approaches can be used to develop an empirically derived understanding of soil erosion in the UK. The second research chapter (Chapter 5) assessed which of two proximal sensing technologies, TLS and SfM-MVS, was best suited to a cost-effective, replicable and robust assessment of soil erosion within a laboratory environment. The final research chapter (Chapter 6) built on the findings of the Chapter 5, using both REO tracers and SfM-MVS to elucidate retrospective information about sediment sources under changing soil erosion conditions, also within a laboratory environment. This chapter will now discuss how the findings of the individual chapters are situated within the broader discourse before articulating the limitations of the research presented herein and suggesting potential areas for future research.

7.1 Existing soil erosion observations

While the core community of UK-based soil erosion researchers have published numerous reviews of the existing soil erosion research in the UK (e.g. Boardman, 2002, 2006, 2013; Boardman et al., 1990; Brazier, 2004; Evans, 1988b, 1995, 2005, Evans et al., 2015, 2017), Chapter 3 presents the most comprehensive independent compilation and review of the existing soil erosion research in the UK, to-date. The study is situated within an extensive history of soil erosion research in the UK, as confirmed by the inclusion of over 1500 individual soil erosion observations within the geodatabase. Within the literature there was a varied array of methods used to monitor soil erosion, reflecting the maturation of the understanding of the importance of soil erosion described by Evans (2010). Accordingly, monitoring techniques have evolved from *ad hoc* assessments (e.g. Evans & Morgan, 1974) arising from the need to alert the wider soil research community to the presence of soil erosion, to formal monitoring programs within experimental catchments (e.g. Deasy et al., 2011). The discourse surrounding the merits of the existing research has also been changeable since Evans' 1971 paper (Evans, 1971). This is perhaps best described by the following quotes from two separate papers led by Evans:

> *"trends in the extent and severity of water erosion in lowland England and Wales cannot be identified with any certainty from the three national monitoring schemes"* (Evans, 2005: 155)

> *"Field-based assessments of water erosion in lowland Britain delivered by a number of strategic campaigns give a consistent picture of the extent, frequency and rate of erosion"* (Evans *et al.*, 2015: 10–11)

Through presenting an independent review of the existing body of work, the results presented in Chapter 3 are perhaps best aligned with the former statement. The compiled data has illustrated that although low relative to rates found in Europe, as summarised by Verheijen et al. (2009), examples of soil erosion rates exceeding the defined tolerable rate of 1 t ha^{-1} yr^{1} do exist in the UK (Figure 3.3). However, given the biased nature of the soil erosion story presented within the existing dataset, it is impossible to ascertain if the frequency and magnitude of soil erosion events in the UK are problematic.

The analysis of the data has identified that there are numerous shortfalls within the methodological approaches of the studies. The difference between soil erosion rates determined by volumetric estimates and ^{137}Cs-based assessments illustrates that, despite the criticism of ^{137}Cs approaches (Evans *et al.*, 2017; Mabit *et al.*, 2013; Parsons & Foster, 2011, 2013), best summarised as a need for a robust understanding of background concentrations, the purely volumetric approach widely adopted in the UK, though rapid in application, does not capture the full extent of soil erosion within arable landscapes (Figure 3.10). This is further reflected in the discrepancies between watercourse turbidity and visible on-site erosion described by Evans (2017). Chapter 3 has also identified that the bias towards sites with a known history or high likelihood of erosion has a significant impact on the distribution and magnitude of erosion rates observed Figure 3.11). Accordingly, this study has substantiated the recommendations of Brazier et al. (2011), and reaffirmed the need for a new un-biased approach to monitoring soil erosion in the UK. Furthermore, the conclusions are also aligned with the global meta-analysis carried out by García-Ruiz et al. (2015) in highlighting the need for a unified approach to soil erosion monitoring and reporting. To this end, on publication of this chapter within a peer-reviewed journal, the geodatabase will be made open-access, with the goal of promoting a collective development towards a national-scale assessment of soil erosion in the UK.

7.2 Quantification of soil erosion using proximal technologies

The application of TLS and SfM-MVS to geomorphic change detection is a rapidly expanding area of research (Eltner *et al.*, 2016; Smith *et al.*, 2015; Telling *et al.*, 2017). SfM-MVS

presents a novel and low cost alternative to TLS, however the quality of the spatial data is, broadly speaking, derived from the estimation of the intrinsic and extrinsic geometry of consumer-grade cameras, rather than the timed return of a precision laser. As a result, there is an emerging body of research testing the performance of SfM-MVS against TLS results for change detection (Castillo *et al.*, 2012; Eltner *et al.*, 2014; Glendell *et al.*, 2017; Ouédraogo *et al.*, 2014). To-date, however, this has been carried out in the absence of true soil erosion measurements, such as those derived from the collection of all exported sediment from known plot areas. In addition to benchmarking against TLS, the precision of SfM-MVS applications are often assessed with the RMSE of independent GCPs. Smith et al. (2015), in reviewing SfM-MVS applications in physical geography, found a linear relationship between the RMSE of GCPs and survey range (i.e. dimensionless precision ratio), and found a median relationship of ca. 1:600 in the existing literature, for survey distances greater than 1 m. Accordingly, through identifying the limitations of TLS and SfM-MVS applications in laboratory settings with reference to 'true' observations of total soil loss, the experimental approach and findings presented in Chapter 5 symbolise a novel contribution to a developing field of research.

While presenting a simple and replicable workflow, the SfM-MVS point clouds produced through this experiment are, to the author's knowledge, of the highest quality achieved within similar environments (Figure 5.1, Figure 5.2,Table 5.1,Table 5.2 and Table 5.3). Consistent with the recent findings of Balaguer-Puig et al. (2017), Eltner et al. (2017) and Prosdocimi et al. (2017), the elevation changes detected by SfM-MVS after filtering with minimum LoD also included non-erosive processes that alter the soil bulk density, such as slaking and compaction. This limited the correlation between soil loss observations and the predictions made by SfM-MVS DoDs, when quantifying soil loss from predominately diffuse processes. The effect of non-erosive changes in surface elevations were, however, less significant for the plot scale rilling experiment (Figure 5.7), illustrating the potential for SfM-MVS applications for laboratory based studies. Conversely, TLS, after filtering with a minimum LoD was not able to detect any elevation changes following the sheetwash experiment and consistently underestimated the volume of soil loss during the rilling experiment (Figure 5.4). Chapter 5 has thus highlighted the need for a full understanding of the limitations of TLS, such as the importance of beam diameter, when using it as a benchmark technology.

The experimental conditions created features that were of a similar scale to those found under natural conditions, within field environments. For example, at the plot scale, rill depths ranged from 3 – 5.5 cm (Figure 5.8), consistent with depths observed by Evans and Morgan (1974) in the UK. Furthermore, increasing the DTM resolution to a maximum of 20 mm, consistent with the field scale applications (Glendell et al., 2017), did not have a significant impact on the soil loss calculations on the plot scale experiments. Consequently, there is potential to build on the understanding developed within this experiment for field scale applications, where pre-calibrated ground-based or near surface (i.e. <3 m) imagery could be used to quantify soil losses to spatial resolutions and precisions similar to those presented in Chapter 5.

7.3 Source apportionment under different soil erosion processes

Through providing information on the role of different soil erosion pathways and sediment transport distances, an understanding of source apportionment is crucial to understanding the mechanisms of soil erosion (Govers *et al.*, 2007; Kinnell, 2005; Parsons *et al.*, 2004; Wainwright *et al.*, 2008b). Accordingly, tracers, both naturally occurring and artificially applied have played an important role in elucidating retrospective information about soil erosion processes. For example, ^{137}Cs approaches have been crucial to developing an understanding of tillage erosion processes (Quine *et al.*, 1997), while REO tracers, through the existence of multiple forms have been used to understand patterns of sediment transport distances both within laboratory environments (Michaelides *et al.*, 2010; Polyakov & Nearing, 2004; Pryce, 2011) and in field scale applications (Kimoto *et al.*, 2006a; Polyakov *et al.*, 2009; Stevens & Quinton, 2008). The experiment presented in Chapter 6, however, is the first example of a stratified approach to tagging with REO tracers. Similarly, while previous studies have used SfM-MVS to identify areas of soil loss or deposition (Balaguer-Puig *et al.*, 2017; Eltner *et al.*, 2017; Smith & Vericat, 2015), the stratified use of the SfM-MVS point cloud is completely novel, to the best of the author's knowledge. Thereby, Chapter 6 has presented a unique assessment of source apportionment under three different soil erosion conditions.

Through presenting a stratified and spatially quantified assessment of source apportionment, the study presented in Chapter 6 was able to ascertain an understanding of the changes in sediment apportionment under different soil erosion conditions (Figure 6.6 and Figure 6.8). Accordingly, Figure 7.1 presents a modified version of the figure included in Section 2.1.1 of the literature review, to illustrate the potential contribution to

understanding of soil erosion processes that could arise from the study. Furthermore, through identifying the spatial distribution and relative contribution of both diffuse and convergent water erosion processes (Figure 6.5), this study has illustrated the potential for similar applications within more controlled experimental settings, such as those designed for specific hypothesis testing, as described by Bryan (2000). The combination of techniques also acted to confirm some of the uncertainties around the SfM-MVS elevation changes identified in Chapter 5, most notably, the depth of change observed during the sheetwash experiments (Figure 6.3 and Figure 6.4). Given the sheetwash experiments had the greatest discrepancies between elevation changes and masses of sediment loss, a combined approach has the potential to evaluate the magnitudes of non-erosive changes within the soil profile (e.g. due to soil compaction or slaking).

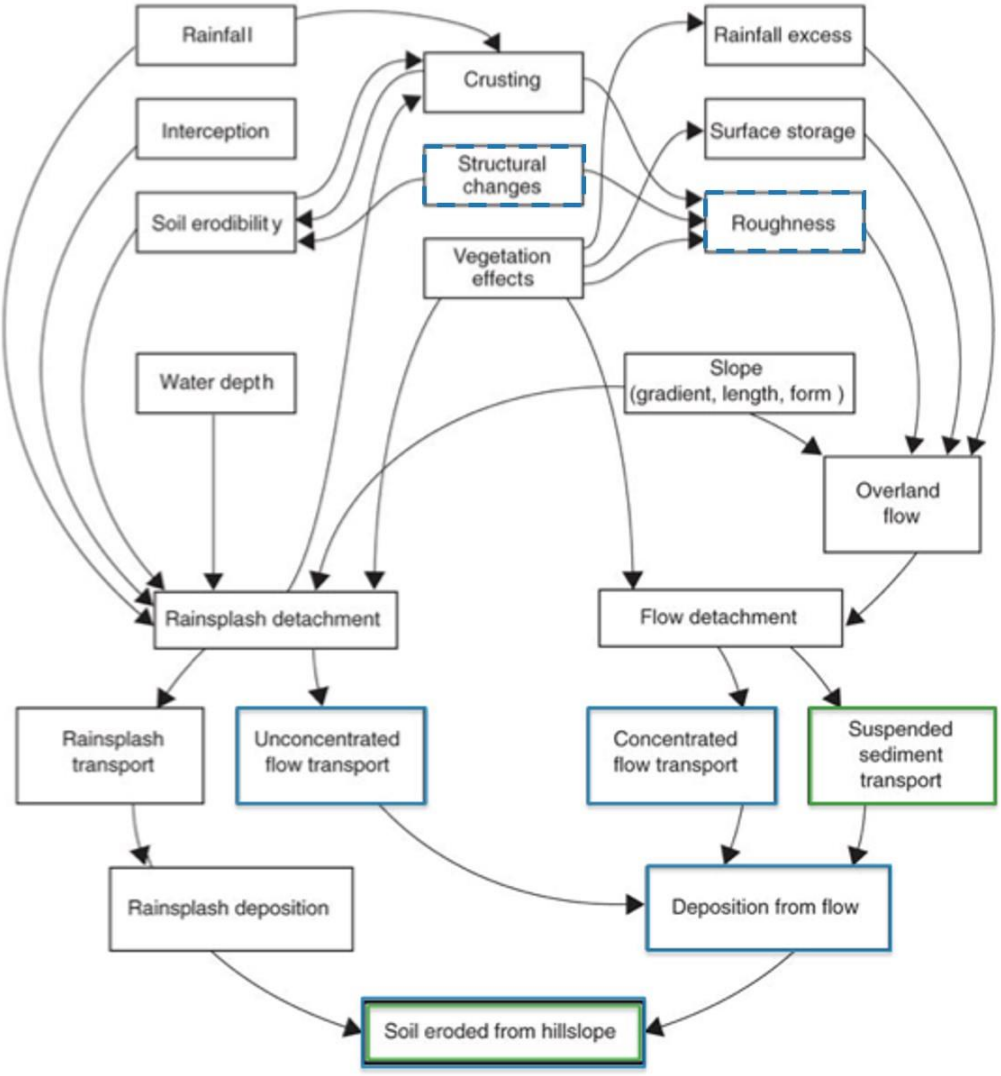

Figure 7.1: Modified complexities of soil erosion processes diagram illustrating the contribution of REOs (green) and SfM-MVS (blue) to the understanding of soil erosion processes. Dashed lines indicates areas of further research (From Brazier, 2013: Figure 15.1, p. 254).

7.4 Study limitations and future research

While Chapter 3 has presented the most comprehensive compilation and assessment of existing soil erosion research in the UK to-date, the strength of the review was limited by an absence of multivariate analysis. Multivariate analysis would have allowed the UK-based findings to be better situated within global discussions on the complexity of interactions between environmental and methodological variables and soil erosion rates, as achieved in the meta-analysis presented by García-Ruiz et al. (2015). However, due to the information content and biased nature of the source literature, it was not possible to carry out a statistically sound multivariate analysis of the geodata in this instance. Accordingly, this research has the potential to provide the impetus needed to improve the reporting of soil erosion studies, while also providing a criteria from which to carry out future assessments of soil erosion in the UK, as listed in Section 3.7 .

The application of a suite of monitoring techniques to laboratory scale soil erosion experiments has illustrated their potential to contribute to our understanding of soil erosion processes. Although the relationship between soil loss and elevation changes were not always consistent, even with the inclusion of conservative LoDs, the resolution and precision of the spatial information attained using the SfM-MVS approach in combination with REO tracers illustrates that the combination presents an exciting platform with great potential to be implemented along-side laboratory-based soil erosion studies. The identification of aggregates and the potential to resolve grains of sand and sub-millimetre elevation changes, from the SfM MVS point clouds, DTMs and DoDs suggests that further studies could be undertaken to extract spatially complex information on erosion processes. For example, changes in surface roughness could be used as a metric to identify slaking rates or be used to further explore how soil microtopography influences soil erosion processes (Anderson & Croft, 2009; Bryan, 2000; Smith, 2014). Furthermore, the smooth flow pathways between groups of aggregates visible on the soil surface following the plot scale sheetwash experiment, were consistent with the sealing of the soil surface by redistributed soil particles. The patterns were also visible within the SfM outputs, and suggest further work could be undertaken to quantify the spatial extent of surface sealing during the experiments.

The trialled precision analysis presented in Section 5.4 could be used for cloud to cloud quantification of change through the adapted Multiscale Model to Model Cloud Comparison

'M3C2' (Lague *et al.*, 2013) method presented by James et al. (2017b). This would perhaps be of most benefit for the compaction and sheetwash experiments, where the resolution of information attainable would be increased through reducing the need to include DTM error. Such approaches could also be used in combination with connectivity indexing maps, similar to Prosdocimi et al. (2017), and a REO-tracer derived understanding of source apportionment, leading to better constraint of process-based models. Furthermore, due to the low number of images and reduced processing times, the experimental set-up could be modified to collect within event changes to surface roughness and flow paths, for example.

Whilst this study has demonstrated that both proximal sensing methods can produce ultra-fine grain data, there is further scope to improve the methods used for both techniques. For example, further experimental work could be undertaken to reveal if the methodological error of scanning the soil surfaces at less than beam diameter had an impact on the magnitude of TLS DTM σ_z and therefore the LoD and ability to quantify sheetwash and sediment deposition. Aside from the methodological improvements already suggested, the quality of the SfM MVS data could be potentially improved further through the use of prime lenses, at the cost of a more expensive set-up. Zoom lenses, with a greater number of moving parts, are particularly susceptible to changes in temperature and humidity levels present within the experimental hall, for example. Consequently, whilst all possible care was taken to minimise changes to the intrinsic lens geometry, some of the variability in SfM MVS model precision could have arisen from subtle changes to the intrinsic geometry due to external environmental conditions.

7.5 Conclusions

This thesis has explored some of the multiple techniques available for building an understanding of soil erosion in the UK. The collation and review of all available UK-based and empirically derived soil erosion observations has confirmed that there is a rich history of soil erosion observations in the UK. However, while there are examples of soil erosion on arable land reaching rates of 91.7 t ha^{-1} yr^{-1}, because of the biased nature of the existing studies, the geodatabase cannot be used for determine if there is a soil erosion problem in the UK. Analysis of the data has illustrated that while environmental controls, such as soil texture has had some impact on the rates of erosion observed, the methodological approach and techniques used has had a significant impact on the distribution of the results. Accordingly, there is a real need for a new approach to monitoring soil erosion nationally.

The experimental chapters have presented a robust assessment of two proximal sensing technologies, TLS and SfM-MVS, and REO tracers in two discrete scales – plot and flume – within a laboratory environment. The assessment of the performance of TLS and SfM-MVS has revealed that while SfM-MVS was the best suited of the two for quantifying soil loss within laboratory environment, non-erosive changes to the soil surface elevation can influence the accuracy of the soil loss estimates regardless of the precision and density of spatial information attained with the technology. The combination of SfM-MVS and REO tracers, however, did elucidate retrospective information on sediment apportionment and provide some insight into the contribution of different soil erosion processes.

Finally, this study has identified that without 'true' observations of soil loss i.e. collection of sediment leaving known plot areas, proxies, such as the novel techniques presented in the experimental work herein (Chapters 4 – 6) and the methods used in the existing landscape scale assessments of soil erosion as included in the database chapter (Chapter 3), are not capable of providing a complete assessment of soil erosion rates. However, this work has indicated that despite this limitation, each technique can present valuable information on the complex and spatially variable nature of soil erosion and associated processes, across different observational environments and scales.

8. SUPPLEMENTARY MATERIAL

Table 8.1: Summary table illustrating the structure of records held within the geodatabase, when limited to records with a presence of erosion.

		Method			Site selection				Erosion risk (Evans, 1990)				
		^{137}Cs	*RSC*	*Volumetric*	*Known*	*Predicted*	*Grid*	*Other*	*1*	*2*	*3*	*4*	*5*
Scale	*Plot*	0	11	10	2	16	0	3	11	0	7	0	2
	Field	14	0	127	45	2	94	0	13	28	24	4	5
	Hillslope	18	9	0	0	24	0	3	11	3	13	0	0
	Catchment	0	0	20	10	10	0	0	1	0	15	0	4
	Regional	0	0	47	0	47	0	0	0	0	0	0	0
Method	^{137}Cs				13	19	0	0	10	3	16	1	2
	RSC				1	15	0	4	12	3	3	0	2
	Volumetric				43	65	94	6	16	27	40	3	7
Site selection	*Known*								2	4	12	1	7
	Predicted								18	3	31	0	0
	Grid								11	24	16	3	3
	Other								7	2	0	0	1

Table 8.2: Processing and error properties following plot scale camera calibration.

	Number of images					
Plot	Camera 1	Camera 2	Camera 3	Reference use	Scalebars (n)	RMSE (mm)
2	28	30	25	Control	77	0.19
				Check	12	0.2
3	30	38	44	Control	78	0.18
				Check	12	0.2
4	32	27	28	Control	78	0.19
				Check	12	0.2
5	29	29	36	Control	78	0.19
				Check	12	0.2

	Control points (n)	Error (mm)				Time (hh:mm)
Plot		x	y	z	RMSE	
2	7	0.25	0.3	0.13	0.42	00:19
	6	0.38	0.3	0.26	0.55	
3	8	0.24	0.29	0.12	0.39	00:36
	5	0.44	0.29	0.25	0.58	
4	7	0.23	0.29	0.11	0.39	00:14
	6	0.36	0.28	0.25	0.52	
5	7	0.23	0.29	0.08	0.38	00:18
	6	0.36	0.29	0.18	0.49	

Table 8.3: SfM MVS processing properties and quality of plot scale experimental models, based on Photoscan metrics.

E	Plot	Reference use	Control points (N)	Error (mm)				GSD (mm/pix)	RMS reprojection (pix)	Time (hh:mm)
				x	y	z	RMSE			
E0	2	Control	27	0.06	0.06	0.10	0.13	0.174	0.416	00:03
		Check	16	0.08	0.11	0.20	0.24			
	3	Control	32	0.06	0.06	0.12	0.15	0.174	0.378	00:03
		Check	11	0.16	0.17	0.22	0.32			
	4	Control	26	0.06	0.04	0.09	0.12	0.174	0.363	00:03
		Check	16	0.09	0.05	0.14	0.18			
	5	Control	29	0.05	0.07	0.11	0.14	0.175	0.368	00:06
		Check	11	0.06	0.06	0.14	0.16			
E1	2	Control	28	0.07	0.05	0.12	0.15	0.174	0.366	00:03
		Check	15	0.08	0.05	0.21	0.23			
	3	Control	26	0.10	0.11	0.13	0.19	0.174	0.341	00:03
		Check	17	0.15	0.17	0.28	0.36			
	4	Control	27	0.09	0.07	0.21	0.24	0.173	0.329	00:05
		Check	12	0.17	0.11	0.26	0.33			
	5	Control	29	0.07	0.07	0.11	0.15	0.173	0.416	00:05
		Check	12	0.09	0.06	0.12	0.16			
E2	2	Control	30	0.05	0.05	0.09	0.11	0.175	0.325	00:03
		Check	11	0.04	0.06	0.12	0.14			
	3	Control	30	0.05	0.05	0.13	0.15	0.175	0.33	00:03
		Check	12	0.08	0.07	0.23	0.25			
	4	Control	26	0.08	0.08	0.20	0.23	0.173	0.385	00:05
		Check	15	0.17	0.15	0.26	0.35			
	5	Control	30	0.07	0.07	0.09	0.13	0.176	0.389	00:03
		Check	13	0.07	0.08	0.13	0.16			
E3	2	Control	30	0.07	0.06	0.06	0.11	0.176	0.316	00:03
		Check	14	0.13	0.08	0.05	0.17			
	3	Control	28	0.11	0.08	0.07	0.15	0.175	0.336	00:36
		Check	16	0.19	0.16	0.10	0.27			
	4	Control	25	0.23	0.10	0.11	0.28	0.175	0.397	00:14
		Check	12	0.35	0.14	0.14	0.40			
	5	Control	26	0.23	0.12	0.10	0.28	0.176	0.325	00:18
		Check	13	0.32	0.22	0.17	0.43			

4000 .ply files found. First file has 6428 points.
Reading point cloud (.ply) files... Done.
Calculating mean point coordinates... Done.
Calculating point precisions and covariances... Done.
Writing text file output: _point_precision_and_covars.txt... Done.
Calculating point precisions and covariances for different numbers of iterations... Done.
Calculating overall georeferencing precision... Done.

Differences between Monte Carlo means and initial error-free values:
(Differences should be small to indicate that sufficient Monte Carlo iterations have been completed).

Rotation (as Euler angles; o, p, k; mdeg):	-0.00150	-0.00182	0.00245
Translation (in X, Y, Z; mm):	0.00001	0.00004	0.00001
Scale (%):	-0.0001		

Overall survey georeferencing precision:

Rotation (as Euler angles; o, p, k; mdeg):	47.905	38.102	31.889
Rotation (around fixed X, Y, Z axes; mdeg):	37.902	47.734	31.497
Translation (in X, Y, Z; mm):	0.17	0.18	0.17
Scale (%):	0.0537		

RMS residual discrepancies on point coordinates after overall georeferencing:

Mean for all points (in X, Y, Z; mm):	0.05	0.04	0.17
Std. dev. across all points (in X, Y, Z; mm):	0.01	0.01	0.00

Calculating shape point precisions and covariances (i.e. excluding overall georeferencing errors)... Done.
Writing text file output: _point_precision_and_covars_shape_only.txt... Done.

Mean point precisions (mm):

Full (X, Y, Z, [Mean], Hz, full magn.:	0.21	0.21	0.28	[0.23]	0.30	0.41
Shape only (X, Y, Z, [Mean], Hz, full magn.:	0.04	0.04	0.16	[0.08]	0.06	0.17

Median point precisions (mm):

Full (X, Y, Z, [Median], Hz, full magn.:	0.21	0.21	0.27	[0.22]	0.29	0.40
Shape only (X, Y, Z, [Median], Hz, full magn.:	0.03	0.03	0.17	[0.04]	0.05	0.19

Generalised survey imaging characteristics:
Max. survey dimension: 0.88 m

Dimensionless relative precision ratios (i.e. mean point precision with respect to):

	Full	Excluding overall georeferencing
Survey extent:	1 : 3,760	1 : 11,200

Point precision analysis complete.

Figure 8.1 : Precision estimates for P5E2 based on methods presented by James et al., (2017b)

```
4000 .ply files found. First file has 7049 points.
Reading point cloud (.ply) files... Done.
Calculating mean point coordinates... Done.
Calculating point precisions and covariances... Done.
Writing text file output: _point_precision_and_covars.txt... Done.
Calculating point precisions and covariances for different numbers of iterations... Done.
Calculating overall georeferencing precision... Done.

Differences between Monte Carlo means and initial error-free values:
(Differences should be small to indicate that sufficient Monte Carlo iterations have been
completed).
Rotation (as Euler angles; o, p, k; mdeg):   -0.00110          0.00448 0.00523
Translation (in X, Y, Z; mm):                          0.00001 0.00006 0.00004
Scale (%):          -0.0002

Overall survey georeferencing precision:
Rotation (as Euler angles; o, p, k; mdeg):   56.764  39.215  33.858
Rotation (around fixed X, Y, Z axes; mdeg):          39.057  56.643  33.504
Translation (in X, Y, Z; mm):                        0.18    0.19    0.19
Scale (%):          0.0574

RMS residual discrepancies on point coordinates after overall georeferencing:
Mean for all points (in X, Y, Z; mm):                0.07    0.05    0.29
Std. dev. across all points (in X, Y, Z; mm): 0.00   0.00    0.00

Calculating shape point precisions and covariances (i.e. excluding overall georeferencing errors)...
Done.
Writing text file output: _point_precision_and_covars_shape_only.txt... Done.

Mean point precisions (mm):
Full (X, Y, Z, [Mean], Hz, full magn.:               0.23    0.23    0.38    [0.28]  0.32    0.50
Shape only (X, Y, Z, [Mean], Hz, full magn.:0.06     0.05    0.28    [0.13]  0.08    0.29

Median point precisions (mm):
Full (X, Y, Z, [Median], Hz, full magn.:             0.22    0.23    0.40    [0.24]  0.32    0.50
Shape only (X, Y, Z, [Median], Hz, full magn.:       0.05    0.04    0.31    [0.06]  0.07    0.33

Generalised survey imaging characteristics:
Max. survey dimension:          0.90 m

Dimensionless relative precision ratios (i.e. mean point precision with respect to):
                    Full            Excluding overall georeferencing
Survey extent:   1 : 3,220                  1 : 7,050

Point precision analysis complete.
```

Figure 8.2: Precision estimates for P5E3 based on methods presented by James et al., (2017b)

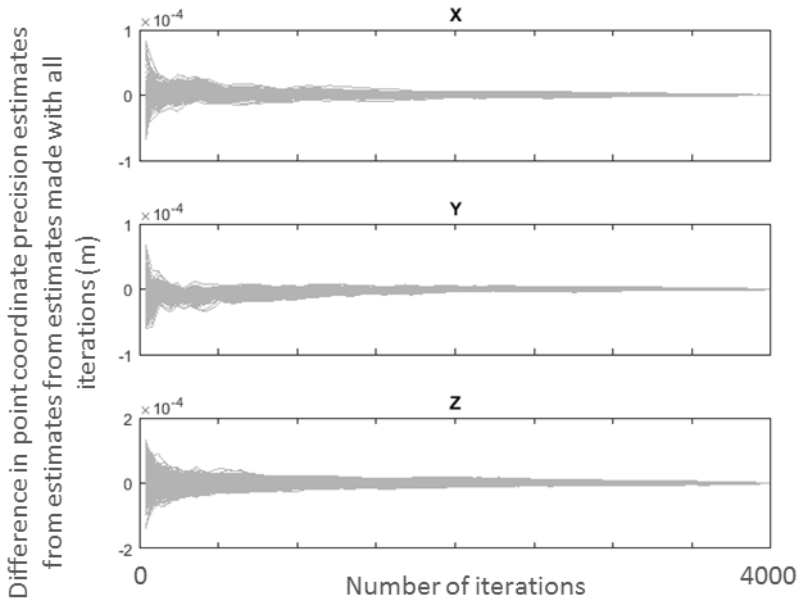

Figure 8.3: Variation in tie point precision as a function of the number of Monte Carlo iterations.

4000 .ply files found. First file has 31265 points.
Reading point cloud (.ply) files... Done.
Calculating mean point coordinates... Done.
Calculating point precisions and covariances... Done.
Writing text file output: _point_precision_and_covars.txt... Done.
Calculating point precisions and covariances for different numbers of iterations... Done.
Calculating overall georeferencing precision... Done.

Differences between Monte Carlo means and initial error-free values:
(Differences should be small to indicate that sufficient Monte Carlo iterations have been completed).

Rotation (as Euler angles; o, p, k; mdeg):	-0.00414	0.00175	-0.00065
Translation (in X, Y, Z; mm):	-0.00014	0.00067	0.00000
Scale (%):	0.0003		

Overall survey georeferencing precision:

Rotation (as Euler angles; o, p, k; mdeg):	38.995	83.719	37.141
Rotation (around fixed X, Y, Z axes; mdeg):	83.615	38.764	36.962
Translation (in X, Y, Z; mm):	0.67	0.65	0.67
Scale (%):	0.0463		

RMS residual discrepancies on point coordinates after overall georeferencing:

Mean for all points (in X, Y, Z; mm):	0.12	0.08	0.25
Std. dev. across all points (in X, Y, Z; mm):	0.00	0.00	0.00

Calculating shape point precisions and covariances (i.e. excluding overall georeferencing errors)... Done.
Writing text file output: _point_precision_and_covars_shape_only.txt... Done.

Mean point precisions (mm):

Full (X, Y, Z, [Mean], Hz, full magn.:	0.89	0.80	1.03	[0.90]	1.19	1.58
Shape only (X, Y, Z, [Mean], Hz, full magn.:	0.07	0.05	0.16	[0.09]	0.08	0.18

Median point precisions (mm):

Full (X, Y, Z, [Median], Hz, full magn.:	0.85	0.77	1.01	[0.86]	1.15	1.53
Shape only (X, Y, Z, [Median], Hz, full magn.:	0.03	0.03	0.09	[0.05]	0.04	0.10

Generalised survey imaging characteristics:

Max. survey dimension:	3.37 m
Mean observation distance:	0.94 m
Mean ground pixel dimension:	0.2 mm

Dimensionless relative precision ratios (i.e. mean point precision with respect to):

	Full	Excluding overall georeferencing
Survey extent:	1 : 3,730	1 : 37,700
Observation distance:	1 : 1,040	1 : 10,500
Pixel size (XY precision):	5.8	0.41 (pixels)
Pixel size (Z precision):	5	0.76 (pixels)

Point precision analysis complete.

Figure 8.4: Precision estimates for F2E2 based on methods presented by James et al., (2017b)

Base formula for determination and application of cell-by-cell LoD using Surfer GridMath

$LoD\ (X) = 1.96 * (A^2 + C^2 + D^2 + F^2 + G^2)^{0.5}$

ELEVATION CHANGE = IF $(X > ((E - B)^2)^{0.5}$,

TRUE = 0,

FALSE = {IF(((E - B) <0), [E - B + (X)], [E - B - (X)]})

Where:
A – CLOUD1 RMSE
B – DEM1
C – DEM1 σ_z
D – CLOUD2 RMSE
E – DEM2
F – DEM2 σ_z
G – REGISTRATION/ALIGNMENT RMSE
X = (1.96 * pow((pow(A,2) + pow(C,2) + pow(D,2) + pow(F,2) + pow(G,2)),0.5))

Therefore:
ELEVATION CHANGE = IF ((1.96 * pow((pow(A,2) + pow(C,2) + pow(D,2) + pow(F,2) + pow(G,2)),0.5)) > pow((pow(E-B,2)),0.5), 0, (IF(((E - B) <0), (E - B + ((1.96 * pow((pow(A,2) + pow(C,2) + pow(D,2) + pow(F,2) + pow(G,2)),0.5)))), (E - B - ((1.96 * pow((pow(A,2) + pow(C,2) + pow(D,2) + pow(F,2) + pow(G,2)),0.5))))))

Actually implemented in surfer:

A – DEM1
B – DEM1 σ_z
C – DEM2
D – DEM2 σ_z
E – CLOUD1 RMSE
F – CLOUD2 RMSE
G – REGISTRATION/ALIGNMENT RMSE

ELEVATION CHANGE = IF ((1.96 * pow((pow(B,2) + pow(D,2) + pow(E,2) + pow(F,2) + pow(G,2)),0.5)) > pow((pow(C-A,2)),0.5) , 0, (IF(((C - A) <0), (C - A + (1.65 * pow((pow(B,2) + pow(D,2) + pow(E,2) + pow(F,2) + pow(G,2)),0.5))), (C - A - (1.65 * pow((pow(B,2) + pow(D,2) + pow(E,2) + pow(F,2) + pow(G,2)),0.5))))))

Figure 8.5: Formula for determination of cell-by-cell LoD using Surfer.

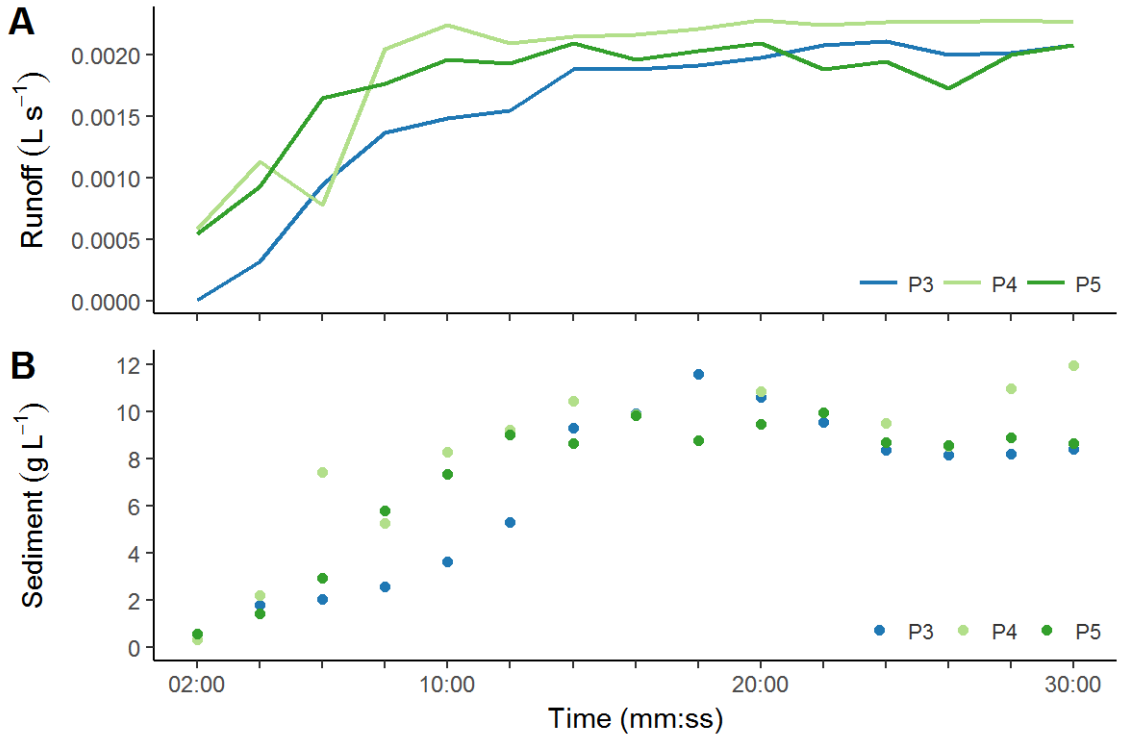

Figure 8.6: Discharge (A) and sediment flux concentrations (B) for the plot scale sheetwash experiment (E2)

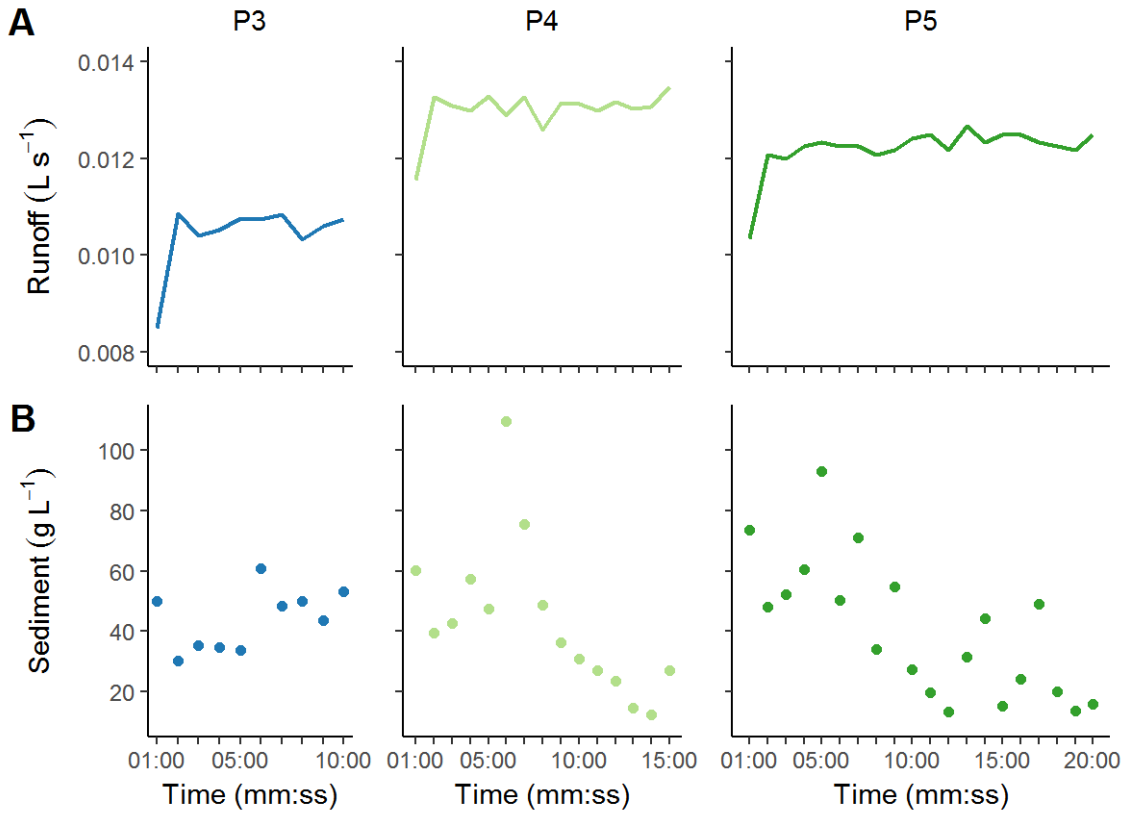

Figure 8.7: Discharge (A) and sediment flux concentrations (B) for the plot scale rilling experiment (E3)

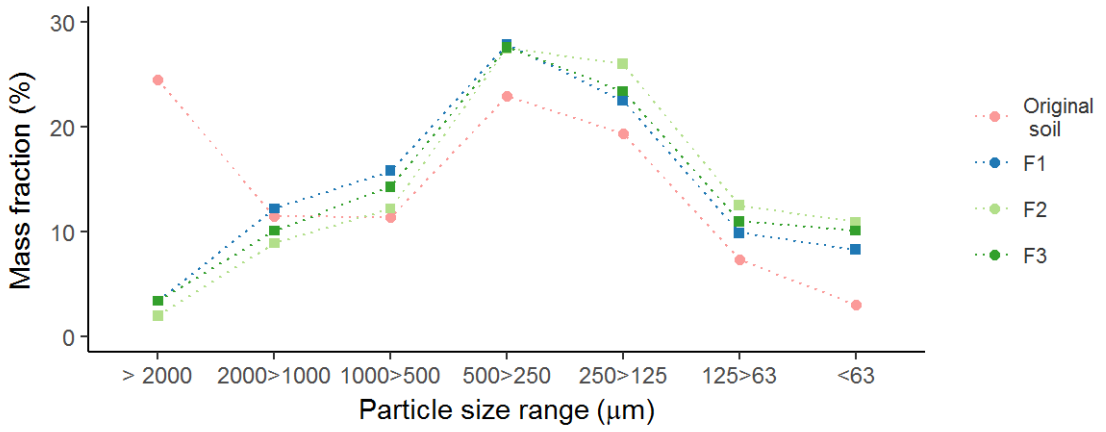

Figure 8.8: The bulked PSD for the sediment collected during the flume rainfall/runoff event (E2), presented as mass faction (%) for each φ interval, presented for all Flumes, while F3 was studied in Chapter 6.

9. REFERENCES

Abrahams AD, Li G, Krishnan C, Atkinson JF. 1998. Predicting sediment transport by interrill overland flow on rough surfaces. *Earth Surface Processes and Landforms* **23**: 1087–1099. DOI: 10.1002/(SICI)1096-9837(199812)23:12<1087::AID-ESP934>3.0.CO;2-4

Alberts EE, Moldenhauer WC, Foster GR. 1980. Soil aggregates and primary particles transported in rill and interrill Flow. *Soil Science Society of America Journal* **44**: 590–595. DOI: 10.2136/sssaj1980.03615995004400030032x

Amundson R, Berhe AA, Hopmans JW, Olson C, Sztein AE, Sparks DL. 2015. Soil and human security in the 21st century. *Science* **348**

Anders N, Masselink R, Keesstra S, Suomalainen J. 2013. High-Res Digital Surface Modeling using Fixed-Wing UAV-based Photogrammetry. *Geomorphometry 2013*. Nanjing, China

Anderson K, Croft H. 2009. Remote sensing of soil surface properties. *Progress in Physical Geography* **33**: 457–473. DOI: 10.1177/0309133309346644

Anderson K, Gaston KJ. 2013. Lightweight unmanned aerial vehicles will revolutionize spatial ecology. *Frontiers in Ecology and the Environment* **11**: 138–146. DOI: 10.1890/120150

Armstrong A, Quinton JN, Heng BCP, Chandler JH. 2011. Variability of interrill erosion at low slopes. *Earth Surface Processes and Landforms* **36**: 97–106. DOI: 10.1002/esp.2024

Asadi H, Ghadiri H, Rose CW, Rouhipour H. 2007. Interrill soil erosion processes and their interaction on low slopes. *Earth Surface Processes and Landforms* **32**: 711–724. DOI: 10.1002/esp.1426

Bakker MM, Govers G, Kosmas C, Vanacker V, Oost K van, Rounsevell M. 2005. Soil erosion as a driver of land-use change. *Agriculture, Ecosystems & Environment* **105**: 467–481. DOI: 10.1016/j.agee.2004.07.009

Balaguer-Puig M, Marqués-Mateu Á, Lerma JL, Ibáñez-Asensio S. 2017. Estimation of small-scale soil erosion in laboratory experiments with Structure from Motion photogrammetry. *Geomorphology* **295**: 285–296. DOI:

10.1016/j.geomorph.2017.04.035

Barneveld RJ, Seeger M, Maalen-Johansen I. 2013. Assessment of terrestrial laser scanning technology for obtaining high-resolution DEMs of soils. *Earth Surface Processes and Landforms* **38**: 90–94. DOI: 10.1002/esp.3344

Bennett JP. 1974. Concepts of mathematical modeling of sediment yield. *Water Resources Research* **10**: 485–492. DOI: 10.1029/WR010i003p00485

Berger C, Schulze M, Rieke-Zapp D, Schlunegger F. 2010. Rill development and soil erosion: a laboratory study of slope and rainfall intensity. *Earth Surface Processes and Landforms* **35**: 1456–1467. DOI: 10.1002/esp.1989

Beven KJ, Brazier RE. 2010. Dealing with Uncertainty in Erosion Model Predictions. *Handbook of Erosion Modelling*. John Wiley & Sons, Ltd, 52–79. DOI: 10.1002/9781444328455.ch4

Bilotta GS, Brazier RE. 2008. Understanding the influence of suspended solids on water quality and aquatic biota. *Water research* **42**: 2849–61. DOI: 10.1016/j.watres.2008.03.018

Bilotta GS, Brazier RE, Haygarth PM, Macleod CJA, Butler P, Granger S, Krueger T, Freer J, Quinton JN. 2008. Rethinking the Contribution of Drained and Undrained Grasslands to Sediment-Related Water Quality Problems. *J. Environ. Qual.* **37**: 906–914. DOI: 10.2134/jeq2007.0457

Bilotta GS, Krueger T, Brazier RE, Butler P, Freer J, Hawkins JMB, Haygarth PM, Macleod CJA, Quinton JN. 2010. Assessing catchment-scale erosion and yields of suspended solids from improved temperate grassland. *Journal of Environmental Monitoring* **12**: 731–739. DOI: 10.1039/b921584k

Blake WH, Walling DE, He Q. 1999. Fallout beryllium-7 as a tracer in soil erosion investigations. *Applied Radiation and Isotopes* **51**: 599–605. DOI: 10.1016/S0969-8043(99)00086-X

Boardman J. 1988. Severe erosion on agricultural land in east Sussex, UK October 1987. *Soil Technology* **1**: 333–348. DOI: http://dx.doi.org/10.1016/0933-3630(88)90013-X

Boardman J. 1995. Damage to Property by Runoff from Agricultural Land, South

Downs, Southern England, 1976-93. *The Geographical Journal* **161**: 177–191. DOI: 10.2307/3059974

Boardman J. 2002. The Need for Soil Conservation in Britain: Revisited. *Area* **34**: 419–427. DOI: 10.2307/20004273

Boardman J. 2003. Soil Erosion and Flooding on the Eastern South Downs, Southern England, 1976-2001. *Transactions of the Institute of British Geographers* **28**: 176–196. DOI: 10.2307/3804444

Boardman J. 2006. Soil erosion science: Reflections on the limitations of current approaches. *CATENA* **68**: 73–86. DOI: http://dx.doi.org/10.1016/j.catena.2006.03.007

Boardman J. 2013. Soil Erosion in Britain: Updating the Record. *Agriculture* **3**: 418–442. DOI: doi:10.3390/agriculture3030418

Boardman J, Burt TP, Evans R, Slattery MC, Shuttleworth H. 1996. Soil erosion and flooding as a result of a summer thunderstorm in Oxfordshire and Berkshire, May 1993. *Applied Geography* **16**: 21–34. DOI: http://dx.doi.org/10.1016/0143-6228(95)00023-2

Boardman J, Evans R. 2006. Britain. *Soil Erosion in Europe*. John Wiley & Sons, Ltd, 439–453. DOI: 10.1002/0470859202.ch33

Boardman J, Evans R, Favis-Mortlock DT, Harris TM. 1990. Climate change and soil erosion on agricultural land in england and wales. *Land Degradation & Development* **2**: 95–106. DOI: 10.1002/ldr.3400020204

Boix-Fayos C, Martínez-Mena M, Arnau-Rosalén E, Calvo-Cases A, Castillo V, Albaladejo J. 2006. Measuring soil erosion by field plots: Understanding the sources of variation. *Earth-Science Reviews* **78**: 267–285. DOI: http://dx.doi.org/10.1016/j.earscirev.2006.05.005

Brasington J, Langham J, Rumsby B. 2003. Methodological sensitivity of morphometric estimates of coarse fluvial sediment transport. *Geomorphology* **53**: 299–316. DOI: 10.1016/S0169-555X(02)00320-3

Brazier RE. 2004. Quantifying soil erosion by water in the UK: a review of monitoring and modelling approaches. *Progress in Physical Geography* **28**: 340–365. DOI:

10.1191/0309133304pp415ra

Brazier RE. 2013. Erosion and Sediment Transport: Finding Simplicity in a Complicated Erosion Model. In: Wainwright J and Mulligan M (eds) *Environmental Modelling: Finding Simplicity in Complexity*. John Wiley & Sons, 253–266

Brazier RE, Anderson K, Benaud P, Evans M, Farrow L, Glendell M, James MR, Lark M, Quine TA, Quinton JN, Rawlins B, Rickson RJ. 2016. *Developing a cost-effective framework to monitor soil erosion in England and Wales. Final report to Defra for project SP1311*.

Brazier RE, Anderson K, Quine TA, Quinton JN, Evans M, Rickson RJ, Bellamy PH, Rawlins B, Ellis M. 2011. *Developing a cost-effective framework for monitoring soil erosion in England and Wales. Final report to Defra for project SP1303*.

Brazier RE, Beven KJ, Freer J, Rowan JS. 2000. Equifinality and uncertainty in physically based soil erosion models: application of the GLUE methodology to WEPP–the Water Erosion Prediction Project–for sites in the UK and USA. *Earth Surface Processes and Landforms* **25**: 825–845. DOI: 10.1002/1096-9837(200008)25:8<825::aid-esp101>3.0.co;2-3

Brazier RE, Bilotta GS, Haygarth PM. 2007. A perspective on the role of lowland, agricultural grasslands in contributing to erosion and water quality problems in the UK. *Earth Surface Processes and Landforms* **32**: 964–967. DOI: 10.1002/esp.1484

Brazier RE, Hutton CJ, Parsons AJ, Wainwright J. 2010. Scaling Soil Erosion Models in Space and Time. *Handbook of Erosion Modelling*. John Wiley & Sons, Ltd, 98–116. DOI: 10.1002/9781444328455.ch6

Brazier RE, Rowan JS, Anthony SG, Quinn PF. 2001. "MIRSED" towards an MIR approach to modelling hillslope soil erosion at the national scale. *CATENA* **42**: 59–79. DOI: http://dx.doi.org/10.1016/S0341-8162(00)00097-7

Bryan RB. 2000. Soil erodibility and processes of water erosion on hillslope. *Geomorphology* **32**: 385–415. DOI: http://dx.doi.org/10.1016/S0169-555X(99)00105-1

Bryan RB, Poesen J. 1989. Laboratory experiments on the influence of slope length on runoff, percolation and rill development. *Earth Surface Processes and Landforms*

14: 211–231. DOI: 10.1002/esp.3290140304

Castillo C, Pérez R, James MR, Quinton JN, Taguas E V., Gómez J a. 2012. Comparing the Accuracy of Several Field Methods for Measuring Gully Erosion. *Soil Science Society of America Journal* **76**: 1319. DOI: 10.2136/sssaj2011.0390

Chambers BJ, Davies DB, Holmes S. 1992. Monitoring of water erosion on arable farms in England and Wales, 1989–90. *Soil Use and Management* **8**: 163–169. DOI: 10.1111/j.1475-2743.1992.tb00915.x

Chambers BJ, Garwood TWD. 2000. Monitoring of water erosion on arable farms in England and Wales. 1990–94. *Soil Use and Management* **16**: 93–99. DOI: 10.1111/j.1475-2743.2000.tb00181.x

Chaplot V, Le Bissonnais Y. 2000. Field measurements of interrill erosion under -different slopes and plot sizes. *Earth Surface Processes and Landforms* **25**: 145–153. DOI: 10.1002/(sici)1096-9837(200002)25:2<145::aid-esp51>3.0.co;2-3

Chapman AS, Foster IDL, Lees JA, Hodgkinson RA. 2005. Sediment delivery from agricultural land to rivers via subsurface drainage. *Hydrological Processes* **19**: 2875–2897. DOI: 10.1002/hyp.5789

Chappell A, Manchester G. 2002. Modelling to reconstruct recent wind erosion history of fields in eastern England . In: Lee JA and Zobeck TM (eds) *ICAR5/GCTE-SEN Joint Conference*, 309–311

Chappell A, Warren A. 2003. Spatial scales of 137Cs-derived soil flux by wind in a 25 km2 arable area of eastern England. *CATENA* **52**: 209–234. DOI: http://dx.doi.org/10.1016/S0341-8162(03)00015-8

Croft H, Anderson K, Kuhn NJ. 2009. Characterizing soil surface roughness using a combined structural and spectral approach. *European Journal of Soil Science* **60**: 431–442. DOI: 10.1111/j.1365-2389.2009.01129.x

Cunliffe AM, Puttock AK, Turnbull L, Wainwright J, Brazier RE. 2016. Dryland, calcareous soils store (and lose) significant quantities of near-surface organic carbon. *Journal of Geophysical Research: Earth Surface* **121**: 684–702. DOI: 10.1002/2015JF003628

D'Oleire-Oltmanns S, Marzolff I, Peter K, Ries J. 2012. Unmanned Aerial Vehicle (UAV)

for Monitoring Soil Erosion in Morocco. *Remote Sensing* **4**: 3390–3416. DOI: 10.3390/rs4113390

Davidson DA, Harrison DJ. 1995. The nature, causes and implications of water erosion on arable land in Scotland. *Soil Use and Management* **11**: 63–68. DOI: 10.1111/j.1475-2743.1995.tb00498.x

Deasy C, Baxendale SA, Heathwaite AL, Ridall G, Hodgkinson R, Brazier RE. 2011. Advancing understanding of runoff and sediment transfers in agricultural catchments through simultaneous observations across scales. *Earth Surface Processes and Landforms* **36**: 1749–1760. DOI: 10.1002/esp.2197

Deasy C, Brazier RE, Heathwaite AL, Hodgkinson R. 2009a. Pathways of runoff and sediment transfer in small agricultural catchments. *Hydrological Processes* **23**: 1349–1358. DOI: 10.1002/hyp.7257

Deasy C, Quinton JN. 2010. Use of rare earth oxides as tracers to identify sediment source areas for agricultural hillslopes. *Solid Earth* **1**: 111–118. DOI: 10.5194/se-1-111-2010

Deasy C, Quinton JN, Silgram M, Bailey AP, Jackson B, Stevens CJ. 2009b. Mitigation Options for Sediment and Phosphorus Loss from Winter-sown Arable Crops. *Journal of Environmental Quality* **38**: 2121–2130. DOI: 10.2134/jeq2009.0028

de Vente J, Poesen J, Verstraeten G, Govers G, Vanmaercke M, Van Rompaey A, Arabkhedri M, Boix-Fayos C. 2013. Predicting soil erosion and sediment yield at regional scales: Where do we stand? *Earth-Science Reviews* **127**: 16–29. DOI: 10.1016/j.earscirev.2013.08.014

Desmet PJJ, Govers G. 1997. Two-dimensional modelling of the within-field variation in rill and gully geometry and location related to topography. *CATENA* **29**: 283–306. DOI: 10.1016/S0341-8162(96)00074-4

Dinno A. 2017. dunn.test: Dunn's Test of Multiple Comparisons Using Rank Sums.

Duck RW, McManus J. 1987. Soil erosion near Barry, Angus. *Scottish Geographical Magazine* **103**: 44–46. DOI: 10.1080/00369228718736686

Duck RW, McManus J. 1994. A long-term estimate of bedload and suspended sediment yield derived from reservoir deposits. *Journal of Hydrology* **159**: 365–373. DOI:

10.1016/0022-1694(94)90267-4

Eltner A, Baumgart P. 2015. Accuracy constraints of terrestrial Lidar data for soil erosion measurement: Application to a Mediterranean field plot. *Geomorphology* **245**: 243–254. DOI: 10.1016/j.geomorph.2015.06.008

Eltner A, Baumgart P, Maas H-G, Faust D. 2014. Multi-temporal UAV data for automatic measurement of rill and interrill erosion on loess soil. *Earth Surface Processes and Landforms* **40**: 741–755. DOI: 10.1002/esp.3673

Eltner A, Kaiser A, Abellan A, Schindewolf M. 2017. Time lapse structure from motion photogrammetry for continuous geomorphic monitoring. *Earth Surface Processes and Landforms*. DOI: 10.1002/esp.4178

Eltner A, Kaiser A, Castillo C, Rock G, Neugirg F, Abellán A. 2016. Image-based surface reconstruction in geomorphometry-merits, limits and developments. *Earth Surface Dynamics* **4**: 359–389. DOI: 10.5194/esurf-4-359-2016

Eltner A, Mulsow C, Maas H. 2013. QUANTITATIVE MEASUREMENT OF SOIL EROSION FROM TLS AND UAV DATA. *International Archives of the Photogrammetry, Remote Sensing and Spatial Information Sciences* **XL**: 4–6

Emmett BA, Reynold B, Chamberlain PM, Rowe E, Spurgeon D, Brittain SA, Frogbrook Z, Hughes S, Lawlor AJ, Poskitt J, Potter E, Robinson DA, Scott A, Wood C, Woods C. 2007. *Countryside Survey: Soils Report from 2007*. Wallingford, Oxfords

Etana A, Larsbo M, Keller T, Arvidsson J, Schjønning P, Forkman J, Jarvis N. 2013. Persistent subsoil compaction and its effects on preferential flow patterns in a loamy till soil. *Geoderma* **192**: 430–436. DOI: 10.1016/j.geoderma.2012.08.015

Evans R. 1971. The Need for Soil Conservation. *Area* **3**: 20–23. DOI: 10.2307/20000505

Evans R. 1988a. *Water Erosion in England and Wales 1982-1984*.

Evans R. 1988b. *Water Erosion in England and Wales 1982-1984 pt.2*.

Evans R. 1990a. Water erosion in British farmers' fields-some causes, impacts, predictions. *Progress in Physical Geography* **14**: 199–219

Evans R. 1990b. Soils at risk of accelerated erosion in England and Wales. *Soil Use and Management* **6**: 125–131. DOI: 10.1111/j.1475-2743.1990.tb00821.x

Evans R. 1995. Some methods of directly assessing water erosion of cultivated land-a comparison of measurements made on plots and in fields. *Progress in Physical Geography* **19**: 115–129

Evans R. 2002. An alternative way to assess water erosion of cultivated land – field-based measurements: and analysis of some results. *Applied Geography* **22**: 187–207. DOI: http://dx.doi.org/10.1016/S0143-6228(02)00004-8

Evans R. 2005. Monitoring water erosion in lowland England and Wales—A personal view of its history and outcomes. *Catena* **64**: 142–161. DOI: 10.1016/j.catena.2005.08.003

Evans R. 2010. Runoff and soil erosion in arable Britain: changes in perception and policy since 1945. *Environmental Science & Policy* **13**: 141–149. DOI: http://dx.doi.org/10.1016/j.envsci.2010.01.001

Evans R. 2017. Factors controlling soil erosion and runoff and their impacts in the upper Wissey catchment, Norfolk, England: A ten year monitoring programme. *Earth Surface Processes and Landforms* **42**: 2266–2279. DOI: 10.1002/esp.4182

Evans R, Boardman J. 2016a. The new assessment of soil loss by water erosion in Europe. Panagos P. et al., 2015 Environmental Science & Policy 54, 438–447—A response. *Environmental Science & Policy* **58**: 11–15. DOI: 10.1016/j.envsci.2015.12.013

Evans R, Boardman J. 2016b. *A reply to panagos et al., 2016 (Environmental science & policy 59 (2016) 53–57*. *Environmental Science & Policy*. DOI: 10.1016/j.envsci.2016.03.004

Evans R, Brazier RE. 2005. Evaluation of modelled spatially distributed predictions of soil erosion by water versus field-based assessments. *Environmental Science & Policy* **8**: 493–501. DOI: http://dx.doi.org/10.1016/j.envsci.2005.04.009

Evans R, Collins AL, Foster IDL, Rickson RJ, Anthony SG, Brewer T, Deeks LK, Newell-Price JP, Truckell IG, Zhang Y. 2015. Extent, frequency and rate of water erosion of arable land in Britain – benefits and challenges for modelling. *Soil Use and Management* n/a-n/a. DOI: 10.1111/sum.12210

Evans R, Collins AL, Zhang Y, Foster IDL, Boardman J, Sint H, Lee MRF, Griffith BA. 2017. A comparison of conventional and 137 Cs-based estimates of soil erosion rates on

arable and grassland across lowland England and Wales. *Earth-Science Reviews* **173**: 49–64. DOI: 10.1016/j.earscirev.2017.08.005

Evans R, Morgan RPC. 1974. Water Erosion of Arable Land. *Area* **6**: 221–225

Farres PJ. 1987. The dynamics of rainsplash erosion and the role of soil aggregate stability. *CATENA* **14**: 119–130. DOI: http://dx.doi.org/10.1016/S0341-8162(87)80009-7

Fisher O. 1868. III.—On the Denudations of Norfolk. *Geological Magazine* **5**: 544–558. DOI: http://dx.doi.org/10.1017/S0016756800197079

Foley JA, DeFries R, Asner GP, Barford C, Bonan G, Carpenter SR, Chapin FS, Coe MT, Daily GC, Gibbs HK, Helkowski JH, Holloway T, Howard EA, Kucharik CJ, Monfreda C, Patz JA, Prentice IC, Ramankutty N, Snyder PK. 2005. Global Consequences of Land Use. *Science* **309**: 570–574. DOI: 10.1126/science.1111772

Foth HD. 1990. *Fundamentals of Soil Science*. John Wiley & Sons

Fullen MA. 1985a. Compaction, hydrological processes and soil erosion on loamy sands in east Shropshire, England. *Soil and Tillage Research* **6**: 17–29. DOI: http://dx.doi.org/10.1016/0167-1987(85)90003-0

Fullen MA. 1985b. Wind erosion of arable soils in east Shropshire (England) during spring 1983. *CATENA* **12**: 111–120. DOI: http://dx.doi.org/10.1016/S0341-8162(85)80010-2

Fullen MA. 1992. Erosion rates on bare loamy sand soils in east Shropshire, UK. *Soil Use and Management* **8**: 157–162. DOI: 10.1111/j.1475-2743.1992.tb00914.x

Fullen MA. 1998. Effects of grass ley set-aside on runoff, erosion and organic matter levels in sandy soils in East Shropshire, UK. *Soil and Tillage Research* **46**: 41–49. DOI: http://dx.doi.org/10.1016/S0167-1987(98)80106-2

García-Ruiz JM, Beguería S, Nadal-Romero E, González-Hidalgo JC, Lana-Renault N, Sanjuán Y. 2015. A Meta-Analysis of soil erosion rates across the world. *Geomorphology* **239**: 160–173. DOI: 10.1016/j.geomorph.2015.03.008

Gerland P, Raftery AE, Ev Ikova H, Li N, Gu D, Spoorenberg T, Alkema L, Fosdick BK, Chunn J, Lalic N, Bay G, Buettner T, Heilig GK, Wilmoth J. 2014. World population stabilization unlikely this century. *Science* **346**: 234–237. DOI:

10.1126/science.1257469

Ghadiri H, Payne D. 1977. RAINDROP IMPACT STRESS AND THE BREAKDOWN OF SOIL CRUMBS. *Journal of Soil Science* **28**: 247–258. DOI: 10.1111/j.1365-2389.1977.tb02233.x

Glendell M, McShane G, Farrow L, James MR, Quinton JN, Anderson K, Evans M, Benaud P, Rawlins B, Morgan D, Jones L, Kirkham M, DeBell L, Quine TA, Lark M, Rickson J, Brazier RE. 2017. Testing the utility of structure-from-motion photogrammetry reconstructions using small unmanned aerial vehicles and ground photography to estimate the extent of upland soil erosion. *Earth Surface Processes and Landforms*. DOI: 10.1002/esp.4142

Gómez-Gutiérrez Á, Schnabel S, Berenguer-Sempere F, Lavado-Contador F, Rubio-Delgado J. 2014. Using 3D photo-reconstruction methods to estimate gully headcut erosion. *CATENA* **120**: 91–101. DOI: 10.1016/j.catena.2014.04.004

Gómez J., Vanderlinden K, Nearing MA. 2005. Spatial variability of surface roughness and hydraulic conductivity after disk tillage: implications for runoff variability. *Journal of Hydrology* **311**: 143–156. DOI: 10.1016/j.jhydrol.2005.01.014

Gómez JA, Nearing MA. 2005. Runoff and sediment losses from rough and smooth soil surfaces in a laboratory experiment. *CATENA* **59**: 253–266. DOI: 10.1016/j.catena.2004.09.008

Govers G, Giménez R, Van Oost K. 2007. Rill erosion: Exploring the relationship between experiments, modelling and field observations. *Earth-Science Reviews* **84**: 87–102. DOI: 10.1016/j.earscirev.2007.06.001

Govers G, Lobb DA, Quine TA. 1999. Preface - Tillage erosion and translocation: emergence of a new paradigm in soil erosion research. *Soil and Tillage Research* **51**: 167–174. DOI: http://dx.doi.org/10.1016/S0167-1987(99)00035-5

Govers G, Poesen J. 1988. Assessment of the interrill and rill contributions to total soil loss from an upland field plot. *Geomorphology* **1**: 343–354. DOI: http://dx.doi.org/10.1016/0169-555X(88)90006-2

Govers G, Quine TA, Desmet PJJ, Walling DE. 1996. THE RELATIVE CONTRIBUTION OF SOIL TILLAGE AND OVERLAND FLOW EROSION TO SOIL REDISTRIBUTION ON AGRICULTURAL LAND. *Earth Surface Processes and Landforms* **21**: 929–946. DOI:

10.1002/(sici)1096-9837(199610)21:10<929::aid-esp631>3.0.co;2-c

Govers G, Vandaele K, Desmet P, Poesen J, Bunte K. 1994. The role of tillage in soil redistribution on hillslopes. *European Journal of Soil Science* **45**: 469–478. DOI: 10.1111/j.1365-2389.1994.tb00532.x

Greenwood P, Walling DE, Quine TA. 2014. Using caesium-134 and cobalt-60 as tracers to assess the remobilization of recently-deposited overbank-derived sediment on river floodplains during subsequent inundation events. *Earth Surface Processes and Landforms* **39**: 228–244. DOI: 10.1002/esp.3442

Grieve IC, Davidson DA, Gordon JE. 1995. Nature, extent and severity of soil erosion in upland Scotland. *Land Degradation & Development* **6**: 41–55. DOI: 10.1002/ldr.3400060105

Guo M, Shi H, Zhao J, Liu P, Welbourne D, Lin Q. 2016. Digital close range photogrammetry for the study of rill development at flume scale. *CATENA* **143**: 265–274. DOI: 10.1016/j.catena.2016.03.036

Guzmán G, Barrón V, Gómez JA. 2010. Evaluation of magnetic iron oxides as sediment tracers in water erosion experiments. *CATENA* **82**: 126–133. DOI: 10.1016/j.catena.2010.05.011

Guzmán G, Quinton JN, Nearing MA, Mabit L, Gómez JA. 2013. Sediment tracers in water erosion studies: current approaches and challenges. *Journal of Soils and Sediments* **13**: 816–833. DOI: 10.1007/s11368-013-0659-5

Gyssels G, Poesen J, Bochet E, Li Y. 2005. Impact of plant roots on the resistance of soils to erosion by water: a review. *Progress in Physical Geography* **29**: 189–217. DOI: 10.1191/0309133305pp443ra

Hairsine PB, Sander GC. 2009. Comment on “A transport-distance based approach to scaling erosion rates”: Parts 1, 2 and 3 by Wainwright et al. *Earth Surface Processes and Landforms* **34**: 882–885. DOI: 10.1002/esp.1782

Harrod T. 1998. *A systematic approach to national budgets of phosphorous loss through soil erosion and surface runoff and National Soil Inventory nodes. Final report to MAFF for project NT1014 (SSLRC project code: JF3181)*. North Wyke

He Q, Walling DE. 1996. Interpreting particle size effects in the adsorption of 137Cs

and unsupported 210Pb by mineral soils and sediments. *Journal of Environmental Radioactivity* **30**: 117–137. DOI: 10.1016/0265-931X(96)89275-7

He Q, Walling DE. 1997. The distribution of fallout 137Cs and 210Pb in undisturbed and cultivated soils. *Applied Radiation and Isotopes* **48**: 677–690. DOI: 10.1016/S0969-8043(96)00302-8

Heng BCP, Chandler JH, Armstrong A. 2010. Applying close range digital photogrammetry in soil erosion studies. *The Photogrammetric Record* **25**: 240–265. DOI: 10.1111/j.1477-9730.2010.00584.x

Hodge R, Brasington J, Richards K. 2009. In situ characterization of grain-scale fluvial morphology using Terrestrial Laser Scanning. *Earth Surface Processes and Landforms* **34**: 954–968. DOI: 10.1002/esp.1780

Holman IP, Hollis JM, Thompson TRE. 2000. *Impact of agricultural soil conditions on floods – autumn 2000. R&D Technical Report W5B-026/TR*. Rio House Aztec West Almonds- bury Bristol BS32 4UD, UK

Idowu OJ, Rickson RJ, Godwin RJ. 2002. Analysis of surface roughness in relation to soil loss and runoff at high rainfall intensities. *Hydrological Processes* **16**: 2339–2345. DOI: 10.1002/hyp.1006

James MR, Robson S. 2012. Straightforward reconstruction of 3D surfaces and topography with a camera: Accuracy and geoscience application. *Journal of Geophysical Research: Earth Surface* **117**: F03017. DOI: 10.1029/2011jf002289

James MR, Robson S. 2014. Mitigating systematic error in topographic models derived from UAV and ground-based image networks. *Earth Surface Processes and Landforms* n/a-n/a. DOI: 10.1002/esp.3609

James MR, Robson S, D'Oleire-Oltmanns S, Niethammer U. 2017a. Optimising UAV topographic surveys processed with structure-from-motion: Ground control quality, quantity and bundle adjustment. *Geomorphology* **280**: 51–66. DOI: http://dx.doi.org/10.1016/j.geomorph.2016.11.021

James MR, Robson S, Smith MW. 2017b. 3-D uncertainty-based topographic change detection with structure-from-motion photogrammetry: precision maps for ground control and directly georeferenced surveys. *Earth Surface Processes and Landforms*. DOI: 10.1002/esp.4125

Jenny H. 1941. *Factors of soil formation: a system of quantitative pedology*. Dover

Jester W, Klik A. 2005. Soil surface roughness measurement—methods, applicability, and surface representation. *CATENA* **64**: 174–192. DOI: 10.1016/j.catena.2005.08.005

Kaiser A, Neugirg F, Rock G, Müller C, Haas F, Ries J, Schmidt J. 2014. Small-Scale Surface Reconstruction and Volume Calculation of Soil Erosion in Complex Moroccan Gully Morphology Using Structure from Motion. *Remote Sensing* **6**: 7050–7080. DOI: 10.3390/rs6087050

Kimoto A, Nearing MA, Shipitalo MJ, Polyakov VO. 2006a. Multi-year tracking of sediment sources in a small agricultural watershed using rare earth elements. *Earth Surface Processes and Landforms* **31**: 1763–1774. DOI: 10.1002/esp.1355

Kimoto A, Nearing MA, Zhang XC, Powell DM. 2006b. Applicability of rare earth element oxides as a sediment tracer for coarse-textured soils. *CATENA* **65**: 214–221. DOI: http://dx.doi.org/10.1016/j.catena.2005.10.002

Kinnell PIA. 2005. Raindrop-impact-induced erosion processes and prediction: a review. *Hydrological Processes* **19**: 2815–2844. DOI: 10.1002/hyp.5788

Kinnell PIA. 2008. Discussion: Misrepresentation of the USLE in "Is sediment delivery a fallacy?" *Earth Surface Processes and Landforms* **33**: 1627–1629. DOI: 10.1002/esp.1629

Kirkbride MP, Reeves AD. 1993. Soil erosion caused by low-intensity rainfall in Angus, Scotland. *Applied Geography* **13**: 299–311. DOI: http://dx.doi.org/10.1016/0143-6228(93)90034-X

Kirkby MJ. 2010. Distance, time and scale in soil erosion processes. *Earth Surface Processes and Landforms* **35**: 1621–1623. DOI: 10.1002/esp.2063

Kirkby MJ, Bracken LJ. 2009. Gully processes and gully dynamics. *Earth Surface Processes and Landforms* **34**: 1841–1851. DOI: 10.1002/esp.1866

Kirkby MJ, Irvine BJ, Jones RJA, Govers G. 2008. The PESERA coarse scale erosion model for Europe. I. - Model rationale and implementation. *European Journal of Soil Science* **59**: 1293–1306. DOI: 10.1111/j.1365-2389.2008.01072.x

Kosmas C, Gerontidis S, Marathianou M. 2000. The effect of land use change on soils

and vegetation over various lithological formations on Lesvos (Greece). *CATENA* **40**: 51–68. DOI: 10.1016/S0341-8162(99)00064-8

Lague D, Brodu N, Leroux J. 2013. Accurate 3D comparison of complex topography with terrestrial laser scanner: Application to the Rangitikei canyon (N-Z). *ISPRS Journal of Photogrammetry and Remote Sensing* **82**: 10–26. DOI: 10.1016/j.isprsjprs.2013.04.009

Lal R. 1998. Soil Erosion Impact on Agronomic Productivity and Environment Quality. *Critical Reviews in Plant Sciences* **17**: 319–464. DOI: 10.1080/07352689891304249

Lane SN, Westaway RM, Murray Hicks D. 2003. Estimation of erosion and deposition volumes in a large, gravel-bed, braided river using synoptic remote sensing. *Earth Surface Processes and Landforms* **28**: 249–271. DOI: 10.1002/esp.483

Le Bissonnais Y, Cerdan O, Lecomte V, Benkhadra H, Souchère V, Martin P. 2005. Variability of soil surface characteristics influencing runoff and interrill erosion. *Catena* **62**: 111–124. DOI: 10.1016/j.catena.2005.05.001

Lei TW, Zhang QW, Zhao J, Nearing MA. 2006. Tracing sediment dynamics and sources in eroding rills with rare earth elements. *European Journal of Soil Science* **57**: 287–294. DOI: 10.1111/j.1365-2389.2005.00737.x

Leys A, Govers G, Gillijns K, Berckmoes E, Takken I. 2010. Scale effects on runoff and erosion losses from arable land under conservation and conventional tillage: The role of residue cover. *Journal of Hydrology* **390**: 143–154. DOI: http://dx.doi.org/10.1016/j.jhydrol.2010.06.034

Lichti DD, Jamtsho S. 2006. Angular resolution of terrestrial laser scanners. *The Photogrammetric Record* **21**: 141–160. DOI: 10.1111/j.1477-9730.2006.00367.x

Lindstrom MJ, Nelson WW, Schumacher TE. 1992. Quantifying tillage erosion rates due to moldboard plowing. *Soil and Tillage Research* **24**: 243–255. DOI: 10.1016/0167-1987(92)90090-X

Lobb DA, Gary Kachanoski R, Miller MH. 1999. Tillage translocation and tillage erosion in the complex upland landscapes of southwestern Ontario, Canada. *Soil and Tillage Research* **51**: 189–209. DOI: http://dx.doi.org/10.1016/S0167-1987(99)00037-9

Lobb DA, Kachanoski RG, Miller MH. 1995. Tillage translocation and tillage erosion on shoulder slope landscape positions measured using 137Cs as a tracer. *Canadian Journal of Soil Science* **75**: 211–218. DOI: 10.4141/cjss95-029

Long EJ, Hargrave GK, Cooper JR, Kitchener BGB, Parsons AJ, Hewett CJM, Wainwright J. 2014. Experimental investigation into the impact of a liquid droplet onto a granular bed using three-dimensional, time-resolved, particle tracking. *Physical Review E* **89**: 32201. DOI: 10.1103/PhysRevE.89.032201

Luscombe DJ, Anderson K, Gatis N, Wetherelt A, Grand-Clement E, Brazier RE. 2014. What does airborne LiDAR really measure in upland ecosystems? *Ecohydrology* n/a-n/a. DOI: 10.1002/eco.1527

Mabit L, Meusburger K, Fulajtar E, Alewell C. 2013. The usefulness of 137Cs as a tracer for soil erosion assessment: A critical reply to Parsons and Foster (2011). *Earth-Science Reviews* **127**: 300–307. DOI: http://dx.doi.org/10.1016/j.earscirev.2013.05.008

Matisoff G, Ketterer ME, Wilson CG, Layman R, Whiting PJ. 2001. Transport of Rare Earth Element-Tagged Soil Particles in Response to Thunderstorm Runoff. *Environmental Science & Technology* **35**: 3356–3362. DOI: 10.1021/es001693m

McHugh M, Harrod T, Morgan RPC. 2002. The extent of soil erosion in upland England and Wales. *Earth Surface Processes and Landforms* **27**: 99–107. DOI: 10.1002/esp.308

Michaelides K, Ibraim I, Nord G, Esteves M. 2010. Tracing sediment redistribution across a break in slope using rare earth elements. *Earth Surface Processes and Landforms* **35**: 575–587. DOI: 10.1002/esp.1956

Micheletti N, Chandler JH, Lane SN. 2014. Investigating the geomorphological potential of freely available and accessible structure-from-motion photogrammetry using a smartphone. *Earth Surface Processes and Landforms* n/a-n/a. DOI: 10.1002/esp.3648

Micheletti N, Chandler JH, Lane SN. 2015. Structure from Motion (SfM) Photogrammetry. *Geomorphological Techniques*. British Society for Geomorphology, 1–12

Montgomery DR. 2007. Soil erosion and agricultural sustainability. *Proceedings of the*

National Academy of Sciences of the United States of America **104**: 13268–72. DOI: 10.1073/pnas.0611508104

Morgan JA, Brogan DJ, Nelson PA. 2017. Application of Structure-from-Motion photogrammetry in laboratory flumes. *Geomorphology* **276**: 125–143. DOI: 10.1016/j.geomorph.2016.10.021

Morgan RPC. 1985a. Soil Erosion Measurement and Soil Conservation Research in Cultivated Areas of the UK. *The Geographical Journal* **151**: 11–20. DOI: 10.2307/633274

Morgan RPC. 1985b. Assessment of soil erosion risk in England and Wales. *Soil Use and Management* **1**: 127–131. DOI: 10.1111/j.1475-2743.1985.tb00974.x

Morgan RPC. 1995. *Soil Erosion and Conservation*. Longman

Morgan RPC, Quinton JN, Smith RE, Govers G, Poesen JWA, Auerswald K, Chisci G, Torri D, Styczen ME. 1998. The European Soil Erosion Model (EUROSEM): a dynamic approach for predicting sediment transport from fields and small catchments. *Earth Surface Processes and Landforms* **23**: 527–544. DOI: 10.1002/(SICI)1096-9837(199806)23:6<527::AID-ESP868>3.0.CO;2-5

Nearing MA, Govers G, Norton LD. 1999a. Variability in Soil Erosion Data from Replicated Plots. *Soil Science Society of America Journal* **63**: 1829. DOI: 10.2136/sssaj1999.6361829x

Nearing MA, Govers G, Norton LD. 1999b. Variability in Soil Erosion Data from Replicated Plots. *Soil Sci. Soc. Am. J.* **63**: 1829–1835. DOI: 10.2136/sssaj1999.6361829x

Nouwakpo SK, James MR, Weltz MA, Huang C-H, Chagas I, Lima L. 2014. Evaluation of structure from motion for soil microtopography measurement. *The Photogrammetric Record* **29**: 297–316. DOI: 10.1111/phor.12072

Ouédraogo MM, Degré A, Debouche C, Lisein J. 2014. The evaluation of unmanned aerial systems-based photogrammetry and terrestrial laser scanning to generate DEMs of agricultural watersheds. *Geomorphology*. DOI: 10.1016/j.geomorph.2014.02.016

Owens PN, Rickson RJ, Clarke MA, Dresser M, Deeks LK, Jones RJA, Woods GA, Van

Oost K, Quine TA. 2006. *Scoping study of soil loss through wind erosion , tillage erosion and soil co-extracted with root vegetables. Final report to Defra for project SP08007*.

Palmer RC, Smith RP. 2013. Soil structural degradation in SW England and its impact on surface-water runoff generation. *Soil Use and Management* **29**: 567–575. DOI: 10.1111/sum.12068

Panagos P, Borrelli P, Meusburger K. 2015a. A New European Slope Length and Steepness Factor (LS-Factor) for Modeling Soil Erosion by Water. *Geosciences* **5**: 117–126. DOI: 10.3390/geosciences5020117

Panagos P, Borrelli P, Poesen J, Ballabio C, Lugato E, Meusburger K, Montanarella L, Alewell C. 2015b. The new assessment of soil loss by water erosion in Europe. *Environmental Science & Policy* **54**: 438–447. DOI: 10.1016/j.envsci.2015.08.012

Panagos P, Borrelli P, Poesen J, Meusburger K, Ballabio C, Lugato E, Montanarella L, Alewell C. 2016. Reply to "The new assessment of soil loss by water erosion in Europe. Panagos P. et al., 2015 Environ. Sci. Policy 54, 438-447-A response" by Evans and Boardman [Environ. Sci. Policy 58, 11-15]. *Environmental Science and Policy* **59**: 53–57. DOI: 10.1016/j.envsci.2016.02.010

Parsons AJ, Brazier RE, Wainwright J, Powell DM. 2006. Scale relationships in hillslope runoff and erosion. *Earth Surface Processes and Landforms* **31**: 1384–1393. DOI: 10.1002/esp.1345

Parsons AJ, Foster IDL. 2011. What can we learn about soil erosion from the use of 137Cs? *Earth-Science Reviews* **108**: 101–113. DOI: 10.1016/j.earscirev.2011.06.004

Parsons AJ, Foster IDL. 2013. The assumptions of science. *Earth-Science Reviews* **127**: 308–310. DOI: 10.1016/j.earscirev.2013.05.011

Parsons AJ, Onda Y, Noguchi T, Patin J, Cooper J, Wainwright J, Sakai N. 2014. The use of RFID in soil-erosion research. *Earth Surface Processes and Landforms* n/a-n/a. DOI: 10.1002/esp.3628

Parsons AJ, Wainwright J. 2006. Depth distribution of interrill overland flow and the formation of rills. *Hydrological Processes* **20**: 1511–1523. DOI: 10.1002/hyp.5941

Parsons AJ, Wainwright J, Abrahams AD. 1993. Tracing sediment movement in interrill overland flow on a semi-arid grassland hillslope using magnetic susceptibility. *Earth Surface Processes and Landforms* **18**: 721–732. DOI: 10.1002/esp.3290180806

Parsons AJ, Wainwright J, Fukuwara T, Onda Y. 2010. Using sediment travel distance to estimate medium-term erosion rates: a 16-year record. *Earth Surface Processes and Landforms* **35**: 1694–1700. DOI: 10.1002/esp.2011

Parsons AJ, Wainwright J, Mark Powell D, Kaduk J, Brazier RE. 2004. A conceptual model for determining soil erosion by water. *Earth Surface Processes and Landforms* **29**: 1293–1302. DOI: 10.1002/esp.1096

Peeters I, Van Oost K, Govers G, Verstraeten G, Rommens T, Poesen J. 2008. The compatibility of erosion data at different temporal scales. *Earth and Planetary Science Letters* **265**: 138–152. DOI: http://dx.doi.org/10.1016/j.epsl.2007.09.040

Pimentel D. 2006. Soil Erosion: A Food and Environmental Threat. *Environment, Development and Sustainability* **8**: 119–137. DOI: 10.1007/s10668-005-1262-8

Pimentel D, Harvey C, Resosudarmo P, Sinclair K, Kurz D, McNair M, Crist S, Shpritz L, Fitton L, Saffouri R, Blair R. 1995. Environmental and Economic Costs of Soil Erosion and Conservation Benefits. *Science* **267**: 1117–1123. DOI: 10.1126/science.267.5201.1117

Plante AF, Duke MJM, McGill WB. 1999. A Tracer Sphere Detectable by Neutron Activation for Soil Aggregation and Translocation Studies. , 1284–1290

Polyakov VO, Kimoto A, Nearing MA, Nichols MH. 2009. Tracing Sediment Movement on a Semiarid Watershed using Rare Earth Elements. *Soil Science Society of America Journal* **73**: 1559. DOI: 10.2136/sssaj2008.0378

Polyakov VO, Nearing MA. 2004. Rare earth element oxides for tracing sediment movement. *CATENA* **55**: 255–276. DOI: http://dx.doi.org/10.1016/S0341-8162(03)00159-0

Polyakov VO, Nearing MA, Shipitalo MJ. 2004. Tracking sediment redistribution in a small watershed: implications for agro-landscape evolution. *Earth Surface Processes and Landforms* **29**: 1275–1291. DOI: 10.1002/esp.1094

Porto P, Walling DE, Capra A. 2014. Using 137Cs and 210Pbe measurements and conventional surveys to investigate the relative contributions of interrill/rill and gully erosion to soil loss from a small cultivated catchment in Sicily. *Soil and Tillage Research* **135**: 18–27. DOI: 10.1016/j.still.2013.08.013

Posthumus H, Deeks LK, Rickson RJ, Quinton JN. 2013. Costs and benefits of erosion control measures in the UK. *Soil Use and Management* n/a-n/a. DOI: 10.1111/sum.12057

Prosdocimi M, Burguet M, Di Prima S, Sofia G, Terol E, Rodrigo Comino J, Cerdà A, Tarolli P. 2017. Rainfall simulation and Structure-from-Motion photogrammetry for the analysis of soil water erosion in Mediterranean vineyards. *Science of The Total Environment* **574**: 204–215. DOI: http://dx.doi.org/10.1016/j.scitotenv.2016.09.036

Pryce O. 2011. Development of Environmental Tracers for Sediments and Phosphorus. Lancaster University

Quine TA. 1999. Use of caesium-137 data for validation of spatially distributed erosion models: the implications of tillage erosion. *CATENA* **37**: 415–430. DOI: http://dx.doi.org/10.1016/S0341-8162(99)00030-2

Quine TA, Govers G, Walling DE, Zhang X, Desmet PJJ, Zhang Y, Vandaele K. 1997. Erosion processes and landform evolution on agricultural land — new perspectives from caesium-137 measurements and topographic-based erosion modelling. *Earth Surface Processes and Landforms* **22**: 799–816. DOI: 10.1002/(SICI)1096-9837(199709)22:9<799::AID-ESP765>3.0.CO;2-R

Quine TA, Walling DE. 1991. Rates of soil erosion on arable fields in Britain: quantitative data from caesium-137 measurements. *Soil Use and Management* **7**: 169–176. DOI: 10.1111/j.1475-2743.1991.tb00870.x

Quine TA, Zhang Y. 2002. An investigation of spatial variation in soil erosion, soil properties, and crop production within an agricultural field in Devon, United Kingdom. *Journal of Soil and Water Conservation* **57**: 55–65

Quine TA, Zhang Y. 2004. Re-defining tillage erosion: quantifying intensity–direction relationships for complex terrain. *Soil Use and Management* **20**: 114–123. DOI: 10.1111/j.1475-2743.2004.tb00346.x

Quinton JN, Catt JA. 2004. The effects of minimal tillage and contour cultivation on surface runoff, soil loss and crop yield in the long-term Woburn Erosion Reference Experiment on sandy soil at Woburn, England. *Soil Use and Management* **20**: 343–349. DOI: 10.1111/j.1475-2743.2004.tb00379.x

R Core Team. 2016. R: A language and environment for statistical computing. R Foundatoin for Statistical Computing: Vienna, Austria

Rai RK, Upadhyay A, Singh VP. 2010. Effect of variable roughness on runoff. *Journal of Hydrology* **382**: 115–127. DOI: 10.1016/j.jhydrol.2009.12.022

Reed AH. 1979. Accelerated erosion of arable soils in the United Kingdom by rainfall and run-off. *Outlook on Agriculture* **10**: 41–48. DOI: 10.1177/003072707901000107

Regnier P, Friedlingstein P, Ciais P, Mackenzie FT, Gruber N, Janssens IA, Laruelle GG, Lauerwald R, Luyssaert S, Andersson AJ, Arndt S, Arnosti C, Borges A V, Dale AW, Gallego-Sala A, Godderis Y, Goossens N, Hartmann J, Heinze C, Ilyina T, Joos F, LaRowe DE, Leifeld J, Meysman FJR, Munhoven G, Raymond PA, Spahni R, Suntharalingam P, Thullner M. 2013. Anthropogenic perturbation of the carbon fluxes from land to ocean. *Nature Geosci* **6**: 597–607

Rickson RJ. 2014. Can control of soil erosion mitigate water pollution by sediments? *Science of The Total Environment* **468–469**: 1187–1197. DOI: http://dx.doi.org/10.1016/j.scitotenv.2013.05.057

Robinson DA, Boardman J. 1988. Cultivation practice, sowing season and soil erosion on the South Downs, England: a preliminary study. *The Journal of Agricultural Science* **110**: 169–177. DOI: doi:10.1017/S0021859600079818

Robinson KM, Bennett SJ, Casalí J, Hanson GJ. 2000. Processes of headcut growth and migration in rills and gullies. *International Journal of Sediment Research* **15**: 69–82

Römkens MJ., Helming K, Prasad S. 2002. Soil erosion under different rainfall intensities, surface roughness, and soil water regimes. *CATENA* **46**: 103–123. DOI: 10.1016/S0341-8162(01)00161-8

Rowan JS, Goodwill P, Greco M. 1995. Temporal variability in catchment sediment yield determined from repeated bathymetric surveys: Abbeystead Reservoir, U.K. *Physics and Chemistry of the Earth* **20**: 199–206. DOI: 10.1016/0079-

1946(95)00024-0

RStudio Team. 2015. RStudio: Integrated Development for R. RStudio, Inc.: Boston, MA

Ruysschaert G, Poesen J., Verstraeten G., Govers G. 2004. Soil loss due to crop harvesting: significance and determining factors. *Progress in Physical Geography* **28**: 467–501. DOI: 10.1191/0309133304pp421oa

Sadeghi SHR, Seghaleh MB, Rangavar AS. 2013. Plot sizes dependency of runoff and sediment yield estimates from a small watershed. *CATENA* **102**: 55–61. DOI: http://dx.doi.org/10.1016/j.catena.2011.01.003

Salles C, Poesen J. 2000. Rain properties controlling soil splash detachment. *Hydrological Processes* **14**: 271–282. DOI: 10.1002/(SICI)1099-1085(20000215)14:2<271::AID-HYP925>3.0.CO;2-J

Schaller N, Kay AL, Lamb R, Massey NR, van Oldenborgh GJ, Otto FEL, Sparrow SN, Vautard R, Yiou P, Ashpole I, Bowery A, Crooks SM, Haustein K, Huntingford C, Ingram WJ, Jones RG, Legg T, Miller J, Skeggs J, Wallom D, Weisheimer A, Wilson S, Stott PA, Allen MR. 2016. Human influence on climate in the 2014 southern England winter floods and their impacts. *Nature Clim. Change* **6**: 627–634

Senbayram M, Bol R, Dixon L, Fisher A, Stevens C, Quinton JN, Fangueiro D. 2015. Potential use of rare earth oxides as tracers of organic matter in grassland. *Journal of Plant Nutrition and Soil Science* n/a-n/a. DOI: 10.1002/jpln.201400465

Seto KC, Fragkias M, Güneralp B, Reilly MK, Pidgeon A. 2011. A Meta-Analysis of Global Urban Land Expansion. *PLoS ONE* **6**: e23777. DOI: 10.1371/journal.pone.0023777

Shahbazi M, Sohn G, Théau J, Menard P. 2015. Development and Evaluation of a UAV-Photogrammetry System for Precise 3D Environmental Modeling. *Sensors* **15**: 27493–27524. DOI: 10.3390/s151127493

Shaw EM. 1994. *Hydrology in Practice*. Chapman & Hall: London, UK

Skinner RJ, Chambers BJ. 1996. A survey to assess the extent of soil water erosion in lowland England and Wales. *Soil Use and Management* **12**: 214–220. DOI: 10.1111/j.1475-2743.1996.tb00546.x

Slattery MC, Bryan RB. 1992. Hydraulic conditions for rill incision under simulated rainfall: A laboratory experiment. *Earth Surface Processes and Landforms* **17**: 127–

146. DOI: 10.1002/esp.3290170203

Smith MW. 2014. Roughness in the Earth Sciences. *Earth-Science Reviews* **136**: 202–225. DOI: 10.1016/J.EARSCIREV.2014.05.016

Smith MW, Carrivick JL, Quincey DJ. 2015. Structure from motion photogrammetry in physical geography. *Progress in Physical Geography*. DOI: 10.1177/0309133315615805

Smith MW, Cox NJ, Bracken LJ. 2011. Terrestrial laser scanning soil surfaces: a field methodology to examine soil surface roughness and overland flow hydraulics. *Hydrological Processes* **25**: 842–860. DOI: 10.1002/hyp.7871

Smith MW, Vericat D. 2015. From experimental plots to experimental landscapes: topography, erosion and deposition in sub-humid badlands from Structure-from-Motion photogrammetry. *Earth Surface Processes and Landforms* **40**: 1656–1671. DOI: 10.1002/esp.3747

Soudarissanane S, Lindenbergh R, Menenti M, Teunissen P. 2009. Incidence angle on the quality of Terrestrial Laser Scanning points. *International Archives of Photogrammetry. Remote Sensing and Spatial Information Sciences* **38**: 183–188

Stevens CJ, Quinton JN. 2008. Investigating source areas of eroded sediments transported in concentrated overland flow using rare earth element tracers. *CATENA* **74**: 31–36. DOI: http://dx.doi.org/10.1016/j.catena.2008.01.002

Stevens CJ, Quinton JN, Bailey AP, Deasy C, Silgram M, Jackson DR. 2009. The effects of minimal tillage, contour cultivation and in-field vegetative barriers on soil erosion and phosphorus loss. *Soil and Tillage Research* **106**: 145–151. DOI: http://dx.doi.org/10.1016/j.still.2009.04.009

Takken I, Govers G, Jetten V, Nachtergaele J, Steegen A, Poesen J. 2001a. Effects of tillage on runoff and erosion patterns. *Soil and Tillage Research* **61**: 55–60. DOI: 10.1016/S0167-1987(01)00178-7

Takken I, Jetten V, Govers G, Nachtergaele J, Steegen A. 2001b. The effect of tillage-induced roughness on runoff and erosion patterns. *Geomorphology* **37**: 1–14. DOI: 10.1016/S0169-555X(00)00059-3

Telling J, Lyda A, Hartzell P, Glennie C. 2017. Review of Earth science research using

terrestrial laser scanning. *Earth-Science Reviews* **169**: 35–68. DOI: 10.1016/j.earscirev.2017.04.007

Tilman D, Cassman KG, Matson PA, Naylor R, Polasky S. 2002. Agricultural sustainability and intensive production practices. *Nature* **418**: 671–7. DOI: 10.1038/nature01014

Torri D, Sfalanga M, Del Sette M. 1987. Splash detachment: Runoff depth and soil cohesion. *CATENA* **14**: 149–155. DOI: 10.1016/S0341-8162(87)80013-9

Van Muysen W, Govers G. 2002. Soil displacement and tillage erosion during secondary tillage operations: the case of rotary harrow and seeding equipment. *Soil and Tillage Research* **65**: 185–191. DOI: 10.1016/S0167-1987(01)00284-7

Van Muysen W, Govers G, Bergkamp G, Roxo M, Poesen J. 1999. Measurement and modelling of the effects of initial soil conditions and slope gradient on soil translocation by tillage. *Soil and Tillage Research* **51**: 303–316. DOI: http://dx.doi.org/10.1016/S0167-1987(99)00044-6

Van Muysen W, Govers G, Van Oost K. 2002. Identification of important factors in the process of tillage erosion: the case of mouldboard tillage. *Soil and Tillage Research* **65**: 77–93. DOI: http://dx.doi.org/10.1016/S0167-1987(01)00282-3

Van Oost K, Govers G, de Alba S, Quine TA. 2006. Tillage erosion: a review of controlling factors and implications for soil quality. *Progress in Physical Geography* **30**: 443–466. DOI: 10.1191/0309133306pp487ra

Van Oost K, Govers G, Desmet P. 2000. Evaluating the effects of changes in landscape structure on soil erosion by water and tillage. *Landscape Ecology* **15**: 577–589. DOI: 10.1023/a:1008198215674

Vandaele K, Poesen J. 1995. Spatial and temporal patterns of soil erosion rates in an agricultural catchment, central Belgium. *CATENA* **25**: 213–226. DOI: http://dx.doi.org/10.1016/0341-8162(95)00011-G

Ventura E, Nearing MA, Amore E, Norton LD. 2002. The study of detachment and deposition on a hillslope using a magnetic tracer. *CATENA* **48**: 149–161. DOI: 10.1016/S0341-8162(02)00003-6

Ventura E, Nearing MA, Norton L. 2001. Developing a magnetic tracer to study soil

erosion. *CATENA* **43**: 277–291. DOI: http://dx.doi.org/10.1016/S0341-8162(00)00149-1

Verheijen FGA, Jones RJA, Rickson RJ, Smith CJ. 2009. Tolerable versus actual soil erosion rates in Europe. *Earth-Science Reviews* **94**: 23–38. DOI: 10.1016/j.earscirev.2009.02.003

Vericat D, Smith MW, Brasington J. 2014. Patterns of topographic change in sub-humid badlands determined by high resolution multi-temporal topographic surveys. *CATENA* **120**: 164–176. DOI: 10.1016/j.catena.2014.04.012

Vinci A, Brigante R, Todisco F, Mannocchi F, Radicioni F. 2015. Measuring rill erosion by laser scanning. *CATENA* **124**: 97–108. DOI: 10.1016/j.catena.2014.09.003

Vrieling A. 2006. Satellite remote sensing for water erosion assessment: A review. *CATENA* **65**: 2–18. DOI: 10.1016/j.catena.2005.10.005

Wainwright J, Parsons AJ, Müller EN, Brazier RE, Powell DM. 2009. Response to Kinnell's "Comment on 'A transport-distance approach to scaling erosion rates: III. Evaluating scaling characteristics of Mahleran.'" *Earth Surface Processes and Landforms* **34**: 1320–1321. DOI: 10.1002/esp.1816

Wainwright J, Parsons AJ, Müller EN, Brazier RE, Powell DM, Fenti B. 2008a. A transport-distance approach to scaling erosion rates: 2. sensitivity and evaluation of Mahleran. *Earth Surface Processes and Landforms* **33**: 962–984. DOI: 10.1002/esp.1623

Wainwright J, Parsons AJ, Müller EN, Brazier RE, Powell DM, Fenti B. 2008b. A transport-distance approach to scaling erosion rates: 1. Background and model development. *Earth Surface Processes and Landforms* **33**: 813–826. DOI: 10.1002/esp.1624

Wainwright J, Parsons AJ, Müller EN, Brazier RE, Powell DM, Fenti B. 2008c. A transport-distance approach to scaling erosion rates: 3. Evaluating scaling characteristics of Mahleran. *Earth Surface Processes and Landforms* **33**: 1113–1128. DOI: 10.1002/esp.1622

Walling DE. 2005. Tracing suspended sediment sources in catchments and river systems. *Science of The Total Environment* **344**: 159–184. DOI: 10.1016/j.scitotenv.2005.02.011

Walling DE. 2008. *Documenting soil erosion rates on agricultural land in England and Wales: Phase 2. Final report to Defra for project SP0413*.

Walling DE, He Q, Quine TA. 1995. Use of caesium-137 and lead-210 as tracers in soil erosion investigations. *IAHS Publications-Series of Proceedings and Reports-Intern Assoc Hydrological Sciences* **229**: 163–172

Walling DE, He Q, Whelan P. 2003. Using 137Cs measurements to validate the application of the AGNPS and ANSWERS erosion and sediment yield models in two small Devon catchments. *Soil and Tillage Research* **69**: 27–43. DOI: 10.1016/S0167-1987(02)00126-5

Walling DE, Quine TA. 1990. Calibration of caesium-137 measurements to provide quantitative erosion rate data. *Land Degradation & Development* **2**: 161–175. DOI: 10.1002/ldr.3400020302

Walling DE, Quine TA. 1991. Use of 137Cs measurements to investigate soil erosion on arable fields in the UK: potential applications and limitations. *Journal of Soil Science* **42**: 147–165. DOI: 10.1111/j.1365-2389.1991.tb00099.x

Walling DE, Russell MA, Hodgkinson RA, Zhang Y. 2002. Establishing sediment budgets for two small lowland agricultural catchments in the UK. *CATENA* **47**: 323–353. DOI: http://dx.doi.org/10.1016/S0341-8162(01)00187-4

Walling DE, YuSheng Z. 2010. A national assessment of soil erosion based on caesium-137 measurements. In: Zlatic´ M (ed) *Advances in GeoEcology*. Catena Verlag, 89–97

Watson A, Evans R. 1991. A comparison of estimates of soil erosion made in the field and from photographs. *Soil and Tillage Research* **19**: 17–27. DOI: http://dx.doi.org/10.1016/0167-1987(91)90106-8

Wheaton JM, Brasington J, Darby SE, Sear DA. 2010. Accounting for uncertainty in DEMs from repeat topographic surveys: improved sediment budgets. *Earth Surface Processes and Landforms* **35**: 136–156. DOI: 10.1002/esp.1886

Wickham H. 2009. ggplot2: Elegant Graphics for Data Analysis. Springer-Verlag: New York, USA

Wickham H. 2016a. scales: Scale Functions for Visualization.

Wickham H. 2016b. stringr: Simple, Consistent Wrappers for Common String Operations.

Wiggs GF., Baird A., Atherton R. 2004. The dynamic effects of moisture on the entrainment and transport of sand by wind. *Geomorphology* **59**: 13–30. DOI: 10.1016/j.geomorph.2003.09.002

Wilke CO. 2017. cowplot: Streamlined Plot Theme and Plot Annotations for "ggplot2."

Zapata F. 2003. The use of environmental radionuclides as tracers in soil erosion and sedimentation investigations: recent advances and future developments. *Soil and Tillage Research* **69**: 3–13. DOI: 10.1016/S0167-1987(02)00124-1

Zhang W, Montgomery DR. 1994. Digital elevation model grid size, landscape representation, and hydrologic simulations. *Water Resources Research* **30**: 1019–1028. DOI: 10.1029/93WR03553

Zhang X, Friedrich J, Nearing M, Norton L. 2001. Potential use of rare earth oxides as tracers for soil erosion and aggregation studies. *Soil Science Society …* **65**: 1508–1515

Zhang X, Nearing MA, Polyakov VO, Friedrich J. 2003. Using rare-earth oxide tracers for studying soil erosion dynamics. *Soil Science Society …* **67**: 279–288